Monitoring the variability of sea level and surface circulation with satellite altimetry

Monitoring van variabiliteit van zeeniveau en oppervlaktecirculatie met satelliet altimetrie
(met een samenvatting in het Nederlands)

Мониторинг изменчивости уровня и поверхностной циркуляции океана посредством спутниковой альтиметрии
(с кратким изложением на русском языке)

Proefschrift

ter verkrijging van de graad van doctor aan de Universiteit Utrecht
op gezag van de Rector Magnificus, Prof. Dr. W.H. Gispen, ingevolge
het besluit van het College voor Promoties in het openbaar te verdedigen

op **donderdag 18 november 2004** des middags om **12:45** uur

door

Denis Volkov

geboren op 30 april 1975 te Taganrog, Rusland

Promotor: **Prof. Dr. W.P.M. de Ruijter**
Instituut voor Marien en Atmosferisch onderzoek Utrecht (IMAU)
Faculteit Natuur- en Sterrenkunde, Universiteit Utrecht

Co-promotor: **Dr. H.M. van Aken**
Afdeling Fysische Oceanografie
Koninklijk Nederlands Instituut voor Onderzoek der Zee

Dit proefschrift werd mede mogelijk gemaakt door financiële steun van de Nederlandse organisatie voor Wetenschappelijk Onderzoek (NWO).

Contents

Chapter 1: Introduction **1**

1.1 Oceanic variability 1
1.2 Changes of sea level 4
1.3 Ocean circulation and its variability 5
1.4 The North Atlantic Ocean and its variability 7
1.5 Overview of the thesis 14

Chapter 2: Monitoring the ocean with satellite altimetry **17**

2.1 Principles of satellite altimetry 17
2.2 Satellite altimetry missions 20
2.3 Altimeter data used in this thesis 22
2.4 Data processing techniques 22

Chapter 3: Seasonal and interannual variability of sea level in the northern North Atlantic **29**

3.1 Introduction 29
3.2 Data used 32
3.3 Observational results 33
3.4 Conclusions 44

Chapter 4: Variability of sea level in the North Pacific and North Atlantic: a comparative analysis **47**

4.1 Introduction 47
4.2 Observational results 50
4.3 Climate-related change 65
4.4 Conclusions 72

Chapter 5: Interannual variability of eddy field and surface circulation in the North Atlantic Ocean **75**

5.1 Introduction 76
5.2 Data and method 78

5.3 Observational results 80
5.4 Conclusions 102

Chapter 6: Propagating features in the eddy field of the North Atlantic Current **105**

6.1 Introduction 105
6.2 Method 106
6.3 Results of the analysis 109
6.4 Conclusions and discussion 115

Chapter 7: Summary and synthesis **117**

References **125**

Samenvatting **135**

Краткое изложение **143**

Acknowledgements **151**

Curriculum Vitae **152**

Chapter 1

Introduction

1.1 Oceanic variability

Definition of oceanic variability

The World Ocean covers 70.8 % of the Earth's surface and, along with the atmosphere, is a highly unsteady and variable dynamic object on the planet. This implies that oceanic properties, influenced by various physical processes, are time-dependent or variable. These properties include characteristics of motion (current velocity components and sea surface state), thermodynamic characteristics defining the state of water (pressure, temperature and salinity) and derived thermodynamic parameters (density, conductivity, entropy, speed of sound and refractive index), and chemical composition (the concentration of dissolved gases and substances, mineral and organic suspended matter). Eventually, a change of the thermodynamic state can lead to a change of seawater volume (sea level) and a phase state (freezing/melting and evaporation/condensation).

Why to study oceanic variability?

Understanding the oceanic variability and the ability to predict it are very important issues for human activity. Nearly all motions, and hence changes, in the ocean and atmosphere are ultimately caused by uneven income of solar radiation. Overall, the earth gains heat at low latitudes and it loses heat at high latitudes. To balance these gains and losses, the ocean and atmosphere transport heat from the tropics to the poles in an approximately equal proportion (Peixoto and Oort, 1992). The oceanic transport of heat features low velocities and high heat capacity compared to the low heat capacity and high velocities in the atmosphere. Due to its enormous potential to store heat, the ocean moderates climate on our planet. The transport of heat is not steady, but varies because of different physical processes. For instance, significant changes in meridional heat transport, particularly in the Atlantic Ocean, may have contributed to the development of ice ages (Dijkstra, 2000). Different physical processes of ocean-atmosphere interaction on shorter time-scales have a great impact on the variations of atmospheric conditions. Therefore, the study of oceanic variability helps to achieve better seasonal and inter-annual forecasts as well as to

understand, identify and predict the changes of climate. The latter is particularly important nowadays, in the light of the anticipated anthropogenic global change. Other activities, like navigation, fisheries, shelf exploration etc. also benefit from the study of the oceanic variability. A principal requirement for navigation and other offshore activities is the knowledge of currents and wave regime. But it is known that the range of the variable part of the direction and velocity of currents is often comparable to or larger then their long-term mean state. The fishing industry also needs information about the variations in the position of oceanic fronts and currents, changes of temperature and salinity of the upper ocean, and other parameters determining the distribution of fish populations in the ocean. At last, everyone is aware that before carrying out any activity on the oceanic shelf, whether it is oil and gas production or coastal protection, the understanding of the oceanic variability and its prediction is crucial.

Classification and causes of oceanic variability

Changes in the oceanic properties can have different spatial and temporal scales. It is important to choose a particular scale of variability during an investigation, because it helps to decide how to handle smaller and larger scales. For example, when we study seasonal changes of sea level, it is not necessary to take into account variations in the solar insolation due to orbital changes or to consider a historical change of the amount of water in the ocean. In this case smaller and larger scale phenomena can be considered as a noise (random component) with given statistical properties. Based on the temporal and spatial scales of changes, Monin et al. (1977) and later Kamenkovich et al. (1986) introduced a classification of the types of variability, observed in the ocean, which can briefly be presented as follows:

1. *Small-scale change* includes capillary and surface gravitational waves, internal gravitational waves, turbulence and other processes with periods of the order of 10 minutes and less and spatial scales from fractions of a millimetre to tens of metres, sometimes kilometres.

2. *Mesoscale change* has periods from hours to a day and spatial scales of hundreds of metres to several kilometres. This type includes tidal fluctuations, induced by the gravitational attraction of the moon and sun, inertial fluctuations that are produced by the inertial forces attendant to the rotation of the earth, and internal waves.

The small-scale and mesoscale changes are not resolved by the present-day satellite altimetry and are not covered by this thesis. However, the mesoscale variations introduce different biases to satellite altimetry data and therefore can be studied using altimeter measurements.

3. *Synoptic variability* is primarily generated by the action of the variable wind on the sea surface, thermal action of the atmosphere, and baroclinic and barotropic instabilities of large-scale currents. The instability processes mainly result in the formation of eddies with spatial scales of the order of 100 km and life times from several days to several months, on occasions to about 1 year and more. Another kind of synoptic variations is the propagation of Rossby waves across the ocean basins.

The term “synoptic variability” was introduced in Kamenkovich et al. (1986) for variability with horizontal scales of the order of the Rossby deformation radius by complete analogy with the atmosphere. However, in the English literature the term “mesoscale

eddies" is more common. To avoid confusion in the following chapters of this thesis the term "mesoscale variability" will be applied for eddies and Rossby waves.

4. *Seasonal variations* (annual cycle) have a yearly period and are caused by the seasonal change of direct insolation, changes of heat and fresh water fluxes (buoyancy fluxes) between the ocean and atmosphere, wind forcing, river discharge, etc. These variations occur everywhere in the ocean, but in particular in the mid-latitudes and in the monsoon regions.

5. *The year-to-year* (inter-annual) *variability* is connected, by definition, with periods over a year and occurs on large spatial scales. This type of variability mainly comprises the change of the oceanic properties, caused by large-scale ocean-atmosphere interaction. The ocean-atmosphere system can undergo internal oscillations caused by instabilities of the circulation due to nonlinear dynamics (Dijkstra, 2000). One of the well-known examples of such oscillations is the El Niño/Southern Oscillation (ENSO) phenomenon, associated with the variations in atmospheric pressure distribution in the equatorial Pacific. These variations cause an anomalous increase of the sea surface temperature (SST) by a few degrees in the eastern Pacific. Another example of the inter-annual change is the North Atlantic Oscillation (NAO), which is a large-scale alteration of the atmospheric pressure difference between the Icelandic Low and Azores High pressure centres. The NAO is characterized by changes in the strength of westerly winds over the North Atlantic (Hurrell, 1995) and associated changes in the oceanic transport (Curry and McCartney, 2001) and SST (Bjerknes, 1964; Daly, 1978).

In fact, the ocean-size spatial scales are inherent to the temporal scales from seasonal and longer. The *inter-decadal* to *centennial* time scales can also be identified. The NAO, for example, among multiple frequencies has an inter-decadal mode. As was observed, sea surface temperature in the North Atlantic was higher during the period 1950-1964 than in 1970-1984 (Kushnir, 1994). A Great Salinity Anomaly in 1967-1972 was suggested to be a recurrent event linked to an approximately 20 year climate cycle, involving changes in the atmosphere, ocean and sea-ice (Mysak, 1990).

The physical mechanisms, which induce changes in the ocean and on the whole planet, can be of external or internal origin. A clear example of an external forcing are variations of insolation: daily variations due to the altitude of the sun over the horizon, seasonal changes due to the tilt of the earth spin axis with respect to the plane of its orbit around the sun (obliquity), annual changes because of the eccentricity of the earth orbit, changes caused by precession and the variations of obliquity and eccentricity (orbital parameters) over long time scales, the variations of sunspots, etc. Another example of externally forced oscillations is the tide. In the essence of the internal forcing lies the interaction between the different components of the geosphere, i.e. atmosphere, hydrosphere, lithosphere, cryosphere and biosphere. The existence of nonlinear processes in each component can lead to a complex character of variability on different time scales.

Monitoring the oceanic variability

The monitoring of the oceanic variability implies the realisation of regular measurements. Depending on the scales a researcher is interested in, these measurements must have a satisfactory spatial and temporal resolution. Oceanographers have been monitoring the ocean by conducting regular surveys, deploying moorings, using drifting buoys and floats,

tidal gauges, and, in the last years, satellite observations. Poor spatial and temporal resolution of *in situ* measurements imposes severe limitations on the study of the oceanic variability. With a few exceptions, hydrographic surveys are rarely conducted on a regular basis and usually measurements are taken in a most favourable season, in terms of weather and sea state. It may take weeks or months for a ship to cross the ocean while the oceanic properties are constantly changing. Therefore, it is almost unfeasible to perform synoptic monitoring and it is very complicated and costly to study large-scale changes using *in situ* instrumentation. The advent of satellite altimetry and especially the latest high-accuracy altimetric missions (joint French/U.S. TOPEX/Poseidon and Jason-1 satellites, and the European Space Agency's ERS-1, ERS-2 and Envisat missions) has given oceanographers a powerful tool to study the variability of sea level and ocean currents (Fu and Cazenave, 2001; Fu et al., 1994). The satellites provide a regular global monitoring of the ocean state and make it possible to resolve the synoptic processes.

1.2 Changes of sea level

The sea surface of an ocean at rest is an equipotential surface, or the geoid, determined by the mean gravity variations on the sea floor, when the attractive forces of all the masses are balanced by the centrifugal forces set up by the rotation of the earth. However, the marine geoid is subject to periodic and non-periodic forcing, caused by heat and fresh water fluxes (buoyancy fluxes), air pressure differences and wind stress, currents, tides, etc. This forcing causes deviations of the sea surface from the geoid.

Changes of sea surface level can be observed by using tidal gauges and by satellite altimetry measurements. The largest portion of the sea level variability is caused by the ocean tides with a global root-mean-square (RMS) of about 32 cm (Fu and Cazenave, 2001). Apart from tides, sea level can vary due to the volumetric changes of the water column at a given location that occur because of the variations of total mass or density. This remaining sea level signal has global RMS≈12 cm (Wunch and Stammer, 1997).

If the long-term changes of the amount of water in the ocean are neglected, the vertically integrated mass of the water column can change because of the mechanical forcing of the atmosphere through wind and pressure. Wind forcing accounts for surface gravity waves, advection, storm surges, etc., while the atmospheric pressure differences cause the sea surface to be depressed/expanded by about 1 cm per 1 mbar change (so called atmospheric loading or inverse barometer effect). Such a response to the atmospheric forcing involves the redistribution of the amount of water between different locations and is called barotropic. The barotropic response occurs on relatively short time scales, generally less than seasonal, although spatial scales can exceed 500 km like in the case of the atmospheric loading.

Changes in density can be caused by the variations in buoyancy fluxes, by the baroclinic instability and the variations of temperature and salinity due to the advection of water masses, when the isopycnal surfaces in the ocean move vertically without changing the mass of the entire water column. Among these variations of sea level are eddies, baroclinic Rossby waves, large-scale seasonal and inter-annual variations. This is the baroclinic response of the ocean and it occurs on synoptic, seasonal and longer time scales.

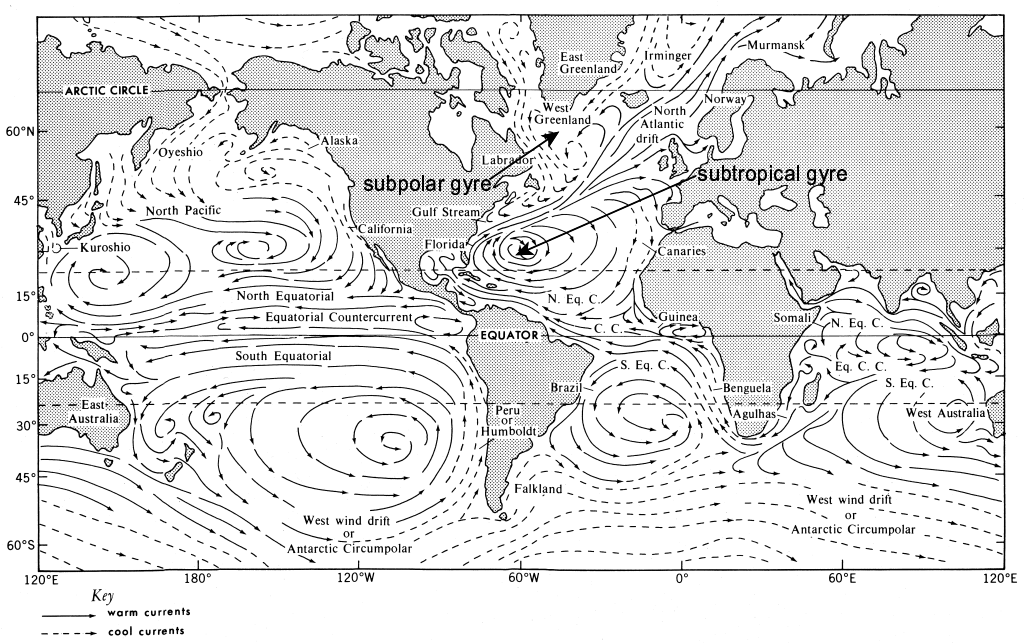

Figure 1.1: *A map of the World Ocean's near-surface circulation (borrowed from Nauw [2003]). Dashed arrows denote cold currents while solid arrows indicate warm currents.*

1.3 Ocean circulation and its variability

The quasi-stationary oceanic circulation acquires momentum and kinetic energy from two sources: (1) from the atmosphere because of the friction of the wind against the sea surface and (2) due to the conversion of the available potential energy of the ocean.

The wind transfers momentum to both the drift currents and to surface and internal waves. The latter, in turn, are capable to transfer their momentum to currents. Furthermore, an uneven wind field and natural barriers (coasts) deviate the sea surface from the geoid creating horizontal pressure gradients and giving rise to the wind-driven gradient currents. The circulation initiated by wind is called the wind-driven circulation. The buoyancy fluxes at the ocean-atmosphere interface are unevenly distributed over the global ocean, which leads to density gradients and unstable stratification. Under such conditions, a part of potential energy, called available potential energy, is released and converted into kinetic energy. The circulation generated by density gradients, determined by the distribution of temperature and salinity, is called the thermohaline circulation. The large-scale mean near-surface circulation (upper thousand metres) is mainly wind-driven, while the much slower deep currents are forced by buoyancy fluxes.

The wind and buoyancy fluxes together form a complex three-dimensional circulation pattern involving surface and deep horizontal currents as well as convergence and divergence zones with intensive vertical motions. The pattern of the near-surface horizontal global oceanic circulation, presented in Figure 1.1, is characterised by the presence of basin-wide anticyclonic gyres north and south of the equator around the corresponding

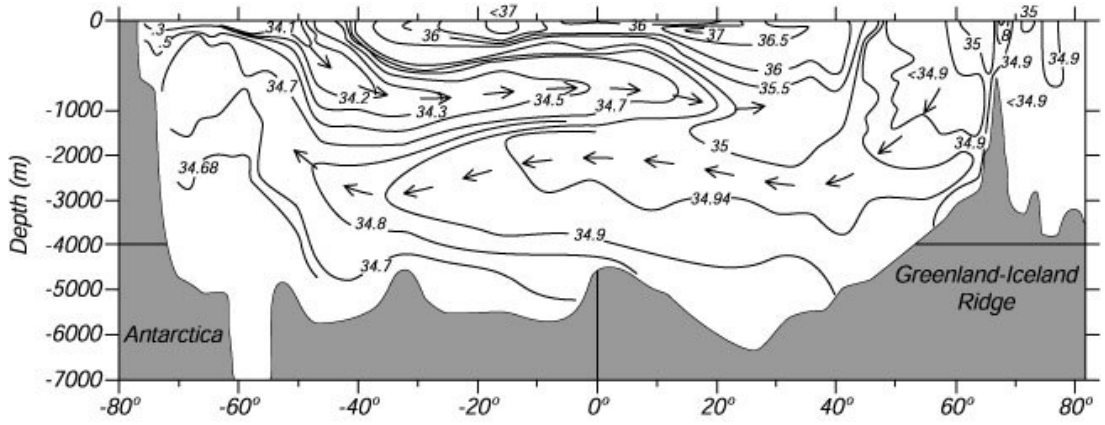

Figure 1.2: *Contour plot of salinity as a function of depth in the western basins of the Atlantic from the Arctic Ocean to Antarctica. The plot clearly shows extensive cores, one at depths near 1000 m extending from 50°S to 20°N, the other at is at depths near 2000m extending from 20°N to 50°S. The upper is the Antarctic Intermediate Water; the lower is the North Atlantic Deep Water. The arrows mark the assumed direction of the flow in the cores. The Antarctic Bottom Water fills the deepest levels from 50°S to 30°N. This figure is borrowed from Steward (2002).*

subtropical centres of high atmospheric pressure. The western peripheries of the gyres are strongly intensified due to the β-effect caused by the rotation of the spherical earth. Here we find the strongest ocean currents, including the Gulf Stream, Kuroshio, Agulhas Current etc. The northern and southern subtropical gyres are separated by equatorial currents, which create equatorial convergence and divergence zones. In the middle and high latitudes a cyclonic atmospheric circulation drives the cyclonic gyres around Antarctica (Antarctic Circumpolar Current, ACC) and around the Icelandic and Aleutian Lows (subpolar gyres). These gyres are separated from the subtropical gyres by a system of oceanic fronts. At high latitudes, in particular in the Atlantic between Norway and Greenland and near Antarctica, an intensive heat loss and subsequent sinking of cold and dense water leads to the formation of deep water. In other regions, the formation of cold and dense water also occurs, but there the surface salinity is not large enough to facilitate its sinking. However, there are some exceptions, such as the Mediterranean Sea, where considerable evaporation makes water sufficiently saline to sink to intermediate depths of the North Atlantic.

The Atlantic Ocean, especially the North Atlantic, is a central area triggering the thermohaline circulation. The vertical salinity profile from the Arctic Ocean to Antarctica, shown in Figure 1.2, depicts the main features of the thermohaline circulation in the Atlantic Ocean. The near-surface layer between 40°S and 40°N is occupied by high-salinity and warm water. The low-salinity water is formed in the upper layer of the subpolar regions of the northern and southern Atlantic Ocean. The latter represents the Antarctic Intermediate Water (AIW) at the bottom of the permanent thermocline and extends northwards at depths near 1000 m. Below this water mass is a core of salty North Atlantic Deep Water (NADW) originating in the subpolar gyre of the North Atlantic.

A very simplified scheme of the three-dimensional wind-driven and thermohaline circulation is called the *Global Conveyor Belt* (Broecker, 1991) and sketched in Figure 1.3. Although this scheme lacks many details, it shows the important elements of oceanic mass transport. The Gulf Stream carries warm and saline water to the far north Atlantic where it becomes denser due to the decrease of temperature. Since it remains more saline than the

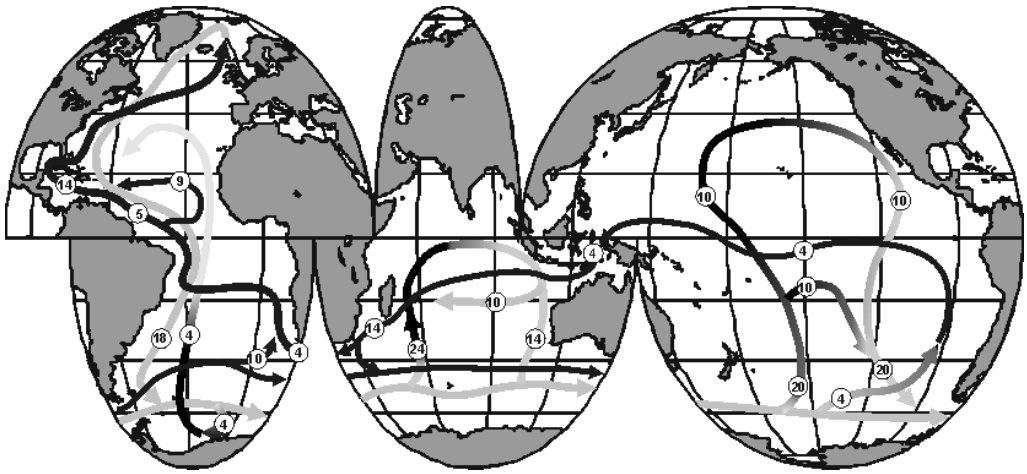

Figure 1.3: *A simplified representation of the global ocean circulation (Global Conveyor Belt). Dark shaded paths indicate near-surface flows while light shaded paths denote deep flows. Numbers show volume transport in Sverdrups (10^6 m^3/s). This figure is based on Schmitz (1995), but borrowed from Bradley (1999).*

surrounding waters, it sinks forming NADW. The latter, in turn, extends southward, reaches the Southern Ocean and mixes with the deep water of ACC, which then enters the Indian and Pacific Oceans. Here, it mixes with the surrounding waters, becomes lighter, returns to the surface in divergence zones and ultimately flows back to the north Atlantic via the system of surface currents.

In reality, the described wind-driven and thermohaline circulation is not steady, but subjected to the variability on different temporal and spatial scales. The variability is mainly caused by the adjustment of the sea surface to changes in atmospheric forcing, buoyancy fluxes and by instabilities in oceanic flows. The changes of the large-scale wind-driven circulation occur on the time-scales from months to decades, whereas the thermohaline circulation varies on much longer climatic time-scales. The scale of the oceanic gyres implies a possible existence of natural periods of the order of few years. If a radius of a gyre is taken 2500 km and the average velocity of the currents around its periphery as 10 cm/s, then the period of this circulation is about 5 years (Monin et al., 1977). One of the most important parts of the variability of the ocean is synoptic, represented mostly by eddies and Rossby waves, which are generated by instabilities of the mean flow due to horizontal and vertical shear and can involve the whole water column.

1.4 The North Atlantic Ocean and its variability

Main topographic features

The North Atlantic Ocean is the best studied ocean basin. The bottom topography of the extratropical part of the ocean is presented in Figure 1.4. The largest topographic feature is the Mid-Atlantic Ridge (MAR), which is located near the centre of the ocean and almost symmetrically divides the entire North Atlantic Ocean floor with an average summit depth of 2500 m. The axis of the MAR is distorted by transversal fracture zones, e.g. Charlie-Gibbs Fracture Zone located at about 52°N. The topography of the MAR is complex and

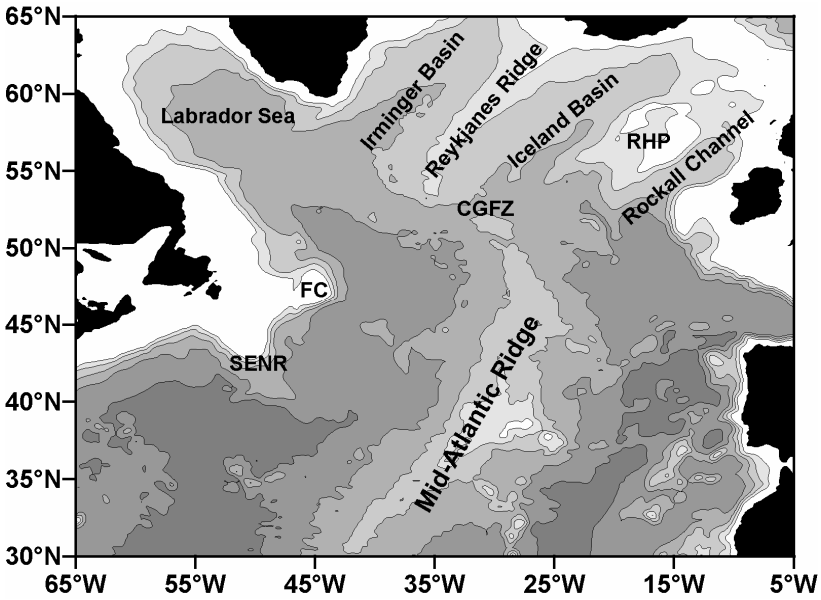

Figure 1.4: *A map showing main features of bottom topography in the extratropical North Atlantic Ocean. The bottom topography is shaded every 1000 m. Abbreviations used: SENR - South East Newfoundland Ridge, FC - Flemish Cap, RHP - Rockall-Hatton Plateau, CGFZ – Charlie-Gibbs Fracture Zone.*

includes seamounts, volcanic islands, banks and troughs. The northern part of the North Atlantic between ≈52°N and 65°N can be divided into several sub-basins due to the topographic features and the distribution of land. Among these sub-basins are the Rockall Channel, Iceland Basin, Irminger Sea bounded by the British Islands, Rockall-Hatton Plateau, Reykjanes Ridge, which is a continuation of the MAR, and Greenland. The bottom topography can have a great impact on surface circulation (e.g. Langseth and Boyer, 1972).

General surface circulation

The general surface circulation in the North Atlantic based mostly on hydrographical observations of the density field is shown in Figure 1.5. An equatorial current system, including a counter current, presents the surface circulation at low latitudes. The circulation in subtropics is characterised by a large anticyclonic gyre as expected from Sverdurp's theory (Sverdrup, 1947), which owes its existence to the low-latitude trade winds and mid-latitude westerly winds.

The western boundary of the subtropical gyre is presented by a strong western boundary current, the Gulf Stream (GS), which flows along the North American Coast. At the site of Cape Hatteras (36°N), the GS leaves the continental slope and veers east. Then, southwest of the Grand Banks it produces numerous and variable meanders. However, it is still clearly identified as a high velocity jet (Rossby, 1996, Käse and Krauss, 1996, Reverdin et al., 2003). At about 55°W a significant weakening of the average flow of the GS occurs while the eddy kinetic energy remains large. Further east, the GS is identified as two current branches centred near 39°N and 41°N (Reverdin at al., 2003).

As the GS approaches the Grand Banks, its northern branch forms the North Atlantic Current (NAC) and its southern branch is connected with the re-circulation gyre and the

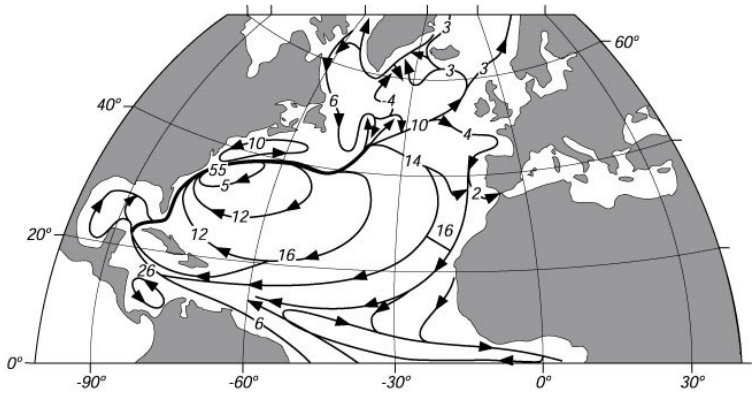

Figure 1.5: *Sketch of the major surface currents in the North Atlantic. Values are transport in Sverdups (1Sv=10^6 m^3/s . From Sverdrup, Johnson, and Fleming (1942: fig. 187), but taken from Steward (2002).*

Azores Current (AC) (Reverdin et al., 2003). A recent study of satellite-tracked drifter trajectories in 1990's suggested existence of three significant anticyclonic re-circulation cells in the North Atlantic. One is situated south of the Gulf Stream extension (50°W, 39°N), another east of the NAC in the Newfoundland Basin (near 45°W, 41°N), and the third is located near 40°W, 50°N and represents the time-averaged northwest corner of the NAC (Fratantoni, 2001). The anticyclonic re-circulation in the Newfoundland Basin was first described by Mann (1967) and is now known as the Mann eddy. It is also observed with surface drifters (McClean et al., 2002). The Mann eddy is situated at the first meander crest of the NAC and is argued to be a permanent feature in the North Atlantic circulation (Rossby, 1996). According to the drifter studies most of the southern branch of the GS contributes to the re-circulation cell rather than feeding the Mann eddy, the NAC or the AC (Reverdin, 2003). The AC appears to be a persistent feature, which feeds into the westward North Equatorial Current (Maillard and Käse, 1989). It is less intensive than the NAC because the Azores Front is much weaker than the Subarctic Front.

The classical scheme of the NAC and its branches, shown in Figure 1.6, was introduced by Dietrich et al. (1980). At about 51°N the NAC turns eastwards, follows the Subarctic Front while loosing its structure as a well-defined jet, and finally crosses the MAR near 52°N (Charlie-Gibbs Fracture Zone). The NAC represents the south-eastern boundary of the cyclonic subpolar gyre in the North Atlantic. Based on the trajectories of satellite-tracked buoys and hydrographic sections, Krauss (1986) concluded that the NAC consists of a frontal jet in the western part of the northern North Atlantic and a broad north-eastern drift further east. Krauss et al. (1987) stated that the appearance of jets between the Azores Front and the Subarctic Front is a transient phenomenon related to the eddy field between the MAR and Grand Banks. During surveys in 1981-1984 two branches of the NAC at 47°N, 41°W were observed. Sy (1988) and later Sy et al. (1992) found clearly defined current branches (jets) in the NAC system dominated by large time-space variability. Sy (1988) presented a scheme where he showed the NAC meandering along the Subarctic Front and still west of the MAR dividing into a branch crossing the ridge as a permanent Subarctic Front, topographically fixed to the Charlie-Gibbs Fracture Zone, and a number of non-permanent current jets between the Subarctic Front and 45°N.

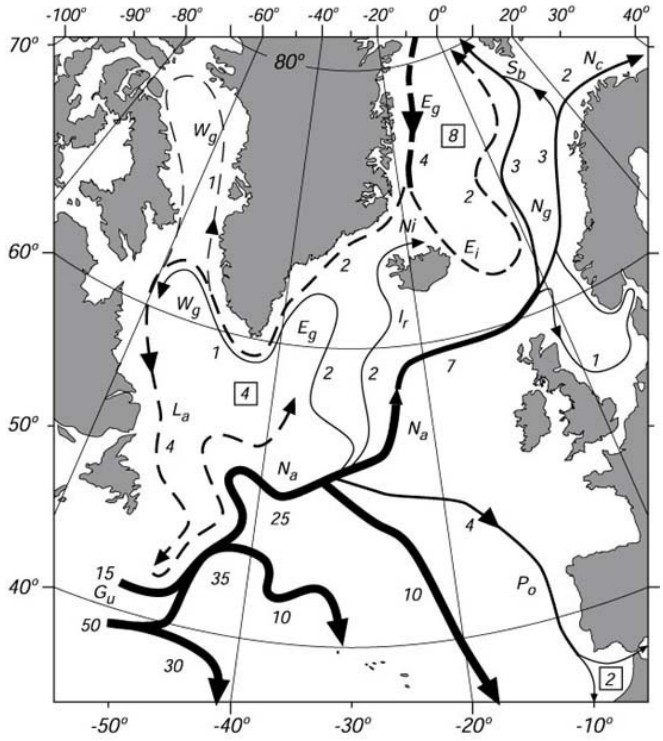

Figure 1.6: *Scheme of major surface currents in the North Atlantic according to Dietriech et al. (1980). The numbers indicate the volume transport in sverdrups (10^6 m^3/s). Abbreviations: E_g - East Greenland Current; E_i - East Iceland Current; G_u - Gulf Stream; I_r - Irminger Current; L_a - Labrador Current; N_a - North Atlantic Current; N_c - North Cape Current; N_g - Norwegian Current; N_i - North Iceland Current; P_o - Portugal Current; S_b - Spitsbergen Current; W_g - West Greenland Current. Numbers within squares indicate the volume of sinking water in Sverdrups (10^6 m^3/s). Solid Lines: relatively warm currents. Broken Lines: relatively cold currents.*

As observed from drifter trajectories (McClean et al., 2002, Flatau et al., 2003), after the NAC has crossed the MAR near the site of the Charlie-Gibbs Fracture zone, it forms two strong branches around the Rockall-Hatton Plateau with a weak flow in between. One flows north-eastward towards Iceland and significantly decelerates at about 60°N while the other branch continues eastwards to 25°W from where it turns north-eastward and ultimately enters the Rockall Channel. The trajectories of the surface drifters, released in the Iceland Basin, showed a north-eastward surface flow towards the Norwegian Sea, surrounding the Rockall-Hatton Plateau (Otto and van Aken, 1996, van Aken and Becker, 1996). A weak southward flow possibly exists on the eastern side of the Reykjanes Ridge (Langseth and Boyer, 1972, Otto and van Aken, 1996, Valdimarsson and Malmberg, 1999, Flatau et al., 2003). Another intensified north-eastward flow is located over the western flank of the Reykjanes Ridge. The large velocity drifter trajectories in this area originate mostly from either the cyclonic circulation in the Irminger Basin or from the Iceland Basin, but not from the north-west corner of the NAC as suggested by the Eulerian mean (Flatau et al., 2003). Approaching Iceland this flow splits into two branches. One becomes the North Icelandic Current, which flows around Iceland, along the Iceland-Faeroe Ridge, and finally contributes to the Norwegian Atlantic Current. The second branch veers west and then flows into the East Greenland Current. This branch is known as the Irminger Current, which carries the major portion of the flow originating from the western flank of the

Reykjanes Ridge. Before reaching the southern tip of Greenland some water of the East Greenland Current turns east and follows the cyclonic circulation in the Irminger Basin (e.g. Reverdin et al., 2003). Another part enters the Labrador Sea and flows north-westward as the West Greenland Current (WGC). The Labrador Sea is characterized by intensive eddy activity, particularly along the wedge of the WGC branching off the continental slope near 61°N – 62°N (Eden and Böning, 2002). In the end, the Labrador Current locks the loop of the cyclonic subpolar gyre. It represents a southward flow along the Labrador coast, which extends southward inshore of the northward NAC.

North Atlantic Oscillation (NAO)

As has already been mentioned, the varying wind stress and buoyancy fluxes at the ocean-atmosphere interface are the prime factors determining the oceanic variability. This means that a major part of oceanic variability is directly or indirectly linked to the atmosphere. The dominant mode of atmospheric behavior in the North Atlantic sector is the North Atlantic Oscillation (NAO), which is more pronounced in winter and accounts for more than one-third of the total variance in sea level pressure (Cayan, 1992). The NAO is a large-scale redistribution of atmospheric mass between the Arctic and the subtropical Atlantic. It fluctuates from one phase to another, being associated with large changes in the mean wind speed and direction over the Atlantic Ocean, the heat and moisture transport between the Atlantic and the neighboring continents, and the intensity and the number of storms, their paths, and their weather (Hurrell et al., 2003).

Since there is no unique way to define the spatial structure of the NAO, many NAO-related indices have been derived. Walker and Bliss (1932) constructed the first index using a linear combination of surface pressure and temperature measurements from weather stations on both sides of the Atlantic. Rogers (1984) used sea level pressure anomalies from Ponta Delgada, Azores and Akureyri, Iceland, while Hurrell (1995, 1996) extended the index further back in time using data from Lisbon, Portugal and Stykkisholmur, Iceland. Normalization is usually used to avoid the time series being dominated by the greater variability of the northern station. Most modern NAO indices are derived either from the simple difference in surface pressure anomalies between various northern and southern locations, or from the principal components of the leading empirical orthogonal function of sea level pressure (Hurrell et al., 2003). The winter NAO index based on the difference of normalized sea level pressure between Lisbon and Stykkisholmur since 1864 (Hurrell, http://www.cgd.ucar.edu/~jhurrell) is shown in Figure 1.7.

The positive phase of the NAO index is characterized by a stronger subtropical high pressure centre and a deeper than usual Icelandic Low. An increased meridional pressure gradient results in stronger westerly winds and winter storms crossing the North Atlantic on a more northeastward track. The negative NAO index phase shows a weak subtropical high and a weak subpolar low. A reduced pressure gradient leads to weaker westerly winds and fewer and weaker winter storms moving on a more west-east pathway.

The variability of the NAO index has a wide range of frequencies. There is little evidence for the NAO to vary on any preferred time scale. Large changes occur between two consecutive winters as well as between different seasons. There are, however, indications that the NAO pattern can persist over several successive winters (Figure 1.7). For example, the 1960s were characterized by unusually high surface pressure and severe

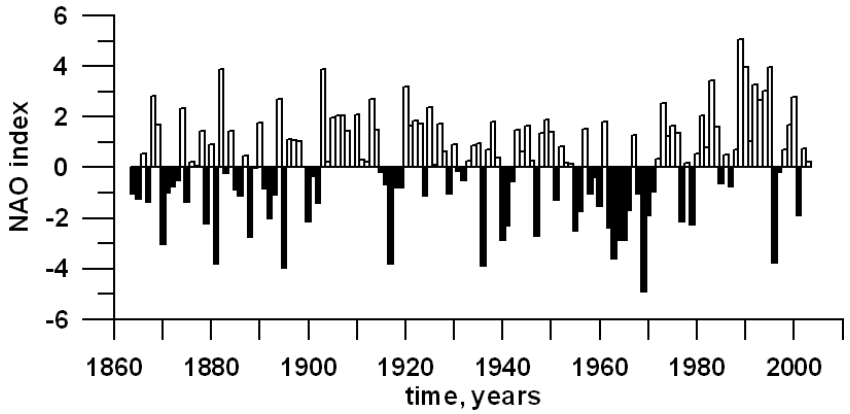

Figure 1.7: *Winter (December through March) index of the NAO based on the difference of normalized sea level pressure (SLP) between Lisbon, Portugal and Stykkisholmur/Reykjavik, Iceland since 1864. The SLP anomalies at each station were normalized by division of each seasonal mean pressure by the long-term mean (1864-1983) standard deviation. Normalization is used to avoid the series being dominated by the greater variability of the northern station. Positive values of the index indicate stronger-than-average westerlies over the middle latitudes. The data are provided by J.Hurrell, http://www.cgd.ucar.edu/~jhurrell.*

winters across northern Europe corresponding to the negative NAO phase. A reversal to a positive phase occurred in the late 1960s reaching strongly positive winter NAO indices at the beginning of 1990s. The inter-annual and inter-decadal fluctuations in the NAO appear to be synchronized with the intensity of wintertime renewal of intermediate and deep waters in the subpolar gyre (Dickson et al., 1996).

The wide range of frequencies inherent to the NAO is consistent with the hypothesis that the variability in the atmospheric system related to the NAO might be of internal origin and is generated within the atmosphere itself. Various scales of nonlinear processes interact with one another and produce random fluctuations. Atmospheric general circulation models provide strong evidence that the basic structure of the NAO arises from the internal, nonlinear dynamics of the atmosphere (Hurrell et al., 2003). Most evidence suggests that the ocean's influence on the NAO is small compared to the internal variability in the atmosphere (Seager et al., 2000). Nevertheless, great heat capacity and connected with it inertia of the ocean can impose time scales leading to low frequency changes in both sea surface temperature and lower tropospheric air temperature (Frankignoul and Hasselmann, 1977; Barsugli and Battisti, 1998).

Past research

Most of our knowledge about the variability of oceanographic parameters comes from hydrographic surveys. As was already mentioned above, hydrographic surveys, with a very few exceptions, do not provide regular observations, contain seasonal bias, and have a limited spatial coverage. In addition, to derive information about sea level from in situ hydrography data it is necessary to make a disputable assumption about the level of no motion. Regular nearly global measurements of sea level became possible only after the advent of satellite altimetry, especially after the launch of the high accuracy TOPEX/Poseidon mission in 1992. There were some studies based on data obtained from earlier Seasat (e.g. Menard, 1983), Geosat and ERS-1 (e.g. Kelly and Gill, 1990; Le Traon

et al., 1990; Tokmakian and Challenor, 1993; Heywood et al., 1994; White and Heywood, 1995) missions. However, these missions lasted a relatively short period and were much less accurate than TOPEX/Poseidon. In the late 1990s effective techniques to merge multisatellite data sets were developed at CLS Space Oceanography Division (Le Traon et al., 1995; Le Traon et al., 1998; Le Traon and Ogor, 1998). The merging of the TOPEX/Poseidon and ERS-1/2 and later Jason-1 and Envisat increased the spatial resolution of data and made it possible to better resolve mesoscale processes.

There were several validation studies aimed to compare the more accurate TOPEX/Poseidon altimeter measurement with corresponding *in situ* surveys (e.g. Morris et al, 1994; Gilson et al., 1998). Seasonal variations of the sea surface height in the North Atlantic were investigated using both satellite altimetry and numerical simulations (e.g. Behringer, 1994; Wang and Koblinsky, 1996; Stammer, 1997; Kelly, 1999; Ferry et al., 2000). Studies by Reverdin et al. (1999), Häkkinen (2001), Esselborn and Eden (2001), Cabanes et al. (2001), Frankignoul et al. (2001) were dedicated to the interannual change of the sea surface height. However, all these studies considered shorter altimeter records than available now. Also, uncertainty remained with regard to the magnitude and relative contribution of the modes of variability in different parts of the North Atlantic.

The studies of the seasonal change of sea level were mostly devoted to very large oceanic scales (Behringer, 1994; Stammer, 1997; Ferry et al., 2000), to the tropical regions (Wang and Koblinsky, 1996) and to the Gulf Stream area (Kelly, 1999), but not to the low-variability northern North Atlantic. The interannual variability of the seawater properties in the northern North Atlantic was mainly studied from hydrographic surveys (e.g. Bersch et al., 1999; Reverdin et al., 1999; Bersch, 2002; van Aken, 2003). Therefore, there is a need for further validation of regular high-accuracy altimeter measurements with hydrographic surveys in this region in order to allow interpretation of satellite altimetry observations in hydrographic terms.

There were numerous studies of the surface circulation pattern in the North Atlantic, mainly performed by using hydrographic surveys and satellite-tracked drifters (e.g. Dietrich et al., 1980; Krauss and Käse, 1984; Krauss, 1986; Krauss et al., 1987; Sy, 1988; Sy et al., 1992; van Aken and Becker, 1996; Otto and van Aken, 1996; Fratantoni, 2001; McClean et al., 2002; Reverdin et al., 2003; Flatau et al., 2003). Drifters may provide longer continuos records than hydrographic surveys. However, their spatial and temporal coverage is not comparable with satellite altimetry and usually they do not resolve the interannual variability. Therefore, drifters have mainly been used to identify mean pathways of oceanic currents. As will be shown in the next chapter, satellite altimetry does not yet provide scientists with accurate geostrophic velocity estimates, but it gives the variable part of geostrophic velocities, which is of key interest for studying the variability of surface currents.

Eddy kinetic energy, derived from drifter trajectories (e.g. Wyrtki et al., 1976; Richardson, 1983; Krauss and Käse, 1984; Otto and van Aken, 1996; Fratantoni, 2001) and from satellite altimetry (e.g. Menard, 1983; Ducet et al., 2000), has also been used to describe the large-scale surface circulation pattern in the North Atlantic. However, only a few studies considered the seasonal or interannual variability of eddy kinetic energy (Stammer and Wunch, 1997; Heywood et al., 1994; White and Heywood, 1995). In particular, the relation between the variability of eddy kinetic energy and large-scale surface circulation has not been well elucidated.

There have been many works coupling the variability of the seawater properties, sea level and surface circulation in the North Atlantic Ocean with the NAO (e.g. Dickson et al., 1996; Taylor and Stephens, 1998; Bersch, 2002; Curry and McCartney, 2001; Esselborn and Eden, 2001; Frankignoul et al., 2001). These studies described changes in the ocean, which were possibly connected to the NAO phase changes. The NAO phenomenon and its relation with the oceanic variability are still poorly understood however, and similar studies based on longer NAO and oceanographic records must be continued.

At last, there will always be a need for more research as the high-accuracy satellite altimetry data are constantly updated due to the continuation of current and the arrival of new altimetry missions. New data will allow us to study longer time scales and to improve the statistics of the synoptic and seasonal change.

1.5 Overview of the thesis

The main purpose of this thesis is to study the variability of the sea level and surface circulation in the extratropical North Atlantic Ocean on the time-scales from weeks to a decade using satellite altimetry data from November 1992 to the latest available. Although the thesis is dedicated to the North Atlantic Ocean, a comparison with the North Pacific Ocean is also included.

The sequence of questions the author wanted to address can be listed as follows: “How was the sea level changing in the northern subpolar part of the North Atlantic and how well it compares with corresponding hydrographic surveys in the same region during the last decade?”, “How was the sea level changing in the extratropical North Atlantic Ocean and what is the relationship of these changes to the simultaneous changes in the extratropical North Pacific Ocean?”, “What were the changes in surface circulation for the last decade inferred from satellite altimetry data?”, “Are the observed large-scale low-frequency changes in sea level and surface circulation the result of an adjustment of the ocean to the atmospheric forcing?”.

The thesis thus comprises two major parts: the variability of sea level and the variability of surface circulation. The specific research objectives can be listed:

- To assess the observed sea surface height variability in the North Atlantic on the time scales from weeks to several years and to determine the magnitude and relative contribution of different signals to the total variance.
- To combine the variations of sea level observed by altimetry with *in situ* hydrographical surveys along the section AR7E in the northern part of the North Atlantic and to interpret the observed change in terms of changes in the properties and distribution of water masses.
- To compare the observed variations of the sea level in the North Atlantic with those in the North Pacific in order to obtain a broader view on the character of the sea level change in the Northern Hemisphere.
- To estimate and interpret the observed variability of eddy kinetic energy and associated variations of surface currents in the North Atlantic Ocean.

- To investigate the relation of the inter-annual changes of sea surface height and surface circulation with the variability of atmospheric circulation over the North Atlantic Ocean.

The thesis is organized as follows:

Chapter 2 introduces the reader to the principles of satellite altimetry measurements, presents the data sets used, and describes the techniques and methods used in this thesis to analyze the data. Only satellite altimetry data are considered in this chapter while the description of other data sets used in the thesis, i.e. hydrographic and climatologic, is included in the following chapters.

Chapter 3 deals with the study of the sea surface height variability in the northern part of the North Atlantic Ocean. Here, the inter-annual, seasonal (annual cycle) and higher frequency (mainly mesoscale eddies) signals are investigated. The parameters and relative contribution to the total variance of each of the investigated modes of variability are estimated. The observed change of sea level in the North Atlantic is related to the variations in atmospheric circulation pattern, which can be expressed in terms of the North Atlantic Oscillation. A comparison of sea surface heights with dynamic heights derived from hydrographical surveys is also performed to allow the hydrographical interpretation of satellite altimetry data.

Chapter 4 presents a comparison of the sea level variability in the extratropical North Atlantic and North Pacific oceans. It is done with the purpose to distinguish peculiarities of the sea level change in both basins, and especially in the low kinetic energy subpolar gyres. As it is done in Chapter 3, the parameters of the mesoscale, seasonal and inter-annual signals in both oceans are estimated and compared. In addition, the leading modes of the interannual variability are determined by means of the Empirical Orthogonal Functions analysis. At the end, this chapter presents a discussion on the climate-related change of the sea level and associated geostrophic circulation in both oceans.

Chapter 5 discusses how satellite altimetry data can be used to study the variability of surface circulation. It presents a detailed description of the observed changes in the eddy kinetic energy (EKE) and altimetry-derived geostrophic velocity anomalies in the North Atlantic Ocean. Special emphasis is given to regional studies: to the high variability Gulf Stream extension and the NAC west of the Mid-Atlantic Ridge, to the relatively lower variability Azores Current, and to the north-eastern (Rockall Channel and Iceland Basin) and north-western (Irminger Sea and Labrador Sea) parts of the North Atlantic. The proposed interpretation relies on the assumption that since the observed EKE is associated with major currents, the variability in EKE reflects the displacements and changes in the intensity of the currents. The latter is discussed by comparing the altimetry-derived EKE with vertical density profiles and dynamic heights in the low EKE northern North Atlantic.

Chapter 6 is a thematic study. It demonstrates an application of the complex singular value decomposition method to the yearly estimates of EKE anomalies in the NAC west of the Mid-Atlantic Ridge. This method was used to test the EKE time series for possible propagating signals.

Thus chapters 3 and 4 are mostly dedicated to the study of the variability of sea level and chapters 5 and 6 deal with questions related to the variability of surface circulation. In the end, the main findings of this thesis are summarized in *chapter 7*.

Chapter 2

Monitoring the ocean with satellite altimetry

Altimetry is a technique for measuring heights. For a detailed presentation of the satellite altimetry techniques and applications the reader is referred to Fu and Cazenave (2001). This chapter aims to briefly describe the principles of satellite altimetry: how it works, what corrections need to be applied and what accuracy is achieved up to date. Also, the present, past and nearest future satellite altimetry missions are discussed. The chapter describes the TOPEX/Poseidon – Jason-1 and ERS-1/2 altimeter data sets used in this thesis to study the variability of sea level and surface circulation. In the end, the techniques applied in this work to obtain the needed oceanographic information are demonstrated.

2.1 Principles of satellite altimetry

The measuring of heights can be achieved by estimating the vertical range R from the satellite to the sea surface (Figure 2.1). Radar altimeters onboard the satellites transmit a short pulse of microwave radiation at high frequency toward the sea surface. A part of this pulse after hitting the sea surface is reflected back to the altimeter. The time t for the pulse to travel from the satellite to the sea surface and back to the satellite, or round trip time, is precisely determined (see Chelton et al. 2001). The time measurement scaled by the speed of light c (at which electromagnetic waves travel in a vacuum) yields the uncorrected range:

$$R^* = ct / 2 \qquad (2.1).$$

Because the electromagnetic waves travel through the atmosphere, they undergo atmospheric refraction. The effects of atmospheric refraction increase the round trip time travel. Therefore, failure to correct for atmospheric refraction results in a range estimate that is longer than the true range. The atmospheric refractivity is determined by the temperature, pressure, water vapour density, cloud liquid water droplet density, presence of raindrops and ionospheric electron density. The correction thus consists of the dry tropospheric refractivity associated with dry gases, the wet tropospheric correction, which includes both the water vapour and the cloud liquid water droplet constituents, and the ionospheric refractivity, which is determined by the dielectric properties of the upper atmosphere associated with the presence of free electrons. Because of the difficulties to

estimate rain effects on the range estimates, the altimeter observations that are likely to be contaminated by rain are flagged and excluded from further geophysical analysis (Chelton et al., 2001). The altimeter range estimates must also be corrected for biases related to the sea state effects: the electromagnetic bias and skewness bias. The electromagnetic bias arises because of the systematic difference between mean sea level and mean scattering surface. The difference is caused by a higher reflection rate of wave troughs than of wave crests because wave troughs are generally flattened and wave crests are peaked. The wind-generated small-scale roughness of the sea surface is greater near wave crests than in wave troughs, further reducing the amount of radar signal reflected back to the satellite by crests. Therefore, the backscattered power measured by altimeters is greater from wave troughs than from wave crests leading to underestimation of the sea level. The skewness bias arises because of the height difference between the mean scattering surface and the median scattering surface. The latter represents the surface actually measured by the onboard tracker, which is designed to determine the half-power point of the return wave front. The corrected range is thus given by

$$R = R^* - \sum_{j=1} \Delta R_j \qquad (2.2),$$

where ΔR_j (j = 1, …) are the corrections for the atmospheric refraction and sea state biases. All ΔR_j, determined for each R^* estimate, are given in the geophysical data record (GDR). The GDR is the format in which each along-track data point is published. It contains a series of different parameters belonging to that data point.

The corrected range measurements vary along the satellite orbit due to the variations in the sea surface height and changes in the satellite altitude relative to the centre of the earth. The latter is caused by the elliptical shape of the orbit and its undulations due to the variations of gravity on the surface of the earth. Therefore, to estimate the sea surface height it is necessary to define the satellite orbit relative to a fixed terrestrial frame. The altitude of the satellite (orbit height) at any instance is determined relative to an arbitrary reference surface, an ellipsoid. This reference ellipsoid is a rough approximation of the earth's shape, a sphere flattened at poles. The precise determination of the satellite position in its orbit (i.e. exact latitude, longitude and altitude coordinates) is one of the major tasks of satellite altimetry. During the last decade significant improvements have been made reducing the root-mean-square errors of estimated orbit height H from ~10 m for GEOS-3 to 2.5 cm for TOPEX/Poseidon (Chelton et al., 2001). This was achieved by improving the model for the earth's gravity field and satellite tracking systems. The TOPEX/Poseidon tracking is performed with the use of the Satellite Laser Ranging (SLR) and the Doppler Orbitography and Radiopositioning Integrated by Satellite (DORIS) systems accompanied by an experimental Global Positioning System Demonstration Receiver (GPSDR). Once the satellite height H is determined, the sea surface height SSH relative to the reference ellipsoid is given by

$$SSH = H - R \qquad (2.3).$$

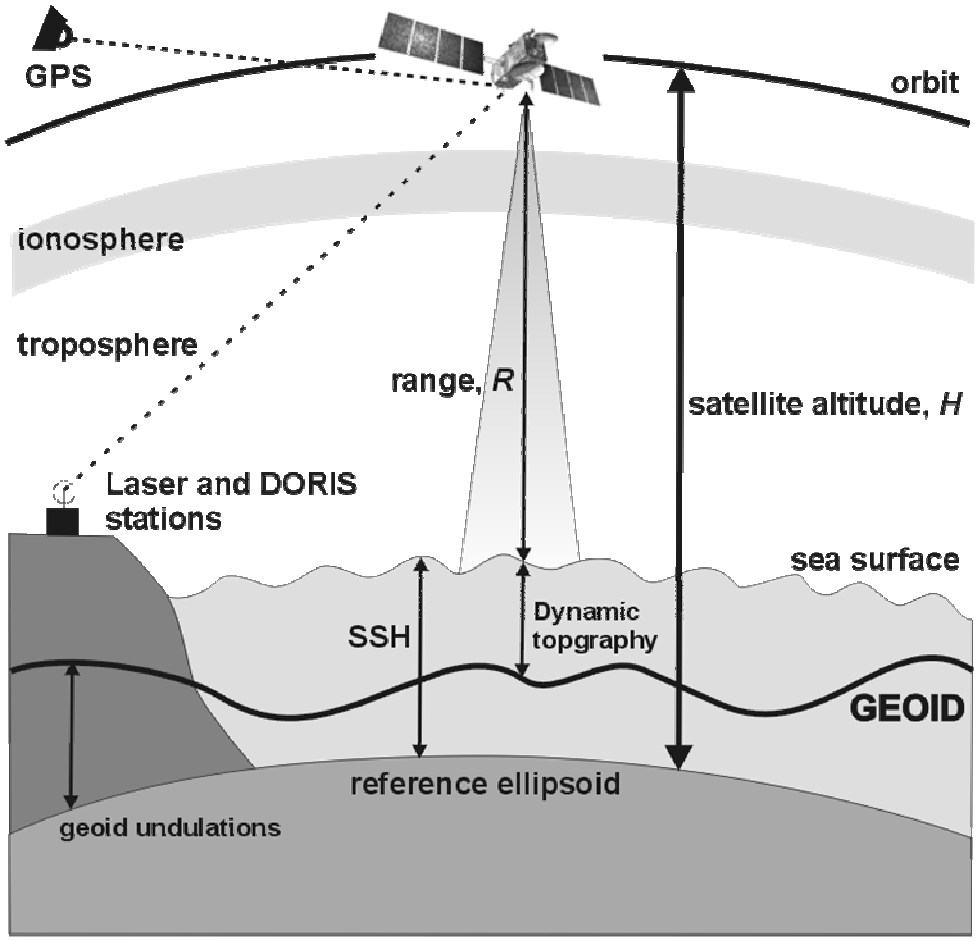

Figure 2.1: *Principle of sea surface height measurements with satellite altimetry.*

The SSH value given by (2.3) is made up by several geophysical effects:

$$SSH = h_G + h_D + h_T + h_A \qquad (2.4).$$

The *SSH* which would exist without any disturbances, an equipotential surface or ocean at rest, is called the marine geoid. The first element of (2.4), h_G, represents the height of the marine geoid undulations relative to the reference ellipsoid. The second element, h_D, is dynamic topography, which is the SSH due to the dynamic effects of geostrophic ocean currents. The dynamic topography, h_D, comprises a permanent stationary component $\overline{h}_D$ and a variable part ζ ($h_D = \overline{h}_D + \zeta$). The former is related to the permanent geostrophic circulation mainly maintained by permanent winds and effects of the earth's rotation while the latter is made up mainly by variable winds, seasonal changes, instability processes etc. The third element, h_T, represents the tidal height and the fourth element, h_A, is the sea level response to atmospheric pressure loading.

The dynamic topography is the prime interest for most oceanographers because it is linked to the geostrophic circulation of the ocean. The surface velocity can be determined from the sea surface slope due to the fact that ocean currents are nearly in geostrophic

balance on time scales longer than a few days and spatial scales longer than a few tens of kilometres. Ideally, the dynamic topography can be estimated by subtracting h_G, h_T and h_A from *SSH*. However, in practice, errors in the present geoid models are still too large on the spatial scales of the mesoscale oceanic processes and exceed the signal in ocean topography. Therefore, the long-term mean sea level is usually subtracted from SSH instead of the geoid, which yields the variable part of the dynamic topography ζ :

$$\zeta = SSH - \frac{1}{N}\sum_{i=1}^{N} SSH_i - h_T - h_A \qquad (2.5),$$

where N – number of measurements used for averaging ($i=1,2,\ldots,N$). The long-term mean SSH is presumed to contain the geoid undulations relative to the reference ellipsoid h_G and the mean dynamic topography $\overline{h}_D$.

Although the periods of leading semidiurnal and diurnal tidal constituents (≈0.5 and 1 day) are much shorter than the repeat period of the satellites with an onboard altimeter, the unresolved tidal variations of SSH alias into the lower frequencies associated with ocean circulation. Therefore, to estimate the dynamic topography, the tidal height h_T, which consists of both the solid earth and ocean tides, must also be removed.

The variations of atmospheric pressure also contribute to the variations of SSH. This is so-called "inverted-barometer response", which amounts to ~1 cm sea level change per 1 hPa change in atmospheric pressure. Since these height variations, h_A, are not connected with the dynamic topography associated with geostrophic ocean circulation, they must also be subtracted from SSH.

2.2. Satellite altimetry missions

Since the first altimeter installed on the manned SKYLAB mission flown in 1973-1974 there has been a number of satellite missions equipped with an onboard altimeter. The present ~5 cm state-of-the-art overall accuracy of the sea surface height estimates has been achieved due to the technological advancements in the orbit determination, improvement of sensors and geophysical algorithms.

Seasat was the first Earth-orbiting satellite designed for remote sensing of the ocean and carried five instruments onboard including a radar altimeter. It was launched in June 1978 into a nearly circular 800 km orbit with an inclination of 108 degrees. The mission ended on October 10, 1978 due to a failure of the vehicle's electric power system. Although only approximately 42 hours of real data were received, the Seasat mission demonstrated the usefulness of microwave sensors to monitor the ocean. The first long-term altimetry mission was the Geosat of the U.S. Navy that was launched in March 1985 and was operational until January 1990. The first 18 months of the Geosat mission were dedicated to the mapping of the global geoid with a spatial sampling interval down to 4 km. Once this part of the mission was over, the satellite was put on a 17-day repeat orbit and provided the scientific community with altimetry data for over three years. The European Space Agency (ESA) launched its first altimeter – equipped European Remote Sensing Satellite – 1 (ERS

– 1) in July 1991. The ERS-1 satellite, launched into a nearly 780 km orbit with an inclination about 100 degrees, was operational until June 1996 on three different orbits: on a 3 – day repeat orbit during validation and sea – ice observations, on a 35 – day repeat cycle for multi-disciplinary ocean observations, and on a 168 – day repeat orbit performing geodetic tasks from April 1994 to March 1995. The first dedicated radar altimeter TOPEX/Poseidon (T/P) satellite was launched on August 10, 1992, as a cooperative space project between NASA (U.S.) and CNES (France). The T/P is equipped with two radar altimeters and precise orbit determination systems, including the DORIS system. The satellite has flown on a nearly 10 – day repeat orbit with an average altitude of 1336 km. The T/P mission achieved an unprecedented accuracy of ~5 cm (Fu et al., 1994). Initially it was planned to be operational for 3 – 5 years. However, the mission was so successful that it still continues providing the scientific community with high quality altimetry data. ERS – 2, the follow-on from ERS – 1, was launched in April 1995 and put on the same 35 – day repeat orbit as ERS – 1 but having a one-day shift. Both satellites were used in tandem from August 1995 to June 1996. The ERS-2 satellite was functional until June 2003 and replaced by Envisat. The Geosat follow-on (GFO) was launched in February 1998. The GFO satellite flies on the same 17 –day repeat orbit as its predecessor with an altitude of 880 km. The prime objective of the GFO mission is to provide the U.S. Navy with real-time ocean topography data. The scientific community has also access to the GFO data through the National Oceanic and Atmospheric Administration (NOAA). The follow-on of the T/P satellite, Jason – 1 was developed by CNES and NASA and launched on December 7, 2001. Jason – 1 is designed to follow the T/P orbit and to provide data of the same quality, if not better. On September 15, 2002 T/P assumed a new orbit midway between its original ground tracks, which are now repeated by Jason – 1. Thus both satellites are being used in tandem doubling the spatial resolution of coverage. The follow-on of ERS – 1 and – 2, the Envisat satellite (Environmental Satellite), was launched on March 1, 2002 with the same 35 – day orbit period. The satellite carries ten complementary instruments including a radar altimeter and precise location system DORIS. Several altimetry missions are scheduled for the nearest future. The Cryosat altimetry satellite, built by ESA, will be launched at the end of 2004. This satellite is designed to monitor the variations in the thickness of land and sea ice cover. Jason – 2 is scheduled to take over and continue the T/P and Jason – 1 mission at the end of 2006. It will probably carry an experimental Wide-Swath Ocean Altimeter (WSOA). The WSOA system will consist of several altimeters mounted on booms. The altimeters will acquire measurements simultaneously thus providing continuous multi-altimeter wide-area coverage.

To study the Earth's gravity field and to develop a more accurate geoid model, which is of the key importance in determining the absolute dynamic topography, GRACE (Gravity Recovery and Climate Experiment) mission has been designed by NASA. Two identical GRACE satellites were launched in March 2002. The spacecrafts are designed to fly about 220 km apart in a polar orbit 500 km above the Earth. The GRACE mission has been mapping the Earth's gravity fields by making accurate measurements of the distance between two satellites, using GPS and a microwave ranging system. The ESA is designing another mission dedicated to measure the Earth's gravity field and to model the geoid with extremely high accuracy (1-2 cm) and spatial resolution (less than 100 km) – GOCE (Gravity Field and Steady State Ocean Circulation Explorer). The GOCE spacecraft is scheduled for launch in 2006 (Tapley and Kim, 2001).

2.3 Altimeter data used in the thesis

The altimeter data, used for the research reported in this thesis, have been produced by the CLS Space Oceanography Division as part of the European Union Environment and Climate (EU ENACT) project (EVK2-CT2001-00117) with support from CNES (Centre National d'Études Spatiales) and distributed by AVISO (Archiving, Validation, and Interpretation of Satellite Oceanography Data) operations centre.

Two altimeter data sets spanning the period from October 1992 to June 2003 were used. The first data set is the merged gridded TOPEX/Poseidon – Jason and ERS-1/2 (henceforth TPJ+ERS) sea level anomaly (SLA) data, and second is the gridded TOPEX/Poseidon (henceforth T/P) – Jason SLA data alone. Jason data replaced T/P data in August 2002. The T/P and Jason satellites have a repeat cycle of about 10 days while their ground tracks are some 315 km apart at the equator – more than the average span of an ocean eddy. On the other hand, ERS – 2 (and earlier ERS – 1) was passing over the same point every 35 days, but the maximum distance between the ground tracks is only 80 km. Therefore, merging the T/P-Jason and ERS-1/2 altimeter data helps to better resolve the mesoscale variability. The merged TPJ+ERS data provide more homogeneous and reduced mapping errors than either individual data set (Ducet el al., 2000). However, it has a gap of more than one year, from 16 December 1993 to 31 March 1995, during ERS-1 ice monitoring and geodetic missions (phases D, E and F). The T/P data alone were used to fill the gap in this period.

The SLA values were obtained relative to a 7-year mean (January 1993 – January 1999) and a specific processing is performed to get an ERS-1/2 mean consistent with a T/P mean (SSALTO/DUACS handbook, 2001). These SLA data $\zeta(x,y,t)$ are mapped on a 1/3° Mercator projection grid. The use of the Mercator projection implies that zonal (Δx) and meridional (Δy) distances between the corners of a grid square remain in a good approximation identical ($\Delta x=\Delta y$) and vary with the cosine of latitude (e.g. from 37 km at the equator to 18.5 km at 60°N/S). Thus the spatial resolution increases with latitude following the increased resolution of the satellite tracks at high latitudes. There is one map every seven days.

The data were corrected for instrumental errors, environmental perturbations (wet tropospheric, dry tropospheric and ionospheric effects), ocean wave influence (sea state bias), tidal influence (most recent GOT99 tidal correction; Ray, 1999), and inverse barometer effect corrected with a variable mean pressure (Dorandeu and Le Traon, 1999). Tidal and inverse barometer corrections for ERS-1/2 are made to be homogenous with T/P. The ERS-1/2 orbit is globally adjusted to the more precise T/P orbit (Le Traon and Ogor, 1998).

2.4 Data processing techniques

Basic statistics

The satellite altimetry data used in this work are organized as gridded maps of sea level anomalies (MSLA). Each grid point (x, y) thus represents a time series of SLA measurements ($\zeta_1,...,\zeta_N$) at times $t=1\ldots N$, which are assumed to be independent and

identically distributed. The mean value of $\overline{\zeta}$ slightly differs from zero because the average *SSH* used to obtain SLA time series was computed over a 7-year time interval, which is shorter than the time series. The variance of SSH is given by

$$\sigma^2{}_{\zeta(x,y)} = \frac{1}{N-1}\sum_{t=1}^{N}\left(SSH_t(x,y) - \overline{SSH(x,y)}\right)^2 = \frac{1}{N-1}\sum_{t=1}^{N}\left(\zeta_t(x,y)\right)^2 \qquad (2.6).$$

To estimate the characteristic magnitude of an SLA time series it is convenient to use a root-mean-square (RMS) value

$$RMS_{\zeta(x,y)} = \sqrt{\frac{1}{N}\sum_{t=1}^{N}\left(\zeta_t(x,y)\right)^2} \qquad (2.7).$$

Covariance and correlation are used to define the degree of dependence between random variables. The latter can belong to both the different time series and to one time series. The covariance between the time series ξ and η is given by

$$\mathrm{cov}(\xi,\eta) = \frac{1}{N-1}\sum_{t=1}^{N}\left(\xi_t - \overline{\xi}\right)\cdot\left(\eta_t - \overline{\eta}\right) \qquad (2.8).$$

In most cases it is more convenient to use a correlation coefficient instead of covariance because it does not depend on the units in which the time series are represented. The correlation coefficient ρ between time series ξ and η is defined by

$$\rho(\xi,\eta) = \frac{\mathrm{cov}(\xi,\eta)}{\sqrt{\sigma_\xi{}^2}\cdot\sqrt{\sigma_\eta{}^2}} \qquad (2.9).$$

Signal decomposition

An SLA time series is a combination of signals with different time scales. The least resolved periodicity is determined by the repeat period of satellites. This implies that nowadays satellite altimetry resolves signals on the time scales from weeks to interannual. Therefore, in this research the SLA time series $\zeta(x,y,t)$ are regarded as a composition of three modes of variability: interannual changes $\zeta_{int}(x,y,t)$, seasonal change (annual cycle) $\zeta_{ann}(x,y,t)$ and high frequency mesoscale signals $\zeta_{mes}(x,y,t)$:

$$\zeta(x,y,t) = \zeta_{int}(x,y,t) + \zeta_{ann}(x,y,t) + \zeta_{mes}(x,y,t) \qquad (2.10),$$

where x and y are spatial coordinates and t is time. The interannual changes comprise all signals with periods over one year and therefore can be estimated by low-pass filtering the

SLA data. This can be done by applying a moving average operation with a window $2w+1$ approximately equal to one year (w=26 weeks):

$$\zeta_{int}(x,y,k) = \frac{1}{2w+1}\sum_{t-w}^{t+w}\zeta(x,y,t), \quad k=1, 2, \ldots,(N-2w), \tag{2.11}$$

where k is the central time of the window and N is the length of the time series. The seasonal change (annual cycle) has a periodic shape given by the physical nature of the process. It can be approximated by a harmonic function with a frequency ω equal to 1 cycle/year:

$$\zeta_{ann}(x,y,t) = A(x,y)\cdot\sin\left[2\cdot\pi\cdot\omega\cdot t+\varphi(x,y)\right], \quad t=1, 2, \ldots, n \tag{2.12}.$$

The amplitude $A(x,y)$ and phase lag $\varphi(x,y)$ of the annual cycle are evaluated in a least squares sense so that the sum of the squared residual SLA is minimized:

$$\sum_{t=1}^{n}\left[\zeta(x,y,t)-\zeta_{ann}(x,y,t)\right]^2 \rightarrow \min_{A(x,y),\varphi(x,y)}, \quad t=1, 2, \ldots, n \tag{2.13}.$$

The remaining part of the variability has periods less than one year and in this thesis it is attributed to the mesoscale change. The relative contribution of each mode of variability to the total variance can be estimated using the determination coefficient:

$$D_k = \frac{\sigma^2(\zeta_k)}{\sigma^2(\zeta)}\cdot 100\% \tag{2.14},$$

where k is the mode of variability (interannual variability, seasonal change or mesoscale variability).

Empirical Orthogonal Functions (EOF) analysis

EOF analysis is a statistical technique for data reduction in large data sets while maintaining as much of the observed variance as possible. It is used to identify patterns of simultaneous variation and gives a measure of the variance explained by each pattern. The time series of oceanic characteristics are determined by numerous factors interacting at different spatial and temporal scales. The EOF method provides a compact description of the temporal and spatial variability of data series in terms of orthogonal functions, or statistical "modes" (Emery and Thomson, 1998). A detailed description of the EOF analysis is given in Preisendorfer (1988).

Let N be the number SLA maps at times $t_n=1,\ldots,n$. Each map consists of SLA measurements $\zeta(\mathbf{x}_m, t)$ at locations, $\mathbf{x}_m=1,\ldots,m$. Thus we can form an SLA data matrix $\mathbf{Z}$:

$$\mathbf{Z} = \begin{bmatrix} \zeta(1,1) & \dots & \zeta(1,n) \\ \dots & \dots & \dots \\ \zeta(m,1) & \dots & \zeta(m,n) \end{bmatrix} \qquad (2.15).$$

The spatial and temporal EOFs can be found by calculating eigenvectors of the covariance matrices **C** given by products $(n\text{-}1)^{-1}\mathbf{Z}\mathbf{Z}^T$ and $(m\text{-}1)^{-1}\mathbf{Z}^T\mathbf{Z}$ correspondingly, where $\mathbf{Z}^T$ is the transpose of **Z**. The temporal EOFs are usually called principal components (PCs) or expansion coefficients. The EOFs and PCs can also be computed in one-step operation known as the singular value decomposition, SVD (Kelly, 1988; Susanto et al., 1990). The central part of the EOF analysis is to solve the eigenvalue problem $\mathbf{C}\varphi=\Lambda\varphi$, where Λ is a diagonal matrix containing the eigenvalues λ_k of **C** and φ are the eigenvectors. The eigenvectors are the EOFs or PCs and eigenvalues λ_k give a portion of the total variance in **C** explained by the mode *k*. There are *m* temporal and *n* spatial modes. In essence, given the condition that the covariance matrix is symmetric, the EOF method decomposes it into a number of orthogonal eigenvectors

$$\mathbf{C} = \lambda_1\varphi_1\varphi_1^T + \lambda_2\varphi_2\varphi_2^T + \dots + \lambda_k\varphi_k\varphi_k^T \qquad (2.16).$$

The eigenvectors are ordered according to the size of the eigenvalues. Usually the first few eigenvalues contain most of the variance. This means that most of the variability in the data set *Z* can be explained by only a few eigenvectors. Thus for each mode we obtain a certain spatial pattern, called the EOF, characterised by its time evolution given by the PC.

It should be mentioned that the EOF analysis is a purely statistical technique for partitioning the variance of a spatially distributed group of concurrent time series. Therefore, no physical or mathematical relationship necessarily exists between the EOFs and natural dynamical processes.

Determining the geostrophic surface circulation

The SSH data, measured by satellite altimetry, reflect the distribution of seawater density. The basic condition for the derivation of the circulation from the ocean's density field is the fact that in the open ocean at latitudes more than a few degrees away from the equator the large-scale flows are nearly in geostrophic and hydrostatic balance, expressed by the following equations:

$$fu = -\frac{1}{\rho}\frac{\partial P}{\partial y} \quad , \qquad (2.17)$$

$$fv = \frac{1}{\rho}\frac{\partial P}{\partial x} \quad , \qquad (2.18)$$

$$\frac{\partial P}{\partial z} = -g\rho \quad , \qquad (2.19)$$

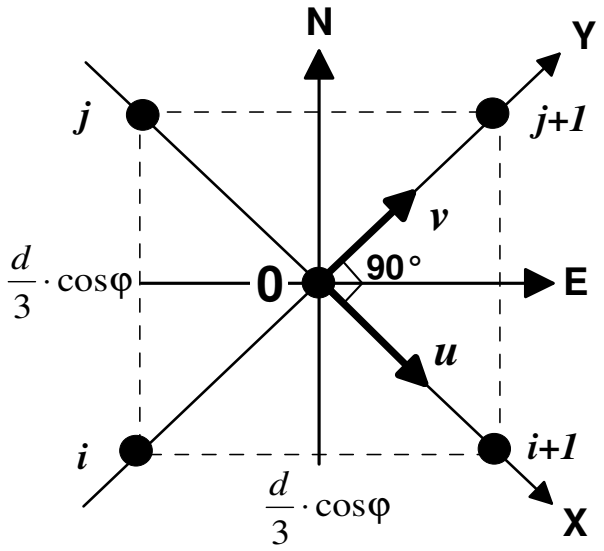

Figure 2.2: *Calculation of eddy geostrophic velocity on a regular 1/3° Mercator grid. 0N, 0E – north and east directions; u, v – eddy geostrophic velocity components; i, i+1, j, j+1 – grid points; d=111.2 km – meridional/zonal distance equivalent to 1° at the equator.*

where P is the pressure, ρ is the density of seawater, z is the depth of the water column, g is the earth's gravity acceleration, $f = 2\Omega\sin\varphi$ is the Coriolis parameter, $\Omega = 7.292\times10^{-5}$ rad/s is the Earth's rotation rate, φ is the latitude, u and v are the zonal and meridional velocity components. We differentiate (2.17) and (2.18) with respect to z and (2.19) with respect to x and y. Then (2.19) is combined with both (2.17) and (2.18). Thus we obtain two equations for the velocity components that after integration over the depth z become

$$\rho u = \frac{g}{f}\int_{z_0}^{z}\frac{\partial\rho}{\partial y}dz + u_0\,, \tag{2.20}$$

$$\rho v = -\frac{g}{f}\int_{z_0}^{z}\frac{\partial\rho}{\partial x}dz + v_0\,, \tag{2.21}$$

Here z_0 is a reference level for integration and u_0 and v_0 are velocities at the reference level. Usually the reference level is chosen to be at great depths where the velocity is traditionally assumed to be close to zero. It is so called "level of no motion". Equations (2.20) and (2.21) are used in dynamical oceanography to derive geostrophic velocities from the *in situ* measured density field. The integral determines the slopes in dynamic heights.

If the geoid was known with an accuracy sufficient for oceanographic purposes then the geostrophic velocities could be computed directly from the gradients of the ocean topography determined by satellite altimetry. In the absence of high-precision geoid models only the variable part of the geostrophic velocities (geostrophic velocity anomalies or eddy geostrophic velocities) can be computed from the altimetry-derived SLA, ζ.

The Mercator projection grid, in which the data are provided, allows a convenient computation of the geostrophic velocity anomalies u' and v'. Apart from the along track analysis, where both u' and v' components are evaluated only at crossovers or by assumption of isotropic velocity variance (Menard, 1983), on the Mercator grid it is possible to compute both u' and v' components using SLA differences between diagonally neighbouring grid points. A precondition for this is that the Mercator projection provides the required orthogonality of u' and v' vectors. Since the T/P orbit inclination equals ~66°, the orthogonality condition is not satisfied in the case of u' and v' calculation at crossovers. This imposes asymmetry between the zonal and meridional velocity vectors.

If axes X and Y are directed as is shown in Figure 2.2, the horizontal components of the geostrophic velocity can be computed by:

$$u' = -\frac{g}{f}\cdot\frac{\partial\zeta}{\partial y} = \frac{g}{f}\cdot\frac{\zeta_i - \zeta_{j+1}}{\sqrt{2\cdot\left(\frac{d}{3}\cdot\cos\varphi\right)^2}} \tag{2.22}$$

$$v' = \frac{g}{f}\cdot\frac{\partial\zeta}{\partial x} = \frac{g}{f}\cdot\frac{\zeta_{i+1} - \zeta_j}{\sqrt{2\cdot\left(\frac{d}{3}\cdot\cos\varphi\right)^2}} \tag{2.23}$$

Since the SLA data, used in this thesis, were computed relative to a 7-year mean SSH, the latter is assumed to be the reference level of no motion. The geostrophic velocity anomalies, computed using (2.22) and (2.23), describe the temporal variation of oceanic geostrophic currents.

Chapter 3

Seasonal and inter-annual variability of sea level in the northern North Atlantic

In this chapter, a study of the seasonal and inter-annual variability of sea level is presented. The seasonal and inter-annual signals were retrieved from the satellite altimetry sea level anomaly (SLA) data over the northern North Atlantic for the time period from October 1992 to June 2003. The contribution of each signal to the total variance was estimated. Both signals appeared to be responsible for a greatest portion of the variability in the northern North Atlantic outside the North Atlantic Current (NAC) and its branches. Large inter-annual variability of the sea level was observed in the Irminger Basin and along the NAC flowing through the Iceland Basin. The inter-annual change of sea level was found to be coherent with the North-Atlantic Oscillation (NAO) index when that changed from its positive to negative phase in the winter of 1995/1996. A significant negative correlation coefficient between the annually averaged SLA and the winter NAO indices was estimated in most parts of the subpolar North Atlantic. The hydrography data obtained during several cruises were also investigated and coupled with the SLA data. The analysis showed a good agreement between the altimeter-derived SLA and hydrography-derived dynamic height anomalies suggesting that the observed changes of sea level in the northern North Atlantic had a baroclinic nature[*].

3.1 Introduction

This study focuses on the northern part of the North Atlantic Ocean from 50°N to 65°N and from 5°W to 45°W (Figure 3.1). This area is an important link in the North Atlantic circulation system, as it comprises the North Atlantic Current (NAC) traveling to the Norwegian Sea and a system of currents composing the North Atlantic subpolar gyre. The subpolar gyre is the formation zone of the deep and intermediate waters of the North Atlantic. Many surveys, mostly performed with surface drifters, have been dedicated to the surface circulation in the North Atlantic Ocean (e.g. Fratantoni, 2001; Käse and Krauss, 1996; Krauss, 1995; Krauss, 1986; Krauss and Käse, 1984; Otto and van Aken 1996; van

[*] This chapter is based on the paper by D.L. Volkov and H.M. van Aken, *Annual and interannual variability of sea level in the northern North Atlantic Ocean*, J.Geophys. Res., 108, 3204, doi:10.1029/2002JC001459, 2003.

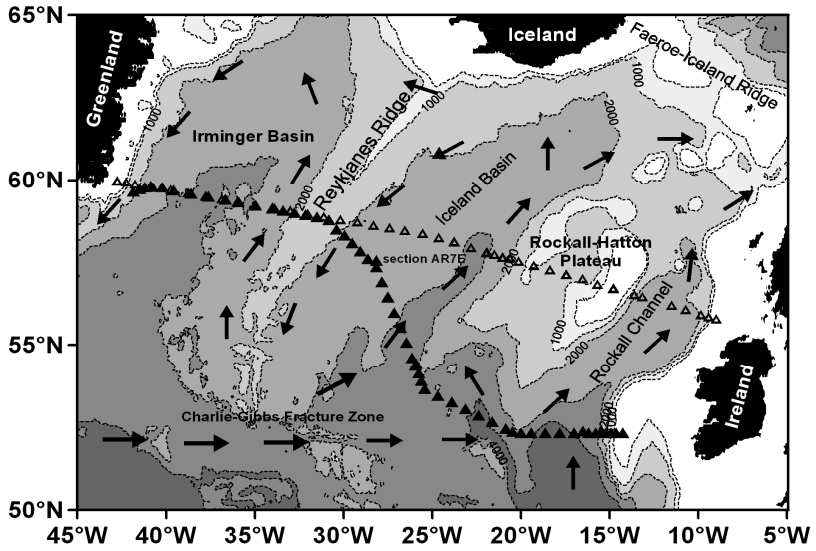

Figure 3.1: *The region of study with bottom topography (m), schematic surface circulation (borrowed from Otto and van Aken, 1996), and two varieties of the AR7E repeat hydrographic section (triangles).*

Aken and Becker, 1996; Valdimarsson and Malmberg, 1999). The mean surface circulation in the North Atlantic was described in chapter 1. Figure 3.1 presents a sketch of major currents in the studied sector of the ocean.

As was described in the previous chapter, three general modes of the sea level variability are distinguished in this thesis: the inter-annual variability, the seasonal change (annual cycle) and the high frequency variability with periods less than one year. The latter is basically represented by eddies and is not covered by this chapter. Here we are only interested in the sea level variations induced by the changes in buoyancy fluxes and advective processes, i.e. changes mainly occurring at seasonal and inter-annual timescales. Since the region is situated in moderate and subpolar latitudes, the contribution of the seasonal and inter-annual changes of the sea level to the overall variability must be important. High variance phenomena (basically eddies) are mainly associated with the NAC, which loses a larger part of its eddy kinetic energy before it reaches the study region (Heywood et al, 1994; Fratantoni, 2001).

The seasonal change or annual cycle of the sea level in the North Atlantic was recently studied by Ferry et al. (2000). They regarded all components that have an impact on the large-scale sea level variability at this timescale. Using both numerical simulation and *in situ* data they concluded that in large parts of the North Atlantic the annual cycle is mainly caused by the steric changes induced by heating. However, on the inter-annual time scales, a contribution to the heat content by advection may become important (Reverdin et al., 1999). The latter can vary due to the changes in the wind stress curl (White and Heywood, 1995). The atmospheric pressure pattern with a characteristic wind stress curl has an oscillating pattern in the North Atlantic and is usually described by the North Atlantic Oscillation (NAO) index (Hurrell, 1995).

As was already reported in chapter 1, the NAO is particularly important during the winter period when it accounts for more than one-third of the total variance in the sea-level pressure (Cayan, 1992). The winter (December through February) NAO indices for the last decade are shown in Figure 3.2.

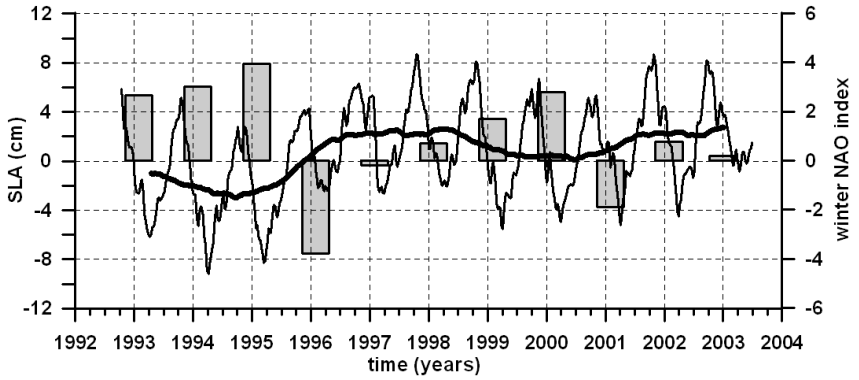

Figure 3.2: *Winter (December through February) NAO indices (vertical bars), and sea level anomalies averaged over the study region with its 1-year window moving average (solid curves).*

Changes in the redistribution of cold, low salinity subarctic water and warm, saline subtropical water in the upper layers of the northern North Atlantic related to the NAO were monitored from the hydrographic data of 1990's (e.g. Bersch et al., 1999; Bersch, 2001). The changes in the local seawater properties may have been caused by the NAO-related large-scale variations in advection and buoyancy fluxes, which also led to a change of sea level. Esselborn and Eden (2001) showed that the sea level variability in the North Atlantic has a dipole pattern which changed sign between 1995 and 1996, following a change of the sign of the NAO index. Reproducing the sea surface height in an ocean general circulation model they concluded that the inter-annual changes in the sea level are mainly induced by variations of the oceanic heat transport. On the basis of model studies, Häkkinen (1999, 2001) also concluded that the low-frequency variations of the sea level in the Gulf Stream area and in the subpolar gyre are mainly determined by the meridional heat transport, which reflects overturning processes in the northern Atlantic. The atmospheric forcing, expressed by the NAO, modulates the variability of the meridional heat transport on the inter-annual time scales. Curry and McCartney (2001) constructed a 50-years oceanic analogue of the atmospheric NAO index as a two-point baroclinic pressure difference between the centers of the North Atlantic subtropical and subpolar gyres. This difference, representing the upper 2000-db eastward baroclinic mass transport between two centers, manifested a relaxation of the Gulf Stream and the NAC during low NAO periods and intensification during high ones.

The study, reported in this chapter, aims to determine the seasonal and inter-annual variations of the sea level in the northern part of the North Atlantic from the satellite altimetry data. One of the objectives is to estimate the contribution of the seasonal and inter-annual variability to the total variance. Although the seasonal change (annual cycle) in the Atlantic Ocean derived from the satellite altimetry data was already studied before (e.g. Behringer, 1994; Ferry et al., 2000), these studies mainly dealt with the large-scale character of the sea level variability. The work, reported in this chapter, focuses on the low kinetic energy region of the North Atlantic Ocean. Another goal is to relate the sea level variations with subsurface changes of temperature and salinity nearly annually measured across the North Atlantic during hydrographic surveys. At last, the inter-annual variations of the sea level will be correlated with the winter NAO indices in order to illustrate a connection between the large-scale processes in the atmosphere and in the ocean.

3.2 Data used

Altimeter data

In this study the merged TPJ+ERS sea level anomaly (SLA) data from October 1992 to June 2003 were used except between 16 December 1993 and 31 March 1995 when the merged data are not available. This time interval was filled up by the T/P only data. The data files also contain mapping errors for every measurement as a percentage of the signal variance. The grid points with the mapping errors exceeding 30% mostly correspond to the shelf areas where tidal aliasing and storm surges are a significant problem whilst the data outside the continental shelves provide a good mapping with small errors compared to the ocean signal that do not greatly contaminate the oceanographic interpretation of the SLA change.

The merged T/P+ERS and T/P only data sets were analysed to understand whether it is acceptable to mix the T/P+ERS and T/P only data to study the seasonal and inter-annual variations of sea level. In particular, the concern is whether the omission of the ERS-1 data would introduce a spurious inter-annual variability into the mixed data set. At large spatial and temporal scales no significant differences between T/P+ERS and T/P data sets are expected since the T/P data were used to correct the ERS data (Le Traon et al., 1995, Le Traon and Ogor, 1998, AVISO handbook, 1998). Mapping errors cause the main discrepancy between the T/P SLA maps and merged T/P+ERS SLA maps. A detailed description of the mapping method is given in Le Traon et al. (1998). The T/P errors are homogeneous in time but have large spatial variability showing a so-called "diamond structure" of the error estimates field with maxima occurring at the centers of the inter-track spaces (diamonds). At high latitudes (higher than 50°N), as the T/P ground tracks become closer to one another, the mapping errors decrease to typical values of ≈30% of signal variance at 60°N. Compared to the T/P only data, the combination of the T/P and ERS-1/2 data sets reduces the mean mapping error by a factor of more than 2 (Ducet et al., 2000).

To assess a discrepancy between the T/P only and T/P+ERS SLA maps both data sets were spanned over two equal time segments, from 22/10/1992 to 06/12/1993 and from 10/04/1995 to 24/05/1996. Thus the time interval when the ERS-1 data are not available was left out of consideration. Then root-mean-squares (RMS) of the T/P and TP/+ERS SLA from each time segment were compared. The RMS of the SLA differences between the T/P and T/P+ERS maps appeared to be less than 20 mm in low-variance areas (over 70% of grid points) besides some centers of the T/P inter-track spaces (diamonds). Only along the NAC, especially in the south-western corner of the region west of the Mid-Atlantic Ridge (high variance area), after subtracting the T/P SLA from the T/P+ERS SLA an obvious "diamond" structure was obtained. Here the T/P+ERS SLA RMS values were usually higher than those of the T/P. This is because the large inter-track distances of the T/P satellite do not allow an adequate mapping of the mesoscale ocean variability. The variance of the T/P+ERS and the T/P SLA differences for both time segments averaged over the study region constitutes approximately 20% of the signal variance.

To show that the inter-annual change is almost intact after the joining of two data sets, mean SLA were calculated for each time segment (42 cycles) of either data set and every grid point. The obtained maps of the mean SLA were spatially smoothed by a median filter over 1 by 1 degree squares. The spatial smoothing was performed because the inter-annual

change of the sea level is a large-scale phenomenon. As a result, the differences between the T/P and T/P+ERS maps were greatly reduced in most areas and slightly exceeded 0.5 cm only in a few number of grid points (less than 20%) whereas the "diamond structure" disappears. In the end, the regional average range of the inter-annual SLA change during the investigated time interval was about 5-6 cm (Figure 3.2) while the regional average of absolute differences between the T/P+ERS and the T/P maps of the inter-annual, spatially smoothed SLA was found to be O(0.3 cm). Hence it is possible to conclude that to study the low-frequency change in low variance areas it is acceptable to fill the gap in the merged TPJ+ERS data by the T/P data. The discrepancy between both data sets was found to be negligible on large spatial and temporal scales.

Hydrographic data

The hydrographic data used in this chapter were obtained during the WOCE (World Ocean Circulation Experiment) and CLIVAR (An International Research Program on CLImate VARiability and Predictability) cruises from 1990 to 2000 along the transatlantic section AR7E, situated between Ireland and Greenland. This section has two varieties: one lies across the Rockall-Hatton Plateau and another surrounds it from the south (Figure 3.1). The hydrographic surveys, studied in this chapter, were conducted in different times of year: basically in August-September (R/V “Meteor”-1991/97, “Valdivia”-1992/96), but also in May, June (R/V “Valdivia”-1999,1995), July (R/V “Tyro” – 1990), December (R/V “Meteor” – 1994) and October (R/V “Pelagia” – 2000). This irregularity introduced a seasonal bias into the data, mainly influencing the upper 200 m water layer. Only one cruise (R/V “Pelagia” in 2000) was conducted along the northern variety of the section. Therefore, the data for the year of 2000 in the southern inlet of the Rockall Channel and south-western Iceland Basin are absent. R/V “Tyro” (1990) did not take any measurements in the central and western parts of the Irminger Basin and the data in this area start in 1991.

NAO index

As has been mentioned the NAO is most pronounced in winter (Cayan, 1992). Therefore, the winter (December through Rebruary) NAO indices based on the differences of normalized sea level pressure between Ponta Delgada, Azores and Stykkisholmur/Reykjavik, Iceland from 1865 to 2003 (from J. Hurrell, 2004; http://www.cgd.ucar.edu/~jhurrell/nao.html) were examined to couple the sea level variations with variations in atmospheric forcing. The sea level pressure anomalies at each station were normalized by division of each seasonal mean pressure by the long-term (1865-2003) standard deviation.

3.3 Observational results

The NAC is characterized by high RMS of SLA associated with intensive eddy activity reaching over 20 cm near 42°W, 50°N (Figure 3.3). In the region where the NAC splits into two branches southwest of the Rockall – Hatton Plateau (Otto and van Aken, 1996; van Aken and Becker, 1996), the RMS values of SLA reach values over 8 cm. The high-RMS

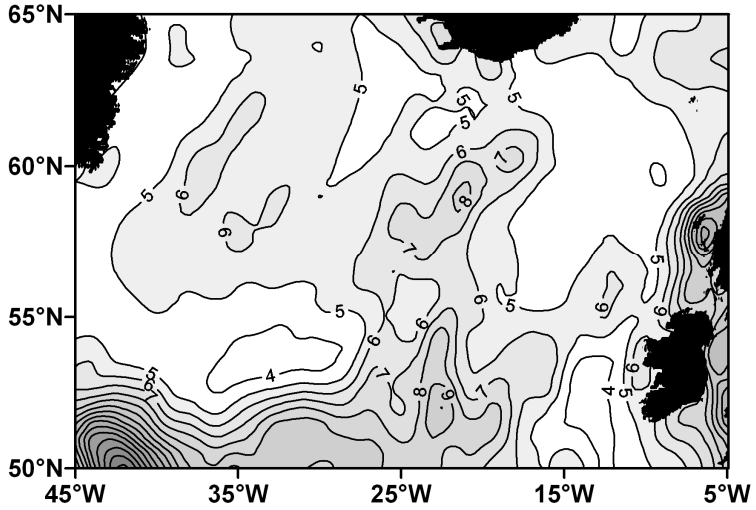

Figure 3.3: *Root-mean-square of sea level anomaly (cm) from October 1992 to July 2003.*

bands reflect the NAC branches in the Iceland Basin and in the Rockall Channel. There are high RMS (over 5 cm) estimates over the Reykjanes Ridge at approximately 56°N-59°N, 31°W-33°W. This area is a likely location where the current flowing along the eastern flank of the ridge crosses it and enters the Irminger Basin (Krauss, 1995; Valdimarsson and Malmberg, 1999).

The SLA data averaged over the study region clearly shows the seasonal signal (Figure 3.2). The spatial averaging suppresses high-frequency signals so that the residual variability is dominated by the seasonal and inter-annual signals. The lowest seasonal sea level was observed in spring whereas the highest seasonal sea level was typical for autumn (Figure 3.2). These variations are out of step with the atmospheric seasons because of the thermal inertia of the sea. The high frequency signals (period < 1 year) appeared to be mainly associated with high eddy activity associated with the NAC band (Figure 3.3). Eddies prevailed in the southwest and gradually decreased in amplitude northwards and eastwards. To visualize the inter-annual change, the SLA data were low-pass filtered by a 1-year moving average. The time-longitude (Hovmöller) diagrams in Figure 3.4 show the inter-annual change in SLA along 52.5°N, 55.5°N and 60.5°N. The most characteristic feature is a sudden increase in the mean sea level, which occurred between 1995 and 1996. In the northern areas the sea level decreased in 2000 and then increased again in 2001. The inter-annual change is also shown as 1-year window moving average of the SLA data averaged over the whole study region (Figure 3.2). The regional mean inter-annual sea level anomaly changed from around -3 cm in 1994 to over +2 cm in late 1996. Then from 1998 to 2000 the sea level decreased at the rate of 2 cm and in the second half of 2000 started to rise again. This change seems to have an inverse relationship with the change of the winter NAO index, which changed from positive to negative in the winters of 1995/1996 and 2000/2001.

Variance explained

After the seasonal and interannual signals had been estimates, as described in Chapter 2, the portion of variance explained by each of them (determination coefficient) was determined.

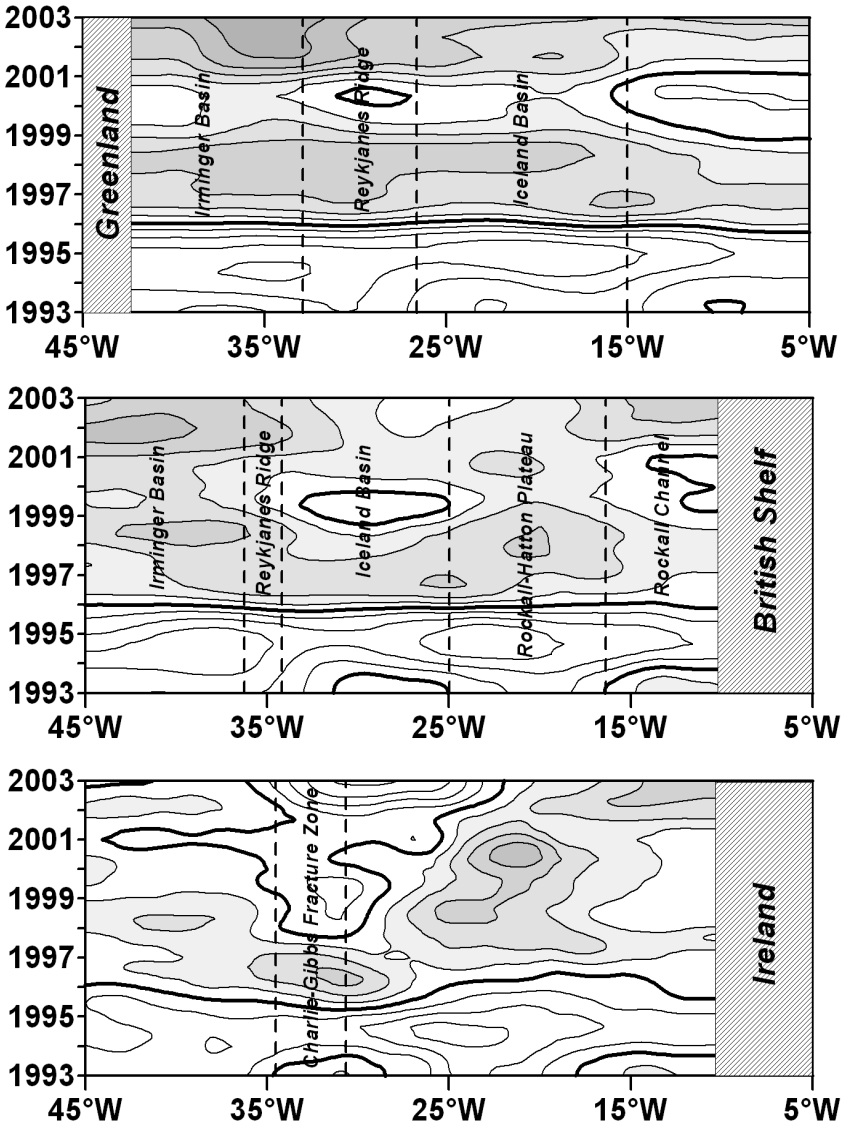

Figure 3.4: *Time-longitude diagrams of the annually averaged SLA (cm) along 52.5°N (bottom panel), 55.5°N (middle panel), and 60.5°N (top panel) with indicated geographical regions. Bold curves denote zero contours. Shaded areas represent positive SLA while blank areas negative SLA. The interval between contours is 1 cm.*

The variance explained by the seasonal change (Figure 3.5, top panel) appeared to explain approximately a half of the total variance in dynamically calm areas as the continental shelf, Rockall-Hatton Plateau, Faeroe-Iceland Ridge and also over the Reykjanes Ridge. Within the NAC band south of 55°N the determination coefficient for the seasonal signal was found to be less than 30%. Along the branches of the NAC in the Rockall Channel and in the Iceland Basin, and also in the Irminger Basin, the seasonal variability explained about 1/3 of the total variance.

The inter-annual signal explained ≈1/3 of the total variance over the Rockall-Hatton Plateau and well over 40% in the Irminger Basin (Figure 3.5, bottom panel). Along the NAC band in the Iceland Basin, where the inter-annual change seems to be as strong as in the Irminger Basin, the determination coefficient was around 20%, which is obviously a result of high eddy activity in this region.

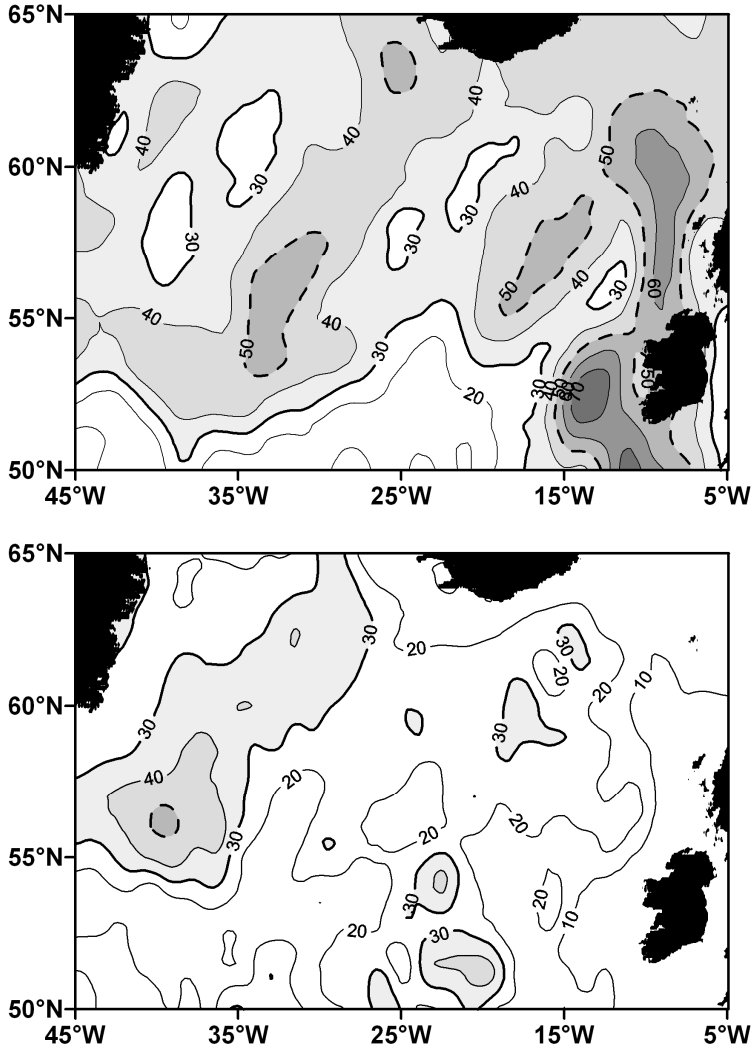

Figure 3.5: *Determination coefficient (%) of the seasonal (top panel) and inter-annual (bottom panel) components of the SLA variability (dashed lines 50%, thick full lines 30%).*

Thus over the largest part of the northern North Atlantic, outside the NAC and its main branches in the Rockall Channel and Iceland Basin, the SLA variability was found to be mostly governed by the seasonal and inter-annual change. The determination coefficient of the combined seasonal and inter-annual signal in these areas exceeded 50%. In some parts of the Irminger Basin the variance explained by these modes of the variability exceeded 70%. Along the NAC the seasonal and inter-annual variability was overpowered by high frequency change (mainly caused by eddies).

Seasonal change

The sea level is at its minimum in spring, after it has lost all the excess heat during the preceding winter and acquired its maximum density. Also, because of the decrease in precipitation at this time the salinity rises increasing the density (The Atlas of the Oceans, 1977). The sea level is at maximum during the autumn period, after the heat has been accumulated. The largest amplitudes of the seasonal SLA, estimated by a harmonic

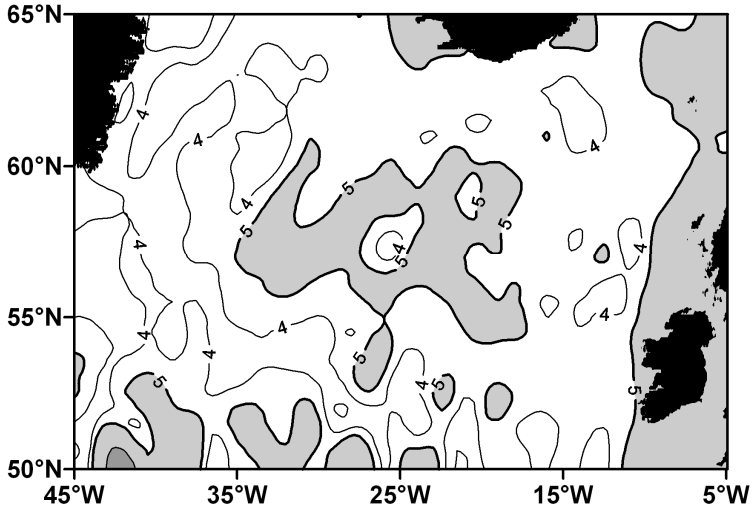

Figure 3.6: *Amplitudes (cm) of the seasonal signal.*

function, were observed in the Iceland Basin and were equal about 5 – 6 cm (Figure 3.6). This is perhaps due to the seasonal shifts of mass in this zone, associated with the shifts of the Subarctic Front, which is usually attributed to the 8°C – isotherm. The seasonal displacements of this isotherm involve the Iceland and Irminger basins (The Atlas of the Oceans, 1977). The other areas have seasonal amplitudes of the order of 3-5 cm. The latter values resemble those, estimated by Ferry et al (2000) from a model simulation of the sea surface height annual harmonic taking into account only the seasonal heat fluxes.

The seasonal change in sea level can be related to a change in the mean temperature of the water column, and therefore with the annual cycle of the sea surface heat budget. When we assume that the salinity profile does not change, nor the total amount of water (constant bottom pressure), the relation between temperature and the sea surface height can be expressed as:

$$\frac{\rho c_p}{A}\frac{\partial(SLA)}{\partial t} = \frac{\partial}{\partial t}\int_{-H}^{SSH}(\rho c_p T)dz \qquad (3.1),$$

where ρ is the density and c_p is the specific heat. A is a vertically averaged thermal expansion coefficient and H is the bottom depth.

Changes in the heat content, causing the steric changes in the sea level, are caused by the net air-sea heat flux Q and advection of heat, so that the final equation is

$$\frac{\rho c_p}{A}\frac{\partial(SLA)}{\partial t} = Q + \int_{-H}^{SSH}(\rho c_p ADV_T)dz \qquad (3.2),$$

where the second term of the right side represents the contribution of the heat advection.

Equation (3.2) shows that, at the annual frequency, the changes in SLA are determined by the seasonal variation in the net sea surface heat flux and the seasonal variation in heat advection. The latter is unknown, but estimates of Q have been published. In this chapter, the monthly mean net heat fluxes, published by Isemer and Hasse (1985), were used. In a statistically stationary situation the annual mean value of Q is completely balanced by the advection term in (3.2). From the remaining part of Q, with annual frequency, it is possible to calculate its contribution to the amplitude of the annual cycle, according to (3.2), assuming that the advection term can be ignored at this frequency. For the 5°-latitude band around 60°N the SLA amplitude of about 3.7 cm was obtained. In the order of magnitude this compares well with the amplitude of around 4.5 cm in this latitude band, derived from the altimetry data. The difference may be explained by the assumption that the advection term does not have an annual cycle and by the influence of precipitation on salinity. Also the estimates of Q by Isemer and Hasse, (1985) may contain systematic errors. Further south, at 57°N where the amplitude of the annual SLA cycle between 35°W and 15°W is largest (≈5.5 cm) the amplitude of the annual Q cycle is about 10% smaller than at 60°N. This suggests a more prominent role of advection in the seasonal SLA signal in the Iceland Basin.

Inter-annual change

The contribution of the inter-annual signal is just a little smaller than the contribution of the annual cycle. Figure 3.7 represents the RMS of the sea level variations estimated from the data obtained after a 1-year window moving average had been applied. The largest RMS values were found along the NAC flowing through the Iceland Basin with secondary maxima in the Irminger Basin. In these regions the RMS estimates of the inter-annual SLA ranged from 3 to over 5 cm. The high RMS estimates of the inter-annual signal in the Irminger Basin are probably a consequence of the strong dependence of the sea level change here upon the temporal restructuring of the NAC branches. The latter possibly causes an increase/decrease of the advection of warm and saline Atlantic water into the Irminger Basin and associated inter-annual displacements of the Subarctic Front leading to a contraction/enlarging of the subpolar gyre. Compared with the RMS estimates of the initial SLA data (Figure 3.3), the variability of the inter-annual SLA (Figure 3.7) has a more expressive maximum in the Irminger and Iceland basins than in the narrow Rockall Channel.

NAO – related change

As has been mentioned before, the inter-annual changes in atmospheric circulation, and therefore atmospheric forcing of the ocean, may be expressed by the North Atlantic Oscillation (NAO) index (see chapter 1). The time series of the SLA averaged over the whole study region and the winter NAO indices (DJF) are shown in Figure 3.2. To define a connection between the NAO and the sea level in the North Atlantic on the inter-annual time scales, the correlation coefficients for each grid point between the annually (from December to November next year) averaged SLA and the winter (DJF) NAO indices were calculated (Figure 3.8). More frequently sampled SLA time series also contain the seasonal signal and higher frequency components (e.g. eddies), which are not generated by the inter-

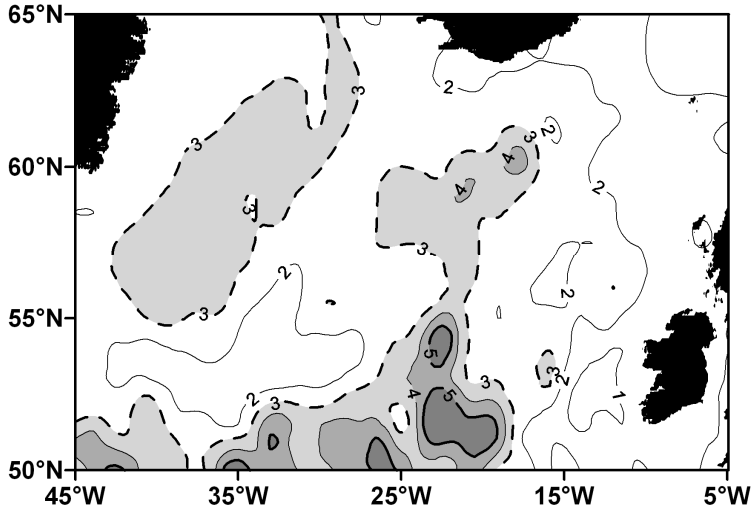

Figure 3.7: *Root-mean-square (cm) of the inter-annual component of the SLA variability. Dashed curves denote 3 cm contours.*

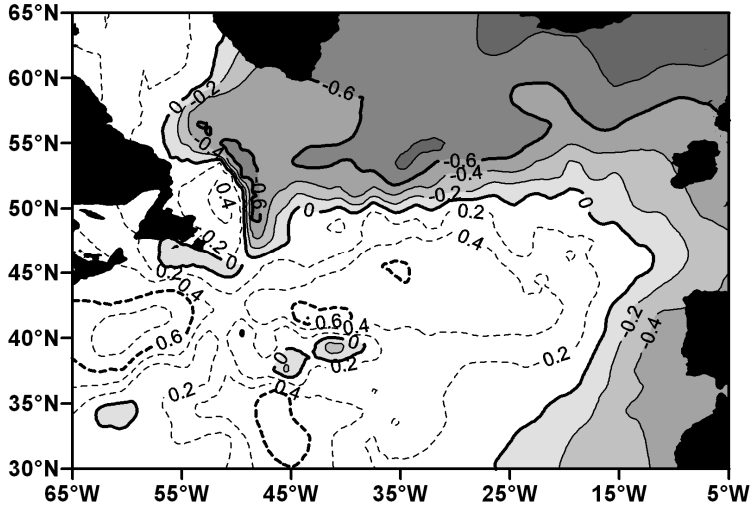

Figure 3.8: *Map of correlation coefficients between the annually averaged SLA and winter (DJF) NAO indices in the extratropical North Atlantic Ocean. Significance level = ±0.6.*

annual changes in the atmospheric forcing, but mainly by the seasonal variations in buoyancy fluxes and, in the case of eddies, by baroclinic and barotropic instabilities. The correlation coefficients were computed for a larger sector of the North Atlantic, which also includes the northern part of the subtropical gyre (5°W-65°W, 30°N-65°N). Prior to the computation, the SLA data were spatially smoothed by a moving average filter over 3º×3º areas. Over most investigated areas of the subarctic North Atlantic Ocean, except the regions where the NAC travels eastwards, a significant negative correlation was found. The 95% significance level for 10 years of data is ±0.6 (Dixon and Massey, 1969). In the subtropical gyre the correlation coefficients are positive, but predominantly not significant.

Thus, it seems probable that changes in the atmospheric forcing over the North Atlantic, related to the NAO, indeed, effect the SLA on the inter-annual time scale. It appeared that on the inter-annual time scale from 1993 to 2003 the North Atlantic Ocean responded to the

atmospheric forcing as a dipole system: during strong/weak westerly winds (positive/negative NAO indices) the sea level increases/decreases in the subtropical gyre and decreases/increases in the subpolar gyre. When the NAO turned from its positive to negative phase in 1995/1996 and 2000/2001, the ocean responded with a sea level rise in the subarctic areas and a decrease in the subtropical areas. It happened that the sea level responded to the changes in the NAO index within one year. This is probably possible due to the presence of the strong North Atlantic Current mainly driven by the atmospheric forcing with its characteristic water properties (warm and saline).

Hydrographic observations

The hydrographic data, obtained from 1990 to 2000 along the section AR7E, confirmed the changes in the spatial distribution of the seawater properties, which were observed by the TOPEX/Poseidon and ERS altimeters as a change of the sea level. A significant change was observed during the change of the NAO phase in 1996. Salinity data unveiled a tongue of saline and warm waters of the NAC penetrating further north and west in the Iceland Basin in 1996 compared with the preceding observations from 1995 (Bersch et al., 1999, Bersch, 2001). In 1997 this penetration of warm and saline water reached deeper layers and almost crossed the Reykjanes Ridge. Analyzing hydrographic data from the 1990's Bersch (2001) arrived to the conclusion that during the periods with weak westerly winds (low NAO index) the eastward transport of the subarctic water with the NAC is reduced and the Subarctic Front is shifted westwards in the Irminger and Iceland Basins. This section attempts to broaden this study by including also the sea level change observed by satellite altimetry. The goal is to analyze how the sea level changed accordingly to the change of the water mass properties and what water masses had a decisive influence on the variations of the sea level. A similar, but more limited, analysis was performed by Reverdin et al. (1999). They compared the sea surface heights measured by satellite altimetry and the dynamic heights for the upper 700 dbar layer along a hydrographic section between Iceland and Newfoundland and found a high correlation between the time series.

As the hydrographic data were obtained in different parts of the year, they are biased by the seasonal change. Mesoscale processes like eddies may also bias the average state of the seawater properties. In order to reduce the influence of eddies, the CTD data from each AR7E survey were spatially averaged in the horizontal domain. For this purpose the sections were divided in four parts, which were chosen in compliance with the main geographical areas restricted by natural topographic boundaries. These parts are (1) the southern inlet of the Rockall Channel, covered by the southern version of the AR7E section (16°W-23°W); (2) the Iceland Basin (restricted by 55°N in the south-east and 2000 m isobath in the northwest corresponding to 30°W); (3) the Reykjanes Ridge (30°W - 33°W); and (4) the Irminger Basin (restricted by 2000 m isobath between the Reykjanes Ridge and Greenland, corresponding to 33°W - 42°W) (Figure 3.1). The number of stations used for averaging in each area is presented in Table 1. Since the position of the Subarctic Front in the Iceland and Irminger Basins may show seasonal and inter-annual variations, the basin-scale averaging is expected to reflect the shifts of the front as well as changes in the seawater properties.

The upper part of the water column contains the relatively warm and saline Subpolar Mode Water (SPMW), which is ultimately converted into the Labrador Sea Water (LSW)

Table 3.1: *Number of hydrographic stations in each area, over which spatial averaging was performed, with indicated geographical boundaries along the AR7E section (see Figure 3.1).*

Time	Research vessel	Southern inlet of the Rockall Channel (16°W -23°W)	Iceland Basin (26°W - 30°W)	Reykjanes Ridge (30°W - 33°W)	Irminger Basin (33°W - 42°W)
July,1990	*Tyro*	8	8	4	…
Aug-Sept, 1991	*Meteor*	12	10	4	12
Aug-Sept, 1992	*Valdivia*	12	11	4	10
December,1994	*Meteor*	10	10	4	7
May-June, 1995	*Valdivia*	13	10	5	11
Aug-Sept, 1996	*Valdivia*	12	11	6	11
Aug-Sept, 1997	*Meteor*	10	12	4	11
May-June, 1999	*Meteor/Valdivia*	11	12	5	10
October, 2000	*Pelagia*	…	…	4	9

by deep convection in the Labrador Sea. The LSW situated below the SPMW is characterized by an intermediate salinity minimum (between 1500 and 2000 dbar), which overlies the North Atlantic Deep Water (NADW). Based on this division the hydrographic data were averaged over 4 layers: 20 – 200 dbar (the choice of 20 dbar was imposed by different start depths in CTD casts), 200 – 800 dbar, 800 – 1500 dbar (800 - 1200 dbar over the Reykjanes Ridge) and 1500 – 2000 dbar. Thus the spatial averaging procedures yielded one characteristic value of temperature and salinity for each area and vertical layer for each cruise. Seasonal bias is significant only in the upper layer. It is assumed in this chapter that the variations below 200 dbar mostly occur on the inter-annual time scale.

To express the change of the seawater properties in terms of the associated sea level change the dynamic heights for the areas of averaging were estimated. The dynamic heights were calculated for each vertical layer and for the 20 – 2000 dbar layer in the southern inlet of the Rockall Channel, in the Iceland and Irminger basins, and for the 20 – 1200 dbar layer over the Reykjanes Ridge. Then in order to compare the obtained results with SLA, the dynamic height anomalies (DHA) were derived relatively to a mean compatible with the mean used to derive the SLA (1992-1999, although there are no hydrographic data for 1993 and 1998).

In Figure 3.9 the regionally averaged DHA, shown for the appropriate time of the year, and the regionally averaged SLA are presented. The SLA were averaged over rectangles encompassing the AR7E section: 52-53°N and 16-23°W in the southern inlet of the Rockall Channel, 55-57°N and 26-28°W plus 57-59°N and 28-30°W in the Iceland Basin, 58-59°N and 30-33°W over the Reykjanes Ridge, 59-60°N and 33-42°W in the Irminger Basin. Another reason for comparing the spatially averaged data instead of *in situ* measurements, besides those mentioned above, was to reduce the impact of errors present in the altimetry data imposed by the accuracy of measurements, which are of the order of 5 cm (Fu et al., 1994), and by the mapping errors, described in the section 3.2.

One can see that the DHA calculated from the hydrography data in most cases coincided very closely with the SLA time series (Figure 3.9). The remaining discrepancy may be induced by several causes. First, it is a possibility to underestimate dynamic heights due to the omission of variability in the water layer below 2000 dbar. Second, the presence of errors imposed by somewhat different scales of spatial averaging of altimetry and hydrography data, different sampling frequencies of satellite- and ship-born measurements

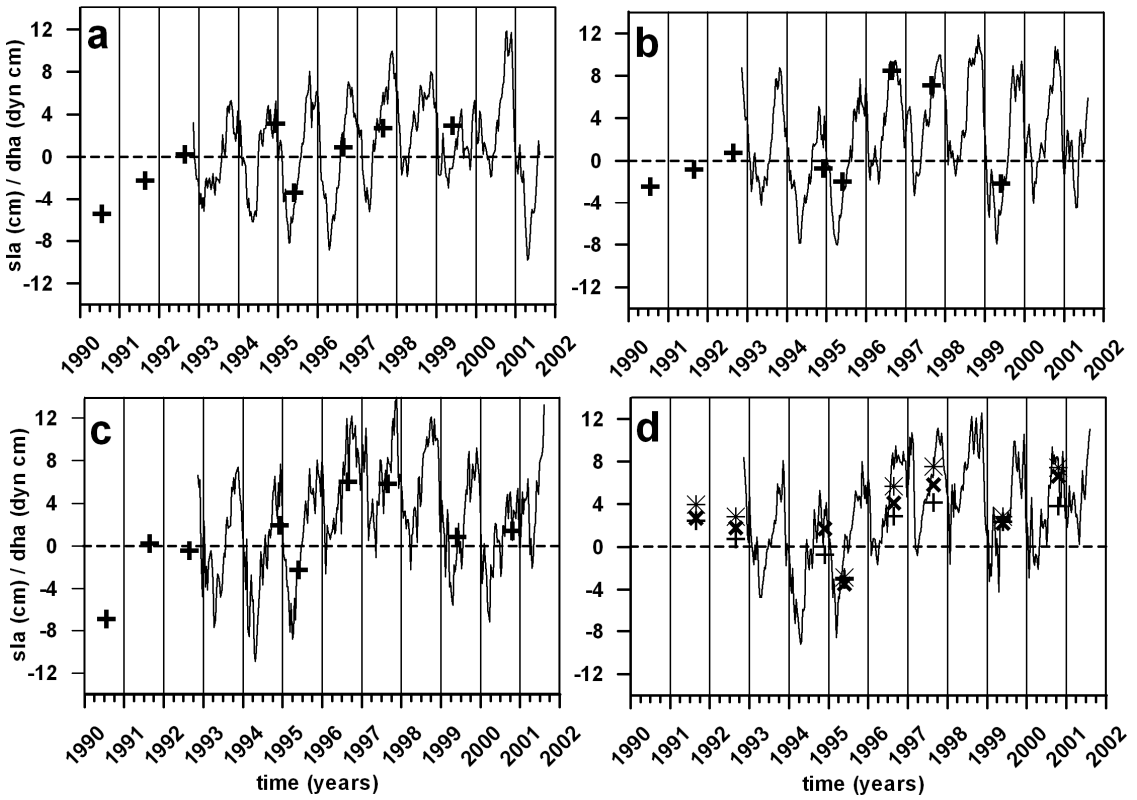

Figure 3.9: *Dynamic height anomalies (DHA) of the 20-2000 dbar layer (crosses) and the mean sea level anomaly (solid line) for (a) the southern inlet of the Rockall Channel, (b) the Iceland Basin, (c) the Reykjanes Ridge (DHA for 20-1200 dbar), and (d) the Irminger Basin. In (d) the DHA for the 20-3000 dbar layer (diagonal crosses) and for the 2-3000 dbar layer (asterisks) are also shown.*

and ultimately the errors in the altimeter measurements. The latter must be reduced by averaging but not completely eliminated. And third, although the same time interval was chosen to calculate a reference level for the DHA (1992-1999) as it was done for the SLA, the averages were not completely adequate due to the irregularity of hydrographic sampling, absence of measurements in 1993 and 1998, etc.

A more complicated situation was observed in the Irminger Basin (Figure 3.9d). One can see that the DHA values (crosses) are lower then the SLA values. Is this discrepancy caused by the reasons mentioned above or it is a consequence of the barotropic compound of the sea level change in this region? Reverdin et al. (1999), investigating the variability of the upper ocean temperature and surface salinity along the section AX2 between Iceland and Newfoundland in 1993-1998, documented that the seasonal amplitude of the dynamic heights in the subpolar gyre is less than that of the sea level observed by the satellite altimetry (30% and more). Nevertheless, since their analysis was based on XBT measurements, it was restricted to 750 dbar (maximum depth of XBT sampling) and could not estimate the steric changes in deeper layers. Accordingly to Dickson et al. (1996) the latter may be important in the Irminger Basin due to deep convection. In order to test this, a larger vertical water column in the Irminger Basin – from 20 to 3000 dbar and from 2 to 3000 dbar was considered, although in the latter case the year of 1994 was missed, as there were no data starting from 2 dbar. Another drawback of this enlarging was that only 4 stations in this basin had depths more than 3000 dbar. T-S diagrams showed a large inter-

Table 3.2: *The determination coefficient (%) of the inter-annual change in dynamic heights calculated for each investigated vertical layer (dbar).*

Area/Vertical layer	2-20 db	20-200 db	200 - 800 db	800 - 1500 db	1500 - 2000 db	1500 - 3000 db
Southern inlet of the Rockall Channel	…	26	41	32	1	…
Iceland Basin	…	32	64	3	1	…
Reykjanes Ridge	…	31	67	2 *(800-1200 db)*	…	…
Irminger Basin	7	28	44	7	…	14

annual change of temperature and salinity in upper 200 dbar and considerable change in deeper water (Bersch et al., 1999). The DHA for 20-3000 dbar (diagonal crosses) and 2-3000 dbar (asterisks) are presented in Figure 3.9d. The agreement between the DHA and SLA was significantly improved, in particular in the later case since in this region of cooling and deep convection the seasonal and inter-annual variations of temperature and salinity in the upper tens of meters are relatively large (shown with numbers below).

In general now it is possible to state that the DHA seem to be highly correlated with the SLA ($r \approx 0.8$). The RMS of differences between the SLA and the DHA were equal 2.5 cm in the southern inlet of the Rockall Channel, 2 cm in the Iceland Basin, 1.8 cm over the Reykjanes Ridge, 3.4 cm for 20 – 2000 dbar and 1.6 cm for 2 – 3000 dbar in the Irminger Basin. This is much less than the range of the observed SLA variability, which was of the order of 20 cm (Figure 3.9). The obtained result is better than in earlier verification studies. For example, Morris and Gill (1994) found an overall RMS difference of 3 cm between the altimeter and tide gauge measurements in the Great Lakes. Gillson et al. (1998) compared the T/P altimetric heights with steric heights calculated from XBT measurements in the North Pacific and obtained a difference of 3.5 cm rms. One of the reasons why the difference between the SLA and the DHA in the study, reported in this chapter, was less than in other studies is the use of the spatially averaged SLA and hydrography data.

The determination coefficients of the DHA variations in each layer were calculated to qualitatively estimate their relative contribution to the overall change of the DHA (Table 2). In all areas the depth interval of 200 – 800 dbar occupied by the SPMW supplied the largest contribution to the change of the sea level on the inter-annual time scale (assuming that the seasonal variations are confined within the upper 200 m): 2/3 of the total variance in the Iceland Basin and over the Reykjanes Ridge and over 40% in the other areas. The determination coefficient for the upper 20 - 200 dbar layer is high, O(30%), but it was biased for some part by the seasonal signal in the upper layer of the ocean since the cruises were conducted in different times of the year. Therefore, the contribution of this layer to the inter-annual change was supposedly smaller than estimated. In the Irminger Basin even the upper 20 m considerably contributed to the steric change of the sea level along with the deep water below 1500 dbar (the determination coefficient = 7 and 14% correspondingly). It is interesting to note a relatively large contribution of 800-1500 dbar layer in the southern inlet of the Rockall Channel (1/3 of the total variance). This is probably due to the inter-annual variations of depth of the permanent thermocline in this region, a feature described

by van Aken (2003). Studying the northern course of the section AR7E he found that the permanent thermocline in 2000 was about 300 dbar deeper than in 1991.

All these results suggest that the inter-annual change of the sea level in the northern North Atlantic Ocean has basically a baroclinic nature so that the sea level did not change due to an increase of the amount of water, but due to a change of thermohaline properties and, consequently, density of the seawater. The findings, reported in this chapter, confirmed that the observed rise of the sea level from 1995 to 1997 was partly caused by the restructuring of the oceanic circulation pattern that brought warm and more saline NAC waters further west along with the contraction of the subpolar gyre and the westward shift of the Subarctic Front (Bersch, 2002). This research confirmed the results obtained by Häkkinen (2001) and Esselborn & Eden (2001) from model studies, stating that the thermohaline circulation variations determine the sea surface height / heat content changes and suggestion made by Reveredin et al. (1999) that a part of the vertically integrated heat content determining the steric sea level is modulated by the advective processes.

3.4 Conclusions

The extraction of the seasonal and inter-annual signals from the altimetry data showed that in the northern North Atlantic both signals were responsible for the greatest part of the observed variance, often surpassing the contribution from mesoscale eddies. The seasonal change appeared to be responsible for ≈1/3 of the total variance in most areas besides the NAC and its branches, where its contribution was <30%, and for more than 50% over dynamically calm areas like the Reykjanes Ridge, Faeroe-Iceland Ridge and the continental shelf. The inter-annual signal was found to be responsible for up to 30% along the branch of the NAC flowing through the Iceland Basin and from 30% to well over 40% in the Irminger Basin. The mesoscale variability, mainly represented by eddies, prevailed along the NAC, where it constituted more than 50% of the total variance.

Maximum amplitudes of the seasonal SLA were observed in the Iceland Basin reaching 5 – 6 cm, whereas in other areas the amplitudes were equal to about 3-5 cm. Following Ferry et al. (2000), the amplitude of the sea level induced by the seasonal net sea surface heat flux variation was estimated. In the order of magnitude it compared with the amplitude derived from the satellite altimetry. At 60°N the annual cycle of the heat flux explained over 80% of the annual SLA cycle, while at 57°N in the Iceland Basin it explained only about 60%. This confirmed that in the northern North Atlantic the seasonal variability of the sea level is mainly caused by the steric effect. Nevertheless, the observed amplitudes of the seasonal signal in the northern part of the Iceland Basin (57°N) are approximately 40% higher than those obtained by using the seasonal net sea surface heat flux. Since advection was neglected computing the amplitudes of the sea level change caused by the seasonal net sea surface heat flux, it is possible to conclude that the advection term (see equation 2) at the seasonal time scale may also be important. The Subarctic Front, to which the NAC is fixed, may have experienced seasonal shifts and thus also contributed to the seasonal sea level amplitudes in the Iceland Basin.

The satellite altimetry and hydrographic data indicated that during the 1990s the sea level experienced a rise from 1995 to 1997 connected with the change of the atmospheric circulation pattern expressed by the NAO index. When the NAO index turned from its

positive phase to strongly negative in 1995-1996, a sea level increase over the northern North Atlantic followed within one year. In 2000-2001 there was another reversal of the NAO index from positive to negative. Although it was much weaker than in 1995-1996, the altimeter data showed that the sea level in the subarctic areas increased again. The NAC with its branches and the Irminger Basin manifested greatest amplitudes of the inter-annual SLA change exceeding 3-5 cm. A significant negative correlation (correlation coefficients <-0.6) was found between the annually averaged SLA and the winter NAO indices in the subarctic North Atlantic. This confirmed strong influence of the atmospheric pressure distribution fluctuations over the North Atlantic on the inter-annual sea level variations.

The hydrographic data also manifested a change of the dynamic heights along the AR7E section associated with the NAO. The dynamic heights of the water column of 20 – 2000 dbar in the southern inlet of the Rockall Channel, Iceland and Irminger basins and over the Reykjanes Ridge appeared to be coherent with SLA. It was shown that the layer 200 – 800 dbar occupied by SPMW had a greatest contribution to the inter-annual dynamic height variations in all mentioned regions. Due to the resemblance of the hydrography derived DHA and altimetry derived SLA it is possible to conclude that the change of the sea level in the northern North Atlantic had a baroclinic nature, i.e. it changed according to the changes of water density mainly influenced by the variations of the net heat flux between ocean and atmosphere and by the changes in advection.

To summarize we may describe the northern North Atlantic Ocean and the atmosphere as an interacting system. Changes in the atmospheric circulation, in particular, weakening or strengthening of westerly winds in the North Atlantic, modulate the inter-annual changes in oceanic circulation and hence redistribution of the warm and saline NAC waters. The baroclinic transport is high/low during strong/weak westerlies, which implies a stronger/weaker horizontal circulation in both subarctic and subtropical gyres (Curry and McCartney, 2001). In the case of weak westerlies (low or negative NAO index), as followed after the dramatic drop of the NAO index in the winter of 1995/1996, the Subarctic Front shifts westwards resulting in an increased lateral heat transport, inducing warming and density decrease in the subpolar gyre (Bersch et al., 1999, Bersch, 2002). It was shown how this process was reflected in the inter-annual variability of the sea level observed by the satellite altimetry and that the change of the sea level was attributed to the thermohaline changes associated with baroclinic transport.

It is not possible to attribute a characteristic period to the inter-annual change of SLA. Firstly, the length of the available SLA time series is not sufficiently long (10 years) and secondly, the oceanic processes taking place in the North Atlantic may be governed by nonlinear ocean-atmosphere interactions, which are still not completely understood. The results presented in this chapter may serve as an illustration of the variability features complementing to our understanding of the ocean – atmosphere interactions over the North Atlantic Ocean.

The main conclusions of this chapter are the following:

1. Outside the NAC the seasonal and inter-annual variability of sea level in the studied area of the northern North Atlantic was responsible for about 2/3 of the total variance.

2. The seasonal change (annual cycle) was found to be responsible for ≈1/3 of the total variance in most areas. In the Iceland Basin, where the observed amplitudes of the annual

cycle appeared to be higher than those derived from the net surface heat flux, a contribution of advection to the annual SLA cycle was suggested.

3. The maximum inter-annual change of sea level was observed in the Irminger Basin (over 40% of the total variance) that suggested a possible importance of advection on these time scales acting along with the inter-annual changes of the net surface heat exchange with the atmosphere.

4. The sea level rise in 1996-1997 followed the dramatic NAO index drop in the winter of 1995-1996 from strongly positive values to strongly negative. Another reversal of the NAO index in winter 2000-2001 was also associated with another rise of the sea level. A significant negative correlation (r=<-0.6) between the winter NAO indices and annually averaged SLA was estimated in the subarctic areas of the North Atlantic.

5. A good agreement between the altimetry derived SLA and hydrography derived DHA was found along the section AR7E, suggesting that the change of the sea level in the study region had a baroclinic nature. The density changes occurring in the SPMW had the largest contribution to the change of the sea level.

Chapter 4

Variability of sea level in the North Pacific and North Atlantic: a comparative analysis

This chapter presents a comparative analysis of the sea level variability in the North Atlantic and North Pacific. As it was done for the northern North Atlantic in the previous chapter, the sea level anomaly signal is represented as a composition of the mesoscale, seasonal and inter-annual components. The magnitude and pattern, characterised by root-mean-square, amplitude, phase, and the amount of variance explained for each component, are studied. The Empirical Orthogonal Functions analysis is used to identify the leading modes of the inter-annual change. A discussion on climate-related change of the sea level and the role of the North Atlantic Oscillation, the El Niño/Southern Oscillation and the Pacific Decadal Oscillation in both oceans is presented[*].

4.1 Introduction

The advent of satellite altimetry has permitted simultaneous monitoring of sea level changes in different parts of the World Ocean, so that different ocean basins can be studied as a complex interconnected system. This is particularly important in the light of the recent debates about anthropogenic Global Change. Such questions like "how is the global sea level changing?", "how is the sea level variability in one part of the World Ocean related to the change in another part?", and "what are the associated changes in oceanic circulation and transport?" can be addressed by satellite altimetry. However, relatively short time series (a little more than 10 years of the high-accuracy TPJ+ERS data at the time when this research was conducted) still impose considerable limitations on identifying the climatic change and distinguishing the Global Change from natural recurrent fluctuations.

This chapter aims to examine the variability of the sea surface height (SSH) in the North Atlantic (NA) Ocean and in the North Pacific (NP) Ocean observed with satellite

[*] This chapter is partly based on the following papers:

1) D.L. Volkov and H.M. van Aken *"Low frequency change of sea level in the North Atlantic Ocean as observed with satellite altimetry"*, In: Satellite altimetry for geodesy, geophysics and oceanography (eds. C.Hwang, C.Shum and L. Jiangcheng), International Association of Geodesy Symposia, Vol. 126, pp. 167-174, Springer-Verlag, 2003.
2) D.L. Volkov and H.M. van Aken *"Climate-related change of sea level in the extratropical North Atlantic and North Pacific in 1993-2003"*, submitted to J. Geophys. Res., 2004.

altimetry from November 1992 to June 2003. The main objective is to compare the magnitudes and patterns of the SSH changes on the mesoscale, seasonal and inter-annual time scales. The study of the sea level variability in the northern NA was presented in the previous chapter. The present chapter broadens that study considering a larger sector of the extratropical NA from 5°W to 65°W and from 30°N to 65°N and by including the 140°E – 240°E, 30°N – 65°N sector of the NP Ocean. Thus these sectors envelope the NP subpolar gyre, the southern part of the NA subpolar gyre, and the northern parts of the subtropical gyres including the western boundary currents, represented by the Gulf Stream and Kuroshio extensions.

Changes in SSH are the result of either changes in the mass of the water column at a given location (barotropic response) or changes in the local density leading to expansion or contraction of the water column (baroclinic response). The latter is also known as the steric change of SSH. The steric changes are thought to dominate SSH variability (e.g. Patullo et al., 1955; Vivier et al., 1999). The major factors determining the variability of altimetric SSH (corrected for tides and inverse barometer effect) include changes in heat and fresh water fluxes at the ocean-atmosphere interface (buoyancy fluxes), the adjustment of the ocean to varying wind stress, eddy formation processes, propagating Rossby waves, equatorially and coastally trapped Kelvin waves, storm surges, etc.

As was done in the previous chapter, we will distinguish three temporal modes of the SSH variability observed by satellite altimetry:

1) mesoscale changes representing all signals with periods less than 1 year, including mainly mesoscale eddies and Rossby waves;
2) seasonal change or annual cycle, which has a period of about 1 year, determined by the seasonal change of insolation and ocean-atmosphere interactions at annual frequency;
3) inter-annual change that is comprised of all detectable signals with periods longer than 1 year and caused by the large-scale variations in buoyancy fluxes, wind forcing and advection.

The first two modes represent large-scale processes and are largely dependent on the oceanic heat and salt content. In the mid-latitude Pacific Ocean, White and Tai (1995) found a good agreement between heat content from expandable bathythermographs (XBTs) and variations of the TOPEX/Poseidon (henceforth T/P) SSH signal. Stammer (1997) found a close resemblance between the observed seasonal change (annual cycle) in the T/P SSH data and steric anomalies estimated from the European Centre for Medium-Range Weather Forecasts sea surface buoyancy fluxes. Gilson et al. (1998) compared the T/P SSH with steric heights calculated from XBT measurements in the North Pacific and concluded that the variability of both is very similar, especially at wavelengths longer than 500 km. In the previous chapter it was shown that the altimetric SSH agree well with the large-scale dynamic height anomalies derived from CTD measurements along the section AR7E in the northern North Atlantic (also see Volkov and van Aken, 2003). Therefore, it was summarized that in the northern NA changes of sea level have a baroclinic nature. Besides the buoyancy fluxes, baroclinic changes can also be induced locally through advection of water masses by fluctuating barotropic currents. In the NA, advection was suggested to be important for both the inter-annual and seasonal changes (Reverdin et al., 1999; Volkov and van Aken, 2003). Stammer (1997) and Isoguchi et al. (1997) showed that after removing the seasonal heating response, the SSH change in the northern North Pacific is governed by

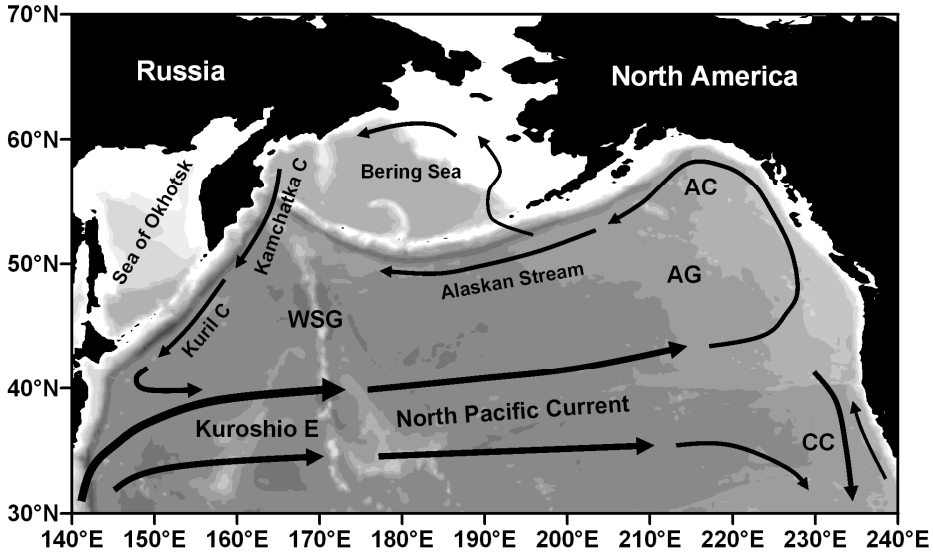

Figure 4.1: *The studied sector of the North Pacific Ocean with bottom topography and schematic surface circulation. Abbreviations: Kuroshio E – Kuroshio extension, CC – California Current, AC – Alaska Current, Kamchatka C – Kamchatka Current, Kuril C – Kuril (Oyashio) Current, WSG – Western Subarctic Gyre, AG – Alaskan Gyre.*

Sverdrup dynamics and can be interpreted as the complex response of the ocean to changes in local and/or non-local wind forcing.

Since, with exception of the directly wind-driven Ekman layer, the ocean circulation to the first degree of accuracy is in geostrophic balance, the large-scale variations of sea level reflect variations of mean currents and hence oceanic transports. The main features of the surface circulation in the NA were already described in the Chapter 1 (see Figure 1.6). The surface circulation in the NP is presented in Figure 4.1. Similar to the NA Ocean, it is characterised by the presence of two ocean scale gyres: the anticyclonic subtropical gyre and the cyclonic subpolar gyre. The Kuroshio Current, the East Kamchatka Current and the Kuril Current (also called Oyashio Current) represent the western boundary currents in the NP. The Kuroshio Current separates from the coast of Japan near 35°N, 140°E (Mizuno and White, 1983) and veers east, creating the Kuroshio extension. The latter has been observed as a zonal jet characterized by large-amplitude meanders and vigorous pinched-off eddies (Qiu, 2003). Further east the Kuroshio extension broadens and loses most of its kinetic energy to become the eastward flowing North Pacific Current (NPC) – the analogue of the North Atlantic Current (NAC). The NPC separates the northern part of the subtropical gyre from the southern part of the subpolar gyre. The subpolar gyre consists of the Western Subarctic Gyre (WSG) and the Alaska gyre (AG) (Qiu, 2002; Musgrave et al., 1992; Reed, 1984). In the vicinity of the North American coast the NPC bifurcates, splitting into the southward California Current and the beginning of the Alaska Current. The Alaska Current flows northward along the coastline of the Gulf of Alaska as the eastern limb of the Alaska gyre and after its south-westward turn it is referred as the Alaskan Stream. A part of the Alaskan Stream enters the Bering Sea through the deep passages of the Aleutian Islands and the rest continues west and constitutes the northern limb of the WSG. When the Alaskan Stream reaches the Kamchatka peninsula the flow turns south-westwards and forms the western extremity of the subpolar gyre. It consists of the East Kamchatka Current

and the Kuril Current. The latter turns eastward around 42°N, east of Hokkaido (Favorite et al., 1976), to merge with the Kuroshio extension and NPC.

In general it can be expected that due to similar forcing mechanisms the magnitude and pattern of the sea level change in the NP are comparable to that in the NA. However, specific geographic and oceanographic conditions may impose differences on the pattern and magnitude of the variability on different time scales. The main geographic and oceanographic differences between the NP and the NA oceans can be listed as follows:

1. The NP is approximately twice as large as the NA. Therefore, the natural time scales of the variability in the NP are longer than in the NA because it takes more time for a signal to propagate across the ocean. The coastal configuration and the bottom relief in the NP are more uniform compared to the NA, where the ocean basin is almost in the middle divided in two parts by the Mid-Atlantic Ridge.
2. In contrast to the NA, the NP Ocean does not have a broad connection with the Arctic Ocean and the exchange between two basins through the shallow Bering Strait is very small. The open connection of the NA with the Arctic Ocean allows an almost unlimited exchange of water masses: warmer and saltier water masses of the NA penetrate deep into the Arctic and on the other hand the northern NA is supplied by the fresher and colder Arctic water.
3. The terrestrial fresh water influx into the NP is much less than in the NA, because the latter is subjected to a bigger river discharge (including arctic rivers) and land ice melting (in Greenland).
4. The NP does not have such subtropical marginal seas like the Mediterranean, which is a source of the saline Mediterranean Sea Water in the NA.
5. The thermohaline forcing in the NP is much simpler than in the NA because there are no deep water sources and the intermediate water sources are weak. Thus the NP is actively ventilated from the north to no more than 2000 metres depth, which coincides with the depth of the wind-driven circulation. Circulation below must be thermohaline, with the source of deep water in the Southern Ocean.

4.1 Observational results

As was done in the previous chapter for the northern NA, the parameters of each investigated signal in the investigated sectors of the NA and NP were estimated at every grid point of the gridded sea level anomaly (SLA) data. The data were low-pass filtered by a moving average with a window equal to 1 year to extract the inter-annual variations. The seasonal change (annual cycle) was approximated by a harmonic sine function. The amplitude and phase of the seasonal change were evaluated by a least squares technique. The mesoscale variability was attributed to residual signals after the inter-annual and seasonal SLA variability has been subtracted from the original SLA data. The magnitude and pattern are characterised by the spatial distribution of amplitude, phase and determination coefficient for the seasonal change, and by the spatial distribution of the root-mean-square (RMS) value and determination coefficient for the mesoscale and inter-annual variability.

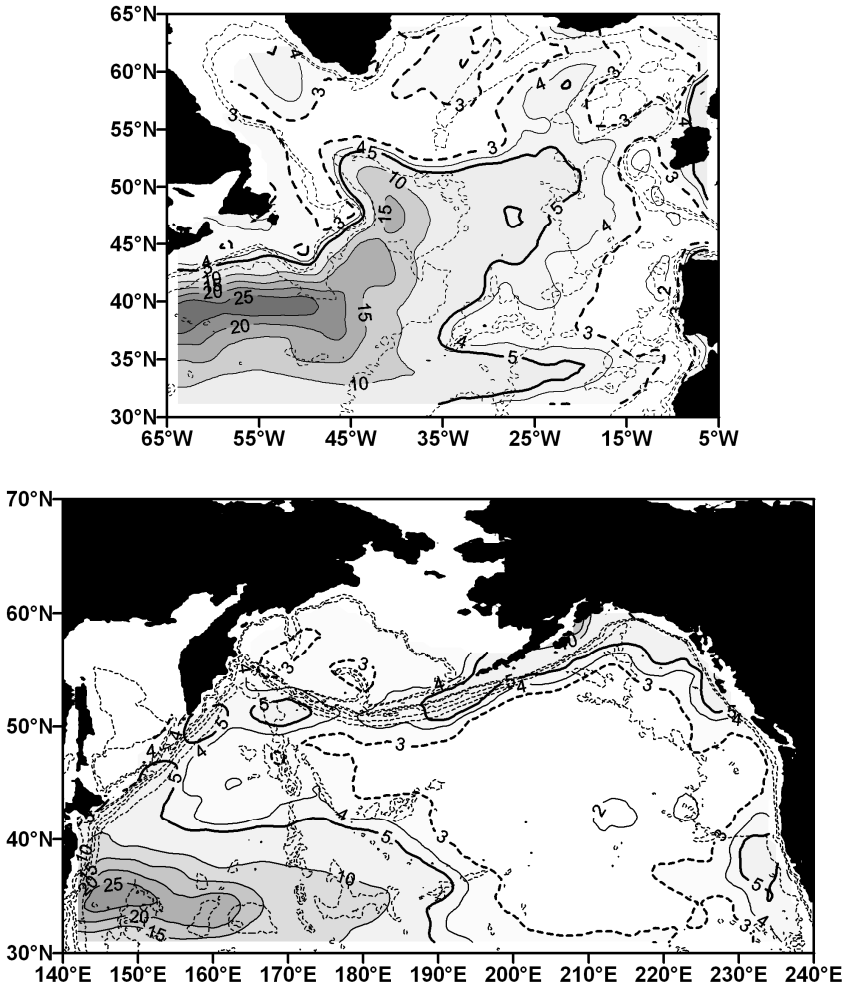

Figure 4.2: *Root-mean-square (cm) of the mesoscale sea surface height variability in the North Atlantic Ocean (top panel) and in the North Pacific Ocean (bottom panel). The bottom topography (dotted lines) is shown at 1000, 2000 4000 and 6000 m.*

Mesoscale variability

The RMS (cm) estimates of the mesoscale variability in the NA and in the NP are shown in Figure 4.2. Since the mesoscale variability is basically associated with eddies, which are mainly generated by barotropic and baroclinic instabilities of currents, the distribution of RMS in both oceans depicts the general pattern of the stronger currents in the surface circulation.

Figure 4.2 (top panel) shows that highest RMS estimates in the NA (over 25 cm) are located in the Gulf Stream extension area. The North Atlantic Current (NAC) and the Azores Current are well outlined by the distribution of RMS, which varies between 5 and 20 cm. In the north-eastern North Atlantic, the branches of the NAC in the Iceland Basin and Rockall Channel are outlined by RMS 3-4 cm. Local maxima of the mesoscale variability in the NA are observed in the Irminger Basin (RMS>3cm) and in the Labrador Sea (RMS>4 cm). The highest RMS of the mesoscale variability in the NP (Figure 4.2, bottom panel), similar to the NA, exceeds 25 cm and is located in the area of the Kuroshio extension. Thus the magnitude of the mesoscale change in both oceans in the areas of the

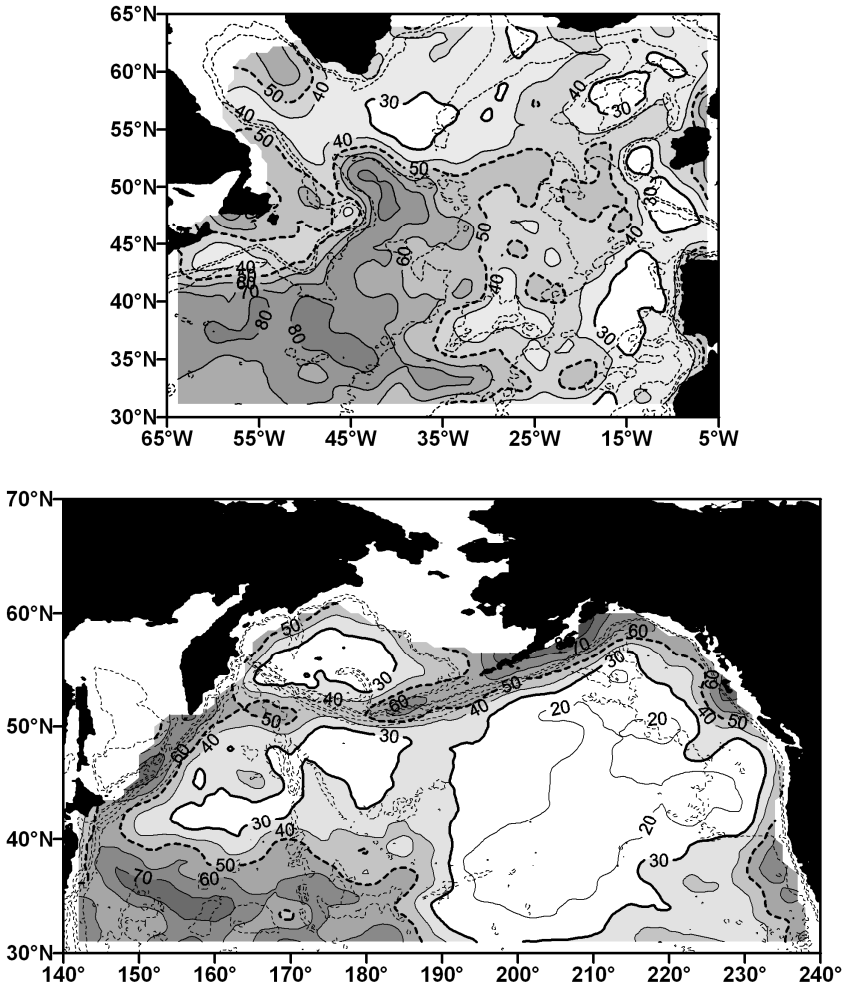

Figure 4.3: *Amount of variance (%) explained by the mesoscale sea surface height variability in the North Atlantic Ocean (top panel) and in the North Pacific Ocean (bottom panel). Bottom topography (dotted lines) is drawn at 1000, 2000, 4000 and 6000 m.*

western boundary currents is comparable. In the western NP where the North Pacific Current flows eastwards, the RMS of the mesoscale variability varies from 3 to 15 cm. These estimates are similar to those observed in the NA. However, in the NA there are two currents characterised by such estimates: the north-eastward NAC and the eastward Azores Current. The existence of these two well-defined current cores is probably related to the open connection with the Arctic Ocean, which allows a divergence of the main eastward currents of the subtropical and subpolar gyres. Due to the geographic northern boundary in the NP, a large north-eastward extension of the subtropical gyre is not possible. Therefore, the eastward circulation in the NP does not diverge into the separate current branches. In the eastern NP, relatively large mesoscale variability (RMS>5 cm) is associated with the California Current flowing south along the North American coast.

Nothing similar is observed in the eastern NA where most of the mesoscale variability is related to the north-eastward drift of the NAC and to the eastward flow of the Azores Current. The mesoscale variability in the subpolar gyres of both oceans also exhibits differences determined by the differences in the surface circulation pattern, which is mainly wind-driven, but transformed according to the coastal configuration and bottom relief.

To estimate the relative contribution of the mesoscale variability into the total SSH variance the determination coefficient was computed as a ratio between the variances of the mesoscale SLA and unfiltered SLA data (Figure 4.3). The mesoscale variability explains over 50% of total variance in the areas of strong currents. In the NA these are the Gulf Stream extension, in the North Atlantic Current, the Azores Current and West Greenland Current (Figure 4.3, top panel). In the NP most of variance explained by the mesoscale variability is associated with the Kuroshio extension, North Pacific Current, California Current, Alaska Current and Alaskan Stream, and with the Kuril Current (Figure 4.3, bottom panel). In contrast to the NA, in the eastern NP there is a large area with very small contribution of the mesoscale signal to the total variability of sea level (<20%). In the centre of the WSG and in the Bering Sea the mesoscale variability also explains less than 30% of total variance. In the NA, the contribution of the mesoscale variability is less than 30% only in the eastern alongshore areas and in the southern section of the subpolar gyre, just north of the Subarctic Front. Apparently the mesoscale variability is overall more dominant in the NA than in the NP Ocean.

To study the temporal change in the mesoscale activity, the RMS value of the mesoscale SLA, calculated with a moving window of approximately 3 months (13 weeks), was estimated. This allowed revealing the seasonal change in the mesoscale activity, mainly induced by the seasonally varying winds. Prior to this operation, the mesoscale SLA was high pass filtered so that signals with quasi-annual periodicity were also filtered out and only signals with periods less than 203 days (29 weeks) remained.

Figure 4.4 shows the moving RMS of the mesoscale SLA averaged over nearly equal areas in the Gulf Stream extension (45°W-65°W, 32°N-42°N) and in the Kuroshio extension (140°-160°, 30°N-40°N) (top panel) , in the North Atlantic Current (25°W-45°W, 40°N-50°N) and in the North Pacific Current (170°-190°, 30°N-40°N) (bottom panel). The time interval when there are no merged TPJ+ERS data available is shaded. The T/P data alone underestimate the mesoscale variability compared to the merged data (Ducet et al., 2000). One can identify seasonal and inter-annual change of the mesoscale activity from the moving RMS (Figure 4.4). The annual maximum of the mesoscale activity occurs predominantly in late summer – autumn months, although some peaks can also be seen in winter. A remarkable feature is that in the Gulf Stream extension the seasonal change of the mesoscale variability is more pronounced than in the Kuroshio extension. This suggests that in the former the mesoscale activity is probably more dependent upon the seasonal variation in the wind stress than in the latter. The maximum mesoscale activity in the Gulf Stream extension was observed in 1997-1998 followed by a decline that reached its minimum in winter 2000/2001. The mesoscale activity in the Gulf Stream extension almost returned to its 1997-1998 level in 2002. In the Kuroshio extension the mesoscale activity was slowly declining from 1995 to the middle of 2000, then peaked in autumn 2001 and decreased again at the end of 2002 (Figure 4.4, top panel). In the NAC, the mesoscale activity was decreasing from 1995 to the winter of 1999/2000 and then started to increase reaching its peak value in the summer of 2002. At the same time, the mesoscale activity was rising from 1996 to a maximum value in the summer of 2001 in the NPC (Figure 4.4, bottom panel).

The temporal change of the RMS of the SLA in other, less energetic, areas of the NA and NP (Figure 4.5) showed different peculiarities at seasonal and inter-annual time scales. In the Iceland Basin (Figure 4.5, a) the RMS value varied within a 1.5 cm range, which

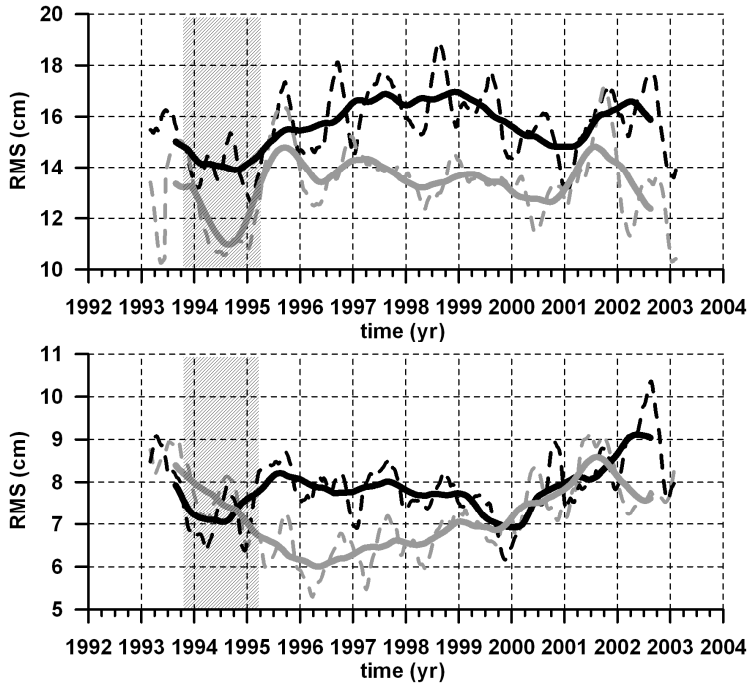

Figure 4.4: *Moving RMS of the mesoscale SLA (cm) with a 3-months window (dashed curves) and a 1-year window (solid curves). Top graph shows the moving RMS averaged in the Gulf Stream extension, 45°W-65°W, 32°N-42°N, (black curves) and in the Kuroshio extension, 140°-160°, 30°N-40°N (grey curves). Bottom graph presents the moving RMS averaged in the North Atlantic Current, 25°W-45°W, 40°N-50°N, (black curves) and in the North Pacific Current, 170°-190°, 30°N-40°N, (grey curves). The time interval, for which there are no merged T/P+ERS data and T/P alone data are used, is shaded.*

constituted 30-40% of the average RMS value (~4 cm) of the mesoscale variability. Maxima RMS values occurred predominantly at the end of autumn and beginning of spring. The inter-annual change of the mesoscale activity here was confined within 1 cm range of RMS and characterised by two depressions in 1996 and in 2001. In the Irminger Basin (Figure 4.5, b) the mesoscale activity had an obvious seasonality with significant intensification in the winter period. The range of the seasonal variations of the RMS value constituted more than 50% of the area average RMS. The variability of the mesoscale activity in the Labrador Sea (Figure 4.5, c) was intensive between 1993 and 1999 and relatively weak starting from the end of 1999 to 2003. The peaks of RMS values in the Labrador Sea appeared to be seasonally modulated with high values occurring mainly in winter.

The seasonal change of the mesoscale activity in the California Current had a range of about 1.5 cm RMS (Figure 4.5, d). The seasonality in mesoscale activity was characterised by intensification in autumn. This compares well with the seasonal change of eddy kinetic energy documented by Kelly et al. (Kelly et al., 1998). The maximum RMS value was observed in autumn 1997 (Figure 4.5, d). The seasonal variation of the mesoscale activity in the Alaska gyre appeared to be more pronounced between 1993 and 1998 than between 1998 and 2003. The strongest peaks were observed in the winters of 1994/1995 and 1997/1998 (Figure 4.5, e). The seasonal change in the mesoscale activity was also well expressed in the WSG with maxima in the winter season, while the inter-annual variation was small (Figure 4.5, f).

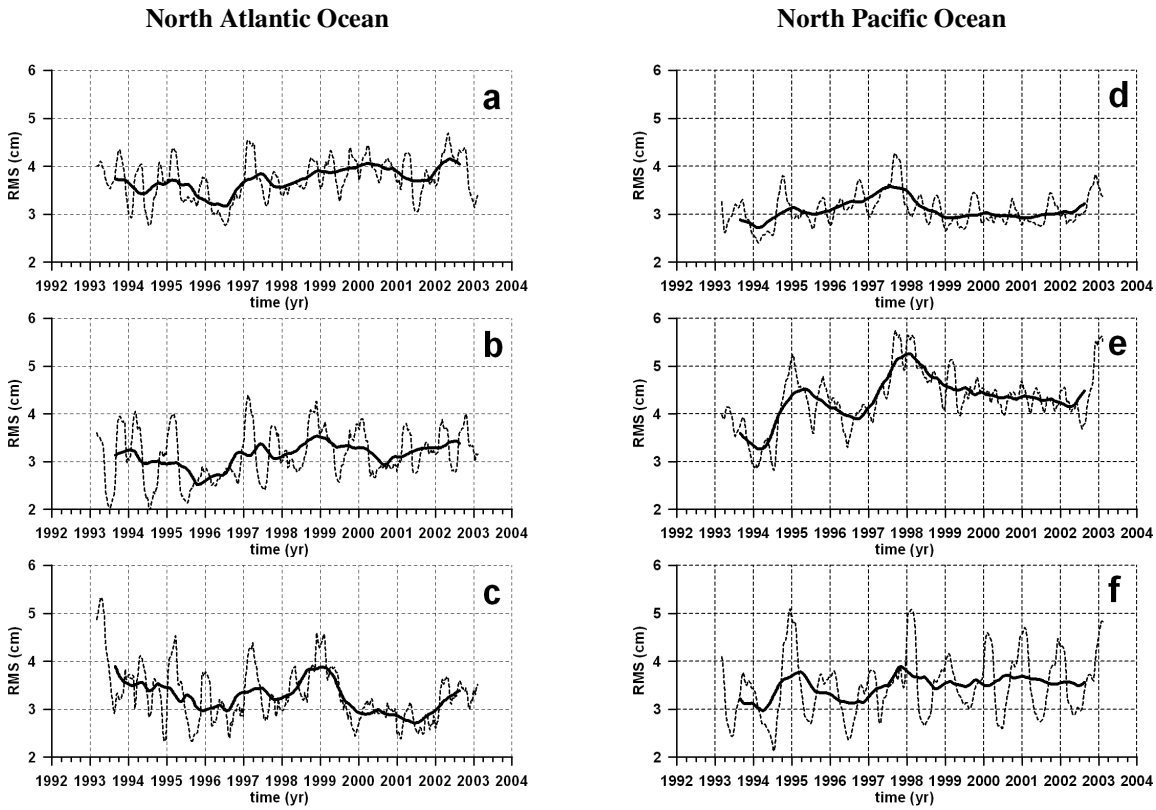

Figure 4.5: *Moving RMS of the mesoscale SLA (cm) with a 3-months window (dashed curves) and a 1-year window (solid curves), averaged over 20°W-30°W, 55°N-60°N in the Iceland Basin (a), over 30°W-40°W, 57°N-62°N in the Irminger Basin (b), over 47°W-55°W, 55°N-60°N in the Labrador Sea (c), over 220°-240°, 30°N-45°N in the Californian Current (d), over 205°-225°, 50°N-60°N in the Alaskan Gyre (e), and over 155°-180°, 45°N-55°N in the Western Subarctic Gyre (f).*

Seasonal change

The seasonal change (annual cycle) of sea level is mainly caused by the steric response to the seasonal variations of heat and fresh water fluxes. In the previous chapter it was shown that in the northern North Atlantic Ocean the contribution of advection to the seasonal variations of sea level may also be important (see also Volkov and van Aken, 2003; Reverdin et al., 1999).

To visualise the seasonal change of the sea level in the North Atlantic and North Pacific, the SLA data were averaged over the calendar seasons (DJF, MAM, JJA, and SON) of all available years (Plate 4.1). The maximum and minimum seasonal sea level in both oceans indeed is mainly associated with maximal thermal expansion of the sea water in autumn (SON) and contraction in spring (MAM).

The seasonal change of SLA also contains information about the seasonal change of geostrophic surface circulation. Therefore, geostrophic velocity anomalies were also estimated from the SLA data (arrows in Plate 4.1). In the NA Ocean the strongest seasonal variations of geostrophic velocities were found in the Gulf Stream extension and in the North Atlantic Current area (Plate 4.1). In the NP Ocean the strongest variations of geostrophic velocities were observed in the Kuroshio extension and in the NPC area and

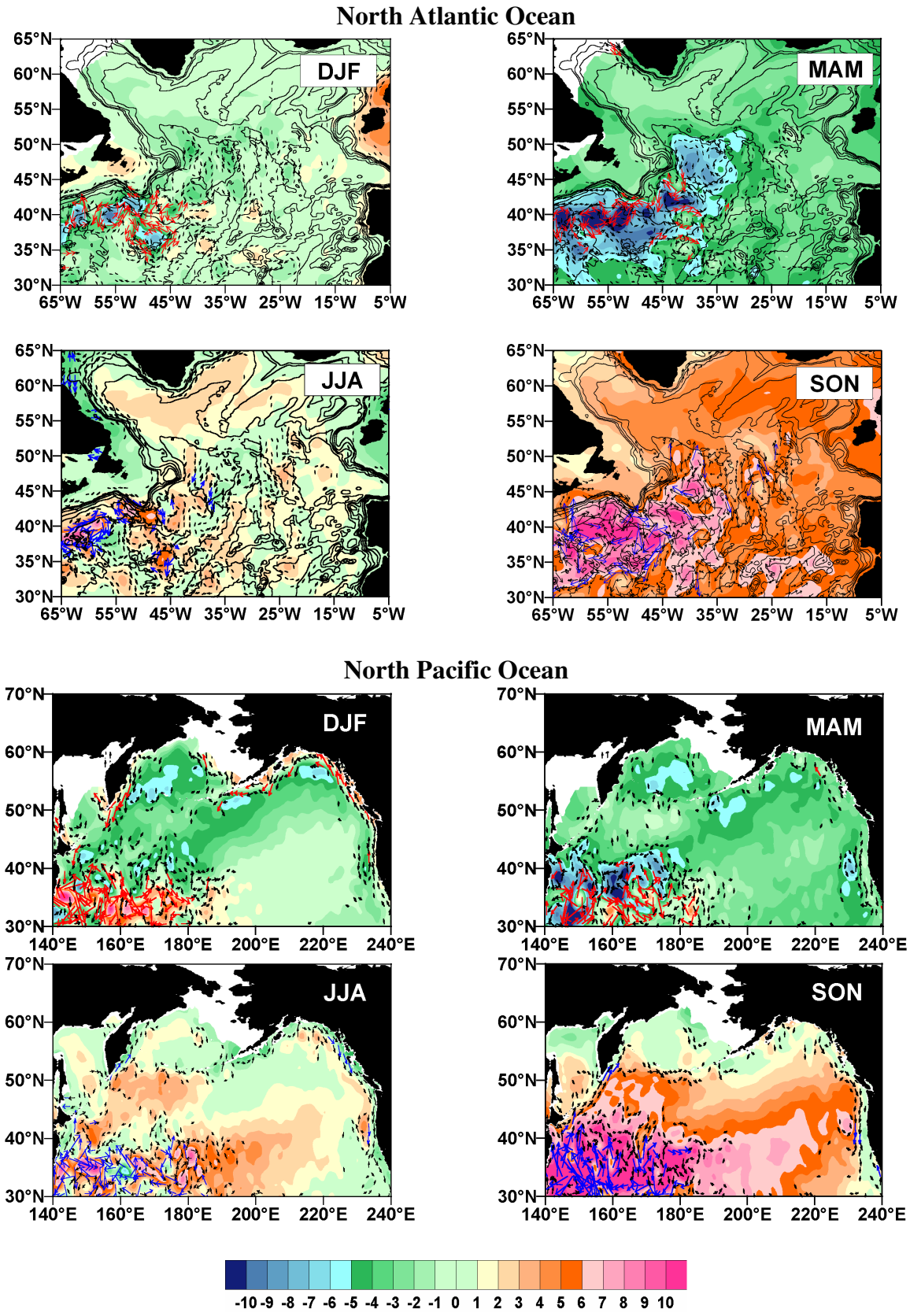

Plate 4.1: *Seasonally averaged SLA data (cm). DJF - winter, MAM - spring, JJA - summer, and SON - autumn. Arrows denote geostrophic velocity anomalies higher than 1 cm/s. The geostrophic velocity anomalies exceeding 3 cm/s are shown by red/blue arrows.*

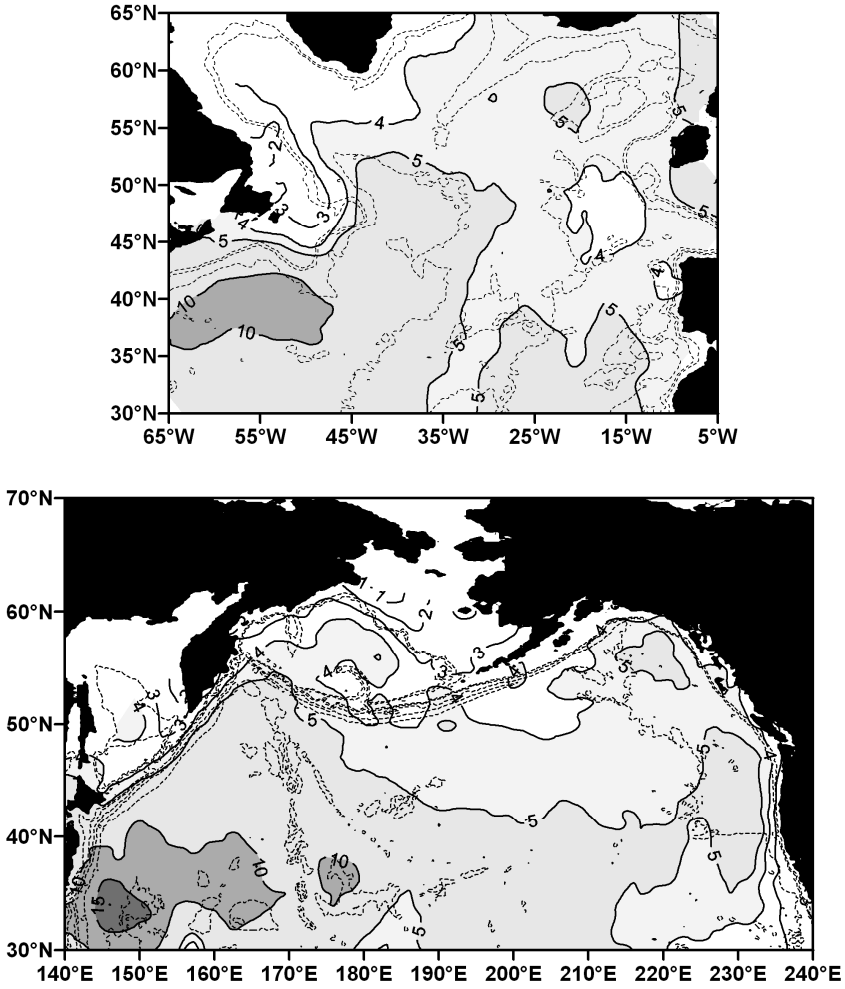

Figure 4.6: *Amplitude (cm) of the seasonal sea surface height change in the North Atlantic Ocean (top panel) and in the North Pacific Ocean (bottom panel). The bottom topography (dotted lines) is shown at 1000, 2000 4000 and 6000 m.*

and significant variations took place along the weaker California, Alaska, Kamchatka and Kuril currents (Plate 4.1). Although the seasonal variations of the position of the western boundary currents are biased by meandering and eddy dynamics, the spatial distribution of the seasonal SLA indicated that the seasonal variability in both the Gulf Stream and the Kuroshio extensions is characterised by meridional displacements of the Subarctic Front and the associated frontal jets. As suggested by the seasonal geostrophic velocity anomalies, the cores of the Gulf Stream and the Kuroshio extensions are possibly at their southernmost positions in spring (MAM) followed by a northward shift reaching extreme northern positions in autumn (SON). This agrees well with the findings of Kelly and Gille (1990) and Kelly et al. (1999) for the Gulf Stream. Kelly and Gille (1990) showed that the Gulf Stream core is situated north of its mean position in the late autumn when the surface transport is maximum, and south of its mean position in the late spring when the surface transport is minimum.

Unlike the NA Ocean, where the seasonal variations of geostrophic flow was mainly observed in the Gulf Stream and the NAC, in the NP Ocean, significant seasonal variability was also observed in the California, Alaska, Kamchatka and Kuril currents. As suggested

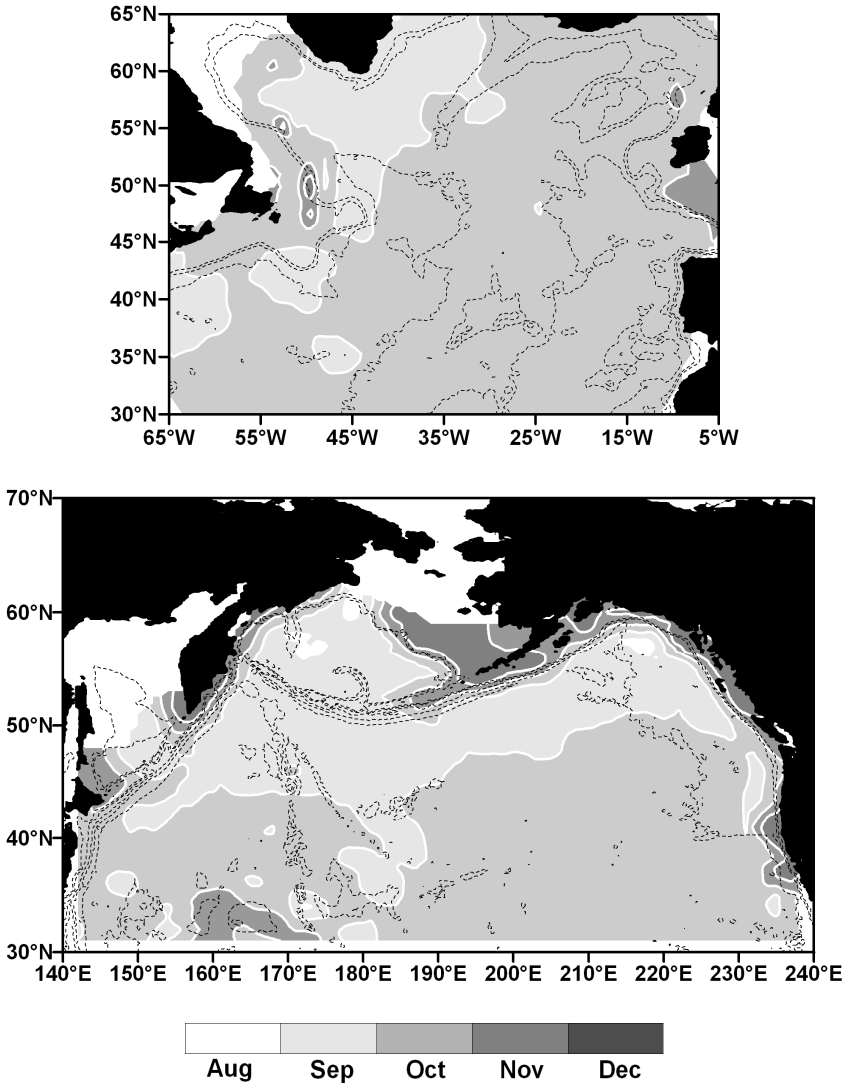

Figure 4.7: *Phase (month of the annual maximum) of the seasonal sea surface height change in the North Atlantic Ocean (top panel) and in the North Pacific Ocean (bottom panel). The bottom topography (dotted lines) is shown at 1000, 2000 4000 and 6000 m.*

by the sea surface slope and geostrophic velocity anomalies (Plate 4.1), the California Current is intensified during autumn (SON) - the season when eddy kinetic energy is maximum (Kelly et al., 1998), and reduced in spring-summer. The Alaska, Kamchatka and Kuril currents appear to be strengthened in winter (DJF) and decelerated in summer (JJA). The seasonal intensification of the California, Alaska, Kamchatka and Kuril currents coincided with maxima in the seasonal mesoscale activity (see Figure 4.5 d, e, and f), described in the previous section. This suggests a connection between the intensity of a flow and associated mesoscale processes, such as meandering and generation of eddies.

The seasonal change of sea level was approximated at each grid point of SLA data (x, y) by a sine function $\zeta_S(x,y,t) = A(x,y) \cdot \sin\left[2 \cdot \pi \cdot \omega \cdot t + \varphi(x,y)\right]$ with a defined frequency ω=1 cycle/year. The amplitude $A(x,y)$ and phase $\varphi(x,y)$ of the seasonal change for the NA and NP are shown in Figures 4.6 and 4.7 correspondingly. For the purposes of plotting the amplitude values were smoothed by a moving average over 2.5°×2.5° areas.

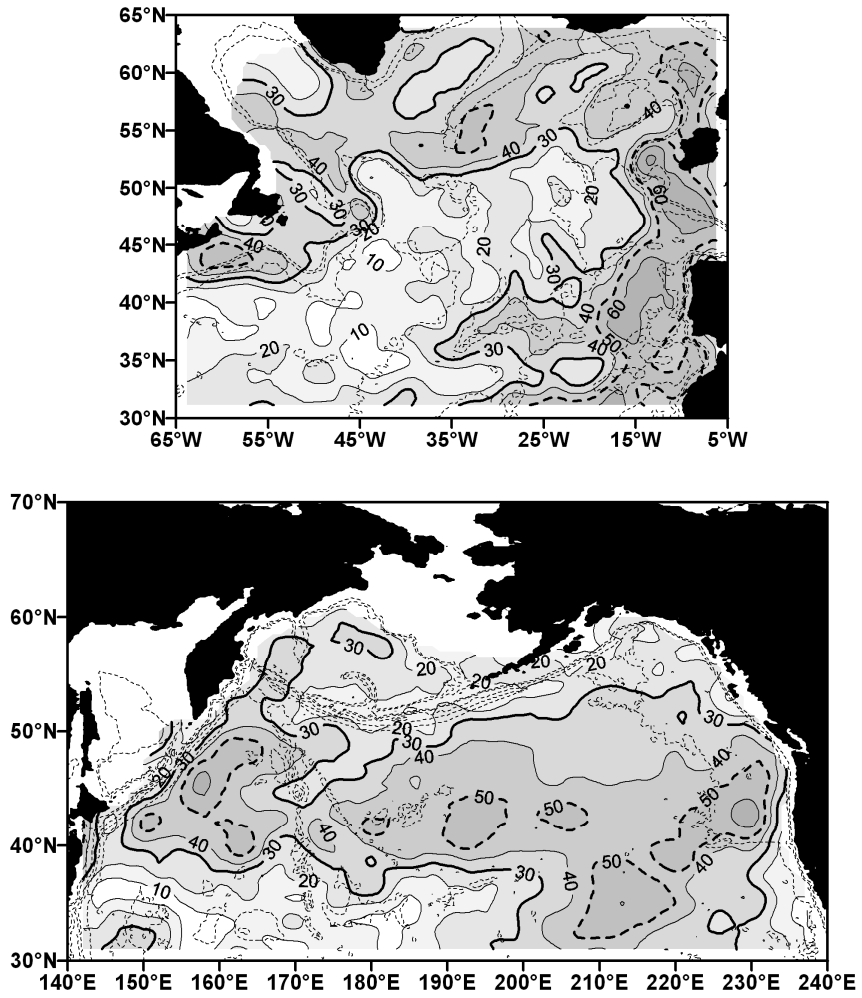

Figure 4.8: *Amount of variance (%) explained by the seasonal sea surface height change in the North Atlantic Ocean (top panel) and in the North Pacific Ocean (bottom panel). Bottom topography (dotted lines) is drawn at 1000, 2000, 4000 and 6000 m.*

The distribution of the amplitude in both oceans appeared to be determined by the features of surface circulation. Maximum amplitudes (over 5 cm) were monitored along the major currents: the Gulf Stream extension, the Kuroshio extension, the NAC and the NPC. In the Kuroshio extension the amplitude of the seasonal sea level change was higher (over 15 cm) than in the considered part of the Gulf Stream extension (over 10 cm). The amplitude of the seasonal SLA in the NAC varied from 4 to 10 cm (Figure 4.6, top panel), whereas in the NPC it varied from 5 to 15 cm (Figure 4.6, bottom panel).

The phase of the seasonal SLA is represented as the month of the annual maximum (Figure 4.7). One can see that in the case of the phase distribution the difference between the NA and the NP is remarkable. In the NP, the phase is distributed mainly zonally (Figure 4.7, bottom panel): the annual maximum of SLA occurs predominantly in October in the southern sector associated with the northern part of the subtropical gyre (south of ~45°N) and in September in the subpolar regions (Alaska gyre and Northwestern Gyre). In the NA, the annual maximum SLA occurs in September mainly in the northwest, the Irminger Basin and the Labrador Sea, and also in the Gulf Stream extension (Figure 4.7, top panel).

The distribution of the determination coefficient of the seasonal change of SLA in both oceans is shown in Figure 4.8. The seasonal variability of SLA explains less than 30% of total variance in the dynamically active areas of major currents where the variability is dominated by the mesoscale processes. In the subpolar regions the determination coefficient of the seasonal SLA is over 30%, sometimes exceeding 50%. In the subpolar NA the highest determination coefficient is observed in the western part of the Iceland Basin, over the Reykjanes Ridge and Rockall Plateau. The seasonal change explains relatively little variance in the centre of the Irminger Basin (less than 30%), where its contribution is comparable to the contribution of the mesoscale variability. In the moderate latitudes of the NP (between about 40 and 50°N) the seasonal change of SLA constitutes over 40-50% of the total variance. A low determination coefficient for the seasonal SLA is observed in the Bering Sea (20-30%). The seasonal signal appeared to be dominant in the eastern areas of the NA (Figure 4.8, top panel), over and next to the continental shelves of Europe and Africa (determination coefficient exceeds 60%). In the eastern NP the seasonal signal is also dominant besides the area in the vicinity of California, where the mesoscale variability of the California Current suppresses other signals (Figure 4.8, bottom panel).

Inter-annual variability

The high resolution gridded data set used in this work is very sensitive to the variations of sea level caused by eddies. This was not a big problem in the northern North Atlantic (Chapter 3), where the variability of sea level is not governed by eddy activity. However, in the dynamically active areas, such as the Gulf Stream and the Kuroshio extensions, the NAC and the NPC, the high frequency variations of sea level may bias the inter-annual signal. This may occur when there are somewhat larger eddies in one year compared to another or the ratio of anticyclonic and cyclonic eddies is different. To reduce the error, a spatial moving average filtering of the SLA data over 5° by 5° squares was applied. Then yearly averages were estimated to visualize the inter-annual change of SLA from 1993 to 2002 (Plates 4.2 and 4.3). One can see that this procedure eliminated most of eddy-like and left only large-scale features in the yearly SLA maps.

It is possible to distinguish the difference between the SLA change in the subpolar and subtropical gyres of the NA and NP. Lowest sea level in the subpolar gyre of the NA (Plate 4.2) was observed in 1994. Then the sea level started to rise until it reached its maximum in 1997-1998 in the Iceland and Irminger Basins and in 1999 in the Labrador Sea. The decrease of the sea level within the subpolar gyre of the NA in 1999 and 2000 was followed by another rise from 2001 through 2002. The subtropical gyre of the NA manifested a minimum SLA in 1996 – 1997 and 2002, and a maximum in 1999 – 2000. In the NP (Plate 4.3), high SLA values were observed in the Kuroshio extension, NPC and in the Alaska gyre adjoining the regions of low SLA in the WSG and to the south-southeast of the NPC in 1993 – 1994. Then, in 1995 – 1997, SLA decreased in the Kuroshio extension, the NPC and the Alaska gyre, and increased in the Bering Sea and in the California Current. The sea level in the Bering Sea and California Current started to decrease in 1998. At the same time the lowering of the sea level continued in the Alaska gyre and in the northern part of the NPC, while a rise of SLA started in the southern sectors of the Kuroshio extension and NPC. The years from 1999 to 2002 were characterised by high SLA in the Kuroshio extension and NPC, associated with the northern part of the subtropical gyre, high SLA in

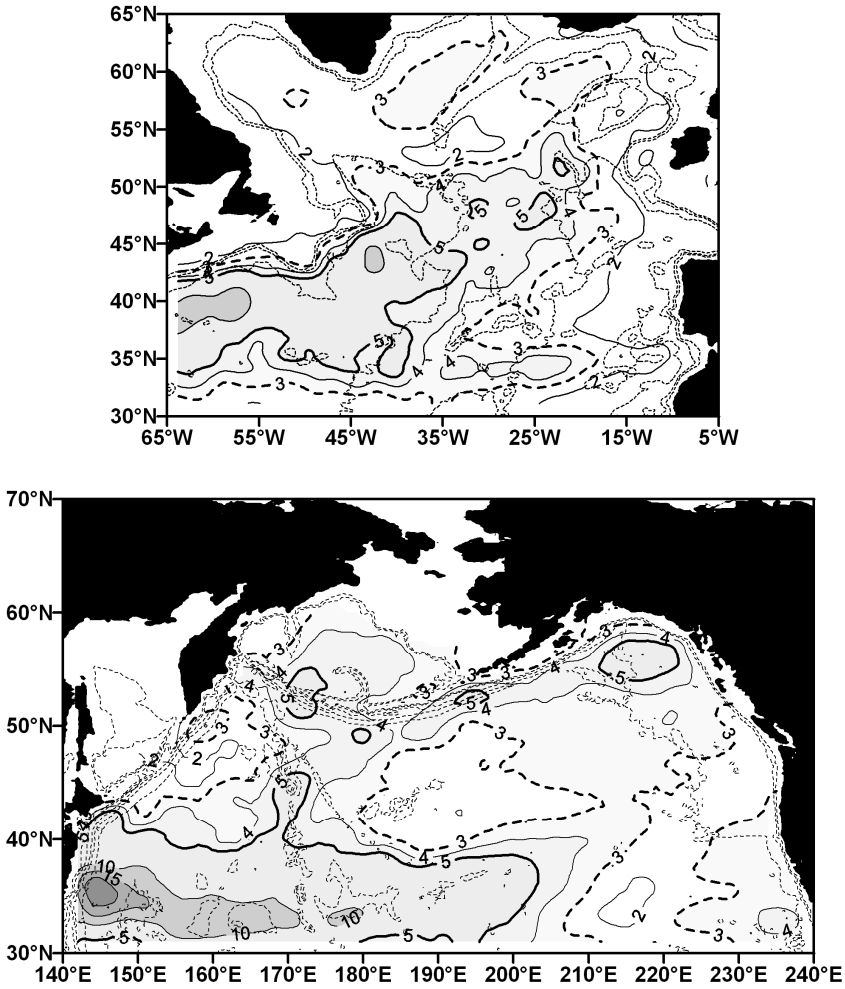

Figure 4.9: *Root-mean-square (cm) of the inter-annual sea surface height variability in the North Atlantic Ocean (top panel) and in the North Pacific Ocean (bottom panel). The bottom topography (dotted lines) is shown at 1000, 2000 4000 and 6000 m.*

the WSG, and low SLA in the Bering Sea, Alaska gyre and California Current.

The yearly averages of SLA also illustrate the most striking features of the inter-annual change of the surface geostrophic circulation (Plates 4.2 and 4.3). The sea surface slopes shown in Plate 4.2 imply that in 1993 – 1994 the Gulf Stream core was located further north than in the following years. At the same time the cyclonic circulation in the Irminger Basin and Labrador Sea was stronger than average. Starting from 1995 and up to 2002 the cyclonic circulation in these areas was slowing down. In 1996 – 1997 the core of the Gulf Stream possibly shifted southward as indicated by a positive SLA centred at about 37°N adjoining a negative SLA at about 40-41°N. The eastward flow associated with the NAC at approximately 45°N was intensified in 1993 – 1995 and especially in 1999 – 2000. As follows from the sea surface slopes in Plate 4.3, in 1993 – 1994 the northern parts of the Kuroshio extension and NPC were intensified and the southern parts were weakened. The Alaska Current at this time was weaker than average as suggested by a positive SLA in the centre of the Alaska gyre. The strength of the Kuroshio extension and the NPC reduced in 1995 – 1997, whereas the intensity of the California Current increased. The Alaskan Current and the Alaskan Stream became stronger in 1997.

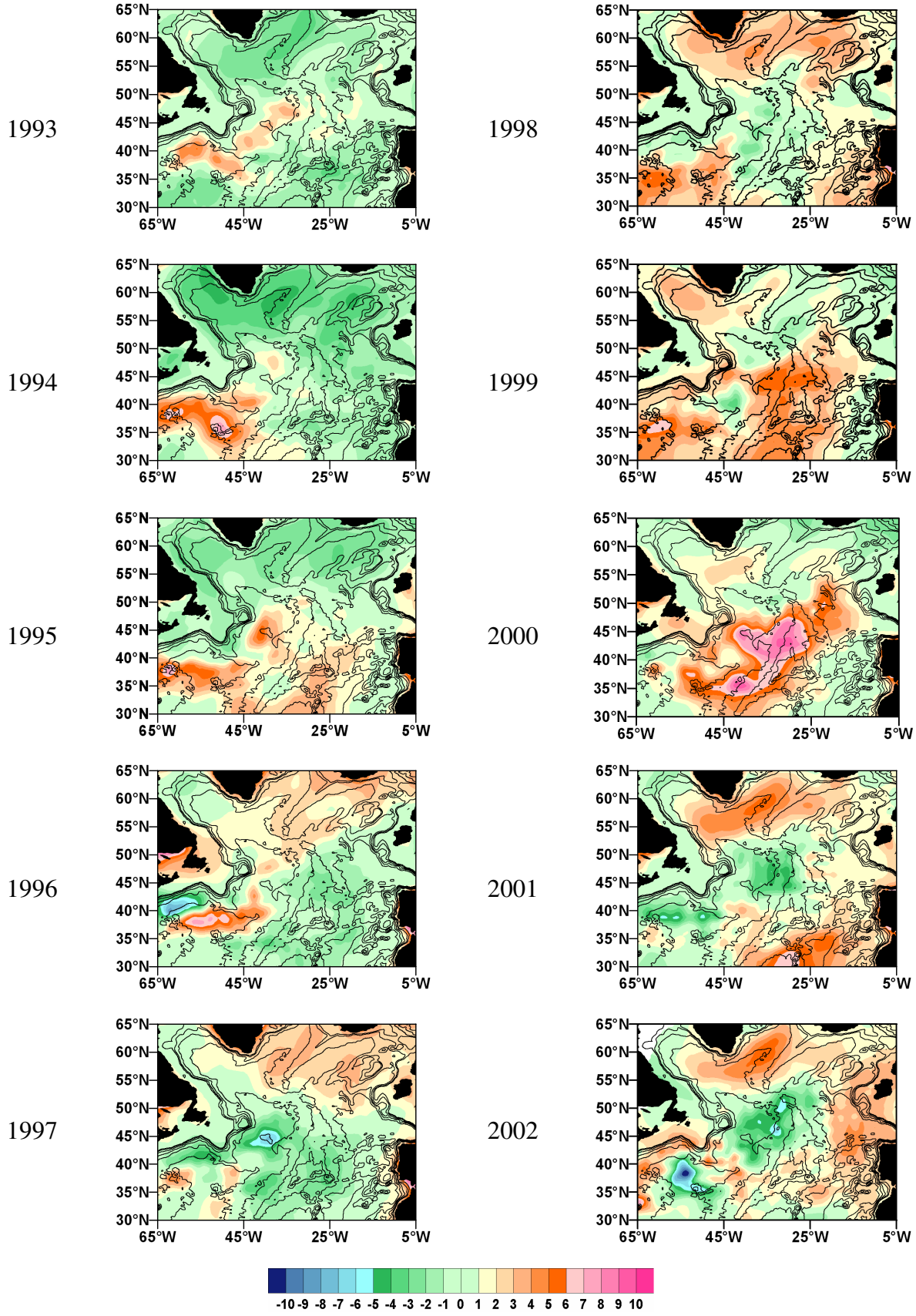

Plate 4.2: *Yearly averaged SLA (cm) in the North Atlantic Ocean. Bottom topography is shown every 1000 m.*

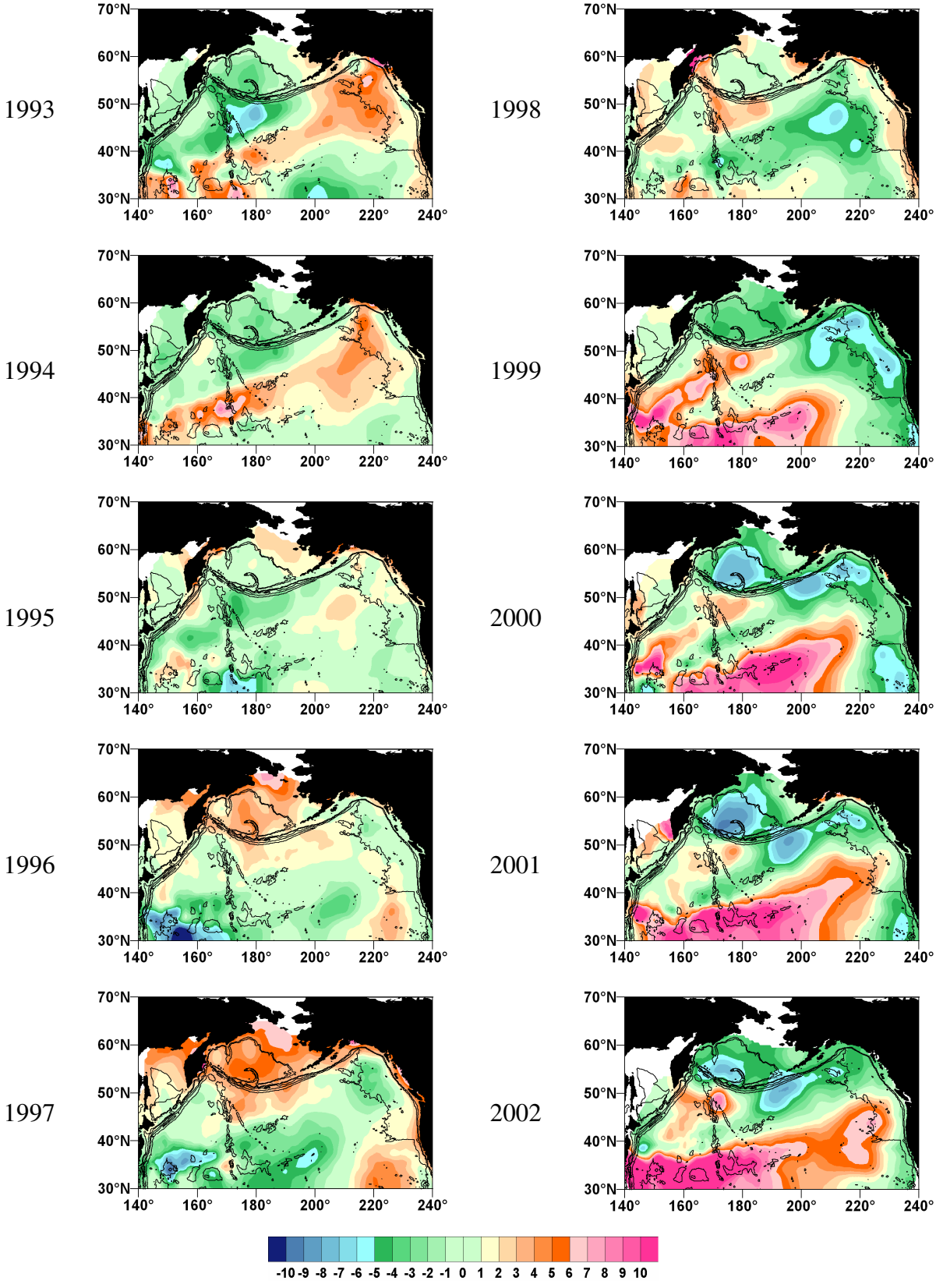

Plate 4.3: *Yearly averaged SLA (cm) in the North Pacific Ocean. Bottom topography is shown every 1000 m.*

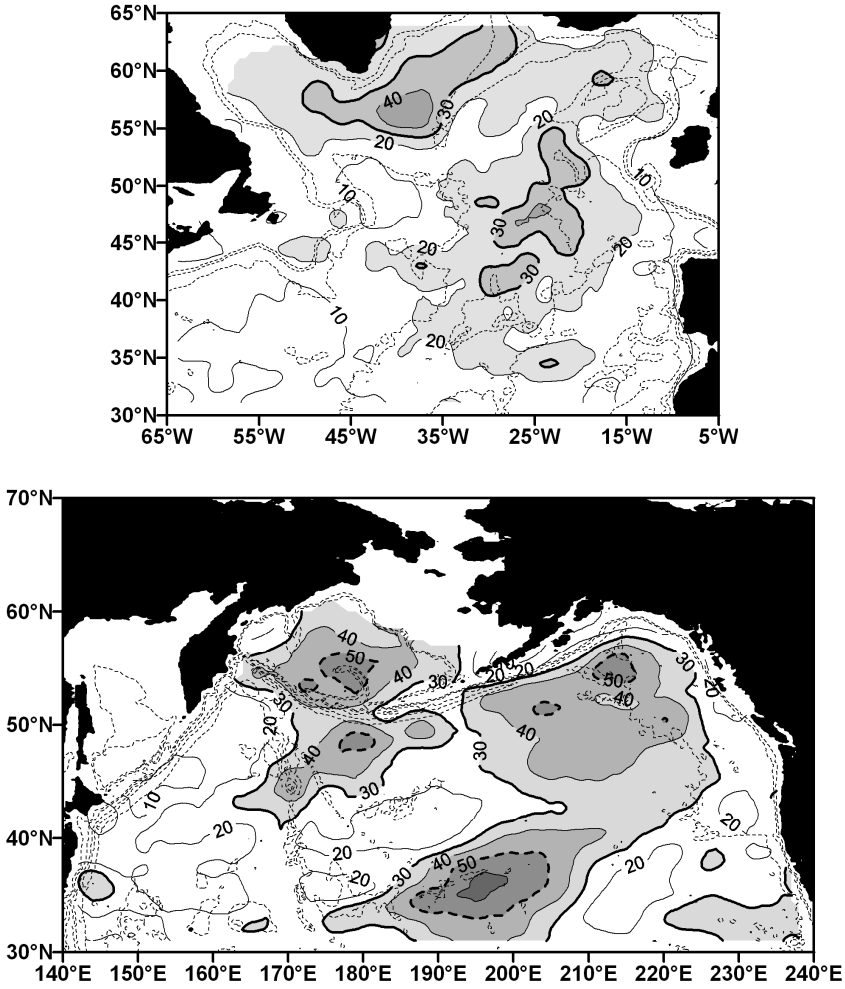

Figure 4.10: *The amount of variance (%) explained by the inter-annual sea surface height variability in the North Atlantic Ocean (top panel) and in the North Pacific Ocean (bottom panel). Bottom topography (dotted lines) is drawn at 1000, 2000, 4000 and 6000 m.*

Starting from 1998 and up to 2002 the intensities of the Kuroshio extension and the NPC were rising possibly accompanied by a gradual northward shift of the current cores. The southward recirculation of the subtropical gyre also increased, eventually facilitating an intensification of the California Current in 2001 – 2002. In 1998 – 2002, an anomalous cyclonic circulation was observed in the Alaska gyre and an anomalous anticyclonic circulation was monitored in the WSG. Starting from 1999 the cyclonic circulation of the Bering Sea intensified reaching a maximum in 2001 and weakened in 2002. As suggested by sea surface slopes there was an increased geostrophic flow into the Bering Sea in 2000 – 2001 originating from the Alaskan Stream.

To estimate the contribution of the inter-annual signal to the total variance, it is necessary to deal with the unfiltered SLA data. To test whether the aliasing of the inter-annual signal (spectral leakage) by individual eddies is important, a yearly moving average of an SLA time series at one grid point in the NAC area (~42°W, 42°N) was compared with a yearly moving average of the same time series but edited by removing several spikes of extreme SLA values associated with eddies. There was no significant difference between the moving averages. Therefore, it seems to be acceptable to estimate the inter-annual

signal by applying a moving average with a window equal to 1 year. The magnitudes and spatial patterns of the inter-annual change of the sea level in the NA and the NP are illustrated in Figures 4.9 and 4.10.

The highest RMS (over 5 cm) of the inter-annual SLA is associated with the Gulf Stream extension and the NAC in the NA (Figure 4.9, top panel), and with the Kuroshio extension and the NPC in the NP (Figure 4.11, bottom panel). The RMS of the inter-annual SLA in the Kuroshio extension (15-20 cm) appear to be higher than that in the Gulf Stream extension (10-15 cm). In the NA, the RMS values are relatively high (over 3 cm) in the Azores Current, in the NAC flowing across the Iceland Basin, and in the Irminger Basin (Figure 4.11, top panel). In the NP, RMS over 5 cm is observed in the Alaska Bay and in the Bering Sea in the vicinity of the Aleutian Islands.

The largest determination coefficient of the inter-annual SLA was observed in the subpolar regions of the NA and the NP, as well as in the eastern halves of the ocean basins: east of the Mid-Atlantic Ridge in the NA and east of the Emperor Seamount Chain and in the Alaska gyre in the NP (Figure 4.10). Thus the spatial pattern observed in the NA is similar to the one in the NP. The determination coefficient of the inter-annual SLA in the NP appeared to be larger than in the NA. In the WSG, the Bering Sea, the Alaska gyre, and in the eastern part of the NPC it varied from 30 to over 50% of the total variance compared to 30-40% in the Irminger Basin and 20-30% in the eastern half of the NA.

Thus it can be summarized that while the spatial patterns of the inter-annual SLA variability in the NA and NP are comparable, the magnitudes are slightly different. As suggested by the RMS values and determination coefficients, the inter-annual SLA signal in the NP is overall more pronounced than in the NA.

4.2 Climate-related change

The forcing mechanism of the seasonal change is quasi-linearly deterministic and depends on the seasonal variations in insolation and ocean-atmosphere interaction. Therefore, the seasonal change has a determined frequency and can be well approximated. The climate-related inter-annual variability, similar to the seasonal change, is also caused by the large-scale variations in ocean-atmosphere interactions. These interactions mainly occur by means of heat and fresh water exchange as well as by means of dynamical forcing (wind stress). However, in contrast to the seasonal change, usually there are no clear linear deterministic mechanisms inducing the climate-related inter-annual variability. Hence, it is possible that the observed inter-annual variability of the sea level can be attributed to the internal variability of the ocean-atmosphere system due to nonlinear physical processes. The latter has been a subject for numerous studies (e.g. Dijkstra, 2000; Nauw, 2003; te Raa, 2003). The Arctic Oscillation/North Atlantic Oscillation (NAO), El Nino/Southern Oscillation (ENSO) and the Pacific Decadal Oscillation (PDO) are referred as the leading modes of the inter-annual variability in the NA and in the NP related to the nonlinear ocean-atmosphere interactions.

The NAO is a dominant mode of the atmospheric processes over the NA Ocean (see Chapter 1), whereas ENSO and PDO refer to the tropical and northern Pacific correspondingly. The PDO term was introduced by Hare (1996) to describe the long-term sea surface temperature (SST) oscillation in the northern Pacific. The PDO phenomenon is

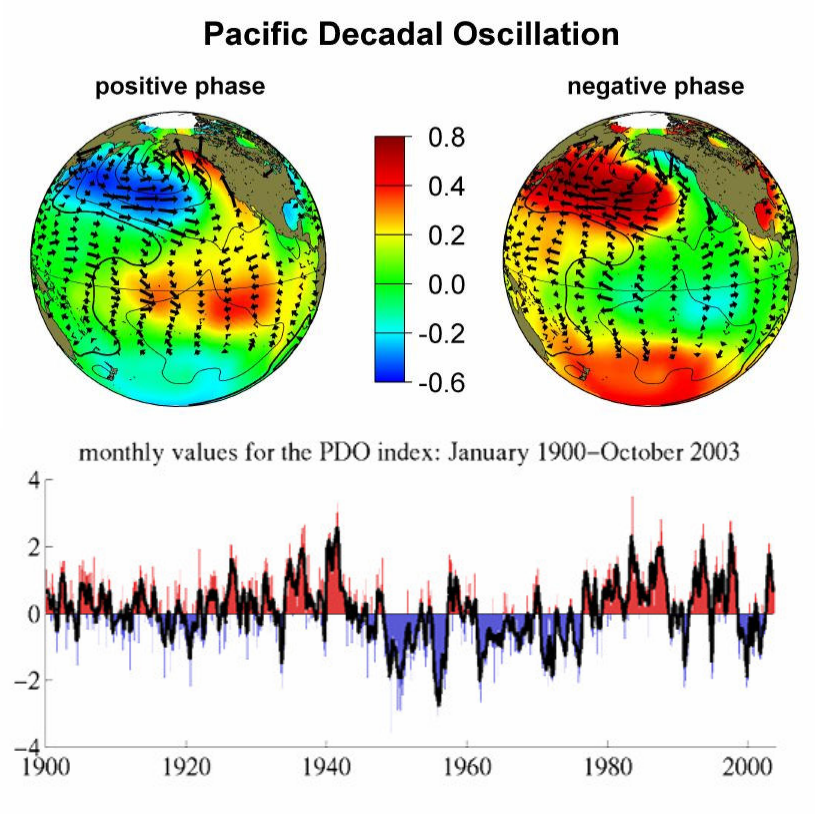

Figure 4.11: *Comparison of sea surface temperature, sea level pressure, and wind stress anomalies in positive versus negative Pacific Decadal Oscillation (PDO) phase (top panel) and monthly values for the PDO index from January 1900 to October 2003 (bottom panel). The figure is borrowed from http://jisao.washington.edu/pdo.*

expressed in terms of the PDO index, which is calculated by spatially averaging the monthly SST of the Pacific Ocean north of 20°N (Mantua, http://jisao.washington.edu/pdo/). The fluctuations of the PDO index from 1900 to the present are shown in Figure 4.11. The positive PDO indices (warm phase) are associated with below normal SSTs in the western and central North Pacific and above normal SSTs along the North America coast. The negative PDO indices (cool phase) correspond to an opposite SSTs distribution. The PDO is often considered as a long-lived El Niño/La Niña-like pattern of climate variability in the Pacific because two oscillations have similar relationships regarding the deviations of SSTs (Zhang et al, 1997). However, PDO events have persisted for 20-30 years (Mantua et al., 1997; Minobe, 1997), while El Niño/La Niña events last typically from 6 to 18 months. Another characteristic distinguishing the PDO from ENSO is that the strongest PDO signal is located in the northern Pacific Ocean, while the strongest ENSO signal is located in the tropical Pacific. Since in this research we are interested in the extratropical parts of the NA and NP, in this section we discuss the connection between the NAO, the PDO, and the inter-annual variability of sea level observed by satellite altimetry.

The Empirical Orthogonal Functions (EOF) analysis was used to identify the dominant modes of the inter-annual sea surface height variability. The advantage of the EOF analysis is that it provides a compact description of the temporal and spatial variability of data in

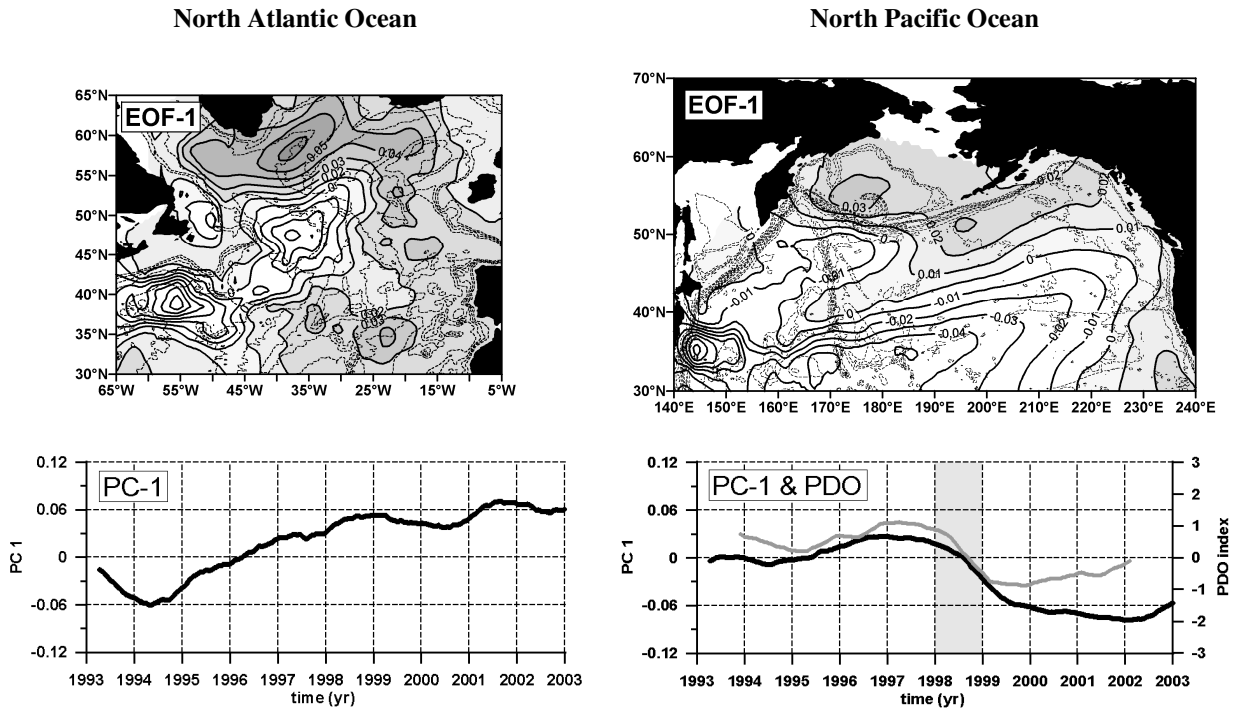

Figure 4.12: *First Empirical Orthogonal Functions (EOF-1) and Principal Components (PC-1) of the inter-annual SLA in the North Atlantic Ocean (left panels) and in the North Pacific Ocean (right panels) explaining 42% and 66% of the total variance respectively. The spacing between contours in the top panels is 0.1. Bottom topography is drawn every 1000 m. The 2-year moving average of the monthly Pacific Decadal Oscillation index is shown together with the PC-1 for the North Pacific Ocean (grey line in the right bottom panel). The period of the PDO phase change is shaded.*

terms of orthogonal functions, or statistical "modes". The dominant modes, usually explaining most of the variance of a spatially distributed series, can be linked to possible dynamical mechanisms. Although no direct or mathematical relationship necessary exists between the statistical EOFs and any related dynamical modes, coupling the dominant modes with other known processes however, can help to understand the forcing mechanisms responsible for a certain pattern of variability. The first empirical modes of the inter-annual SLA data in the NA and NP, described by the spatial (EOF-1) and temporal (PC-1) functions, are shown in Figure 4.12.

The first empirical mode explains 42% of the variance in the NA Ocean and exhibits a dipole pattern of the sea level variability (Figure 4.12, left panels). The EOF-1 and PC-1 suggest that a gradual quasi-linear rise of the sea level from 1993 to 2003 occurred in the subpolar and eastern areas of the studied sector of the NA. At the same time the sea level was decreasing in the Gulf Stream extension and in the NAC area, west of the Mid-Atlantic Ridge. In the NP Ocean, the first empirical mode also displays a dipole pattern of the sea level variability and accounts for 66% of the variance (Figure 4.12, right panels). The EOF-1 and PC-1 indicate that in 1998 there was a reversal between the two centres of the inter-annual variability of sea level: one located in the Kuroshio extension and NPC, and another in the Bering Sea. In 1998, the sea level started to decrease in the Bering Sea, in the areas of the Alaska Current, the Alaskan Stream and the California Current, accompanied by an increase in the northern part of the subtropical gyre (compare with Plate 4.3). Thus the first empirical modes of the inter-annual sea level change in the NA and NP during the decade

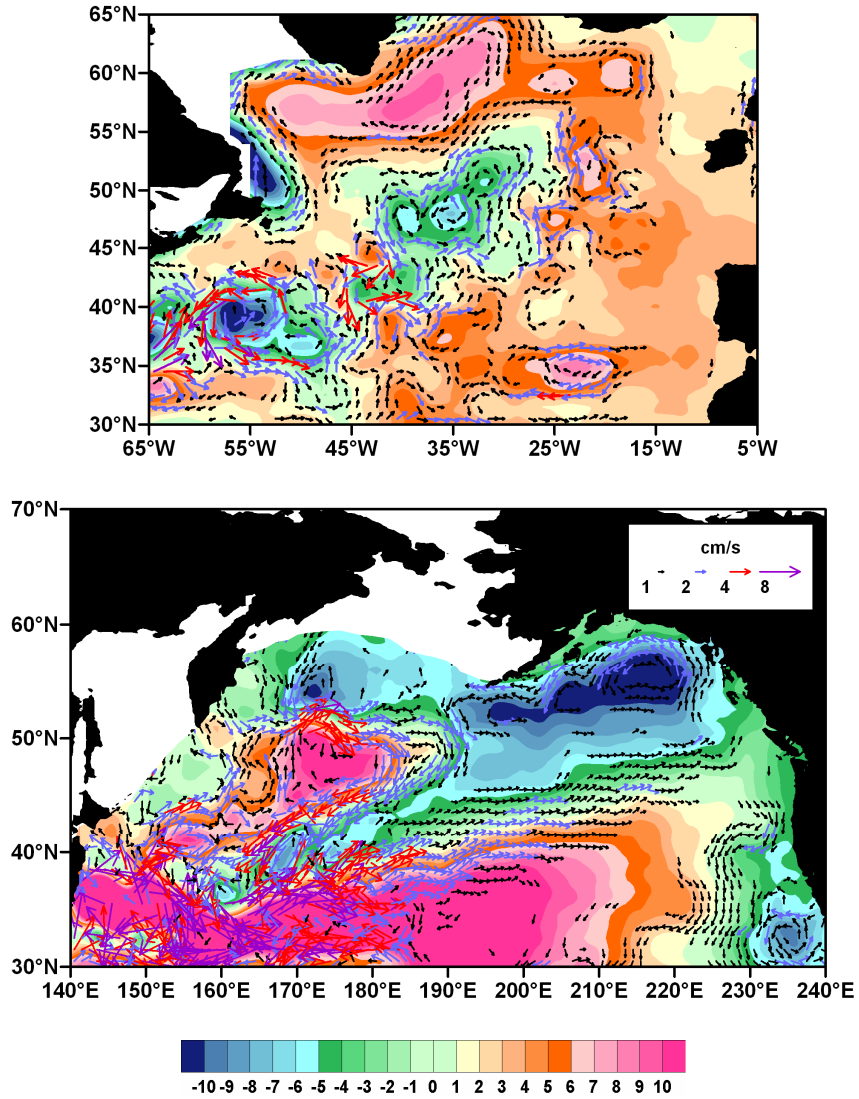

Figure 4.13: *Maps of geographical distribution of sea level trends (cm) and geostrophic velocity anomaly trends (cm/s) over December 1992 – November 2002 in the North Atlantic Ocean (top panel) and in the North Pacific Ocean (bottom panel).*

of 1993-2003 suggest an almost out-of-phase character of the variability in both oceans. While in the subpolar and eastern NA the sea level increased, in the subpolar NP and in the California Current the sea level decreased.

In order to approximate the linear change of sea level during the decade of the TPJ+ERS measurements (December 1992 – November 2002) the linear trends in the SLA data were estimated by regression. The geostrophic velocity anomalies associated with the sea level trends were also computed to demonstrate the corresponding trends in the surface geostrophic circulation. Figure 4.13 illustrates the geographical distribution of the sea level and geostrophic velocity anomaly trends over the investigated time interval in the NA (top panel) and the NP (bottom panel).

The observed decadal changes in the sea level in the NA are substantially different from those in the NP. In the subpolar and eastern areas of the NA the sea level was rising while in the areas of the GS and the NAC it was decreasing. The maximum rise was observed in

the Labrador Sea (over 7 cm) and in the Irminger Basin (about 10 cm). The maximum decrease (10 – 15 cm) occurred in the Gulf Stream extension. A similar spatial pattern of the sea level trends in the NA from 1993 to 1998, computed from the T/P altimetry data and the yearly mean temperature data for the upper 500 m, was obtained by Cabanes et al. (2001). However, on the longer time period from 1955 to 1996, the steric sea level trends for the upper 3000 m estimated by Cabanes et al. (2001), showed that the sea level was decreasing in the subpolar regions and increasing in the subtropical regions of the NA. Thus, taking into account the observed sea level rise in the subpolar regions of the NA during the last decade, it is possible to suggest an existence of inter-decadal gyre-scale variability in the North Atlantic Ocean.

The decadal trends of the geostrophic velocity anomalies in the NA (Figure 4.13, top panel) suggest that the cyclonic circulation in the subpolar gyre (Labrador Sea and Irminger Basin) declined. The decline of the subpolar NA circulation, manifested in altimeter data, direct current-meter observations, and hydrographic data, was also described by Häkkinen and Rhines (2003). The geostrophic currents in the Labrador Sea and Irminger Basin decelerated at the rate of 2 – 3 cm/s (see arrows in Figure 4.13, top panel). A slowdown of the geostrophic velocities also occurred in the NAC and in the Gulf Stream. The northern wall of the NAC associated with the Subarctic Front as well as the NAC flow around the Newfoundland Rise decelerated at the rate of 2 – 4 cm/s. On the other hand the eastward flow of the NAC along 45°N intensified. The geostrophic velocities reduced in the northern part of the Gulf Stream extension (around 40°N), but intensified in the southern part (around 35°N). This suggests a possible southward shift of the Gulf Stream extension core during the last decade. Decadal changes also occurred in the Azores Current. As suggested by the decadal trends in geostrophic velocity anomalies the core of the Azores Current located at 33°N decelerated while intensification took place at the northern boundary of the current. Such a change in the geostrophic flow indicates that the Azores Current shifted northward.

In the NP the decadal increase of the sea level (over 10 cm) was associated with the Kuroshio extension, the NPC and with the WSG. At the same time the sea level lowered in the Bering Sea, Alaska gyre and near the Californian coast (Figure 4.13, bottom panel). Such a decadal trend is well captured by the first empirical mode of the inter-annual SLA (Figure 4.14, right panels). The pattern of the decadal sea level change in the NP from December 1992 to November 2002, shown in Figures 4.12 (right panels) and 4.13 (bottom panel), is almost opposite to that obtained by Cabanes et al. (2001). On the basis of satellite altimetry observations from 1993 to 1998 and the 5-year mean temperature data for 3000 m depth from 1955 to 1996, they showed that the sea level was rising in the subpolar NP and along the North American coast and decreasing in the areas occupied by the Kuroshio Current and the NPC. The difference between the results documented by Cabanes et al. (2001) and obtained in this work suggests that after 1998 there was a drastic change in the NP, which forced the sea level trends to change sign. This change is well portrayed by the PC-1 of the inter-annual SLA in the NP (Figure 4.12, bottom right panel). After 1998 the sea level started to rise in the subtropical gyre and to decrease in the subpolar gyre (compare with Plate 4.3). As follows from Figure 4.12 (bottom right panel), the PC-1 of the inter-annual SLA in the NP is coherent with the yearly moving average of the monthly PDO index for the same time interval. This is not surprising as the sea level is directly dependent upon the SST. Some researches believe that a flip from positive to negative PDO

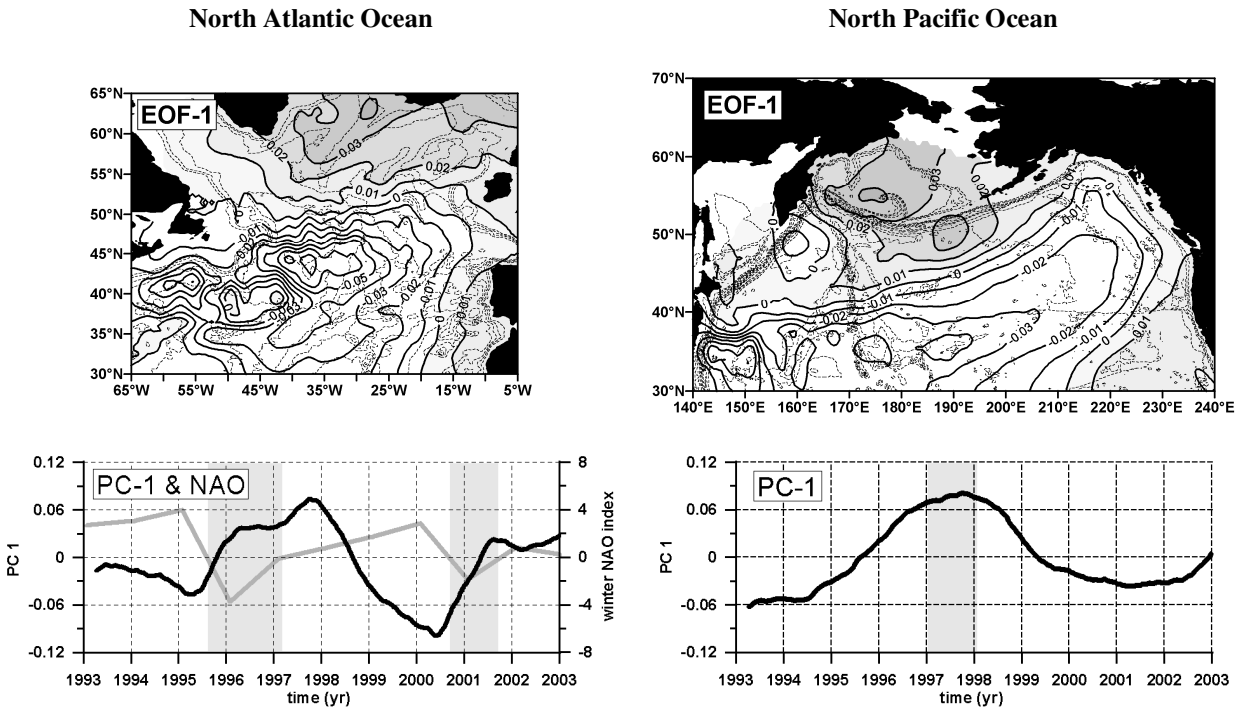

Figure 4.14: *First Empirical Orthogonal Functions (EOF-1) and Principal Components (PC-1) of the detrended inter-annual SLA in the North Atlantic Ocean (left panels) and in the North Pacific Ocean (right panels) explaining 47% and 51% of the total variance respectively. The spacing between contours in the top panels is 0.1. Bottom topography is drawn every 1000 m. The winter (DJF) NAO indices are shown together with the PC-1 for the North Atlantic Ocean (grey line in the left bottom panel). The periods with the negative NAO indices and the period of the 1997-ENSO event are shaded.*

phases may have taken place in 1998, coinciding with the demise of the 1997/1998 El Niño and the beginning of the ongoing La Niña episode (Mantua, 1999). The La Niña events are characterised by the westward propagation of the positive SST anomalies in the tropical Pacific, which are ultimately entrained into the Kuroshio Current and into the NPC. In order to verify whether this flip of the PDO phase really occurred and it was not just a short-term fluctuation caused by a strong 1997/1998 El Niño event we need at least several more years of observations. The positive trends in the sea level in the eastern and subpolar NP and the negative trends in the NP subtropical gyre from 1955 to 1996, estimated by Cabanes et al. (2001), are possibly the result of the PDO-related interdecadal variability. As follows from the variation of the PDO index over the past century (Figure 4.11, bottom panel), the period between 1942-43 and 1976-77 corresponds to the negative (cool) phase and the period between 1976-77 and 1998 corresponds to the positive (warm) phase. Such a sequence of the negative and positive PDO phases would result in positive sea level trends in the subpolar and eastern NP, and negative sea level trends in the NP subtropical gyre.

Figure 4.13 (bottom panel) depicts the decadal trends in geostrophic velocity anomalies associated with the sea level trends in the NP. It is seen that the change, which occurred in 1998, induced a strong intensification of the geostrophic flow of the Kuroshio extension at around 35°N at the rate of about 10 cm/s and a 2 – 8 cm/s increase of geostrophic velocities in the NPC. The cyclonic circulation in the Alaska gyre intensified and the geostrophic velocities in the Alaska Current increased by about 2 cm/s. Intensification also took place in the California Current where the southward geostrophic flow increased by about 1 – 2

cm/s. An anomalous anticyclonic geostrophic flow developed in the WSG suggesting a deceleration of the Alaskan Stream along the Aleutian Islands and its possible deviation south-westwards.

One can see that the spatial patterns of the observed sea level trends in both oceans (Figure 4.13) are identical to the spatial patterns of the EOFs-1 of the inter-annual SLA data (Figure 4.12). Thus the first empirical modes seem to describe long-term, possibly inter-decadal, variations of the sea level in both oceans. Therefore, in order to find the dominant modes of the SLA changes at shorter inter-annual time scales, a linear trend approximated by regression can be removed from the inter-annual SLA prior to the EOF analysis. In this case the first empirical mode of the inter-annual SLA explains 47% of the variance in the NA, and 51% of the variance in the NP. The spatial EOFs-1 of the detrended inter-annual SLA displayed dipole gyre-scale oscillatory patterns in both oceans (Figure 4.14, top panels). The temporal evolution of these patterns is portrayed by the PCs-1 (Figure 4.14, bottom panels).

The EOF-1 pattern of the detrended inter-annual SLA in the NA (Figure 4.14, top left panel) is quite different from the EOF-1 of the original inter-annual SLA, containing the linear trend (Figure 4.12, top left panel). It suggests that an increase/decrease of the sea surface height in the subtropical gyre, associated with a corresponding intensification/relaxation of the subtropical anticyclonic circulation, was accompanied by a decrease/increase of the sea surface height in the subpolar gyre, associated with a strengthening/weakening of the subpolar cyclonic circulation. The PC-1 (Figure 4.14, bottom left panel) indicates that the sea level in 1995 – 1997 and in 2001 – 2001 raised in the subpolar gyre and lowered in the subtropical gyre. In 1997 – 1998 the sea level was at its decadal maximum in the subpolar gyre, and in 1999 – 2000 it was at its decadal maximum in the subtropical gyre (compare with Plate 4.2).

In the NP, the detrending operation only introduced a correction to the EOF-1, computed from the non-detrended data (compare top right panel in Figure 4.14 with top right panel in Figure 4.14). The EOF-1 and PC-1 of the detrended inter-annual SLA in the NP depicted a simultaneous drop of the sea level in the subtropical gyre and a rise in the Bering Sea peaking in 1997. The latter coincided with an increase of the sea level in the subpolar gyre of the NA illustrated by the first empirical mode of the detrended inter-annual SLA (Figure 4.14, left panels). After 1997 an increase of the sea level in the subtropical gyre and a decrease in the subpolar gyre of the NP took place. Thus the inter-annual variability of the detrended inter-annual SLA during 1993 – 2003 in both oceans was dominated by the gyre scale changes. As suggested by the PCs-1 of the detrended inter-annual SLA, the changes in the NA and in the NP were coherent only during 1996 – 1998, but not at the beginning and at the end of the time series (Figure 4.14, bottom panels).

The EOF-1 and PC-1 of the detrended inter-annual SLA in the NA appeared to be correlated with the variations of the winter NAO index. The NAO is most pronounced in winter and the winter season has strongest inter-decadal variability (Cayan, 1992; Hurrell, 1995). When the NAO index changed from positive to negative values in 1995-1996 and in 2000-2001 the sea level responded with a rise in the subpolar and a decrease in the subtropical gyres (also see Esselborn and Eden, 2001; Volkov and van Aken (2), 2003). In the NP, the removal of the decadal trend did not greatly change the spatial pattern of the inter-annual change depicted by the EOF-1 of the inter-annual SLA (Figure 4.12, top right

panel), but it filtered out a part of the inter-decadal signal possibly associated with the PDO. The PC-1 of the detrended SLA in the NP, presented in Figure 4.14 (bottom right panel), highlights the change of sea level due to an unusually strong 1997/1998 El Niño event. The 1997 peak in the PC-1 is associated with the lowest SLA observed in the northern part of the subtropical gyre from 1993 to 2003. Thus, distinctly from the NA, in the NP the first empirical mode of the non-detrended inter-annual SLA (Figure 4.14, right panels) possibly contains both the inter-annual change due to the ENSO event in 1997 and to the longer-term PDO-related variability. The similarity of the EOFs-1 of the detrended and non-detrended inter-annual SLA is due to the similar spatial patterns of the ENSO- and PDO-induced deviations in SSTs (Zhang et al, 1997).

4.5 Conclusions

We have studied over 10 years of the TPJ+ERS satellite altimetry observations in the North Atlantic Ocean and in the North Pacific Ocean. The comparative analysis of the sea level variability in both oceans gave following results:

1) The spatial pattern of the mesoscale variability depicts the general surface circulation suggesting that the mesoscale variability is mainly induced by the barotropic and baroclinic instability of currents. The magnitude of the mesoscale variability in both oceans expressed by the RMS estimates is comparable and peaks (RMS>25 cm) in the Gulf Stream and Kuroshio extensions. In the NA the mesoscale variability is dominant along the Gulf Stream extension, NAC, the Azores Current and in the Labrador, where it is responsible for over 50% of the total variance. In the NP the mesoscale variability explains more than 50% of the total variance along all major currents: in the Kuroshio extension, NPC, California Current, Alaska Current and Alaskan Stream, Kuril and Kamchatka currents. The mesoscale variability was found to be overall more dominant in the NA than in the NP Ocean.

2) The mesoscale variability is subject to seasonal variations, possibly induced by the seasonal variations in wind stress. It appeared that the seasonal variations in mesoscale activity are more important in the subpolar regions of the NA and the NP, where the range of the variations in seasonal RMS of the mesoscale signal is often comparable with its long-term RMS. In most parts of the subpolar regions the maximum RMS of the mesoscale signal is characteristic for late autumn-winter period.

3) The seasonal change (annual cycle) of sea level outlines seasonal variations in the geostrophic surface circulation. In the NA and NP the strongest seasonal variations in geostrophic velocities were observed in the Gulf Stream and Kuroshio extensions, in the NAC and the NPC. As was shown by the seasonal geostrophic velocity anomalies, the Gulf Stream and Kuroshio extensions appeared to be subject to meridional shifts of flow intensity. In the NP, significant seasonal variability of geostrophic velocities was also observed in the California, Alaska, Kamchatka and Kuril currents.

4) The amplitudes of the seasonal SLA (generally between 4 and 10 cm) were found to be comparable in most parts of the NA and NP. The seasonal change in both oceans appeared to be responsible for less than 30% of the variance along major current systems, and over 40-50% of the variance in the eastern and subpolar areas. The largest difference between the NA and NP was found in the spatial distribution of phase of the seasonal

signal. In the NP the phase happened to be distributed mainly zonally with maximum annual SLA observed predominantly in October in the subtropical gyre and in September in the subpolar gyre. In most parts of the NA the maximum annual SLA was observed in October besides the Gulf Stream extension, Irminger basin and Labrador Sea, where the maximum SLA was found in September.

5) The spatial patterns of the inter-annual change of the sea level in the NA and in the NP were found to be comparable. The RMS of the inter-annual signal appeared to be a little larger in the NP than in the NA. In the Kuroshio extension the RMS exceeded 15 cm while in the Gulf Stream extension the RMS was about 10 cm. In the subpolar gyre of the NP the RMS of the inter-annual variability exceeded 5 cm in the Alaska gyre and near the Aleutian Islands, whereas in the subpolar NA the RMS values over 3 cm were observed only in the Irminger and Iceland basins. The relative contribution of the inter-annual change to the total variance appeared to be larger in the NP than in the NA. The determination coefficient of the inter-annual signal in the NP exceeded 40-50% in the Alaska gyre, WSG, and in the Bering Sea, as well as in the north-eastern extremity of the subtropical gyre.

6) The decadal trends of SLA showed that between 1993 and 2003 the sea level was rising in the eastern and subpolar NA, in the subtropical NP and in the WSG. At the same time the sea level was decreasing in the Gulf Stream and NAC in the NA, and in the California Current, Alaska gyre and Bering Sea in the NP. The decadal trends in both the NA and the NP were well portrayed by the first empirical modes of the inter-annual SLA. The difference of the estimated sea level trends with earlier studies suggests a possible existence of inter-decadal variability in both oceans. The long-term positive global sea level trend is generally believed to be an indication of the global sea level rise associated with global warming. However, it is necessary to realise that the inter-decadal variability may hide the true picture. Since the observations of the sea level variability by tidal gauges are spatially irregular and there are no sufficiently long time series of precise altimeter measurements, the estimated global sea level rise may contain errors due to subsampling and bias introduced by spatially non-uniform inter-annual and inter-decadal variability.

7) In the NP the inter-annual variability of SLA was basically associated with a dipole inter-gyre oscillation pattern, highlighting the contrast between the subpolar and subtropical gyres. The first empirical mode of the inter-annual SLA variability (66% of the variance) was found to be coherent with the PDO index. The positive PDO phase was associated with years 1993-1997. During this time relatively high sea level in the eastern parts of the NP and in the subpolar gyre with centre in the Bering Sea was observed. A switch between the two PDO regimes may have possibly occurred in 1998. Starting from 1998 and up to the end of 2002 the sea level started to rise in the northern part of the subtropical gyre and to decrease in the eastern areas, Alaska gyre and in the Bering Sea.

8) The first empirical mode of the detrended inter-annual SLA in the NA (47% of the variance) displayed a dipole inter-gyre variability pattern. The dipole structure of the EOF-1 and the temporal evolution of this mode depicted by the PC-1 showed that when the sea level increased in the subpolar gyre, a decrease occurred in the subtropical gyre, and vice versa. The dipole inter-gyre variability appeared to be related to the NAO. When the winter (DJF) NAO index changed its sign from positive to negative in the winter of 1995/1996 and after in the winter of 2000/2001, the sea level rose in the subpolar gyre and decreased in the subtropical gyre. Thus the variations of the winter NAO index appeared to be negatively correlated with the variability of the sea level in the subtropical gyre and positively

correlated with the variability of the sea level in the subtropical gyre. The first empirical mode of the detrended inter-annual SLA in the NP (51% of the variance) highlighted the change of sea level due to an unusually strong 1997/1998 El Niño event. The EOF-1 patterns of the detrended and non-detrended inter-annual SLA in the NP were found to be similar, which is possibly related to the similarity of spatial patterns of the ENSO- and PDO-induced deviations in SSTs.

Chapter 5

Inter-annual variability of eddy field and surface circulation in the North Atlantic Ocean

The distribution of surface eddy kinetic energy (EKE) depicts main oceanic surface circulation features. The interannual variability of EKE and associated geostrophic velocity anomalies in the North Atlantic Ocean were analyzed to describe the variations in oceanic currents between 1993 and 2002. The sea level anomaly maps of the combined Topex/Poseidon + ERS-1/2 (TP+ERS) satellite altimetry data were used to derive EKE. The study focused on the areas of the Gulf Stream extension (GS), North Atlantic Current (NAC), Azores Current (AC), and the northeastern (Rockall Channel and Iceland Basin) and northwestern (Irminger Basin and Labrador Sea) North Atlantic. The interannual variability of the altimetry-derived EKE field in the GS extension area reflected the meridional displacements of the GS core described in earlier studies. The interannual change of EKE in the AC was characterized by high values in 1993-1995 followed by lower EKE in subsequent years. The interannual variability of EKE in the NAC area west of the Mid-Atlantic Ridge exhibited an anti-phase change between the band centred near 47°N and two bands on either side centred near 43°N and near 50°N. In the Rockall Channel the geostrophic velocity anomalies indicated an intensified north-eastward flow in 1993 – 1995 followed by a relaxation in 1996 – 2000. The EKE band associated with the NAC branch in the Iceland Basin was found to be extended further west after 1996, possibly following the shift of the Subarctic Front, induced by the North Atlantic Oscillation (NAO). A rise of EKE was observed in the Irminger Basin from 1995 to 1999. This rise may have been associated with large anticyclonic geostrophic velocity anomalies, which indicated significant weakening of the cyclonic circulation in the Irminger Basin after 1996, and/or with possibly intensified eddy generation mechanisms due to the NAO – induced approach of the Subarctic Front. The interannual change of EKE in the Labrador Sea did not appear to always follow the atmospheric forcing expressed by the NAO. Therefore, other eddy generation mechanisms can be important[*].*

[*] This chapter is based on the paper by D.L. Volkov *'Interannual variability of the altimetry-derived eddy field and surface circulation in the extratropical North Atlantic Ocean in 1993-2001'*, J. Phys. Oceanogr., in press, 2004.

5.1 Introduction

Satellite altimetry provides an efficient tool to study oceanic circulation (for detailed information about the possibilities of satellite altimetry see Fu & Cazenave, 2001). Ocean currents can be decomposed into a large-scale mean geostrophic flow, a mesoscale eddy component, which is also assumed to be in geostrophic balance, and the non-geostrophic Ekman drift, produced by the varying wind forcing. Satellites measure sea surface heights (SSH) with respect to a reference ellipsoid. Ideally, the equipotential surface (geoid) should be subtracted from SSH to obtain the absolute dynamic topography. The latter would determine two first components of ocean currents: permanent mean geostrophic flow and variable geostrophic eddies. Unfortunately, present geoid models are not accurate enough to estimate the dynamic topography except at very long wavelengths. The latter is generally not suitable for oceanographic purposes, because on the spatial scales of mesoscale ocean features (few tens of km) the geoid errors are much larger than the oceanic signal. Therefore, instead of the geoid a long-term mean sea level is subtracted from the SSH to obtain the variable part of dynamic topography, or sea level anomaly (SLA) - a deviation of the SSH from its long-term mean state. In this case only the eddy geostrophic component can be determined. In other words, we are able to calculate the geostrophic velocity anomalies where the long-term mean sea level is taken as a reference zero-level.

In the absence of the absolute geostrophic velocity estimates, the present research assumes a possibility to study the large-scale oceanic circulation and its variability using a derivative parameter – eddy kinetic energy (EKE). This assumption relies on the fact that, due to the eddy generation mechanisms, most of EKE is concentrated along the main oceanic frontal zones associated with major currents (Richardson, 1983; Krauss and Käse, 1984). The EKE receives contribution from mesoscale vortices, Rossby and Kelvin waves, and temporal variations of the large-scale current pattern. Therefore, it is likely that the variations of EKE reflect the spatial and temporal changes in the location and intensity of the currents (Heywood et al., 1994; White and Heywood, 1995).

This study focused on the 5°W-65°W, 30°N-65°N sector of the North Atlantic Ocean (Figure 5.1). The surface circulation in the Northern Atlantic is governed by the Gulf Stream (GS) in the west, the Azores Current (AC) in the south at about 33°N-35°N and the North Atlantic Current (NAC), which separates the anticyclonic subtropical and cyclonic subpolar gyres. The GS extension south of the Grand Banks, encompassed by the region studied here, represents a highly variable meandering jet characterized by intensive eddy activity (Rossby, 1996; Käse and Krauss, 1996). Position of the GS in this area has manifested seasonal and interannual meridional shifts (Ionov et al, 1986; Kelly et al., 1999; Reverdin et al, 2003). After crossing the Southeast Newfoundland Ridge, the GS divides into two branches: the southern branch creates the AC flowing to the east and the northern branch becomes the NAC. The AC has been observed by ship-borne measurements (Sy, 1988; Klein and Siedler, 1989), drifters (Fratantoni, 2001; Reverdin et al., 2003) and satellite altimetry (e.g. Tokmakian and Challenor, 1993). It is less manifested than the NAC due to the fact that the Azores front is much weaker than the Subarctic Front (Käse and Krauss, 1996). The classical picture of the NAC and its branches presented by Dietrich et al. (1975) was lately reviewed by Krauss (1986) and Krauss et al. (1987). Based on the trajectories of satellite-tracked buoys and hydrographic sections the NAC was described as a superposition of a broad west wind drift and a frontal jet in the western part of the North

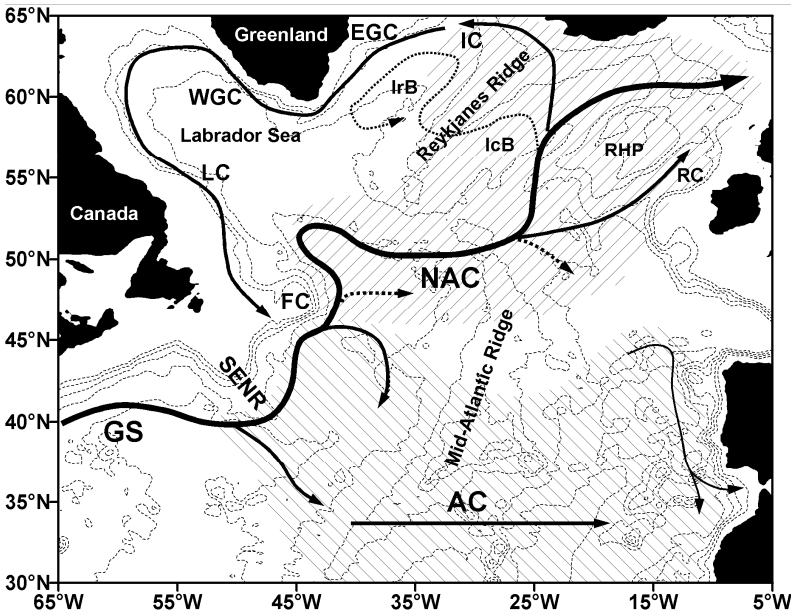

Figure 5.1: *The investigated sector of the North Atlantic Ocean with plotted bottom topography, which is drawn every 1000 m, and surface circulation. The right tilted shading indicates the area where the warm waters of the North Atlantic Current flow towards the north. The left tilted shading represents a part of the subtropical anticyclonic gyre (adapted from Krauss, 1986). Abbreviations used: GS - Gulf Stream extension, NAC - North Atlantic Current, AC - Azores Current, IC - Irminger Current, WGC - West Greenland Current, EGC - East Greenland Current, LC – Labrador Current, RC - Rockall Channel, RHP – Rockall Hatton Plateau, SENR - South East Newfoundland Ridge, FC - Flemish Cap, IcB – Iceland Basin, IrB – Irminger Basin.*

Atlantic (Figure 5.1). Krauss et al. (1987) stated that non-permanent jets appear between the Azores and Subarctic fronts as a transient phenomenon related to the eddy field between the Mid-Atlantic Ridge (MAR) and Grand Banks. According to Sy (1988), west of the MAR the NAC divides into a part which is fixed to the permanent Subarctic Front, and into one or more transient current branches between the front and 45°N.

From previous studies, the NAC proved to be the main source of EKE for the northern North Atlantic (Krauss and Käse, 1984). Although there have been many studies dedicated to the North Atlantic Ocean, and to the NAC in particular, some disputes regarding branching of currents, their preferred paths etc. still remain actual. A large number of investigations have been devoted to the EKE distribution, derived basically from satellite-tracked drifter measurements and in the recent time from satellite altimetry (e.g. Wyrtki et al., 1976; Richardson, 1983; Menard, 1983; Krauss and Käse, 1984; Heywood et al., 1994; White and Heywood, 1995; Fratantoni, 2001; Reverdin et al., 2003). However, so far there is little information available about the variability of the EKE field, especially interannual, which is closely related to the variability of currents. This lack of knowledge is mainly caused by the irregularity and poor spatial resolution of ship-borne and drifter surveys. The advent of satellite altimetry has facilitated the study of oceanic variability in time and space, especially following the launch of the Topex/Poseidon (T/P) mission in October 1992 (Fu et al, 1994).

The study of the seasonal variations in EKE field can help to understand whether the direct atmospheric forcing by fluctuating winds, which is usually stronger during winter, can be an effective mechanism for generating much of the observed oceanic mesoscale

variability. While a wind-induced barotropic variability of O(1 cm^2/s^2) constitutes a significant fraction of total EKE in the deep ocean, it appeared to be of minor importance in the surface layer (Stammer and Böning, 1996, Stammer and Wunsch, 1999). Studying four years of T/P data, Stammer and Wunsch (1999) showed that over most of the mid- and low-latitude oceans and along major oceanic fronts, seasonal variations of EKE are negligible. Thus, the major source of the near-surface eddy activity is attributed to the baroclinic and barotropic instability of major oceanic flows. However, seasonally varying EKE is observed in some regions with high wind energy, notably in the northeastern Pacific and in the northern North Atlantic (Stammer and Wunch, 1999). White and Heywood (1995) described the seasonal differences in EKE in the northern North Atlantic and related them to the varying wind forcing.

Heywood et al. (1994) and then White and Heywood (1995), using data from T/P (October 1992 - September 1994) and preceding Geosat (December 1987 - December 1988) and ERS-1 (May 1992 - April 1993) altimetry missions, showed that the EKE field in the North Atlantic manifests changes at interannual timescales. Their studies confirmed a close relationship between EKE and mean currents, constrained by topography (Heywood et al., 1994), and suggested that outside the strong currents in the subpolar gyre, eddies are primarily driven by wind stress (White and Heywood, 1995).

Since that time the accurate T/P data have been obtained for more than 10 years. These data are constantly being updated due to the successful continuation of the T/P mission and the start of the Jason-1 mission in October 2001 as a successor of T/P. This paper aims to describe the interannual variability of EKE in the North Atlantic Ocean (30-65°N, 5-65°W) as it appeared in satellite altimetry data from October 1992 to February 2002. The horizontal displacements of major currents and changes of their intensity are expected to be reflected in the spatial and temporal variations of the EKE field. Special emphasis is given to regional studies: to the high variability GS extension and NAC areas west of the MAR, to the relatively lower variability AC, and to the northeastern (Rockall Channel and Iceland Basin) and northwestern (Irminger Basin and Labrador Sea) parts of the North Atlantic Ocean. The surface circulation changes depicted by the varying EKE distribution are compared with the North Atlantic Oscillation (NAO). The NAO is a filtered simplification of the atmospheric forcing with an emphasis on the zonal winds expressed by the NAO index (for detailed information about the NAO see Hurrell, 2003).

The subsequent information is organized as follows. In section (2), the altimeter data used and the calculation of EKE are described. The results of the study are presented in section (3), where the mesoscale sea level change, mean EKE field and its comparison with the hydrographic observations, and the interannual variability of EKE in several regions are discussed in detail. Section (4) reviews main conclusions of the study.

5.2 Data and method

The SLA data used in this study are the combined T/P + ERS-1/2 (henceforth TP+ERS) and T/P alone from October 14, 1992 to February 13, 2002. The combined TP + ERS data compared to T/P data alone have a better spatial coverage, and thus provide more homogeneous and reduced mapping errors, more realistic sea level and geostrophic velocity statistics (Ducet et al., 2000). Hence, it is expected that most of the ocean eddy energy will be conserved in the combined data. However, there are no combined TP+ERS-1 maps

available between January 1994 and March 1995 (ERS-1 ice monitoring and geodetic missions) and the T/P alone data are used to fill this gap.

The geostrophic velocity anomalies were computed as it is described in Chapter 2 and used to monitor the relative changes of the annual mean surface circulation from year to year. Following Menard (1983), the surface eddy kinetic energy (EKE) is estimated as half the sum of the squared eddy velocity components in two directions X and Y averaged over N weeks (since there is one map every 7 days):

$$EKE = \frac{1}{2N}\sum_{t=1}^{t+N-1}\left[(u')^2 + (v')^2\right] \qquad (5.1).$$

The averaging in (5.1) was performed using moving averages for N=53 to reveal the interannual change and for N=5 to resolve the seasonal signal.

The EKE values calculated from the combined T/P+ERS data were compared with those derived from the T/P alone data set in order to assess the discrepancy imposed by the different spatial resolution. The largest absolute difference between both data sets was observed along the major currents where variability is largest: the GS, the NAC and the AC (not shown). The largest relative difference (taking into account the magnitude of EKE) is observed mainly in the low-variability eastern North Atlantic and in the NAC area east of the Grand Banks. Here, the T/P-derived EKE constitutes from 40 to 90% of the T/P+ERS -derived EKE. The minimum percentage is located at the centres of the T/P inter-track spaces ("diamonds"). Along the GS extension the T/P-derived EKE generally makes up 70-100% of the T/P+ERS values except at some "diamonds" where it varies from 40 to 70%. This discrepancy is caused by the large T/P inter-track distances at low latitudes and it tends to increase towards the lower variability eastern North Atlantic. In the north, where the tracks of T/P get closer, the agreement between two EKE estimates is fairly good. The T/P data make up 70-100% of the EKE derived from the T/P+ERS data north of 53ºN. Thus, this comparison showed to what degree the T/P alone data underestimate mesoscale variability and how this underestimation is distributed over the North Atlantic. Hence, one has to be careful when interpreting the time series of EKE. It is necessary to bear in mind that the magnitude of EKE in 1994 and 1995 is underestimated relative to the T/P+ERS-derived values. In the following analysis of EKE variability, when a more accurate temporal structure was a priority, the T/P-derived EKE was used.

To visualise the interannual change, EKE was calculated for years 1993 and 1996 - 2001 using the T/P+ERS data, and for years 1994 and 1995 using the T/P data alone. Each year starts in December. Thus 9 independent estimates from December 1992 to December 2001 were yielded. In order to reduce the underestimation of EKE by the T/P data, a seven years average of the ratio $EKE_{T/P+ERS}/EKE_{T/P}$, leaving out the years of 1994 and 1995, was estimated for each grid point and used as a coefficient to correct the T/P-derived EKE values in 1994 and 1995. The application of the coefficient to the seven years (1993, 1996 - 2001) of the T/P-derived EKE significantly reduced the discrepancy between the individual T/P+ERS and T/P EKE estimates in the lower latitudes. In the high variability regions of the GS extension and the NAC, and in the eastern part of the North Atlantic the corrected T/P-derived EKE became in general no more than 10% different from the T/P+ERS-derived EKE. However, the applied correction did not greatly reduce the difference between the T/P- and T/P+ERS-derived EKE estimates in the subarctic North Atlantic. In

the low-variability area between the north-western corner of the NAC and the Irminger Basin, the difference even increased (not shown). Therefore, to study the interannual change of EKE, a correction for years 1994 and 1995 was applied in the GS extension, in the AC and in the NAC areas, but no correction for years 1994 and 1995 was applied in the northeastern and northwestern North Atlantic.

5.3 Observational results

Mesoscale variability

In this study, the SLA time series $\zeta(x,y,t)$ were regarded as a composition of three modes of variability: interannual changes, annual cycle and high frequency signals $\zeta(x,y,t)= \zeta_i(x,y,t)+ \zeta_a(x,y,t)+ \zeta_m(x,y,t)$. The interannual changes ζ_i occur basically due to the variations of oceanic heat and salt content, induced by changes of heat and fresh water exchange between ocean and atmosphere, and large-scale changes of advection, caused by the varying wind stress curl. The annual cycle ζ_a (harmonic period = 1 year) mainly reflects variations of sea level due to the seasonal changes of insolation and connected with it changes of heat and fresh water fluxes between the ocean and atmosphere. As recently was shown (Volkov and van Aken, 2003), the sea level in the northern North Atlantic Ocean, in particular north of 52ºN -53ºN is subject to significant seasonal (up to 30-50% of total variance) and interannual variations (up to 20-40% of total variance). All signals having periods shorter than one year are considered here as high frequency signals or mesoscale variability ζ_m. It is assumed that the mesoscale variability is generally represented by mesoscale eddies generated by instability processes and topographic effects. Besides this, other processes like long baroclinic Rossby waves and shifts of the main currents also contribute to this group. This section aims to characterize the portion of variance the mesoscale change ζ_m is responsible for.

To reveal and subsequently extract the interannual change $\zeta_i(x,y,t)$, the SLA data $\zeta(x,y,t)$ were filtered with a running mean over a period of about one year (N=53 samples in 7-day sampling period altimetry data). This permitted capturing all the interannual variability detectable on the investigated time interval. The harmonic annual cycle has a determined shape and frequency, given by its physical nature, and it was approximated by a sine function $\zeta_a(x,y,t)=A(x,y)\cdot\sin[2\cdot\pi\cdot\omega\cdot t+\varphi(x,y)]$ with a frequency $\omega=1$ cycle/year. Amplitude A and phase φ were estimated using a least-squares method. Subsequently, both the interannual signal and annual cycle were subtracted from $\zeta(x,y,t)$.

The root-mean-square (RMS) of the residual mesoscale variability $\zeta_m(x,y,t)$ is shown in Figure 5.2. The RMS distribution outlines the main surface circulation pattern in the North Atlantic (compare with Figure 5.1). The maximum RMS of $\zeta_m(x,y,t)$ is observed along the GS extension (over 25 cm RMS). At the site where the GS is transformed to the NAC flowing north along the Grand Banks and the AC heading to the southeast-east (35°N -40°N, 45°W) the RMS of $\zeta_m(x,y,t)$ is around 15 - 20 cm. Further east and northeast, the AC and the NAC are detectable as mesoscale SLA fields outlined by 3-5 cm RMS values. There are relatively high RMS values (over 3 cm RMS) in the Iceland Basin and in the Labrador Sea. Relatively low RMS values were observed in the Rockall Channel (2-3 cm).

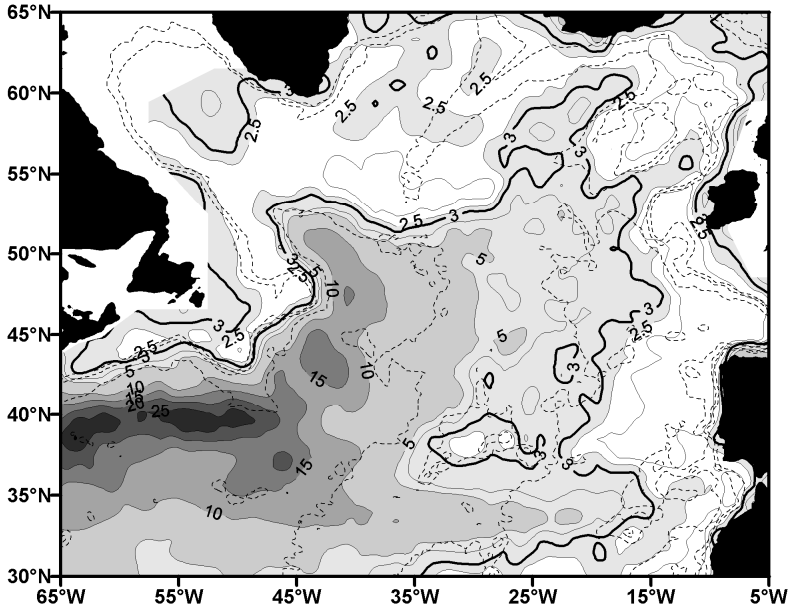

Figure 5.2: *Root-mean-square of mesoscale SLA (cm) after the annual cycle and the inter-annual signal have been subtracted. Bottom topography represented by thin dashed contours is drawn every 1000 m.*

Finally, the determination coefficient of $\zeta_m(x,y,t)$ was calculated to evaluate the relative contribution of the mesoscale sea level variability to the total variance (Figure 5.3). As one would expect the maximum values are typical for dynamic zones where the mesoscale change overpowers the low-frequency variability. Along the GS, NAC and the AC west of the MAR the determination coefficient of the mesoscale variability exceeded 50-70%. It reached 90% in the Northwest Corner of the NAC near 50°N, 40-45°W and in the AC region near 34°N, 44°W. The Northwest Corner, as a retroflection area of the NAC, was already proven to be highly variable in intensity and position of the stream (e.g. Lazier, 1994). The distribution of the determination coefficient west of the MAR outlines a band of the NAC at about 47°N where the portion of the mesoscale variability exceeds 60%. This band can possibly be connected with the above-mentioned branching of the main NAC stream (Krauss, 1986; Krauss et al., 1986; Sy, 1987; Sy et al., 1991). East of the MAR the determination coefficient is generally above the 30% level with relatively high values along the AC (over 50%). Only in the most eastern areas and some regions of the northern North Atlantic the mesoscale processes constitute less than 30% of total variance. Another maximum, where the determination coefficient exceeds 50%, is observed in the Labrador Sea. Elevated drifter-derived EKE values confirming the importance of mesoscale processes in the Labrador Sea were recently documented by Fratantoni (2001) and Reverdin et al. (2003).

Mean eddy kinetic energy field

The mean EKE field, calculated over the investigated time interval besides the period when the combined data are not available (~8 years), depicts the main areas of eddy generation associated with the GS, AC, the NAC and its branches (Figure 5.4). The maximum EKE exceeding 2500 cm^2/s^2 is observed along the GS to the south of the Newfoundland Rise.

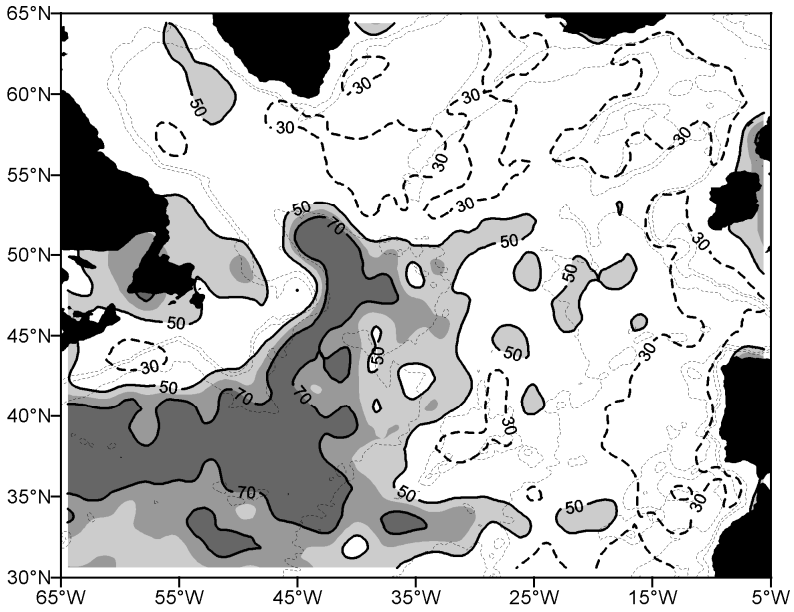

Figure 5.3: *Determination coefficient (%) of the residual SLA after the annual cycle and the inter-annual signal have been subtracted. Bold dashed contours delineate 30% level and bold continuous contours delineate 50 and 70% levels. Bottom topography represented by thin dashed contours is drawn every 1000 m.*

The AC, flowing eastward, was seen along 33-34°N and has EKE in the range of 50-200 cm²/s². In the NAC, traveling to the north along the Grand Banks, EKE ranges from 500 to 1000 cm²/s². It almost approaches 1500 cm²/s² at about 43°N, 43°W and 46°N, 41°W. The site around 43°N, 43°W is associated with a large anticyclonic quasi-permanent Mann Eddy (Mann, 1967; Rossby, 1996). It is well defined in the average drifter-derived current velocity fields (Reverdin et al., 2003; Fratantoni, 2001). The current reaches the MAR with EKE equal to 150-200 cm²/s². In the eastern part of the North Atlantic Ocean, behind the ridge, EKE mainly varies from 25 to 100 cm²/s². From Figure 5.4 one can see that the NAC is indeed the main source of eddies in the North Atlantic Ocean. The 50 cm²/s² contour nearly coincides with the Subarctic Front at about 52°N. The EKE field outlines the NAC as a superposition of a broad west wind drift and a frontal jet crossing the MAR at the Charlie-Gibbs Fracture Zone (Krauss, 1986). After having crossed the ridge, the NAC veers to the north continuing to flow into the Iceland Basin along with some water entering the Rockall Channel. It is interesting to note a relatively high EKE area on the northwestern flank of the Rockall-Hatton Plateau (EKE>100 cm²/s²). Quasi-permanent eddies, existing here, are possibly generated by baroclinic instability of the current flowing along the Subarctic Front over the steeply sloping bottom relief and partly perhaps by shedding off the southeastern wedge of the plateau. Some water of the NAC re-circulates along the eastern slope of the Reykjanes Ridge in the Iceland Basin (Otto and van Aken, 1996; Valdimarsson and Malmberg, 1999) and possibly crosses it at approximately 57ºN. It is suggested by a relatively high RMS of the mesoscale SLA (Figure 5.2) and EKE (Figure 5.4). On the western flank of the Reykjanes Ridge and in the center of the Irminger Basin an elevated EKE area (25-50 cm²/s²) is observed. It corresponds to a poleward current that is a persistent feature on the western flank of the ridge originating from at least 57°N (Reverdin et al., 2003). The East and West Greenland Currents are also seen in Figure 5.4

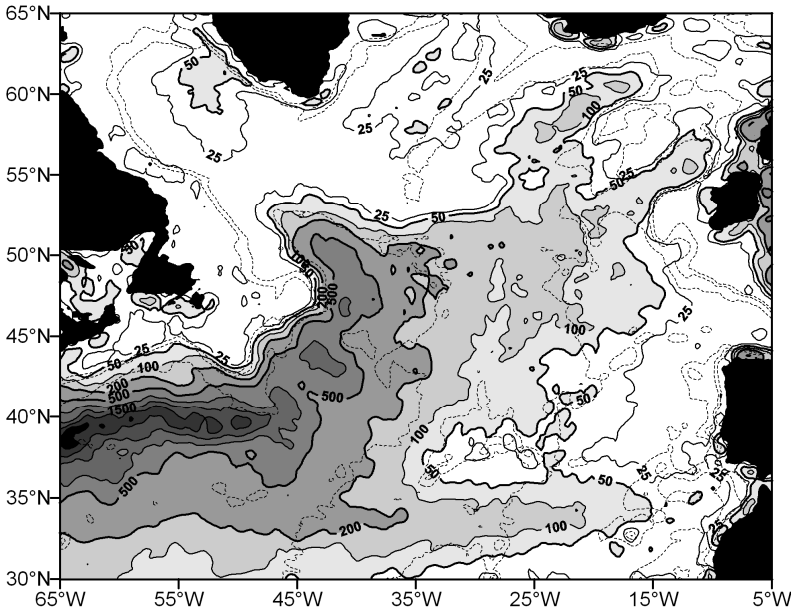

Figure 5.4: *Mean eddy kinetic energy (cm²/s²) in the North Atlantic Ocean computed from the combined T/P+ERS satellite altimetry data. Bottom topography represented by thin dashed contours is drawn every 1000 m.*

with EKE values ranging from 25 to 50 cm²/s². There is a local EKE maximum (>50 cm²/s²) in the Labrador Sea associated with the West Greenland Current.

Along the GS extension, the estimates of EKE by Menard (1983) from SEASAT altimeter data are in the range of 400-1600 cm²/s². These estimates are significantly lower than those obtained in this and other studies because of the poorer spatial resolution of the grid produced from SEASAT ground tracks, different sampling periods and smoothing techniques. Le Traon and Rouquet (1990) and later Heywood et al. (1994) calculated surface EKE from Geosat and ERS-1 data sets and obtained values larger than those of Menard. The largest values for ERS-1 (May 1992 – April 1993) were found in the GS extension (>1000 cm²/s²) and along the NAC as it flows around the Flemish Cap (500 – 1000 cm²/s²). The lowest EKE (mainly 50 – 200 cm²/s²) was estimated in the low variability regions east of the MAR and in the subpolar gyre. The Geosat EKE estimates (January-December 1987 and 1988) compared to ERS-1 (May 1992 – April 1993) showed larger values along the NAC (>1000 cm²/s²). Later, White and Heywood (1995) obtained four years average EKE for Geosat (1987, 1988) and T/P (1992/1993, 1993/1994). In their study EKE exceeded 1000 cm²/s² along the GS extension and the NAC, decreasing to ~200 cm²/s² at the MAR and to 20-200 cm²/s² in the low variability regions. Ducet et al. (2000) first computed EKE using the high-resolution (0.25° x 0.25°) combined T/P + ERS-1 and – 2 SLA data which yielded EKE levels 30% higher than from the T/P SLA data alone. The combined data appear to be more suitable for EKE derivations because it better resolves mesoscale features unlike the individual data sets. The mean EKE field presented in this study (Figure 5.4) compares well with Ducet et al. (2000), especially in terms of depiction the surface circulation pattern in the Northern Atlantic. However, the computed EKE appears to be somewhat lower in the low variability regions of the northern and eastern North Atlantic. This discrepancy can be attributed to more sophisticated data preprocessing

techniques applied to the data set used in the present study resulting in noise reduction (SSALTO/DUACS User Handbook, 2001).

The drifter-derived EKE appears to be approximately two to four times higher than corresponding values derived from satellite altimetry in some low variability areas outside the GS extension and NAC flowing along the Newfoundland Rise (Otto and van Aken, 1996; Fratantoni, 2001; Reverdin et al., 2003). This discrepancy is thought to be a result of differences in spatial resolution and sampling period of drifter and altimeter measurements. Another reason for the difference between altimeter- and drifter-derived EKE is the assumption of geostrophy when we calculate EKE from the satellite altimetry data and impossibility to estimate ageostrophic motions. This becomes especially important in the areas outside the strong currents because there hardly exists a significant slope of sea surface to associate with the geostrophic motion, but the variable Ekman drift may account for a greatest portion of all motions.

Comparison with hydrography data

To illustrate how the maxima of surface EKE depict the frontal zones and associated with them currents, hydrographic data were also investigated. The focus is on the northern part of the North Atlantic Ocean (5°W-45°W, 50°N-65°N), comprising the transatlantic Ireland-Greenland AR7E section performed along two tracks: one across the Rockall – Hatton Plateau and another surrounding it from the south – southwest (Figure 5.5, b). The hydrographic data at this section were obtained from 1990 to 2003. In total, the data from twelve cruises conducted in different times of the year, but mainly in August – September, were studied. There were 4 cruises performed along the northern version of AR7E and 8 cruises performed along the southern version of AR7E (Table 5.1). R/V Tyro did not take any measurements in the central and western Irminger Basin in 1990; therefore, the data in this area start in 1991.

The altimetry-derived EKE was compared with the density profiles and dynamic heights obtained during the cruises. Figure 5.5 presents the averaged density profiles for the northern (4 cruises) and southern (8 cruises) varieties of AR7E section (Figure 5.5, a, c), and long-term average EKE (7 years of data excluding 1994 and 1995) (Figure 5.5, b). The density profiles were plotted only for upper 1000 dbar since the horizontal density gradient does not significantly change below. Dynamic heights between 200 dbar and 2000 dbar isobaric surfaces were also coupled with EKE (not shown). The choice of the 200 dbar – 2000 dbar depth range reduced the seasonal bias, which may be large in upper 200-m layer.

As seen in Figure 5.5, across both the northern and southern varieties of AR7E section the cores of long-term averaged EKE (Figure 5.5, b) coincided with maximum horizontal density gradients (Figure 5.5, a and c), associated with the NAC to the south and southwest of the Rockall-Hatton Plateau, and in the Iceland Basin. The cores of EKE in these areas were also found to coincide with the largest dynamic height slopes across the NAC. Dome-shaped isopicnal surfaces and corresponding local maxima of the altimetry-derived EKE in the Irminger Basin reflected a poleward flow along the western flank of the Reykjanes Ridge and an equatorward East Greenland Current (EGC) along the eastern coast of Greenland. The density profiles and dynamic heights for individual cruises and corresponding EKE also showed a good agreement (not shown).

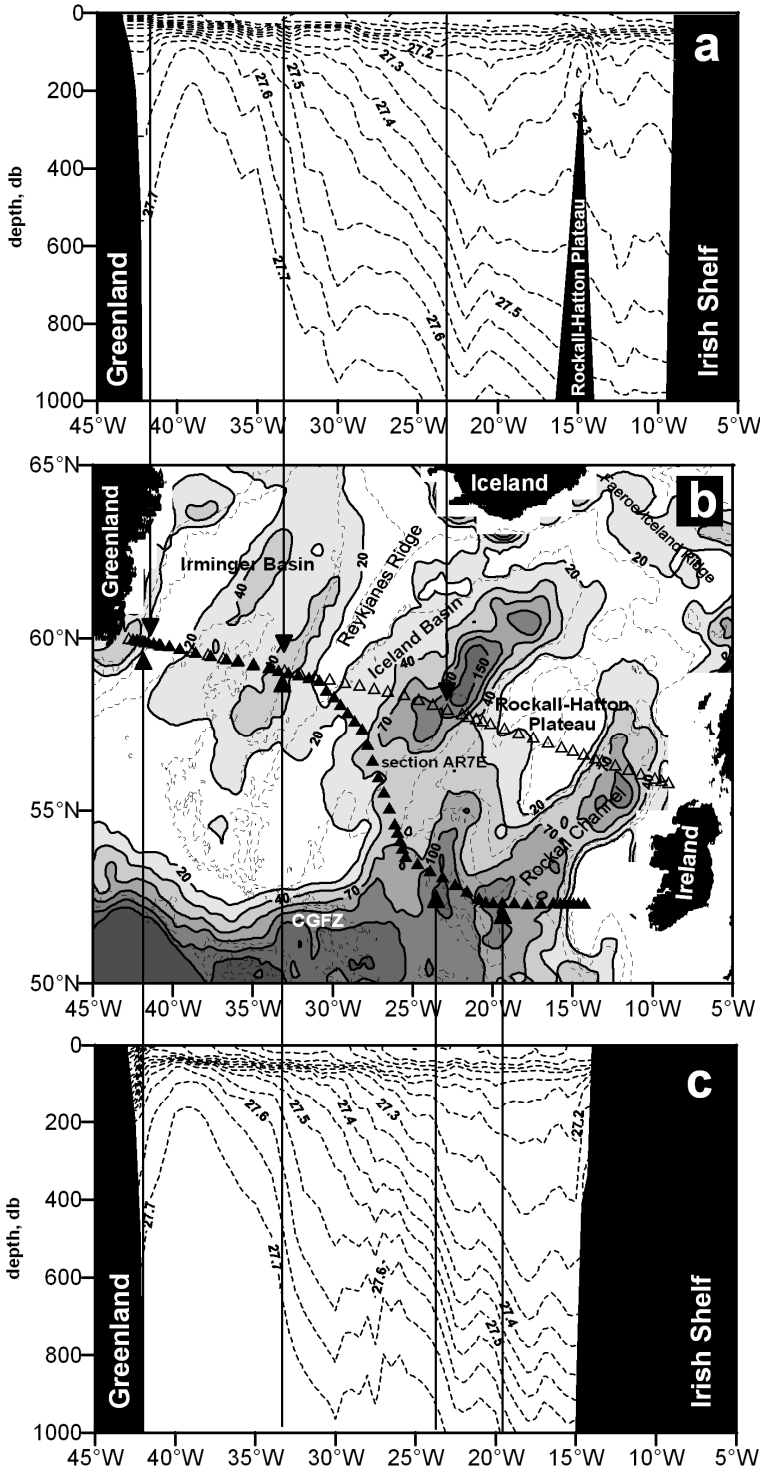

Figure 5.5: *(a) Averaged density anomaly (kg/m^3) profile for the northern variety of AR7E section; (b) northern part of the North Atlantic with plotted average EKE (cm^2/s^2) and both northern (filled triangles) and southern (semi-filled triangles) varieties of AR7E section. The bottom topography is shown every 1000 m; (c) averaged density anomaly (kg/m3) profile for the southern version of AR7E section. Arrows show the position of frontal zones.*

Thus, the hydrographic data presented an observational evidence that high EKE cores are basically confined to oceanic fronts, supporting the hypothesis of hydrodynamical instability mechanisms as the primary source of the mesoscale eddy fields. As the present analysis showed, the latter is possibly valid not only for the high gradient strong currents like GS and NAC west of the MAR, but also for lower gradient frontal zones and associated with them weaker currents (the NAC in the Iceland Basin, poleward flow over the western flank of the Reykjanes Ridge, EGC etc.). In the end, it should be noted that the time scale of the dissipation processes of EKE is apparently so small that EKE does not diffuse very far from the generation area giving us an opportunity to track the paths of currents.

Inter-annual variability of EKE

Surface circulation in the North Atlantic Ocean experiences considerable interannual variations: ocean gyre circulation changes (Curry and McCartney, 2001), meridional shifts of the GS (Ionov et al, 1986; Taylor and Stephens, 1998; Rossby and Benway, 2000; Frankignoul et al., 2001; Reverdin et al, 2003), non-permanent branching of the NAC west of the MAR (Sy, 1987; Sy et al., 1991; Käse and Krauss, 1996), changes of the NAC in the Iceland Basin (Bersch, 2002) and Rockall Channel (Holliday, 2003), variations in the Irminger Basin (Flatau et al, 2003) and Labrador Sea (Han and Tang, 2001) etc. Based on the theoretical assumptions and observational evidence presented above, changes of the altimeter-derived EKE from year to year are expected to reflect the interannual variability of the large-scale surface currents.

The EKE anomalies estimated as a deviation from a mean value for years 1993 - 2001 are presented in Plate 5.1. To estimate the EKE anomalies the TP+ERS – derived mean EKE was calculated over 7 years leaving out years 1994 and 1995, whereas 9 years of the T/P measurements were used to estimate the T/P-derived mean EKE. A correction for the T/P-derived EKE in 1994 and 1995 was applied. As one can see, the spatial distribution of the EKE field in the North Atlantic in 1993-2001 was subject to significant spatial and temporal interannual changes possibly connected with the variability of major currents. The magnitude of the EKE anomaly exceeded 500 cm^2/s^2 along the GS extension and NAC, which constitutes around 25% of maximum EKE magnitude in these high variance areas of the North Atlantic.

Gulf Stream extension (GS)

As shown in Plate 5.1, the GS south of the Newfoundland Rise during the studied time interval experienced meridional shifts of EKE. In 1993 and 1994 positive EKE anomalies were observed along 40°-42°N adjoining the area with negative EKE anomalies further south. Then EKE at 40°-42°N decreased in 1995 and from 1997 to 1999 and in 2001 positive anomalies were observed at about 36°-38°N.

The GS path as it turns east at Cape Hatterras experiences wavelike motions associated with meandering and meridional shifts. Observations have shown that the interannual variations in the meridional position of the GS path are possibly connected with changes in atmospheric forcing (e.g. Kelly et al.; 1996). Taylor and Stephens (1998) studying the interannual changes in the position of the northern wall of the GS from 1966 to 1996 showed that the latitude of the GS is correlated with the NAO index; a positive NAO phase

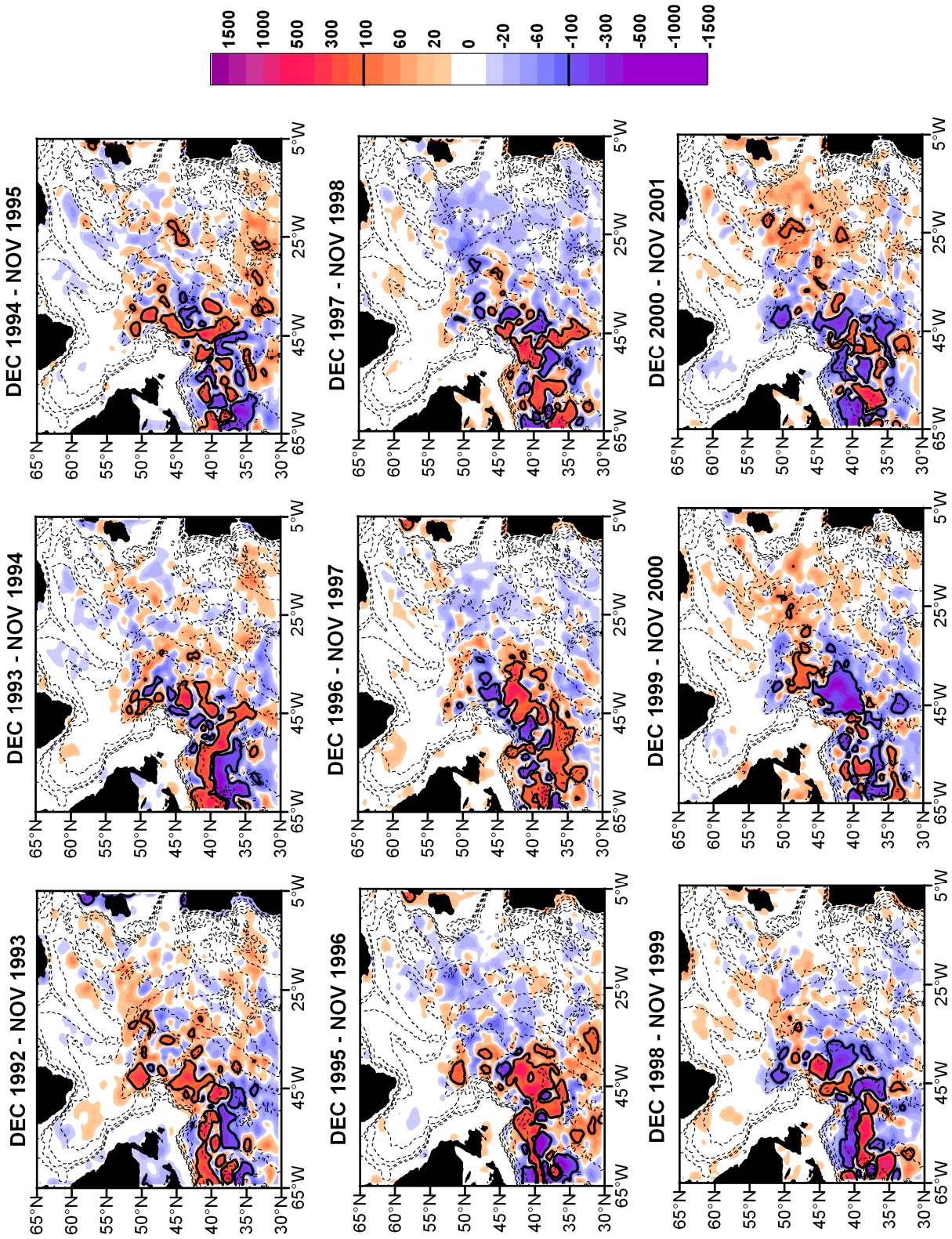

Plate 5.1: *Maps of annual mean (from December to November) eddy kinetic energy anomalies (sm²/s²) in the North Atlantic Ocean. The anomalies for years 1994 and 1995 were computed using the gridded corrected T/P data as a deviation from nine-year mean. The anomalies for other years were computed using the combined T/P+ERS data as a deviation from seven-year mean leaving out the years of 1994 and 1995. Bold isoline indicate ±100 cm²/s² level of EKE anomaly. Dashed isolines denote bottom topography, which is drawn every 1000 meters.*

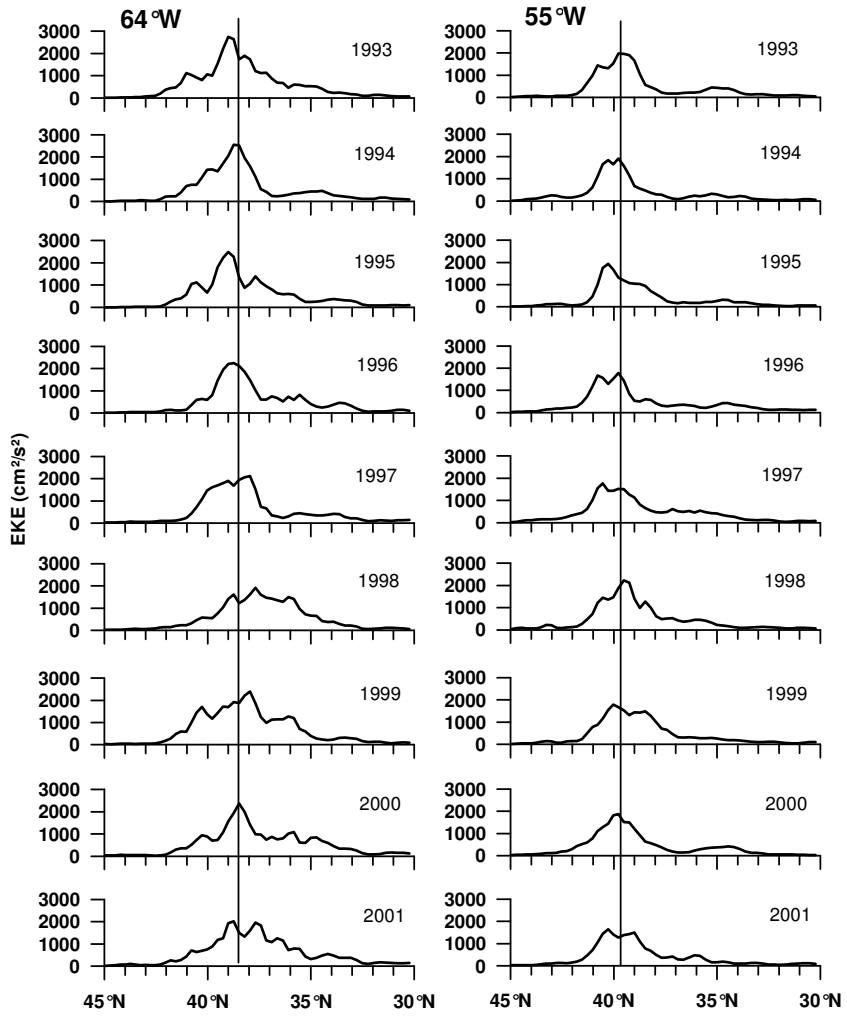

Figure 5.6: *Lateral meridional distribution of EKE (cm²/s²) at 64°W and 55°W across the Gulf Stream from 1993 to 2001. Vertical lines indicate nine-year average position of the highest EKE peak.*

associated with stronger westerly winds favours more northerly position of the GS path about 2 years later. Rossby and Benway (2000) suggested that meridional displacements of the GS can be caused by a time-varying transport of Labrador shelf water. The latter affects the surface salinity, which is correlated with the NAO with a lag of about 1.5 year. Frankignoul et al. (2001) determined the position of the GS from the along-track altimetry data using the method of Kelly and Gille (1990). They concluded that northward (southward) displacements of the GS occur 11 to 18 months after the NAO has reached the extreme of a positive (negative) phase.

The maps of absolute annual mean EKE and geostrophic velocity anomalies in the GS area are presented in Plate 5.2. The highest EKE values and the widest EKE band can be seen in the area of the New England Seamount chain at about 63°W-65°W. Between 50°W and 65°W the core of largest EKE was observed at 38°N-41°N and experienced meridional displacements within about 2° longitudinal band. The interannual variability of the meridional EKE structure of the GS at 64°W and 55°W is shown in Figure 5.6. It is seen that at 55°W and 65°W the core of maximum EKE was within 1° distance from the 9-year average position. The most northerly position of the EKE core was observed from 1993 to

1996 at 65°W and from 1993 to 1997 at 55°W. In 1998 the core of EKE was at its southernmost location. This coincides well with the position of the GS in the findings of Frankignoul et al. (2001), Rossby and Benway (2000), and Taylor and Stephens (1998). Since the NAO turned from a positive to a strongly negative phase in 1995/1996 (Hurrell, 2003; http://www.cgd.ucar.edu/~jhurrell/nao.html), the southward shift of EKE in 1998 corresponds to the southward shift of the GS core observed about 2 years after the reversal of the NAO phase. In 2000 the core of EKE returned to its 9-year average position. In 2001 a peak of EKE was again present to the south of the average position probably following another negative winter NAO index in 2000. The interannual variability of the geostrophic velocity anomalies, shown in Plate 5.2, confirms the lateral shifts of velocity. Although the pattern is confused by meanders and eddies, it is seen that from 1993 to 1995 predominantly eastward anomalous velocities were concentrated along ~40°N adjoining the band of mostly westward velocities in the south along ~38°N. Then from 1997 through 1998 the situation reversed with the eastward velocity anomalies situated to the south of the westward ones.

The EKE distribution in the GS extension area (Plate 5.2) shows a gyre-like feature located at about 37°N, 53°W and outlined by approximately 300 cm^2/s^2 contour. This is possibly a reflection of an anticyclonic recirculation gyre. Such a gyre was mentioned by Fratantoni (2001) on the basis of drifter data and it is seen on the maps of average current velocities presented in Reverdin et al. (2003).

To summarise, it is possible to state that the interannual variability of the altimetry-derived EKE field in the GS extension area reflects the meridional displacements of the GS core, which also was detected using other techniques.

North Atlantic Current (NAC)

Plate 5.1 depicts tremendous spatial and temporal interannual variations of EKE along the NAC between 25°W and 45°W that occurred in 1993-2001. The variability is especially reflected in the meridional shifts of maximum and minimum EKE values in the area to the west of the MAR. The maps of the yearly absolute EKE and geostrophic velocity anomalies in the NAC area are presented in Plate 5.3. Relatively high EKE cores possibly connected with the NAC jets occasionally appeared on the background of the NAC northeastern drift at about 43°N, 47°N and 50°N. These cores were mostly associated with the increased eastward, north-eastward flow as suggested by the geostrophic velocity anomalies (Plate 5.3). The northern wall of the NAC is associated with the Subarctic Front and is fixed at 50°N-52°N (Figure 5.4, Plate 5.3). It appears that the 45°N-48°N area varies out of phase with the two areas on either side along 42°N-43°N and 49°N-52°N. When high EKE anomalies were observed along 42°N-43°N and 49°N-52°N (Plates 5.1 and 5.3 - years 1993, 1994, 1997, 1998), an opposite situation occurred along 45°N-48°N (Plates 5.1 and 5.3 – years 1995, 1999, 2000, 2001). This is confirmed by the first Empirical Orthogonal Function (EOF-1) of the EKE time series explaining 35% of the total variance in 25°W-45°W, 40°N-55°N domain (Figure 5.7). One can see that EOF – 1 depicts a three-zoned standing oscillation pattern with two side bands varying out-of-phase with the central band. The same pattern of the EKE variability in the NAC was also depicted by EOF – 1, explaining 20% of the total variance, computed for the whole domain (5°W-65°W, 30°N-65°N) of the study (not shown).

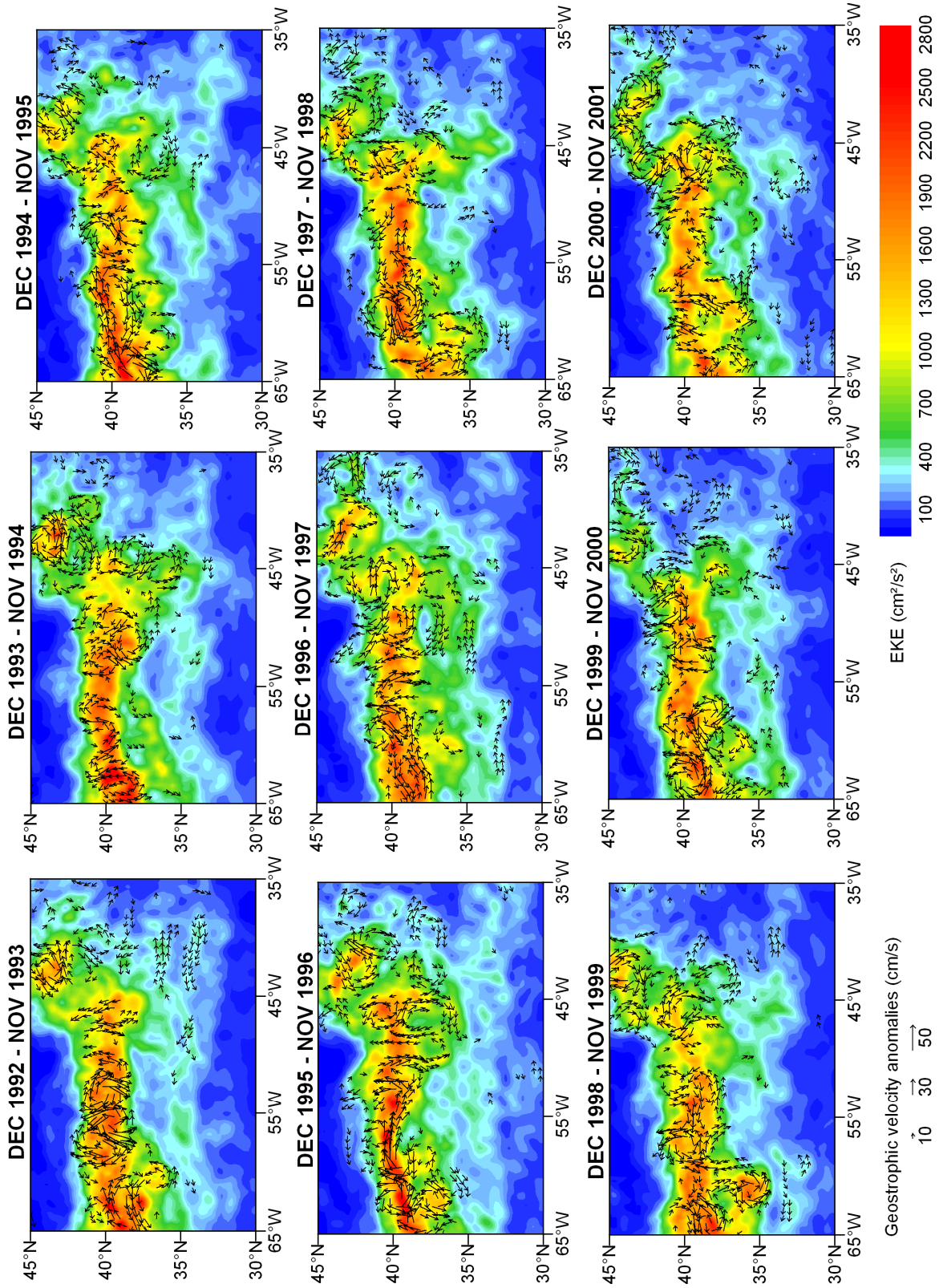

Plate 5.2: *Maps of annual mean EKE (cm²/s²) and geostrophic velocity anomalies in the Gulf Stream extension area. EKE was computed from the combined T/P+ERS satellite altimetry data for years 1993, 1996 – 2001 and from T/P data alone for years 1994 and 1995 with a correction factor applied. The vectors of velocity anomalies are shown only starting from 10 cm/s.*

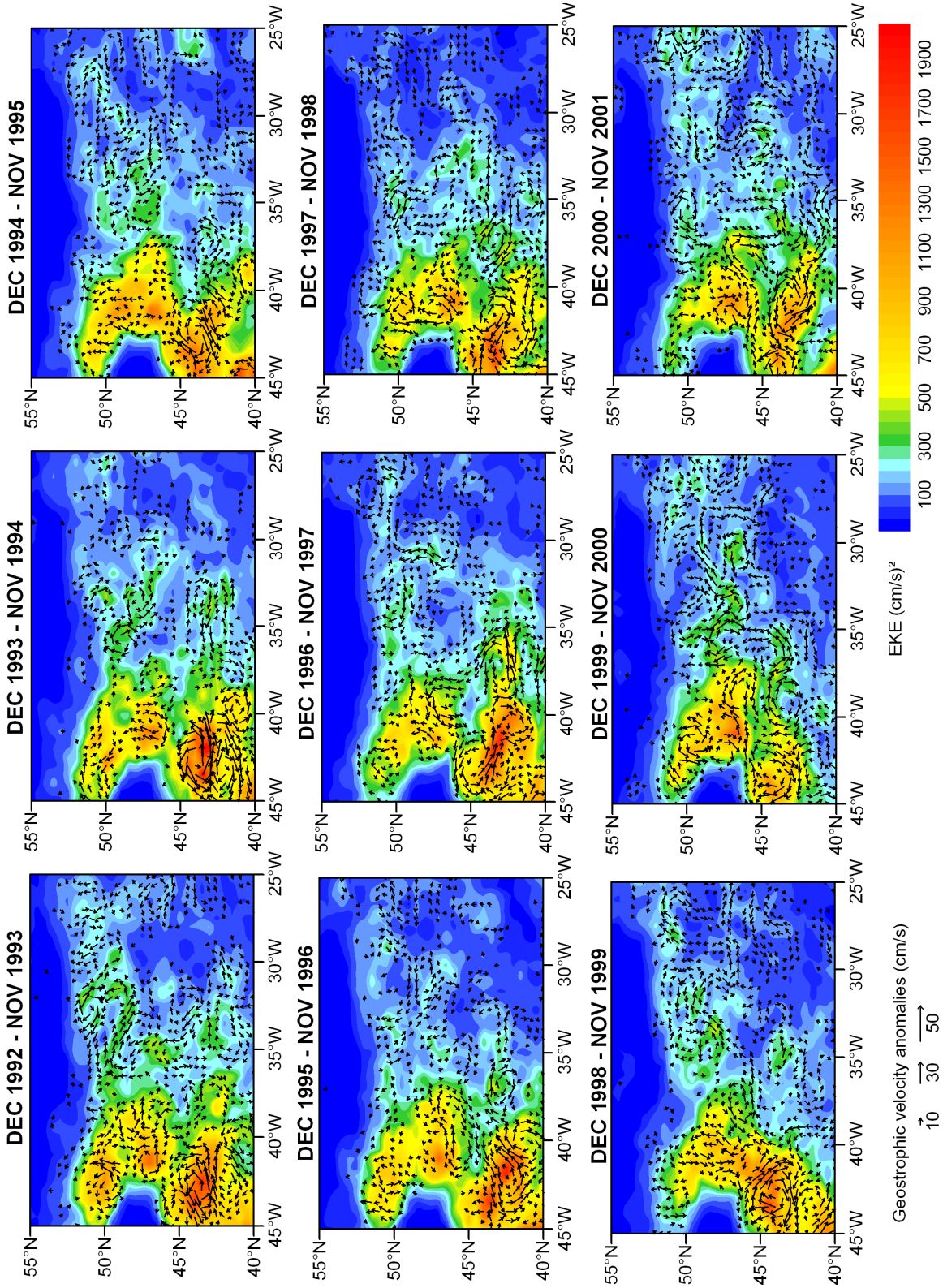

Plate 5.3: *Maps of annual mean EKE (cm²/s²) and geostrophic velocity anomalies in the North Atlantic Current area. EKE was computed from the combined T/P+ERS satellite altimetry data for years 1993, 1996 – 2001 and from T/P data alone for years 1994 and 1995 with a correction factor applied. The vectors of velocity anomalies are shown only starting from 10 cm/s.*

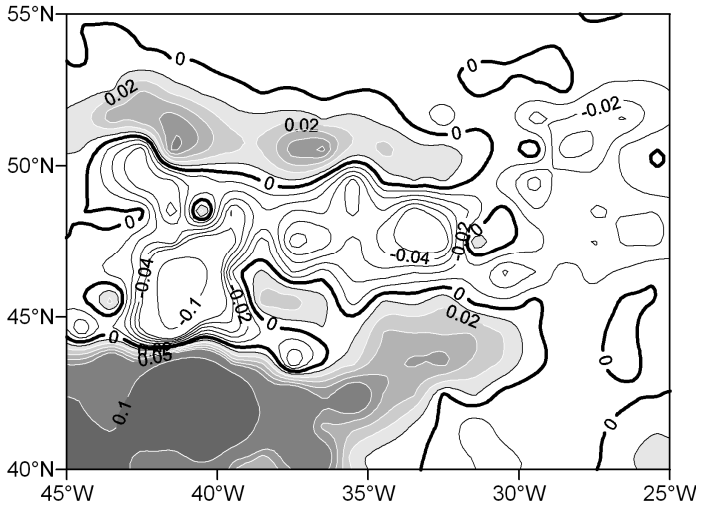

Figure 5.7: *First Empirical Orthogonal Function (EOF-1) of the T/P – derived EKE in the region of the North Atlantic Current explaining 35% of total variance. Before the computation of EOF the data were smoothed by a mean value over 1°x1°. Bold contour delineates zero level.*

A Hovmöller diagram in Figure 5.8 displays the temporal variation of EKE and geostrophic velocity anomalies averaged over a longitudinal band between 38°W and 42°W. The band lies across the NAC flowing north along the Flemish Cap (Figure 5.4, Plate 5.3). Here, the T/P SLA data alone were used to obtain a uniform EKE time-series and T/P+ERS SLA data to estimate geostrophic velocity anomalies. Although the EKE values were underestimated, they did not greatly deteriorate the spatial and temporal pattern of the interannual change. As seen in Figure 5.6, predominantly eastward/westward anomalous velocities are associated with the areas of positive/negative EKE anomalies. This suggests that in the NAC an increase/decrease of EKE mainly reflects an intensification/relaxation of the eastward current. However, in the areas where westward flows exist, for example, in the southern part of the Mann Eddy, an increase of EKE can also be associated with westward anomalous velocities.

The observed EKE anomalies are possibly connected with the NAC branches and can perhaps be an indicator of their strength. For example, in 1993-1994, 1996-1997 the positive EKE anomalies were observed at ~43-44°N and 50°N. This coincided with the strengthening of the eastward flows at these positions suggested by the geostrophic velocity anomalies shown in Plate 5.3. The eastward velocities in 1993 coincided well with an elevated EKE band extending from ~50°N and possibly representing the northern NAC branch. In 1994 this branch became weaker veering south. In 1995 the distribution of EKE was characterized by increased EKE along ~47°N and decreased EKE to the north and south (Figure 5.8, Plate 5.3). The eastward flow intensified around 40°W, but further east the directions of geostrophic velocity anomalies are more chaotic possibly due to high eddy activity. In 1996 – 1997 there was a very large positive EKE anomaly at 42-43°N in the area of the anticyclonic Mann Eddy. At that time the band of elevated EKE and eastward geostrophic velocity anomalies at 42-43°N extended further east up to the MAR. As suggested by Plate 5.3 in 1999 – 2000 most of the NAC waters possibly turned northeastward at ~44-47°N, which coincided with the occurrence of positive EKE anomalies at this site (Figure 5.8).

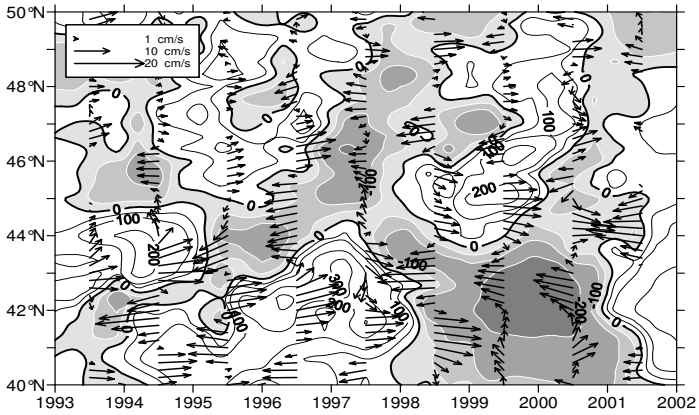

Figure 5.8: *Time-latitude diagram of the T/P-derived EKE (cm²/s²) anomalies and T/P+ERS – derived geostrophic velocity (cm/s) anomalies averaged over a longitudinal band between 42°W and 38°W. Shaded areas represent negative EKE anomalies while blank areas denote positive EKE anomalies.*

Azores Current (AC)

The AC is generated near the Southeastern Newfoundland Ridge where a part of the flow veers southeastward (Figure 5.1). A part of this flow is possibly incorporated in the anticyclonic gyre centered at about 37°N, 53°W and already mentioned above. Another part of the flow continues to move southeastward reaching 33°N – 34°N (Reverdin et al., 2003). The anticyclonic eddies east of the NAC are reported to play an important role in forming the AC. The water from their eastern flank can join the southeastward flow (Käse and Krauss, 1996). At 33°N – 34°N the current turns directly to the east and is traceable as a zonal band with relatively large EKE up to approximately 10°W (Figure 5.4), which is known as the AC proper. Some water from the anticyclonic Mann Eddy may also contribute to the AC, which was documented by Reverdin et al. (2003) on the basis of a drifter study. The maps of annual mean absolute EKE and geostrophic velocity anomalies are shown in Plate 5.4. The interannual variability of EKE in the AC from 1993 to 2001 was characterized by lateral shifts of the EKE core and changes of magnitude (Plate 5.1, 5.4). The largest positive EKE anomalies were observed in 1993-1995 followed by relatively low EKE in subsequent years, which is possibly connected to the relaxation of westerly winds after 1996 expressed by the NAO index. The width of the high EKE band associated with the AC is also subjected to the interannual variations. In 1993 the maximum EKE extended along ~33°N-34°N and was associated with an intensified eastward flow, suggested by the eastward geostrophic velocity anomalies along the EKE core (Plate 5.4). Westward geostrophic velocity anomalies were present to the north and south of the high EKE band. In 1995 the eastward geostrophic velocities at 33°N-34°N decreased while they increased at ~35-36°N and ~31-32°N. The latter was accompanied by a widening of the elevated EKE band in the AC. In the following years EKE in the AC became lower, especially east of the MAR (east of ~35°W-30°W). In 2001 eastward geostrophic velocity anomalies were observed at 34°N-35°N between 35°W-27°W, and at 36°N east of 22°W, adjoining westward geostrophic velocity anomalies to the south suggesting a northward shift of the AC.

Northeastern North Atlantic

This section focuses on the area 5°W - 35°W, 50°N - 65°N where the NAC, after it has crossed the MAR, turns towards north – northeast. There it meets the Rockall-Hatton Plateau (RHP) and splits into two branches: one continuing to flow northward across the Iceland Basin and another, directed to the northeast along the narrow Rockall Channel. The surface circulation in this region was described by Otto and van Aken (1996) on the basis of drifter data.

The maps of annual mean EKE and geostrophic velocity anomalies in the region during the investigated time interval derived from the combined TP + ERS data are presented in Plate 5.5. The geostrophic velocity anomalies were smoothed by moving average over 5×5 grid points. Eddy kinetic energy is subjected to noticeable interannual changes along the NAC branches in the Iceland Basin and Rockall Channel. To trace the temporal change of the NAC branches the T/P-derived EKE values were averaged over three sub-areas in both the Iceland Basin and Rockall Channel (Figure 5.9), where the NAC branches were found. The distribution of surface EKE was the main criterion for choosing the sub-areas for averaging. The northernmost area in the Iceland Basin (IcB-1) is characterized by highest EKE. The other two areas (IcB-2 and IcB-3) were selected to follow the changes of width of the NAC branch in the Iceland Basin. In the Rockall Channel one area represents the inner part (RC-2) with largest observed EKE values while the other two areas represent the outlet region in the northeast (RC-1) and the inlet region in the southwest (RC-3).

According to Stammer and Wunsch (1999) the seasonal change of EKE can be important in this part of the North Atlantic. Therefore, to better understand the relation between the atmospheric forcing and surface circulation presumably reflected by EKE, the time series of EKE calculated over 5 successive weeks to resolve the seasonal signal were compared with the seasonal NAO indices. The latter are based on the difference of normalized sea level pressures between Ponta Delgada, Azores and Stykkisholmur/Reykjavik, Iceland (Hurrell, http://www.cgd.ucar.edu/~jhurrell). Figure 5.9 presents the time series of EKE and NAO index for each sub-area in the Iceland Basin and Rockall Channel.

From 1993 to 1995 there was a relatively narrow high EKE band to the southwest of the RHP outlined by 50 cm^2/s^2 contour (Plate 5.5). This band was connected with the high EKE area in the Iceland Basin. As suggested by the geostrophic velocity anomalies in the Iceland Basin, in 1993 there was a northeastward anomalous flow south of 57°N along the eastern flank of the Reykjanes Ridge to the area with largest EKE and a narrow southward anomalous flow over the western slope of the RHP. This can indicate a stronger NAC flow further west of the RHP, a weaker flow in the vicinity of the RHP, and a suppressed southwestward recirculation along the eastern flank of the Reykjanes Ridge. Northeastward velocity anomalies were also observed in the Rockall Channel from 1993 to 1995 suggesting a possible strengthening of the eastern branch of the NAC. Then in 1996 a decrease of EKE occurred in the area southwest of the RHP and the contour of 50 cm^2/s^2 shifted further west (Plate 5.5, Figure 5.9). The geostrophic velocity anomalies in the Iceland Basin show a reversal in the year of 1996 compared to 1993. The NAC flow over the western slope of the RHP and the southwestward recirculation along the eastern flank of the Reykjanes Ridge probably intensified. The NAC branch in the Rockall Channel perhaps

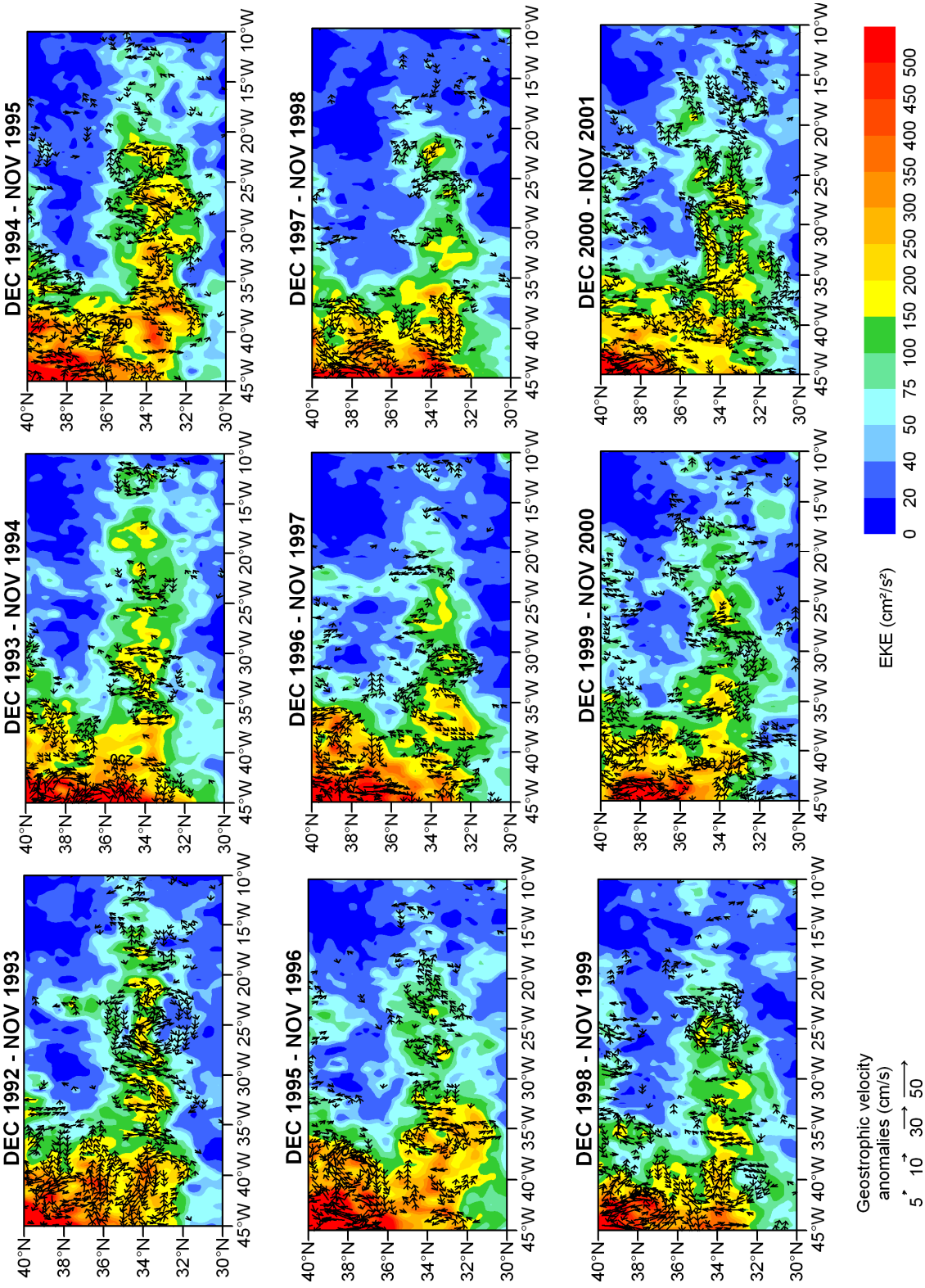

Plate 5.4: *Maps of annual mean EKE (cm²/s²) and geostrophic velocity anomalies in the Azores Current area. EKE was computed from the combined T/P+ERS satellite altimetry data for years 1993, 1996 – 2001 and from T/P data alone for years 1994 and 1995 with a correction factor applied. The vectors of velocity anomalies are shown only starting from 5 cm/s.*

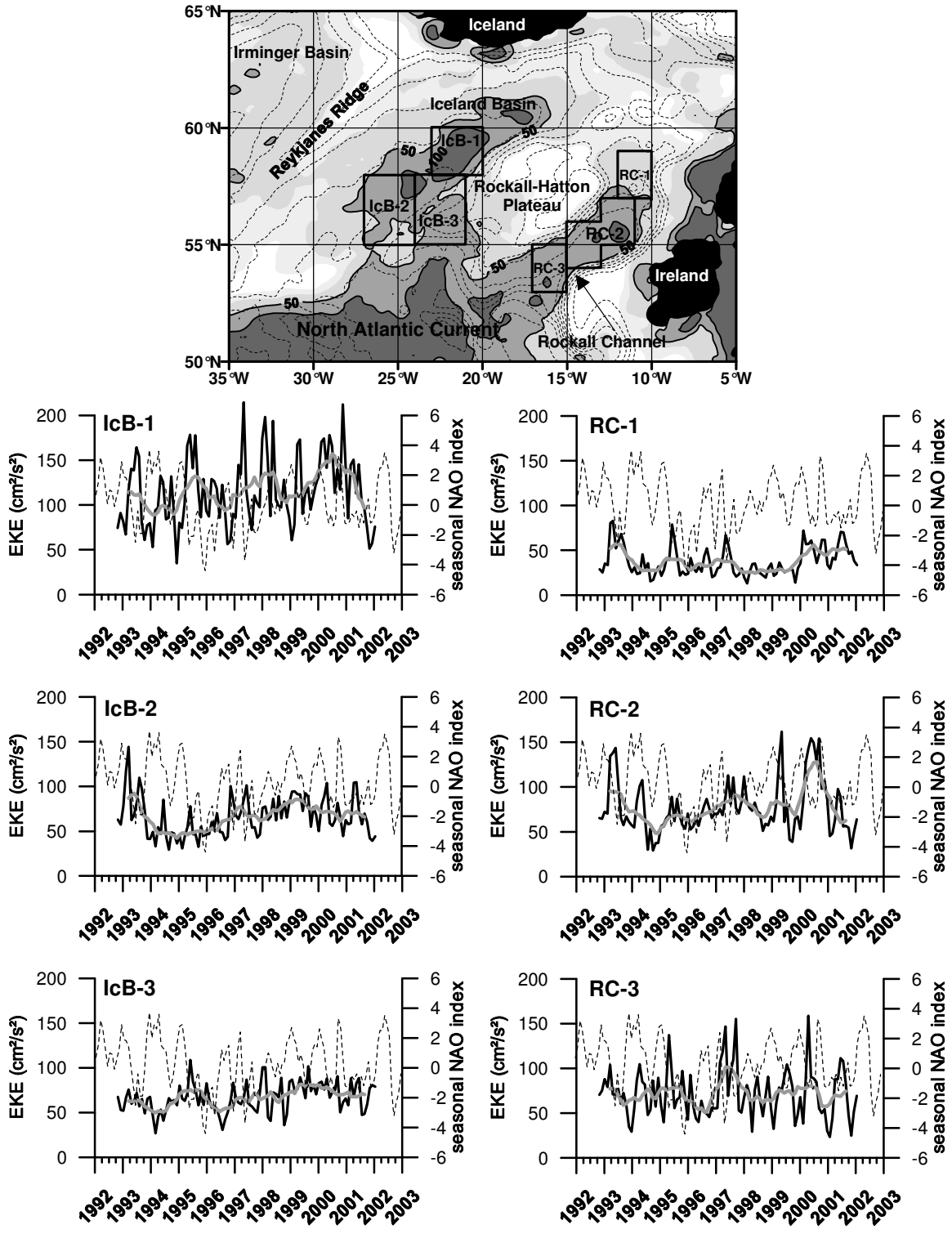

Figure 5.9: *Mean EKE (cm²/s²) in the northeastern North Atlantic with the indicated areas used for averaging (top panel); the time series of EKE (black bold line), computed over each 5 weeks and averaged over IcB-1, IcB-2 and IcB-3 in the Iceland Basin, and RC-1, RC-2 and RC-3 in the Rockall Channel and their yearly running means (grey bold line); seasonal normalized NAO index (thin dashed line). Bottom topography in the top figure is drawn every 500 m.*

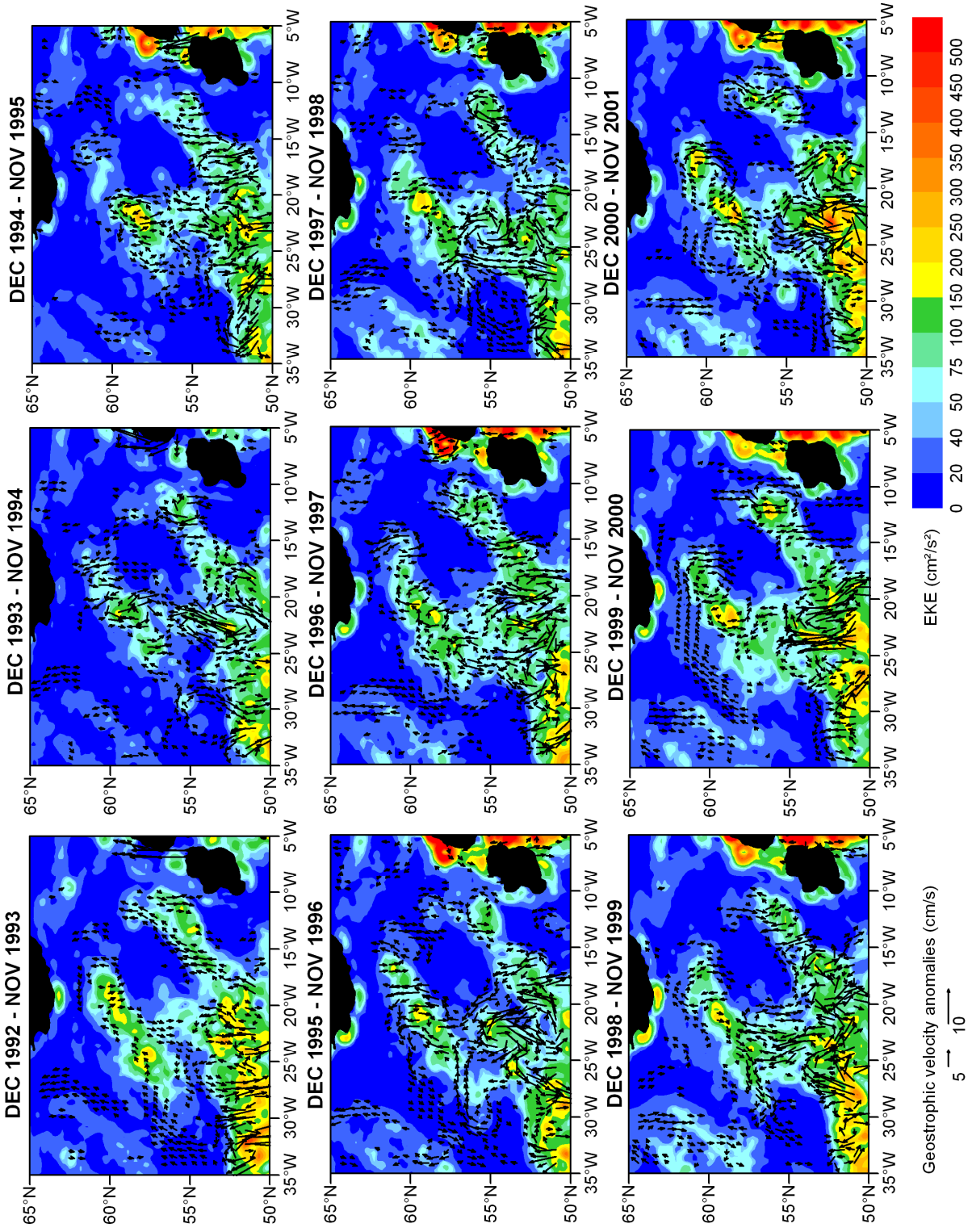

Plate 5.5: *Maps of annual mean EKE (cm²/s²) and geostrophic velocity anomalies in the northeastern North Atlantic. EKE was computed from the combined T/P+ERS and T/P alone (year 1994 and partly 1995) satellite altimetry data (no correction applied for years of 1994 and 1995). The vectors of velocity anomalies are shown starting from 1 cm/s.*

became weaker in 1996 through 1998 since the geostrophic velocity anomalies were predominantly directed southwest or confused (Plate 5.5). Starting from 1997 the band of large EKE southwest of the RHP widened with its western boundary shifting up to ~28°W probably following the NAO – induced shift of the Subarctic Front, which was monitored by hydrographic studies (Bersch, 2002; Verbrugge and Reverdin, 2003).

The variability of EKE in the northeastern part of the North Atlantic exhibited considerable seasonality (Figure 5.9). The seasonal change of EKE overpowered the interannual change. In most cases peaks of EKE occurred in spring and appeared to follow after the peaks of high NAO indices in winter. In the Iceland Basin and southern inlet of the Rockall Channel EKE was low in 1996 after the change of the NAO phase from positive to negative. The peaks of the observed EKE do not always correspond to the peaks in the NAO index, which suggests that the atmospheric forcing is not the only factor determining EKE in this region.

The interannual variability of EKE in the Iceland Basin and Rockall Channel is lower than the seasonal change and difficult to interpret. Figure 5.9 shows that EKE in the western sector of the NAC in the Iceland Basin (IcB-2) after a peak value in 1993 was not high in 1994 – 1995 compared to the years after 1996 while a peak EKE in the eastern sector (IcB-3) was observed in 1995. Eddy kinetic energy increased in both southern sectors in 1996 - 1999 with larger EKE values in the western sector of the NAC (Figure 5.9), which supports the widening of the elevated EKE band in the Iceland Basin outlined by Plate 5.5 after 1996.

It was recently shown that the interannual variations in temperature and salinity in the Rockall Channel are basically modulated by changes in regional circulation (Holliday, 2003). The Rockall Channel is subjected to the influence of Western North Atlantic Water (WNAW) coming together with the NAC and Eastern North Atlantic Water (ENAW) flowing in from the south. The first is cooler and fresher relative to the latter. Holliday (2003) showed that maximum temperature and salinity in the Rockall Channel occurred along with the minimum of WNAW influx (in early 1980s and late 1990s). Plate 5.5 shows that the geostrophic velocity anomalies in the Rockall Channel were mostly directed northeastward in 1993-1995 and southwestward in 1996-2000 indicating correspondingly a strengthening and a relaxation of the average northeastward flow. Thus a strengthening/relaxation of the flow coincides with an increased/decreased transport of WNAW confirming the findings of Holliday (2003). However, no clear evidence of this circulation changes can be obtained from the variability of EKE alone. This is not surprising as the Rockall Channel is a complex, topographically constrained region, where the bottom relief, the balance between the WNAW and ENAW inflow from the south, and the atmospheric forcing are all factors determining the magnitude of EKE.

Northwestern North Atlantic

The maps of annual mean EKE and geostrophic velocity anomalies in the northwestern North Atlantic Ocean for the investigated time interval are shown in Plate 5.6. The geostrophic velocity anomalies were smoothed by a moving average over 5×5 grid points. As was done for the northeastern part of the North Atlantic, EKE calculated for each 5-week interval was averaged over 57°N -63°N, 32°W -38°W in the Irminger Basin (IrB), 57° N-63°N, 49°W-56°W area in the Labrador Sea (LS) and over 58°W-62°N, 41°W-42°W

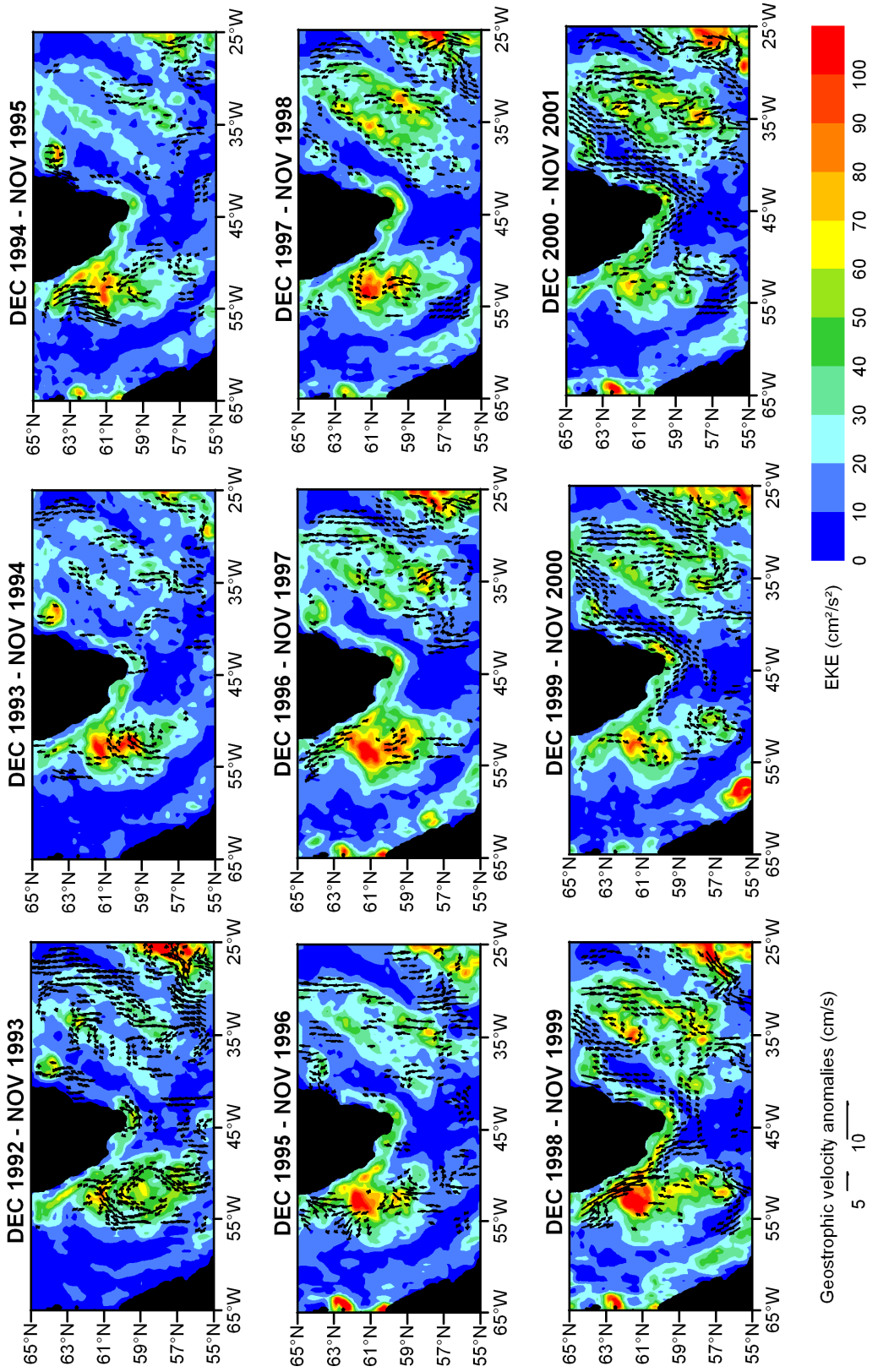

Plate 5.6: *Maps of annual mean EKE (cm²/s²) and geostrophic velocity anomalies in the Irminger Basin and Labrador Sea. EKE was computed from the combined T/P+ERS and T/P alone (year 1994 and partly 1995) satellite altimetry data (no correction applied for years of 1994 and 1995). The vectors of velocity anomalies are shown starting from 1 cm/s.*

in the East Greenland Current (EGC) (Figure 5.10).

Most of EKE in the Irminger Basin is concentrated along two bands parallel to each other and to the Reykjanes Ridge. The most prominent feature of the observed interannual change is the rise of EKE in the Irminger Basin that started in 1995 and reached its maximum in 1998-1999. Then EKE decreased in 2000 and increased again in 2001 (Figure 5.10, Plate 5.6). As was recently documented (Flatau et al., 2003), the circulation changes in the northwestern North Atlantic between 1992 and 1998 were characterized by intensification/relaxation of the cyclonic circulation in the Irminger Basin during positive/negative NAO phase. It is seen in Plate 5.6 that there was an intensified poleward flow along the western flank of the Reykjanes Ridge and predominantly southward velocity anomalies were observed in the Labrador Sea in 1993 – 1995 when the wind stress was strong (Han and Tang, 2001). This confirms the findings of Flatau et al. (2003). After the switch of the NAO phase from positive to negative that occurred in 1996 the pattern of anomalous circulation reversed and southward velocity anomalies were present along the western flank of the Reykjanes Ridge (years 1997-2001) and western coast of Greenland (years 1998-2001), and northward anomalies were observed along the eastern coast of Greenland (years 1998-2001). The reversal of the geostrophic velocity anomalies coincided with an overall sea level rise in the subarctic North Atlantic (Reverdin et al., 1999; Volkov and van Aken, 2003). The latter followed the NAO-induced increase of the heat content of the subarctic North Atlantic and a westward shift of the Subarctic Front, which facilitated the advection of warm and saline NAC water into the subpolar gyre (Verbrugge and Reverdin, 2003; Volkov and van Aken, 2003; Bersch, 2002; Bersch et al., 1999).

The seasonal change of EKE in the Irminger Basin is considerably lower than the interannual (Figure 5.10). The peaks of highest EKE did not occur only in winter when the wind stress is maximum so that the atmospheric forcing does not seem to be directly responsible for the interannual change of EKE in this region. The rise of EKE that occurred in the Irminger Basin from 1995 to 1999 and in 2001 could possibly be a reflection of the large velocity anomalies connected with the relaxation of the large-scale subpolar gyre and the decrease of the surface cyclonic flow. On the other hand, the distribution of large yearly geostrophic velocity anomalies is not only related to the large EKE areas (Plate 5.6). This is not surprising since EKE is a measure of geostrophic velocity variance over yearly time intervals. Another contribution to the rise of EKE in the Irminger Basin could be associated with eddy generation mechanisms at the Subarctic Front, which underwent the NAO-induced westward shift (Bersch, 2002). It appears that the rise of EKE involves two bands: easternmost in the vicinity of the Reykjanes Ridge and westernmost in the center of the Irminger Basin (Plate 5.6). It can be suggested that while the easternmost band is associated with the frontal northeastward flow along the western flank of the Reykjanes Ridge (Figure 5.5), the westernmost band of EKE owes its existence to the convectively generated near-surface front. The presence of two parallel EKE bands in the Irminger Basin still poses a question, however, and in order to address it, an additional research is needed.

The variability of EKE in the East Greenland Current (EGC) exhibited apparent seasonality (Figure 5.10). Maxima EKE values are generally associated with autumn period that coincides with the time of maximum seasonal sea level occurrence (Volkov and van Aken, 2003). Therefore, high autumn EKE in the EGC may be caused by seasonal variation of geostrophic flow determined by the seasonal change of the sea level near Greenland.

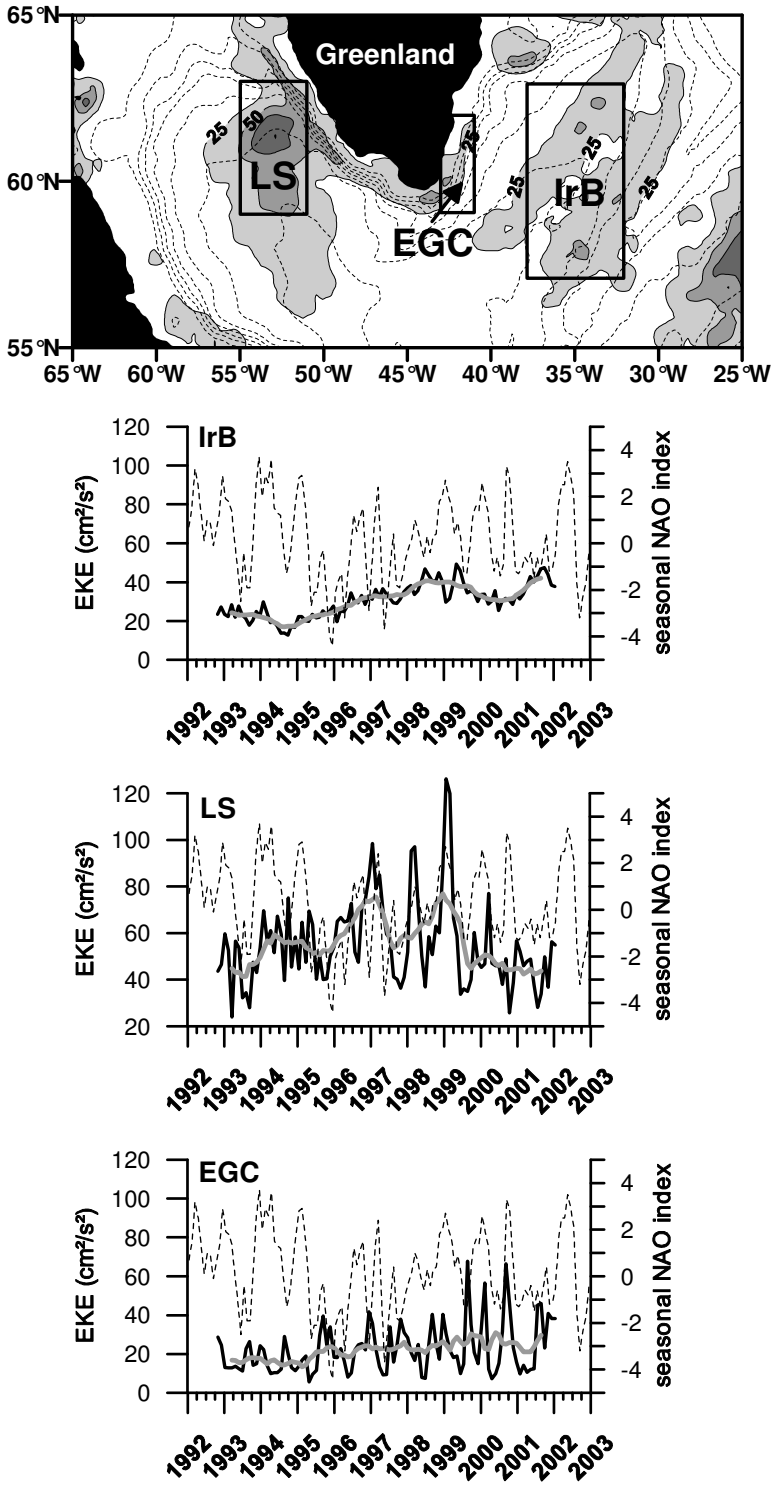

Figure 5.10: *Mean EKE (cm²/s²) in the northwestern North Atlantic with the indicated areas used for averaging (top panel); the time series of EKE (black bold line), computed over each 5 weeks and averaged over IrB in the Irminger Basin, LS in the Labrador Sea, and EGC in the East Greenland Current areas, and their yearly running means (grey bold line); seasonal normalized NAO index (thin dashed line). Bottom topography in the top figure is drawn every 500 m.*

In the Labrador Sea the variability of EKE is more complex (Figure 5.10). Figure 5.10 shows that the seasonal change of EKE is well pronounced and in some years appeared to be coherent with the seasonal NAO index. Maximum values of EKE were found to be associated with the high winter NAO indices from 1998 to 2001, but not in the early part of the record. On the basis of T/P and hydrographic data, Han and Tang (2001) found a positive correlation between the changes of total southward volume transport in the Labrador Sea in spring/summer and the winter NAO index. This is confirmed by the geostrophic velocity anomalies in the Labrador Sea, which were mainly directed southwards in 1993 – 1995 (Plate 5.6). However, the direct atmospheric forcing does not appear to be the prime factor determining the variability of EKE in the Labrador Sea. As seen in Figure 5.10, EKE was fairly low during high winter NAO indices in 1993 – 1995 and the greatest EKE occurred in the winters of 1996/97 (negative NAO index), 1997/98 and 1998/99. A recent study by Eden and Böning (2002) suggested that the source of the large EKE in the Labrador Sea can be related to the formation of eddies from the West Greenland Current (WGC) due to barotropic instability in the local topographical conditions. Eddies are formed at the location where the steep continental slope of Greenland adjoins the slightly sloping shelf area to the north. Thus the varying EKE field in the Labrador Sea, besides the direct atmospheric forcing, can be modulated by instability of the WGC flowing over the abruptly changing topography.

5.4 Conclusions

This study has attempted to contribute to our knowledge of the interannual variability of the surface currents in the North Atlantic Ocean. The surface EKE was used to analyze the interannual variability of the position and intensity of surface currents. It was shown that EKE is subject to significant interannual variations throughout the North Atlantic as well as to seasonal changes in the northern parts, in particular, in the Iceland Basin, Rockall Channel and Labrador Sea.

The mean EKE field, computed from the combined T/P+ERS altimetry data, is concentrated along major frontal currents and thus outlines the main surface circulation pattern (Figure 5.4). The largest EKE exceeding 2500 cm^2/s^2 was found in the GS extension area. The NAC was observed as a broad northeastward drift with EKE ranging between 1000 cm^2/s^2 in the west and 100 cm^2/s^2 in the east of the current. The AC was represented by EKE of 50 – 200 cm^2/s^2 between about 32°N – 36°N. The mesoscale variability, which largely determines the EKE field, appeared to be responsible for over 50% of total sea level variance in the high variability areas of the GS, NAC and AC.

The hydrographic data obtained from 1990 to 2003 in the northern North Atlantic showed that the position of high EKE cores corresponded to the position of frontal zones depicted by the density distribution and dynamic heights. This confirmed the theory that the instability processes along the frontal currents can possibly be the main source of eddy energy in the ocean, while the time scale of the dissipation mechanisms appears to be so small that EKE does not diffuse far from the source area. Thus it was concluded that in the absence of sufficiently accurate dynamic topography for the estimation of absolute currents, EKE can be used as a proxy to determine the position and analyze the intensity of oceanic currents.

The interannual variability of EKE in the GS extension area was expressed by meridional displacements within a 2-degrees band. The meridional displacements of the EKE core were characterized by a most northerly position in 1993-1996 followed by a southward shift. The most southern position was reached in 1998, approximately 2 years after the NAO had reversed to its extreme negative phase in 1996. The shift of EKE was accompanied by lateral restructuring of the geostrophic velocity anomalies along the GS extension indicating an intensification of the southern flank of the current after 1996. These findings corresponded to those documented by Frankignoul et al. (2001), Rossby and Benway (2000), and Taylor and Stephens (1998), who found approximately similar time lag between the shifts of the GS core and NAO events. Thus the core of EKE in the GS extension area appeared to be mainly associated with the core of the current.

The inter-annual change of EKE in the NAC west of the Mid-Atlantic Ridge was found to be governed by variations in EKE distribution between three zones centered at ~43°N, ~47°N and 50°N possibly connected with the current jets. This research showed that, on the interannual timescale, EKE in the central zone varied out-of-phase with the side zones. It appeared that positive EKE anomalies in the NAC were generally associated with eastward geostrophic velocity anomalies whereas negative EKE anomalies corresponded to anomalous westward velocities. This implies that when the eastward flow at ~43°N and ~50°N strengthens, the eastward flow at ~47°N becomes weaker and vise versa.

This research showed that EKE in the AC in 1993 – 1995 was larger than in subsequent years, especially east of the Mid-Atlantic Ridge. The decrease of EKE could possibly be induced by the overall weakening of eastward flow due to the relaxation of westerly winds associated with the negative NAO indices in winter of 1995/96 and 1996/97.

The interannual change of EKE in the Iceland Basin reflected the earlier monitored NAO – induced westward shift of the Subarctic Front that occurred after 1996. In the Rockall Channel the geostrophic velocity anomalies indicated an intensified northeastward flow in 1993 – 1995 followed by a relaxation in 1996 – 2000. In both the Iceland Basin and Rockall Channel the seasonal change of EKE was found to overpower the interannual change, especially in the high EKE area northwest of the RHP.

The present research confirmed the previously documented changes in the circulation within the subpolar gyre: the intensification/relaxation of the cyclonic circulation during the positive/negative phase of NAO. In the Irminger Basin the seasonal changes of EKE were found to be lower than the interannual changes. The rise of EKE from 1995 to 1999 and in 2001 was attributed to two possible sources. Firstly, the large geostrophic velocity anomalies that indicated the significant weakening of the cyclonic circulation. Secondly, the instability processes at the Subarctic Front, which is subject to the NAO-induced shifts towards the Irminger Basin. In the Labrador Sea the seasonal change of EKE was found to overpower the interannual change. The seasonal and interannual variability of EKE here did not appear to be completely coherent with the atmospheric forcing expressed by NAO. Therefore, other processes like seasonally modulated instability of the WGC under specific topographical conditions may possibly be very important.

Chapter 6

Propagating features in the eddy field of the North Atlantic Current

The variations of eddy kinetic energy (EKE) can presumably be used as a proxy to identify changes in the position of current jets. The interannual variability of EKE in the North Atlantic Current (NAC) west of the Mid-Atlantic Ridge has exhibited meridional displacements of EKE anomalies. An increase/decrease of EKE in the NAC was found to be mainly associated with an intensification/relaxation of the predominantly north-eastward NAC flow. The main objective of the research reported in this chapter was to detect propagating signals in the EKE field using Complex Singular Value Decomposition (CSVD) analysis. It appeared that the first empirical mode showed a three-zoned oscillating pattern. Two side bands, associated with the Mann Eddy and the northern wall of the NAC, were found to vary out-of-phase with the central band centred near 47°N. A quasi-meridional propagation of the interannual EKE signal downstream the NAC was identified. Almost two EKE waves were observed between 1993 and 2003 with a period of about 6 years. However, due to the insufficient data record it is neither possible to estimate the typical frequency of the observed propagation of EKE anomalies, nor to state that this propagation has a regular occurrence. The inter-annual change inside the Mann Eddy south of 44°N appeared to be dominated by standing oscillations. The interannual change of EKE in the NAC was related to the NAO. Large positive EKE anomalies south of 45°N appeared after the NAO had changed from positive to negative phase in the winters of 1995/1996 and 2000/2001. The observed pattern of the variability and the propagation of EKE signal in the NAC might be a result of (1) the meridional shifts of the NAC core and/or (2) the successive intensifications of already existing branches[*].*

6.1 Introduction

In the previous chapter it was shown that temporal variations of EKE reflect temporal variations of currents. The variability of the surface circulation can be studied using the time series of EKE. The study, presented in this chapter, focuses on the 30°W-50°W, 35°N-55°N geographical domain. The surface circulation in this region is governed by the North

[*] This chapter is based on the paper by D.L. Volkov *"Propagating features in the eddy field of the North Atlantic Current"*, Geophys. Res. Lett., in press, 2004.

Atlantic Current (NAC). The NAC is a direct continuation of the Gulf Stream (GS) extension and represents a broad easterly drift with a maximum flow at the Subarctic Front (Krauss, 1986) (Figure 5.1). The GS forms the NAC after it crosses the Southeast Newfoundland Ridge. East of it, the NAC turns north, flows around the Flemish Cap, makes a loop northeast of Newfoundland, then veers east and crosses the Mid-Atlantic Ridge (MAR) at about 52°N, being probably fixed to the Charlie-Gibbs Fracture Zone. The area near 42°N and 42°W is identified as a centre of a permanent anticyclonic gyre (Mann, 1967), also known as the Mann Eddy. It is well defined in the average drifter-derived current velocity fields (Reverdin, 2003). Dietrich et al. (1975) presented a branch of the NAC turning eastward just south of the Flemish Cap and forming the northern extremity of the Mann Eddy. Drifter measurements at the northern edge of the Mann Eddy (at about 45°N) showed that buoys were moving further east with high speeds and large meanders (Krauss and Meincke, 1982). In contrast to Dietrich et al. (1975), Krauss (1986) and Krauss et al. (1987) did not document any permanent branching of the NAC, but stated that jets occasionally appear at different locations. Largest EKE in the NAC is closely associated with the regions of strong mean flow and large speed (1 m/sec) drifter trajectories (Reverdin et al., 2003).

The interannual variability of EKE in the region of study from 1993 to 2002 showed meridional displacements of EKE anomalies (deviations from long-term mean) (Chapter 5; Volkov, in press). A peculiar property of these displacements was an almost out-of-phase change of EKE in three areas: (1) the anticyclonic Mann Eddy centred at about 42°N and 42°W, (2) the site of a possible branching of the NAC at 45°N-47°N, and (3) the northern wall of the NAC at the Subarctic Front (near 52°N) (Figure 5.7; Figure 6.1, b). The change occurred in the way that when positive EKE anomalies were observed near latitudes of 42°N-43°N and 52°N, negative EKE anomalies were seen in between, near 47°N. Then the situation reversed with large EKE along 47°N and low EKE on either side. Such a variability pattern of EKE may reflect the meridional movements of the NAC core and/or the redistribution of transport between different NAC branches.

This chapter aims to investigate the character of the interannual variability of EKE in the NAC west of the Mid-Atlantic Ridge. The first question to be addressed is how the variability of EKE in the NAC reflects changes in the large-scale surface circulation. The second and principal task is to test the EKE time series for propagating signals. The final objective is to relate the interannual variability of EKE and surface circulation to the variable atmospheric forcing expressed by the winter (December through February) North Atlantic Oscillation (NAO) index.

6.2 Method

The combined TPJ+ERS sea level anomaly (SLA) maps from October 1992 to July 2003 were used to compute the u' and v' geostrophic velocity anomalies and EKE as described in Chapter 2. The interannual EKE was computed over yearly time intervals using a 53 weeks sliding window. The geostrophic velocity anomalies were estimated for each SLA map and then low-pass filtered using a moving average operation with a window of 53 weeks to make the velocity estimates consistent with EKE. The correlation coefficient between the filtered geostrophic velocity anomalies and the interannual EKE was computed at each grid

point to investigate how the large-scale surface circulation changes depend on the changes in EKE.

The complex singular value decomposition (CSVD) analysis was used to detect propagating structures in the time series of EKE. The variability of the EKE field associated with the variability of currents is a result of a superposition of various determinants interacting at different space and time scales. An efficient technique for compressing the variability of any time series data into a smaller number of independent pieces of information is the empirical orthogonal functions (EOF) analysis, also known as the principal component analysis (PCA) (Preisendorfer, 1988) (see Chapter 2). This analysis decomposes the spatial and temporal variability of data series into orthogonal functions or statistical modes, i.e. it retrieves the most significant phenomena reducing the amount of data. However, conventional EOF analysis can only be used for detecting standing oscillations. The Complex EOF analysis has shown to be a useful technique to identify propagating signals (Horel, 1984; Merrifield and Guza, 1990). The procedure is to derive complex time series formed with the original data field $d_x(t)$ in the real part and its Hilbert transform $d_x^H(t)$ in the imaginary part:

$$D_x(t)=d_x(t)+i\cdot d_x^H(t), \tag{6.1}$$

where x denotes spatial location and t is time. The Hilbert transform represents a filtering operation in which the amplitude of each spectral component remains unchanged but the phase is shifted by $\pi/2$. Expanding the scalar time series $d_x(t)$ as a Fourier series over all frequencies, ω, the complex time series are

$$D_x(t)=\sum_{\omega}\left[A_x(\omega)\cdot\cos(\omega\cdot t)+B_x(\omega)\cdot\sin(\omega\cdot t)\right]+i\cdot\left[B_x(\omega)\cos(\omega\cdot t)-A_x\sin(\omega\cdot t)\right] \tag{6.2}$$

After the complex time series have been formed, the following steps of computing complex EOFs are identical with the conventional EOF analysis. For large data sets the analysis becomes computationally impractical because of the use of a covariance matrix (Kelly, 1988). Therefore, this study uses the CSVD method, for which it is not needed to compute or store a covariance matrix (Susanto et al., 1998). The CSVD approach provides a one-step operation for computing the various components of the eigenvalue problem (eigenvectors, eigenvalues and principal components) and represents considerable savings in computations over the conventional EOF approach making the analysis simpler and faster (Kelly, 1988).

Before carrying out the CSVD analysis, the EKE data were smoothed by averaging over 1° by 1° squares. Then a complex $m \times n$ matrix **D** was created according to (6.1). Each row (m) of **D** is a time series for a given location and each column (n) of **D** is a map. In matrix notation the CSVD becomes

$$\mathbf{D} = \mathbf{USV}^T, \tag{6.3}$$

where the columns of the complex matrix **U** ($m \times m$) are the eigenvectors of spatial covariance matrix $\mathbf{DD}^T$ while the columns of the complex **V** ($n \times n$) are the eigenvectors of the temporal covariance matrix $\mathbf{D}^T\mathbf{D}$. The latter are also called 'principal components'. **S** is a

real $m \times n$ matrix containing s singular values on the diagonal. To see the connection between the EOF method and SVD decomposition, consider the covariance matrix **R** of **D**, taking into account that $\mathbf{U}^T\mathbf{U}=\mathbf{I}$ and $\mathbf{V}^T\mathbf{V}=\mathbf{I}$ become unitary:

$$\mathbf{R}=\mathbf{D}^T\mathbf{D}=(\mathbf{USV}^T)^T(\mathbf{USV}^T)=\mathbf{VS}^T\mathbf{U}^T\mathbf{USV}^T=\mathbf{VS}^T\mathbf{SV}^T \quad (6.4a)$$

$$\mathbf{R}=\mathbf{DD}^T=(\mathbf{USV}^T)(\mathbf{USV}^T)^T=\mathbf{USV}^T\mathbf{VS}^T\mathbf{U}^T=\mathbf{US}^T\mathbf{SU}^T \quad (6.4b)$$

Since the EOF method yields the matrix of eigenvalues $\mathbf{\Lambda}$ such that $\mathbf{R}=\mathbf{C\Lambda C}^T$, where **C** is the matrix of eigenvectors, then $\mathbf{\Lambda}=\mathbf{S}^T\mathbf{S}$ and singular values s are the square roots of the nonzero eigenvalues λ. Each eigenvalue λ_i gives a measure of the fraction of the total variance in **R** explained by the mode i. This fraction is found by dividing the λ_i by the sum of all the other eigenvalues.

As follows from (6.4), the only difference between **U** and **V** is how the singular values are grouped and which is identified with the spatial function and which with the temporal function. In this research the eigenvectors in **U** are called the complex empirical orthogonal functions (CEOFs) and the eigenvectors in **V** are called the complex principal components (CPCs). The former shows the spatial distribution of the variability pattern coupled with each eigenmode while the latter depicts the temporal change of the modal pattern of **D**.

The spatial amplitude function is defined as the real part of a complex matrix A_s and the temporal amplitude function is defined as the real part of a complex matrix A_t:

$$\mathbf{A}_s=\mathbf{US} \quad (6.5a),$$

$$\mathbf{A}_t=\mathbf{VS}^T \quad (6.5b).$$

Spatial and temporal phase functions for each mode i are defined as

$$\theta_i(x)=\tan^{-1}(\mathrm{Im}[U_i(x)]/\mathrm{Re}[U_i(x)]), \quad (6.6a)$$

$$\varphi_i(t)=\tan^{-1}(\mathrm{Im}[V_i(t)]/\mathrm{Re}[V_i(t)]), \quad (6.6b).$$

The temporal phase $\varphi_i(t)$ describes the temporal variation of phase associated with **D** for each eigenmode, while the spatial phase $\theta_i(x)$ shows the relative phase of fluctuations among the various spatial locations where **D** is defined. In analogy with simple waves, a wavenumber, frequency and phase speed for each mode i can be estimated by

$$k_i=d\theta_i/dx \quad (6.7a)$$

$$\omega_i=d\varphi_i/dt \quad (6.7b)$$

$$c_i=\omega_i/k_i \quad (6.7c).$$

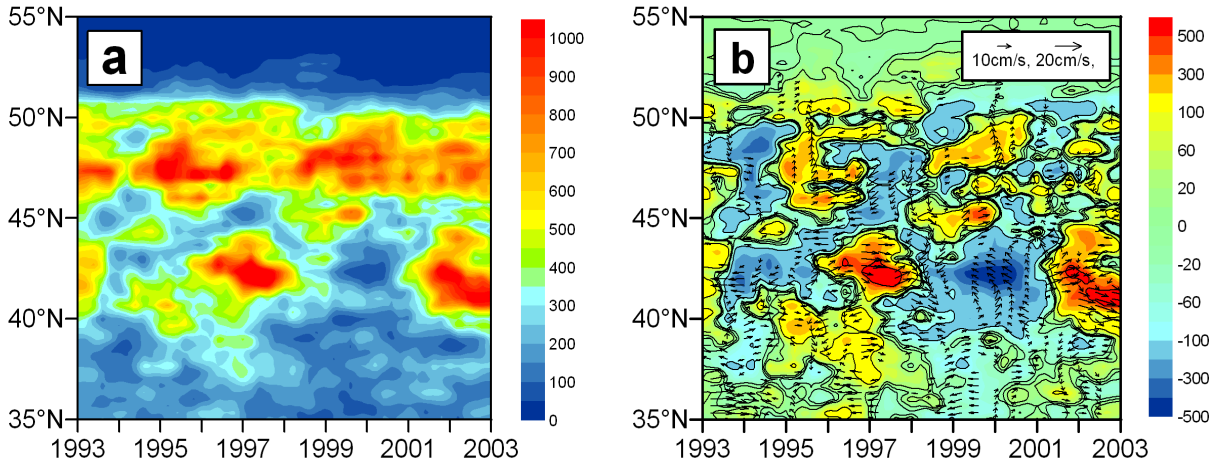

Figure 6.1: *The Hovmöller time-latitude diagrams of absolute EKE* (a) *and EKE anomalies* (b) *(cm²/s²) at 40°W.*

In this chapter only the first CEOF and CPC are considered, because higher modes are not statistically significant. The spatial pattern corresponding to the CEOF-1 mode is presented as a homogeneous correlation map. The homogeneous correlation map is determined as the vector of correlation coefficients between the real part of CPC-1 and the EKE values in the original data field $d_x(t)$ at each grid point. It is a useful indicator of the spatial localization of the co-varying part between the original data field and its empirical mode. If to take a square of the correlation coefficient at a particular grid point and to multiply it by 100, the obtained value would show the percentage of variance accounted for by a mode.

6.3 Results of the analysis

Interannual variability of EKE in the NAC

The temporal change of the interannual EKE across the NAC flowing along 40°W is shown in Figure 6.1a. The 40°W meridional section is characterised by the existence of two large EKE areas. The southern area, centred near 42°N, is associated with the Mann Eddy. The northern large EKE area is centred near 47°N and possibly indicates the place where most of the NAC waters turn east. Further eastward at 35°W, the meridional distribution of EKE is more diverse and shows maxima at 42-44°N, 47-48°N, and near 50°N (not shown). The Mann Eddy is characterized by very large interannual variations of EKE ranging from less than 100 cm²/s² to almost 1000 cm²/s². The most striking feature observed from the interannual variability of EKE is the appearance of two maxima in the Mann Eddy in 1996-1998 and from 2001. The observed increase of EKE in the Mann Eddy followed the change

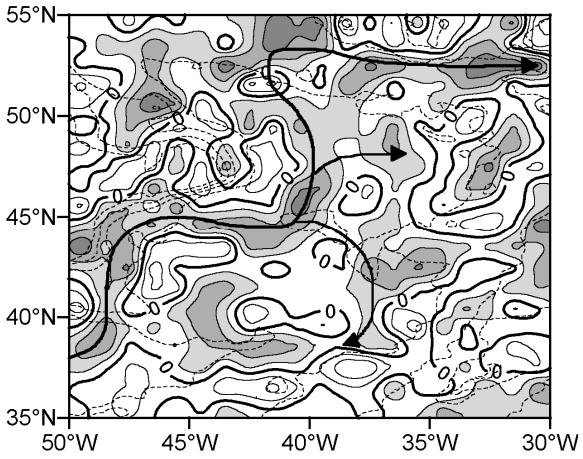

Figure 6.2: *Correlation map between the interannual EKE estimates and north-eastward component of geostrophic velocity anomaly. Contours are drawn every 0.1. Positive contours are shaded. The bottom topography (dashed contours) is drawn every 1000 m. The NAC course is presented by curves with arrows.*

of the NAO phase from positive to negative in the winters of 1995/1996 and 2000/2001. At the same time a decrease of EKE occurred at 47°N, which suggests an almost out-of-phase character of the interannual variability of EKE in the Mann Eddy and in the region north of it (Figure 6.1b).

EKE and large-scale surface circulation

EKE is a measure of the variability of the current over a particular time interval. The current velocity varies due to the changes in u' and v'. The latter can have a different sign at any time and, therefore, large EKE can presumably indicate both a strengthening and a relaxation of the absolute current. However, strong frontal currents, like the NAC, are baroclinically less stable and subject to large meandering and eddy activity. The intensity of the instability processes is directly proportional to the density gradients at frontal surfaces and hence to the strength of the current velocity. Symbolically the change of EKE due to the interconversions of kinetic energy can be presented as $d(EKE)/dt = \{MKE \rightarrow EKE\} + \{PE \rightarrow EKE\} - D_{EKE}$, where $\{MKE \rightarrow EKE\}$ is the transfer of kinetic energy between the mean and eddy fields, $\{PE \rightarrow EKE\}$ is the interconversion between available potential energy (PE) and EKE, and D_{EKE} is the viscous dissipation of EKE (Drijfhout, 1992; Wood, 1988). The latter is always negative in the absence of surface stress forcing factors. The term $\{MKE \rightarrow EKE\}$ represents the barotropic instability while the term $\{PE \rightarrow EKE\}$ denotes the baroclinic instability. Model experiments (Wood, 1988) showed that at the beginning of the model run a baroclinic growth phase takes place when EKE increases at the expense of PE. The barotropic instability [$\{MKE \rightarrow EKE\} > 0$] during this phase is weak. This process is followed by a second phase in which strong Reynolds stress convergences start feeding a mean flow [$\{MKE \rightarrow EKE\} < 0$]. Therefore, any changes of EKE generally reflect the changes of available PE supply and, hence, the displacements of isopicnic surfaces and consequently oceanic fronts and associated currents. Theoretically, an increase of density gradient leads to the strengthening of the frontal

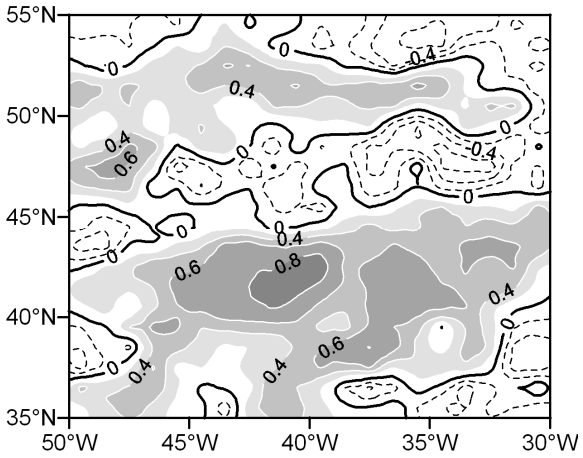

Figure 6.3: *Spatial pattern of the CEOF-1 of the interannual EKE anomalies, presented as a homogeneous correlation map, determined as the vector of correlation coefficients between the real part of the CPC-1 and the EKE values. Contours are drawn every 0.2. Negative contours are dashed.*

current and is associated with an increase of available potential energy, which in turn gives a rise to EKE.

Figure 6.2 presents the map of correlation coefficients between the local diagonal geostrophic velocity anomaly components v' directed northeast and the EKE estimates at each grid point. Since the NAC represents a broad eastward to north-eastward drift (Krauss, 1986), positive correlation is found along the main paths of the flow, especially around the Grand Banks. The positive correlation between the north-eastward component of the geostrophic velocity anomaly and EKE implies that an increase of the latter is associated with an intensification of the north-eastward flow. Thus this chapter confirms the statement made in Chapter 5 that in the NAC an increase/decrease of EKE mainly reflects an intensification/relaxation of the current.

Propagating features in the EKE field

The EKE signal in the Mann Eddy considerably overpowers the EKE signal in other regions of the NAC. Therefore, before performing the CSVD analysis the EKE data were normalized with the standard deviation so that each grid point has an equal contribution to the EKE variability pattern. The CSVD analysis separated the variability of EKE into modes that are uncorrelated and orthogonal to each other. The whole idea of using the CSVD approach is to reduce dimensionality of the data and to identify the mode(s) with physically significant eigenvalues, which represent a major part of the variance. The eigenvalues, derived from the singular values s, showed that the three leading complex EOF modes account for 63% of the total variance. Individually, they explain 28% (CEOF-1), 21% (CEOF-2) and 14% (CEOF-3) of the variance. The interannual EKE time series, used in this study, have 10 independent estimates. Therefore, the CSVD analysis was cut off at the first mode as higher modes are not significant for such a small sample.

The spatial pattern associated with the CEOF-1 is shown in Figure 6.3 as a homogeneous correlation map as described above. The CEOF-1 exhibits a three-zoned variability pattern extending over the entire research domain. There are two zonal bands

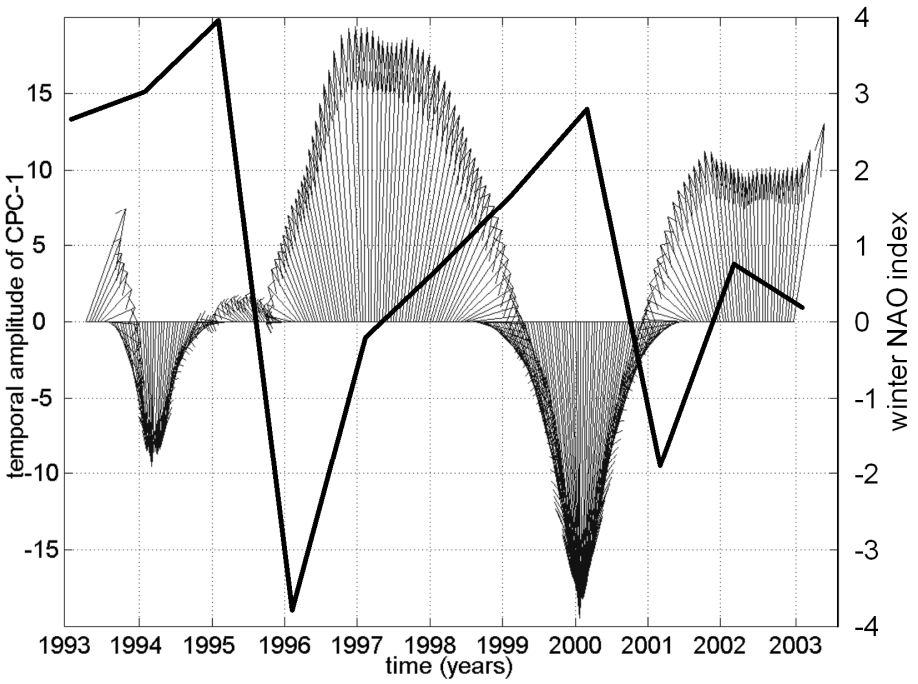

Figure 6.4: *Feather plot of the vectors set up by imaginary and the real parts of the temporal amplitude function of the first empirical mode (CPC-1) and the winter (December through February) NAO indices (from Hurrell, http://www.cgd.ucar.edu/~jhurrell).*

with positive correlation coefficients, coincident with the northern wall of the NAC near 50°N and with the Mann Eddy centred near 42°N. In between, there is a band with negative correlation coefficients, associated with a possible branching of the NAC near 47°N. Such a variability pattern implies that when positive EKE anomalies take place in the Mann Eddy and along the northern wall of the NAC at 50-52°N, an opposite situation occurs at 45-48°N. Thus two side bands vary out-of-phase with the central band. The northern band is much less energetic than the two other (Figure 6.1). Therefore, the redistribution of EKE between the Mann Eddy and the band centred near 47°-48°N determines most of the EKE variability in the NAC. In Figure 6.3 one can see that the correlation between the CPC-1 and the original EKE time series is largest in the Mann Eddy and exceeds 0.8 at about 41°W, 41°N, which means that the first empirical mode accounts here for over 64% of the variance. In the central band near 47°N the CEOF-1 mode explains up to about 1/3 of the variance at 34°W.

The feather plot of the vectors set up by the imaginary and real parts of the temporal amplitude function A_t of the first empirical mode (CPC-1) is shown in Figure 6.4. The CPC-1 shows how the spatial pattern of EKE, depicted by the CEOF-1, was changing during the studied time interval. Since there is a nonzero imaginary part or phase information, the vectors in the feather plot have a clockwise rotation. This proves that indeed there is a propagating pattern in the observed variability of EKE in the NAC. There would be no phase information (imaginary part of $A_t = 0$) and the vectors would be vertical if no propagating pattern existed in the EKE data. The temporal amplitude function shows that in the NAC area one complete wave existed from 1993 to 2003. Two troughs in 1994

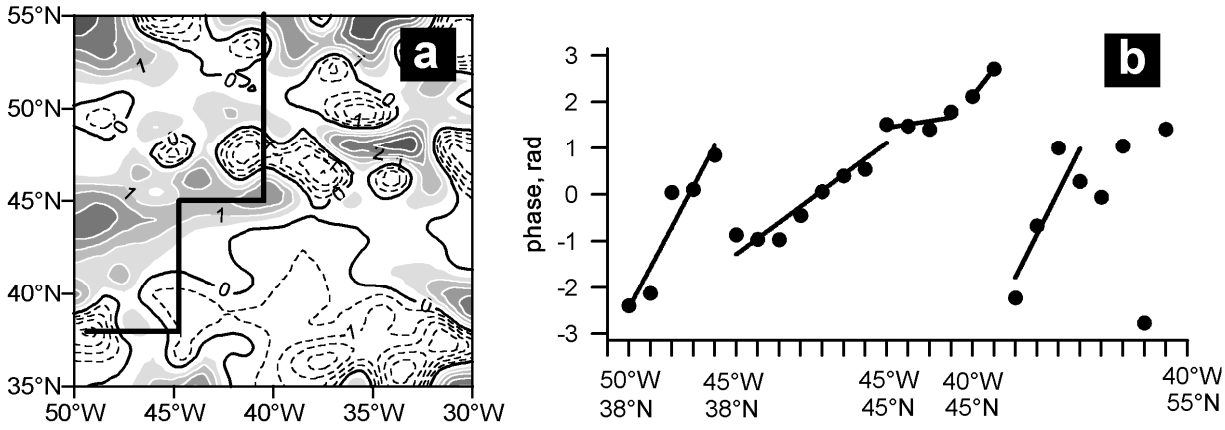

Figure 6.5: *The distribution of the spatial phase function (rad) of the first empirical mode (a) and the variation of the spatial phase function along the thick broken line (b). Contours in (a) are drawn every 0.5 rad and the negative contours are dashed. The dots in (b) indicate the observed values and the solid lines are their linear fits or slopes calculated by regression.*

and in 1999-2000 and two crests in 1996-1997 and in 2001-2002 can be seen in CPC-1 (Figure 6.4). Thus the period of the first empirical mode from 1993 to 2003 is approximately 5-6 years. However, the length of the EKE time series studied here is too short to derive the true periods of the waves, and the waves can be irregular. Therefore, the period of 5-6 years is an approximation valid only for the investigated time interval.

The temporal change of the first empirical mode described by the CPC-1 appears to be a good approximation of the interannual variability of EKE in the NAC. The CPC-1 peaks in 1996-1997 and in 2001-2002 (Figure 6.4) correspond to the large positive EKE anomalies in the Mann Eddy and negative EKE anomalies at around 47°N (Figure 6.1b). The CPC-1 depression in 1994 and a very large depression in 1999-2000 (Figure 6.4) resemble the negative EKE anomalies in the Mann Eddy and positive EKE anomalies near 47°N (Figure 6.1b). The CPC-1 is found to be coherent with the change in the winter NAO index (Figure 6.4). During 1993-2003 the NAO index changed its sign from positive to negative twice in the winter of 1995/96 and in the winter of 2000/01. Thus the results, presented in this study, suggest that a transition from a positive to a negative NAO phase is associated with an increase of EKE in the Mann Eddy and a decrease in the area north of it, centred near 47°N.

The spatial phase function of the first empirical mode $\theta_{CEOF\text{-}1}(x)$ is presented in Figure 6.5a. The spatial phase does not considerably change in the Mann Eddy, which suggests an almost stationary wavelike pattern. The phase structure becomes more complicated north of the Mann Eddy. The contours of constant phase are generally perpendicular to the NAC core, flowing around the Grand Banks. A gradual change of the spatial phase also takes place in the western part of the Mann Eddy along the NAC core. This suggests that there is an along stream quasi-meridional propagation of the EKE anomalies in the NAC area. Figure 6.5b displays the spatial phase function along the NAC path approximated by a broken line in Figure 6.5a. The spatial derivative of $\theta_{CEOF\text{-}1}(x)$ represents wave number k, defined by the equation (6.7a). As follows from Figure 6.5b, the mean wave number along the NAC flowing around the Grand Banks is not constant but always positive for each segment of the line. Along the NAC path indicated by the broken line (Figure 6.5a), the wave numbers are $k\approx0.01$ rad/km at 38°N, $k\approx0.003$ rad/km at 45°W, $k\approx0.001$ rad/km at 45°N, and $k\approx0.007$-0.008 rad/km at 40°W. The numbers suggest that on the western rim of

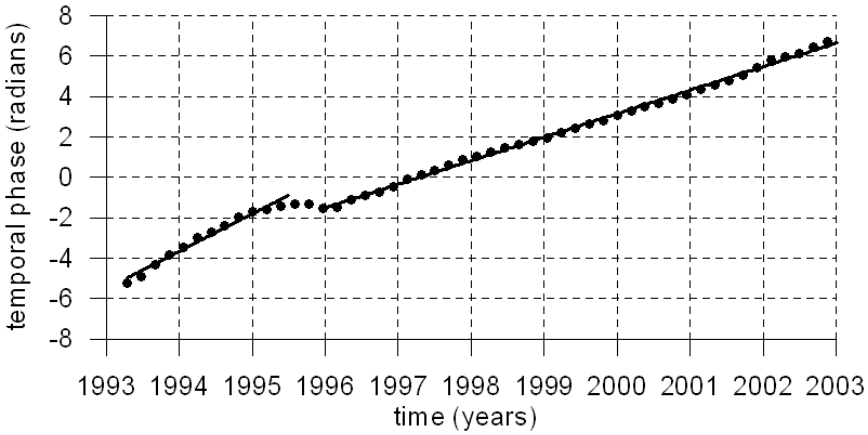

Figure 6.6: *The temporal phase function (rad) of the first empirical mode. The dots indicate the observed values and the solid lines are their linear fits or slopes for limited periods calculated by regression.*

the Mann Eddy the wave lengths, defined by $\lambda=2\pi/k$, are larger than west of 45°W and north of 45°N (2000 km compared to 600-900 km) and there is almost no propagation along 45°N on the northern rim of the Mann Eddy. The positive sign of k denotes that the CEOF-1 mode propagates along stream northward.

Figure 6.6 displays the temporal phase function of the first empirical mode $\varphi_{CEOF\text{-}1}(t)$. The slope of the temporal phase function represents the angular frequency $\omega_{CEOF\text{-}1}$, defined by the equation (6.7b). The angular frequency equals approximately $\pi/3$ rad/year (1 cycle in 6 years), besides the very beginning of the time series, when $\omega_{CEOF\text{-}1}$ was about 2 rad/year. This shows that between 1993 and 2002 nearly two energy waves passed the area.

The phase speed $c_{CEOF\text{-}1}$, defined by the relation (6.7c), is not constant along the NAC. Assuming that the typical frequency for years 1993-2003 is $\pi/3$ rad/year, the phase speed estimates along the NAC path indicated by the broken line in Figure 6.5a are $c\approx100$ km/year at 38°N, $c\approx350$ km/year at 45°W, and $c\approx130$ km/year at 40°W. It should be noted that these numbers are rough approximations. However, they reflect main characteristics of the along stream propagation of the EKE anomalies, depicted by the CEOF-1. The propagation appears to be much faster on the western rim of the Mann Eddy. Hardly any propagation of the EKE anomalies exists inside the Mann Eddy since the spatial phase function in this region is almost uniform (Figure 6.5a).

After performing the CSVD analysis, the EKE time series were reconstructed using only the first empirical mode according to the relation (6.3). Thus, a filtered data set associated only with the CEOF-1 was formed. To illustrate the temporal variability of the EKE anomalies across the NAC, the Hovmöller diagrams displaying the variability of EKE along the broken line in Figure 6.5a and meridional section at 40°W are shown in Figures 6.7a and 6.7b. One can see that the reconstructed data indeed exhibits a northward propagation of the EKE anomalies. As follows from Figure 6.7, the EKE anomalies propagated downstream the NAC. Figure 6.7b does not show any propagation up to 44°N, which implies that inside the Mann Eddy the variability of EKE was characterized by stationary oscillations (standing waves). No propagation was detected on the northern rim of the Mann Eddy at 45°N (Figure 6.7a). Figures 6.7 confirm the change of the phase speed, estimated earlier from the angular frequency and wave number. The propagation of

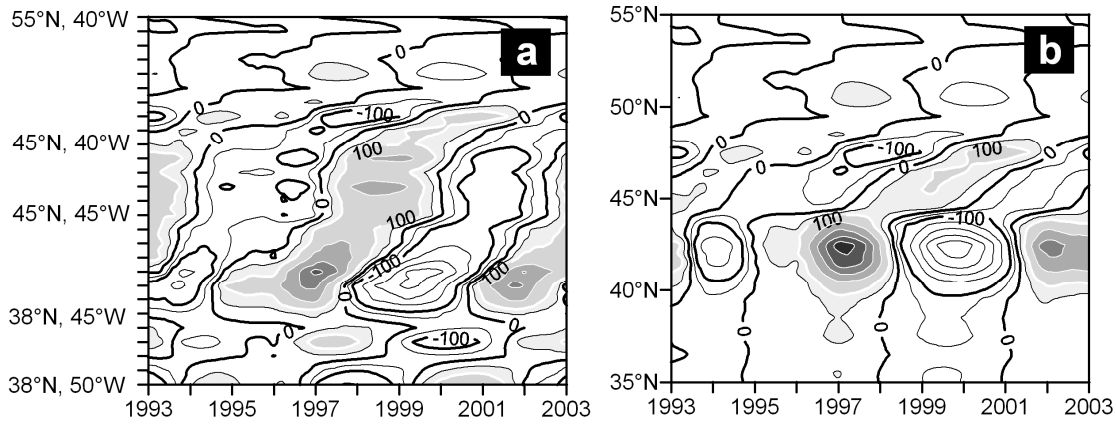

Figure 6.7: *The Hovmöller time-latitude diagrams of the reconstructed EKE anomalies (cm²/s²) (a) along the broken line in Figure 6.5a and (b) along 40°W. Areas with positive EKE anomalies are shaded.*

EKE anomalies on the western rim of the Mann Eddy appeared to be faster than up- and downstream the NAC.

East of the NAC core clear structure of the northward propagation of EKE anomalies was not found, which is probably the consequence of intensive eddy activity in the region and the meandering of jets.

6.4 Conclusions and discussion

In this chapter the interannual variability of EKE in the NAC west of the Mid-Atlantic Ridge from 1993 to 2003 was analyzed. At 40°W meridional section lying across the NAC, flowing around the Grand Banks northward, most of EKE was found to be concentrated in the Mann Eddy and east of the Flemish Cap near 47°N. These areas are reported to be the places where irregular branching occurs. Very large interannual variations of EKE were found in the Mann Eddy. The largest EKE reaching approximately 1000 cm²/s² was observed in 1996-1997 and 2001-2002 while in 1999-2000 EKE was less than 100 cm²/s². The maxima in 1996-1997 and 2001-2002 followed the change of the NAO phase from positive to negative in the winters of 1995-1996 and 2000-2001. At the same time EKE near 47°N decreased.

It was shown that in the NAC an increase/decrease of EKE mainly reflects an intensification/relaxation of the current velocity. Positive correlation was found between the EKE in the NAC core and the north-eastward component of the geostrophic velocity anomaly, suggesting a direct dependence between the variability of EKE and the north-eastward flow of the NAC.

The main objective of this study was to reveal propagating signals in the EKE field using the CSVD approach. The first leading empirical mode of the normalized EKE accounted for 28% of the total variance. The spatial pattern of the CEOF-1 exhibited a three-zoned oscillation pattern. Two zonal bands, associated with the Mann Eddy and the northern wall of the NAC centred at approximately 42°N and 50°N respectively, appeared to vary out-of-phase with the central band centred near 47°N. The complex temporal amplitude function of the first empirical mode with a nonzero imaginary part indicated an

existence of propagating signals in the EKE field. It was shown that the EKE anomalies associated with the first empirical mode propagated downstream the NAC, flowing around the Grand Banks. The propagation was found to be faster on the western rim of the Mann Eddy than up- and downstream the NAC. Inside the gyre no propagation was detected and the variability of EKE there appeared to be mainly characterised by stationary oscillations. Almost two EKE waves with a period of 5-6 years were identified during the studied time interval. The true period of the waves could not be determined however, because the length of the investigated time series was only 10 years and the waves can be aperiodic.

One of the most important findings is that positive EKE anomalies propagating northward are possibly associated with the NAO. A large positive anomaly at about 42°N appeared in 1996/1997 after the NAO index changed sign from positive to negative in the winter of 1995/1996. This anomaly reached the latitude of 47°N in 2001. Next positive EKE anomaly at 42°N followed another change of the NAO phase in the winter of 2000/2001. Thus it is likely that the atmospheric circulation plays an important role in determining the interannual variability of EKE in the NAC, and it is a possible driving force for the observed along stream propagation of the EKE signal.

The propagating EKE signals in the NAC, depicted by the first empirical mode of the inter-annual variations in EKE, indicated successive along stream changes in the intensity of eddy activity. The EKE anomalies propagating downstream the NAC, flowing around the Grand Banks, could be a reflection of meridional displacements of the NAC branches (jets), their intensification and relaxation at different locations across the area of the predominantly eastward drift. The NAO-related increase of EKE in the Mann Eddy in 1996-1997 and in 2001-2002 was likely accompanied by corresponding intensification of the NAC branch extending further east. Then, according to the detected propagation phenomenon, this branch possibly shifted northward and reached the latitude of about 47°N in 1999-2000, which corresponded to a local increase of the eastward flow at this time (see Chapter 5; Volkov, 2004). It is possible that the propagating EKE anomalies followed the NAO-induced meridional shifts of the wind stress. Further analysis of the inter-annual variations in the wind stress over the region is needed to support this suggestion.

Chapter 7

Summary and synthesis

Variability in the ocean occurs on different temporal (from seconds to inter-annual and longer) and spatial scales (from millimetres to ocean-scale). The main objective of this thesis was to study the climatic variability of the sea level and surface circulation in the North Atlantic Ocean observed with satellite altimetry. The variability of sea level is a good indicator of changes occurring in the upper ocean water properties (expansion and contraction of the water column due to changes in temperature and salinity) and in the oceanic circulation (shifts in the position of currents and fronts).

The advent of satellite altimetry has significantly facilitated the study of the variability of the sea level and surface circulation (Fu and Cazenave, 2001). Satellites, equipped with an on-board altimeter, provide frequent, regular, and nearly global measurements of the sea surface height. The surface geostrophic circulation can be determined from the ocean dynamic topography, which is the difference between the sea surface height and the height of the geoid. This thesis uses data from the latest high-accuracy altimetric missions, performed by the US/French (NASA/CNES) TOPEX/Poseidon and Jason-1 satellites, and the European Space Agency's ERS-1 and -2 satellites. From the launch of the TOPEX/Poseidon on August 10, 1992 to the present, more than 10 years of high-accuracy data have been collected. The combination of data from different altimetry missions provides a better spatial coverage (Ducet et al., 2000). The temporal resolution of data is determined by the repeat period of the satellite and for the data, used in this thesis, it is equal about 10 days (the repeat period of the TOPEX/Poseidon and Jason-1 satellites). Such a repeat period resolves mesoscale and larger processes in the ocean. Therefore, this thesis deals with the variability at the mesoscale, seasonal and inter-annual time scales. Variations of sea level at these time scales are mainly induced by the variations of heat and fresh water fluxes (buoyancy fluxes) at air-sea interface, the variations of heat and salt budget due to the advection of water masses with different properties, eddy generation mechanisms due to the instability of oceanic currents, Rossby waves, etc.

Several specific questions were addressed by this thesis. It was shown how the sea level in the extratropical North Atlantic Ocean was changing during the investigated time interval from 1993 to 2003. The mesoscale, seasonal and inter-annual modes of the variability were revealed, and the magnitude and relative contribution of each mode to the total variance was assessed. The inter-annual change of the sea surface height in the northern North Atlantic, measured with altimetry, was coupled with *in situ* observations along the

transatlantic section AR7E, repeated almost every year from 1990 to 2003 in the framework of the WOCE (World Ocean Circulation Experiment) and CLIVAR (CLImate VARiability) hydrographic programs. This allowed interpreting the observed inter-annual change of sea level in terms of changes in the sea water properties and the distribution of water masses. A next step was to understand whether the changes observed in the extratropical North Atlantic are different from those in the extratropical North Pacific. The magnitudes, spatial patterns, and also trends of the observed variations of sea level and associated surface circulation were compared. The variability of surface circulation was studied using yearly estimates of EKE as a proxy to define the course of major currents. One of the important issues illustrated by the thesis is the probable dependence of the inter-annual variations of sea level and surface circulation upon the corresponding changes in the atmospheric circulation pattern, related to the ocean-atmosphere interactions. The leading modes of these interactions in the North Atlantic and North Pacific ocean basins are known as the North Atlantic Oscillation (NAO) and the Pacific Decadal Oscillations (PDO). The NAO and PDO indices were coupled with the observed inter-annual variations of sea level and surface circulation.

In chapter 3, it was shown that the seasonal and inter-annual signals of the sea level variability are dominant in the northern North Atlantic Ocean (north of 50°N). The seasonal variability, outside the North Atlantic Current, appeared to supply the largest contribution to the total variance, ranging from 30% to over 50%. The inter-annual change was found to be the most pronounced in the Irminger Basin, where its relative contribution to the total variance exceeded 40%. The largest amplitudes (5-6 cm) of the seasonal sea surface height variations were observed in the Iceland Basin and attributed to the seasonal shifts in the position of the Subarctic Front in this area. A branch of the North Atlantic Current associated with the Subarctic Front flows through the Iceland Basin and also experiences seasonal displacements and changes in the intensity. Since the seasonal variations of the sea level were not completely explained by the seasonal variations of the heat flux, advective changes in the position of the Subarctic Front probably contributed to the seasonal change of the sea level in the Iceland Basin. As suggested by Reverdin et al (1999), advection plays an important role in the inter-annual variations of sea level.

At inter-annual timescales the sea level in the northern North Atlantic, measured by altimeters, exhibited an overall increase from a minimum level in 1994 to a maximum in 1997-1998. Then the sea level decreased and from 2000 started to rise again. The hydrographic data, obtained during the WOCE and CLIVAR cruises at the transatlantic section AR7E, confirmed the change of the sea level, observed by altimetry. A good agreement was found between the altimetric sea surface heights and the hydrographic dynamic heights, derived from temperature and salinity, at large spatial scales. This implies a basically baroclinic character of the observed sea level change, i.e. the variations of sea level can be explained mainly by the variations in the sea water properties. This differs from a barotropic change of sea level. The barotropic change is caused by the variations of the amount of water, which is probably more important in the coastal regions and marginal seas. It was found that the 200-800 dbar layer occupied by the Subpolar Mode Water (SPMW) has the largest contribution to the inter-annual variations of the dynamic heights along the section AR7E. SPMW is produced by mixing and subsequent convection of the subtropical and polar water masses (McCartney and Talley, 1982). It occupies

approximately the upper 1000 m water layer and represents the most dynamic water mass in the northern North Atlantic. The major role of this layer in the inter-annual variations of sea level was expected, because it is here that the large variations in advection and buoyancy fluxes take place. The inter-annual change of the sea level in the North Atlantic appeared to be correlated with changes in the winter (December through February) NAO index.

It was shown that on the inter-annual time scales the extratropical North Atlantic Ocean responds to the atmospheric forcing, expressed by the winter NAO index, as a dipole system (e.g. Esselborn and Eden, 2001). The atmospheric pressure distribution, and consequently, the winds over the ocean differ between positive and negative NAO phases. The atmospheric pressure pattern during a positive/negative NAO phase is characterised by the strong/weak Azores High and deep/weak Icelandic Low pressure centres (Hurrell et al., 2003). During a positive NAO phase, associated with strong westerly winds, the sea level is high in the subtropical gyre and low in the subpolar gyre. When the NAO phase changes from positive to negative and the westerly winds become weaker, as happened twice during the studied time interval, the sea level in the subpolar gyre rises while in the subtropical gyre it decreases. On the one hand, a restructuring of the atmospheric pressure and circulation during a negative NAO phase brings warm air in the northern and north-western areas of the subpolar North Atlantic Ocean. This leads to a warming of the ocean in these areas by means of buoyancy fluxes. On the other hand, a change in the atmospheric circulation pattern by means of the variable wind stress influences the pattern of the large-scale oceanic circulation. During a negative NAO phase the westerly winds become weaker, which reduces the eastward transport of the SPMW and leads to the westward shift of the Subarctic Front in the Iceland Basin (Bersch, 2001). The latter increases the transport of the North Atlantic Current waters into the northern and north-western areas of the subpolar North Atlantic. Thus the advection of warm and more saline waters also contributes to the rise of the sea level in the subpolar regions.

In chapter 4, the magnitudes and spatial patterns of the sea level variability at mesoscale, seasonal and inter-annual time scales in the extratropical North Atlantic Ocean were compared with those in the extratropical North Pacific Ocean. It was shown that the spatial patterns of the mesoscale, seasonal and inter-annual variability in both oceans resemble the local features of surface circulation. In the North Atlantic, the open connection with the Arctic Ocean permits a large north-eastward extension of the subpolar gyre. This causes a divergence of the main eastward currents, which produces a wide area with relatively large mesoscale variability, associated with the generally north-eastward flow of the North Atlantic Current and the eastward Azores Current. In the North Pacific, a similar north-eastward extension of the subpolar gyre is not possible due to the geographic boundaries and the narrowness of the shallow Bering Strait. Therefore, the area with large mesoscale variability in the North Atlantic is wider than in the North Pacific, and the mesoscale variability in the former appeared to be overall more dominant than in the latter. In the eastern part of the North Pacific the mesoscale variability was found to be very small except in the rim currents along the North American coast. In the North Atlantic relatively large mesoscale variability was observed almost everywhere in the northern part of the subtropical gyre (north of 30°N). The mesoscale variability shows seasonal variations, probably caused by the seasonally varying wind stress. In both oceans the largest seasonal

variations in the mesoscale variability were observed in the subpolar regions. The largest corresponding sea surface height variance was mainly observed in late autumn-winter period. This period coincides with the period of the largest wind stress, which supports the dependence of the seasonal variations of the mesoscale activity upon the seasonally varying winds. The seasonal change of the sea level in the North Atlantic and North Pacific appeared to have a similar magnitude and spatial pattern. However, a difference was found in the spatial distribution of the phase of the seasonal signal. In the North Pacific the seasonal phase appeared to be distributed zonally with a maximum sea level occurring in October in the subtropical gyre and in September in the subpolar gyre. In the North Atlantic, the September maximum of the sea level in the subpolar gyre was observed only in the Irminger Basin and in the Labrador Sea. Such a phase distribution in the North Atlantic is possibly caused by the existence of the poleward flow and associated penetration of the North Atlantic Current waters into the far northern parts of the North Atlantic Ocean. The seasonal variations of the sea level in the Gulf Stream and Kuroshio extensions exhibited seasonal meridional shifts of the flow intensity: to the south in spring and to the north in autumn. The observed magnitude of the inter-annual variability in the North Pacific appeared to be larger than in the North Atlantic while the spatial patterns were found to be similar.

An attempt was made to analyse the climate-related change of the sea level and surface circulation in both the North Atlantic Ocean and the North Pacific Ocean. In the context of this thesis the climate-related change is referred to the inter-annual and inter-decadal variations associated with non-linear ocean-atmosphere interactions. The first empirical modes of the inter-annual change of the sea level in both oceans exhibited dipole oscillation patterns. In the North Atlantic Ocean, the first empirical mode depicted a quasi-linear increase of the sea level during the decade of 1993-2003 in the subpolar and eastern areas. This increase was accompanied by a decrease of the sea level in the Gulf Stream extension and in the North Atlantic Current west of the Mid-Atlantic Ridge. In the North Pacific Ocean, the first empirical mode illustrated a step-like change of the sea level that occurred in 1998. In this year the sea level started to decrease in the subpolar regions, particularly in the Bering Sea, and to rise in the northern part of the subtropical gyre. The first empirical mode of the sea level variability at the inter-annual time scale in the North Pacific was found to be coherent with a low-pass filtered PDO index. Although a little more than ten years of the time series, studied in this thesis, are too short to investigate the climate-related change, some conclusions were made taking into account previous studies (Cabanes et al., 2001; Häkkinen and Rhines, 2004). The linear trends of the sea level in the North Atlantic and the North Pacific, estimated by regression, appeared to have identical spatial pattern with the first empirical modes of the sea level variability on the inter-annual time scale. Thus it was concluded that the first empirical modes describe a long-term, inter-decadal change of sea level. These trends differ from those described by Cabanes et al. (2001) for an earlier period. For the period 1955 to 1996 they found negative trends of the steric sea level in the subpolar gyre and positive trends in the subtropical gyre of the North Atlantic Ocean, which is opposite to what was observed from 1993 to 2003. In the North Pacific Ocean from 1955 to 1996 negative trends of the sea level existed in the subtropical gyre while positive trends were found for the subpolar and eastern areas. Thus a reversal of the sign of the sea level trends, possibly associated with the inter-decadal variability, occurred in both oceans. The PDO *per se* is defined as the inter-decadal mode of the variability over

the North Pacific. The NAO shows multiple frequencies, but has an inter-decadal mode as well (see chapter 1). The change of the sea level trends in the North Pacific, possibly related to the PDO, occurred in 1998. To understand whether it was a flip from one PDO phase to another and not just a short-term fluctuation caused by the strong 1997/1998 El Niño and following La Niña events, we need at least several more years of observations. As it was shown in chapter 3, in the subpolar North Atlantic Ocean the inter-annual change of the sea level from 1993 to 2003 was correlated with the winter NAO index. The rise of the sea level in the subpolar North Atlantic followed changes of the NAO phase from positive to negative in the winters of 1995/1996 and 2000/2001. The sea level trends in the North Atlantic, observed from 1993 to 2003, resemble the negative NAO conditions. However, having such a short sample it is not possible to say whether these conditions are going to persist or that the changes of the NAO phase were only short-term fluctuations. From what was observed, a suggestion was made that at the inter-decadal time scale the sea level in the North Atlantic varies out-of-phase with the sea level in the North Pacific. A simultaneous rise of the sea level in the subpolar and eastern North Atlantic and a decrease in the Gulf Stream extension and in the North Atlantic Current are possibly accompanied by a decrease of the sea level in the subpolar and eastern North Pacific and a rise in the Kuroshio extension and in the North Pacific Current. The decadal trends of the sea level in both oceans also depicted the decadal trends in the surface geostrophic circulation. The latter showed a slowdown of the subpolar and subtropical gyres of the North Atlantic and an intensification of the subpolar and subtropical gyres of the North Pacific. Flatau et al. (2003) and Häkkinen and Rhines (2004) also documented a decline of the subpolar North Atlantic circulation.

In chapter 5, the variability of the surface eddy kinetic energy (EKE) was analysed to study the inter-annual change of the position and intensity of main currents in the extratropical North Atlantic Ocean. The proposed interpretation relies on the fact that the currents are the major source of eddy energy, which is mainly generated through the instability processes of frontal flows. It was shown that largest EKE is concentrated along major frontal currents of the North Atlantic. A comparison between the density distributions along the AR7E repeat section and the surface EKE demonstrated that large EKE cores coincided with high density gradient frontal zones. Thus it was shown that in the absence of sufficiently accurate geostrophic velocity estimates from altimetry data, EKE can be a useful parameter to monitor the variability of surface circulation. A detailed description of the inter-annual change of EKE and associated surface circulation in several regions of the extratropical North Atlantic was presented. In the Gulf Stream extension, the inter-annual variability of EKE and geostrophic velocity anomalies revealed meridional displacements of the current core. The southernmost position was monitored in 1998, approximately 2 years after the change of the NAO phase from positive to negative in the winter of 1995/1996. The inter-annual variability of EKE in the North Atlantic Current was dominated by the redistribution of EKE between three zones centred near 43°N, 47°N and 50°N. The southern zone is associated with the anticyclonic Mann Eddy. The two other possibly represent the branches of the North Atlantic Current flowing eastward. It appeared that when positive EKE anomalies were observed in the Mann Eddy and along the northern wall of the North Atlantic Current near 50°N, negative EKE anomalies were found near 47°N, and vice versa. Positive/negative EKE anomalies in the North Atlantic Current generally corresponded to

the eastward/westward geostrophic velocity anomalies. Since the North Atlantic Current represents on average a broad eastward to north-eastward drift, the positive/negative EKE anomalies were associated with strengthening/weakening of the eastward flow. In the Azores Current, the maximum EKE was observed in 1993-1995 followed by a decrease in subsequent years. Such a decrease was interpreted to be a result of a weakening of the current, induced by a relaxation of the westerly winds in 1996. The inter-annual change of EKE and geostrophic velocity anomalies reflected the above-mentioned westward shift of the Subarctic Front in the Iceland Basin that occurred after 1995. It was demonstrated that the north-eastward flow in the Rockall Channel was more intensive in 1993-1995 than in the following years. In both the Iceland Basin and the Rockall Channel the seasonal signal of the EKE variability with maxima predominantly in the winter period overpowered the inter-annual signal. This suggests a connection between EKE and the seasonally varying wind stress, which is maximum in winter. A long-term trend of rising EKE was monitored in the Irminger Basin. This basin appeared to be the only area of the subpolar North Atlantic where the seasonal change in EKE was found to be smaller than the inter-annual change. In the Irminger Basin, EKE was found to be concentrated along two parallel bands. The observed rise of EKE involved both bands. However, it was not associated with an intensification of the surface circulation. As it was shown in other studies (e.g. Flatau et al., 2003) and confirmed in chapter 5, the cyclonic circulation of the North Atlantic subpolar gyre declined. It was suggested that the westward shift of the Subarctic Front reaching the Irminger Basin, induced by the NAO, might have promoted eddy generation processes and caused the observed increase of EKE in the Irminger Basin. This shift might have effected the easternmost band of EKE in the Irminger Basin while the westernmost band is likely maintained by a convectively generated near-surface front in the centre of the Irminger Basin. In the Labrador Sea the variability of EKE appeared to be very complex. The seasonal signal significantly overpowered the inter-annual signal. Maximum EKE was observed during the high NAO indices in the winters of 1996/1997, 1997/1998, and 1998/1999, but not in the early part of the record.

In chapter 6, the inter-annual EKE time series in the North Atlantic Current between the Grand Banks and the Mid-Atlantic Ridge were analysed to detect propagating features. This study was motivated by the observed peculiarities of the EKE distribution in this region, described in chapter 5. Most of EKE was found in the Mann Eddy and east of the Flemish Cap near 47°N. The propagating signals in the EKE field were revealed using the Complex Singular Value Decomposition analysis, which is a version of the Complex Empirical Orthogonal Functions analysis. It was shown that the EKE signal associated with the first empirical mode propagates downstream the North Atlantic Current, flowing around the Grand Banks. During the studied time interval from 1993 to 2003 almost two EKE waves with a period of about 6 years were observed. It appeared that the EKE signal propagates faster on the western rim of the Mann Eddy than further up and downstream of it. No propagation was monitored inside the Mann Eddy and the inter-annual variability there was characterised by standing oscillations. The inter-annual change of EKE in the North Atlantic Current was found to be coherent with the NAO. Positive EKE anomalies were monitored in the Mann Eddy in 1996-1997 and 2001-2002 right after the NAO index turned from its positive to negative values in the winters of 1995/1996 and 2000/2001. The 1996-1997 positive EKE anomaly, observed in the Mann Eddy, reached the latitude of 47°N in

2000. The positive EKE anomalies in the North Atlantic Current appeared to be mainly associated with an intensified eastward flow. Having a short record of observations it is not possible to state whether the observed propagation is a periodic feature and whether it has a definite period. It is likely that the propagation is related to meridional shifts of the North Atlantic Current branches. The monitored coherence with the NAO suggests a connection with the atmospheric forcing. Since the surface circulation is generally wind driven, the meridional shifts of currents, depicted by the propagating EKE signal, may be caused by meridional shifts of the wind stress.

References

Atlas of the Oceans, *Atlantic and Indian Oceans*, vol. II, Gorshkov, S.G. (ed.), Ministry of Defence of the USSR - Navy, St. Petersburg, 1977.

Barsugli, J.J., and D.S. Battisti, *The basic effects of atmosphere-ocean thermal coupling on midlatitude variability*, J. Atmos. Sci., 55, 477-493, 1998.

Behringer, D.W., *Sea surface height variations in the Atlantic Ocean: a comparison of TOPEX altimeter data with results from an ocean data assimilation system*, J. Geophys. Res., 99, 24685-24690, 1994.

Bersch, M., *North Atlantic Oscillation – induced changes of the upper layer circulation in the northern North Atlantic Ocean*, J. Geophys. Res., 107, 3156, doi: 10.1029/2001JC000901, 2002.

Bersch, M., J. Meincke, and A. Sy, *Interannual thermohaline changes in the northern North Atlantic 1991 – 1996*, Deep Sea Res., part II, 46, 55-75, 1999.

Bjerknes, J., *Atlantic air-sea interaction*, Adv. Geophys., 10, 1-82, 1964.

Bradley, R.S., *Paleoclimatology: reconstructing climates of the quaternary,* Academic Press, New York, USA, 1999.

Broecker, W.S., *The Great Ocean Conveyor,* Oceanography, 4, 79-89, 1991.

Cabanes, C., A. Cazenave, C. Le Provost, *Sea level rise during past 40 years determined from satellite and in situ observations*, Science, 294, 840-842, 2001.

Cayan, D.R., *Latent and sensible heat flux anomalies over the northern oceans: the connection to monthly atmospheric circulation*, J. Climate, 5, 354-369, 1992.

Chelton, D.B., J.C. Ries, B.J. Haines, L.-L. Fu, and P.S. Callahan, *Satellite altimetry,* In: *Satellite altimetry and earth science*, L.-L. Fu and A. Cazenave, Eds., Academic Press, International Geophysics Series, V69, 2001.

Curry, R.G., and M.S. McCartney, *Ocean gyre circulation changes associated with the North Atlantic Oscillation*, J. Phys. Oceanogr., 31, 3374-3400, 2001.

Daly, A.W., *The response of North Atlantic sea surface temperature to atmospheric forcing processes*, Q.J.R. Meteorol. Soc., 104, 363-382, 1978.

Dickson, R.R., J. Lazier, J. Meincke, P. Rhines, and J. Swift, *Long-term coordinated changes in the convective activity of the North Atlantic*, Progr. Oceanogr., 38, 241-295, 1996.

Dietrich, G., K. Kalle, W. Krauss, and G. Siedler, *General Oceanography*, 2nd ed, Ney York: John Wiley and Sons, 1980.

Dijkstra, H.A., *Nonlinear physical oceanography*. Kluwer Academic Publishers, Dordrecht, The Netherlands, 480 pp., 2000.

Dixon, W.J., and F.J. Massey, *Introduction to statistical analysis*, 3rd ed., 638 pp., McGraw-Hill, N.Y., 1968.

Dorandeu, J. and P.-Y. Le Traon, *Effects of global mean atmospheric pressure variations on mean sea level changes from TOPEX/Poseidon*, J. Atmos. Oceanic Technol., 16, 1279-1283, 1999.

Drijfhout, S.S., *On the eddy heat transport in the ocean*, PhD thesis, ISBN 90-393-0014-3, pp.151, 1992.

Ducet, N., P.Y. Le Traon, and G. Reverdin, *Global high-resolution mapping of ocean circulation from Topex/Poseidon and ERS-1 and -2*, J. Geophys. Res., 105, 19477-19498, 2000.

Eden, C., and C. Böning, *Sources of eddy kinetic energy in the Labrador Sea*, J. Phys. Oceanogr., 32, 3346-3363, 2002.

Emery, J.E. and R.E. Thomson, *Data analysis methods in physical oceanography*, Elsevier, pp.634, 1998.

Esselborn, S., and C. Eden, *Sea surface height variability in the North Atlantic Ocean related to the North Atlantic Oscillation*, Geophys. Res. Lett., 28, 3473-3476, 2001.

Favorite, F., A.J. Dodimead, and K. Nasu, *Oceanography of the subarctic Pacific Region, 1962-72*, Bull. Int. North Pac. Fish. Comm., 33, 1-187, 1976.

Ferry, N., Reverdin, G., Oschlies, A., *Seasonal sea surface height variability in the North Atlantic Ocean*, J. Geophys. Res.,105, 6307-6326, 2000.

Flatau, M.K., L. Talley, and P.P. Niiler, *The North Atlantic Oscillation, surface current velocities, and SST changes in the Subpolar North Atlantic,* J. Climate, 16, 2355-2369, 2003.

Frankignoul, C., G. de Coëtlogon, T.M. Joyce, and S. Dong, *Gulf Stream variability and ocean-atmosphere interactions*, J. Geophys. Res., 31, 3516-3529, 2001.

Frankignoul, C., and K. Hasselmann, *Stochastic climate models, part II: application to sea-surface temperature variability and thermocline variability*, Tellus, 29, 289-305, 1977.

Fratantoni, D.M., *North Atlantic surface circulation during 1990's observed with satellite-tracked drifters*, J. Geophys. Res., V106, C10, 22067-22093, 2001.

Fu, L-L. and A. Cazenave, (eds.), *Satellite altimetry and earth sciences: a handbook of techniques and applications*, Academic Press, International Geophysics Series, V69, 2001.

Fu, L-L., E.J. Christensen, C.A. Yamarone Jr., M. Lefebvre, Y. Menard, M.Dorrer, and P. Escudier, *Topex/Poseidon mission overview*, J. Geophys. Res., 99, 24369-24381, 1994.

Gilson, J., D. Reommich, B. Cornuelle, and L.-L. Fu, et al., *Relationship of Topex/Poseidon altimetric height to steric height circulation in the North Pacific*, , J. Geophys. Res., 103, 27947 – 27965, 1998.

Han, G. and C.L. Tang, *Interannual variations of volume transport in the western Labrador Sea based on TOPEX/Poseidon and WOCE data*, J. Phys. Oceanogr., 31, 199-211, 2001.

Hare, S.R., *Low frequency climate variability and salmon production*, Ph.D. dissertation, School of Fisheries, University of Washington, Seattle, 1996.

Heywood, K.J., E.L. McDonagh, and M. White, *Eddy kinetic energy of the North Atlantic subpolar gyre from satellite altimetry,* J. Geophys. Res., 99, 22525-22539, 1994.

Holliday, N.P., *Air-sea interaction and circulation changes in the Northeast Atlantic*, J. Geophys. Res., 108, 3259, 2003.

Horel, J.D., *Complex principal component analysis: theory and examples*, J. Climate App. Meteor., 23, 1660-1673, 1984.

Häkkinen, S. and P.B. Rhines, *Decline of subpolar North Atlantic circulation during the 1990s*, Science, 304, 555-559, 2003.

Häkkinen, S., *Variability in sea surface height: a qualitative measure for the meridional overturning in the North Atlantic*, J. Geophys. Res., 106, 13837-13848, 2001.

Häkkinen, S., *Variability of the simulated meridional heat transport in the North Atlantic for the period 1951-1993*, J. Geophys. Res., 104, 10991-11007, 1999.

Hurrell, J.W., Y. Kushnir, M. Visbeck, and G. Ottersen, *An Overview of the North Atlantic Oscillation*. In: *The North Atlantic Oscillation: Climate Significance and Environmental Impact*, J.W. Hurrell, Y. Kushnir, G. Ottersen, and M. Visbeck, Eds.. Geophysical Monograph Series, 134, pp. 1-35, 2003.

Hurrell, J.W., *Influence of variations in extratropical wintertime teleconnections on Northern Hemisphere temperature*, Geophys. Res. Lett., 23, 665-668, 1996.

Hurrell, J.W., *Decadal trends in the North Atlantic Oscillation: reginal temperatures and precipitation*, Science, 269, 676-679, 1995.

Ionov, V.V., G.L. Weatherly, and R. Harkema, *On the temporal variability of the surface Gulf Stream and near-bottom flows*. J. Geophys. Res., 91, 2661-2666. 1986.

Isemer, H.-J. and Hasse, L., *The Bunker Climate Atlas of the North Atlantic Ocean*. Volume I: *Observations*. Springer-Verlag, Berlin, 1985.

Isoguchi, O., H. Kawamura, and T. Kono, *A study on wind-driven circulation in the subarctic North Pacific using Topex/Poseidon altimeter data*, J. Geophys. Res., 102, 12457-12468, 1997.

Kamenkovich, V.M., M.N. Koshlyakov, A.S. Monin, *Synoptic eddies in the ocean*, D. Riedel Publ. Co., Dordrecht, The Netherlands, 433 pp., 1986.

Kelly, K.A., S. Singh, and R.X. Huang, *Seasonal variations of sea surface height in the Gulf Stream region*, J. Phys. Oceanography, 29, 313-327, 1999.

Kelly, K.A., R.C. Beardsley, R. Limeburner, K.H. Brink, J.D. Paduan, T.K. Chereskin, *Variability of the near-surface eddy kinetic energy in the California Current based on altimetric, drifter, and moored current data*, J. Geophys. Res., 103, 13067-13083, 1998.

Kelly, K.A., M.J. Caruso, and S. Singh, *Observations of atmosphere-ocean coupling in midlatitude western boundary currents*, J. Geophys. Res., 101, 6295-6312, 1996.

Kelly, K.A., *The meandering of the Gulf Stream as seen by the Geosat altimeter: surface transport, position, and velocity variance from 73° to 46°W*, J. Geophys. Res., V96, C9, 16721-16738, 1991.

Kelly, K.A. and S.T. Gille, *Gulf Stream surface transport and statistics at 69°W from the Geosat altimeter*, J. Geophys. Res., V95, C3, 3149-3161, 1990.

Kelly, K.A., *Comment on "Empirical orthogonal function analysis of advanced very high resolution radiometer surface temperature patterns in Santa Barbara Channel" by G.S.E. Lagerloef and R.L. Berstein*, J. Geophys. Res., 93, 15753-15754, 1988.

Klein, B., and G. Siedler, *On the origin of the Azores Current*, J. Geophys. Res., 94, 6159-6168, 1989.

Krauss, W., *Currents and mixing in the Irminger Sea and in the Iceland Basin*. J. Geophys. Res., 100, 10851-10871, 1995.

Krauss, W., Fahrbach, E., Aitsam, A., Elken, J. and Koske, P., *The North Atlantic Current and its associated eddy field southeast of Flemish Cap*, Deep-Sea Res., V34, No.7, pp. 1163-1185, 1987.

Krauss, W., *The North Atlantic Current*, J. Geophys. Res., 91, 5061-5074, 1986.

Krauss, W. and R.H. Käse, *Mean circulation and eddy kinetic energy in the eastern North Atlantic*, J. Geophys. Res., 89, 3407-3415, 1984.

Krauss, W. and J. Meincke, *Drift buoy trajectories in the North Atlantic Current*, Nature, 296, 737-740, 1982.

Käse R.H. and W. Krauss, *The Gulf Stream, the North Atlantic Current, and the origin of the Azores Current,* In: The warmwaterspere of the North Atlantic Ocean (ed. W. Krauss), Gebrüder Borntraeger, Berlin-Stuttgart, 1996.

Kushnir, Y., *Interdecadal variations in North Atlantic sea surface temperature and associated atmospheric conditions*, J. Phys. Oceanography, 7, 141-157, 1994.

Langseth M.G., Jr. and D. Boyer, *The effect of the Reykjanes Ridge on the flow of water above 2000 meters*, In: *Studies in physical Oceanography*, 2, ed. A.L. Gordon, 93-114, 1972.

Lazier, J.R.N., *Observations in the Northeast Corner of the North Atlantic Current*, J. Phys. Oceanogr., 24, 1449-1463, 1994.

Le Traon, P.Y., and F. Ogor, *ERS-1/2 orbit improvement using Topex/Poseidon: the 2 cm challenge*, J. Geophys. Res., 103, 8045-8057, 1998.

Le Traon, P.Y., F. Nadal, N. Ducet, *An improved mapping method of multi-satellite altimeter data*, J. Atm. Ocean. Techn., 25, 522-534, 1998.

Le Traon, P.Y., P. Gaspar, F. Bouyssel, H. Makhmara, *Using TOPEX/POSEIDON data to enhance ERS-1 data*, J. Atm. Ocean. Techn., 12, 161-170, 1995.

Le Traon, P.Y. and M.C. Rouquet, *Spatial scales of mesoscale variability in the North Atlantic as deduced from Geosat data,* J. Geophys. Res., 95, 20267-20285, 1990.

Maillard and Käse, *The near-surface flow in the subtropical gyre south of the Azores*, J. Geophys. Res., 94, 16133-16140, 1989.

Mann, C.R., *The termination of the Gulf Stream and the beginning of the North Atlantic Current,* Deep-Sea Res., 14, 337-359, 1967.

Mantua, N.J., *The Pacific Decadal Oscillation and climate forecasting for North America*, Climate Risk Solutions newsletter, 1999.

Mantua, N.J., S.R. Hare, Y. Zhang, J.M. Wallace, R.C. Francis, *A Pacific interdecadal climate oscillation with impacts on salmon production*, Bulletin of the American Meteorological Society, 78, 1069-1079, 1997.

McCartney, M.S. and L.D. Talley, *The Subpolar Mode Water of the North Atlantic Ocean*, J. Phys. Oceanography, 51, 1169-1188, 1982.

McClean, J.L., P.M. Poulain, J.W. Pelton, and M.E. Maltrud, *Eulearian and lagrangian statistics from surface drifters and a high-resolution POP simulation in the North Atlantic*, J. Phys. Oceanography, 32, 2472-2491, 2002.

Menard, Y., *Observations of eddy field in the Northwest Atlantic and Northwest Pacific by SEASAT altimeter data*, J. Geophys. Res., 88, 1853-1866, 1983.

Merrifield, M.A. and R.T. Guza, *Notes and correspondence. Detecting propagating signals with complex empirical orthogonal functions: a cautionary note*, J. Phys. Oceanogr., 20, 1628-1633, 1990.

Minobe, S., *A 50-70 year climate oscillations over the North Pacific and North America*, Geophys. Res. Lett., 24, 683-686, 1997.

Mizuno, K., and W.B. White, *Annual and interannual variability in the Kuroshio Current System*, J. Phys. Oceanogr., 13, 1847-1867, 1983.

Monin, A.S., V.M. Kamenkovich, V.G. Kort, *Variability of the oceans*, J. Willey & Sons, Inc., , 241 pp., 1977.

Morris, C. and S. Gill, *Evaluation of the Topex/Poseidon altimeter system over the Great Lakes*, J. Geophys. Res., 99, 24527-24539, 1994.

Musgrave, D.L., T.J. Weingartner, and T.C. Royer, *Circulation and hydrography in the northwestern Gulf of Alaska*, Deep-Sea Res., 39, 1499-1519, 1992.

Mysak, L., D.K. Manak, and R.F. Marsden, *Sea-ice anomalies observed in the Greenland and Labrador Seas during 1901-1984 and their relation to an interdecadal Arctic climate cycle*, Climate Dynamics, 5, 111-133, 1990.

Nauw, J.J., *Low-frequency variability of the wind-driven ocean circulation*, PhD thesis, ISBN 90-393-3425-0, pp.158, 2003.

Otto, L., and H.M. van Aken, *Surface circulation in the northeast Atlantic as observed with drifters,* Deep-Sea Res. I, 43, 467-499, 1996.

Patullo, J.G., W.H. Munk, R. Revelle, and E. Strong, *The seasonal oscillation in the sea level*, J. Marine Res., 14, 88-155, 1955.

Peixoto, J.P., and A.H. Oort, *Physics of Climate*, AIP Press, New York, 1992.

Preisendorfer, R.W., *Principal component analysis in meteorology and oceanography*, Elsevier, Oxford-New York-Tokyo, pp. 425, 1988.

Qiu, B., *Kuroshio Extension variability and forcing of the Pacific Decadal Oscillation: responses and potential feedback*, J. Phys. Oceanogr., 33, 2465 – 2482, 2003.

Qiu, B., *Large-scale variability in the midlatitude subtropical and subpolar North Pacific Ocean: observations and causes*, J. Phys. Oceanogr., 32, 353-375, 2002.

Ray, R. *A global ocean tide model from TOPEX/Poseidon altimetry, GOT99.2*, NASA Tech. Memo. NASA/TM-1999-209478, 58 pp., Goddard Space Flight Center, NASA Greenbelt, MD, USA, 1999.

Reed, R.K., *Flow of the Alaskan Stream and its variations*, Deep-Sea Res., 31, 369-386, 1984.

Reverdin, G., P.P. Niiler, and H. Valdimarsson, *North Atlantic Surface currents*, J. Geophys. Res., 108, C1, 3002, 2003.

Reverdin, G., N. Verbrugge, H. Valdimarsson, *Upper ocean variability between Iceland and Newfoundland, 1993-1998*, J. Geophys. Res., 104, 29599-29611, 1999.

Richardson, P.L., *Eddy kinetic energy in the North Atlantic from surface drifters*, J. Geophys. Res., 88, 4355-4367, 1983.

Rogers, J. C., *The association between the North Atlantic Oscillation and the Southern Oscillation in the Northern Henisphere*, Mon. Wea. Rev., 112, 1999-2015, 1984.

Rossby, T., and R.L. Benway, *Slow variations in mean path of the Gulf Stream east of Cape Hatteras*, Geophys. Res. Lett.,**27**, 117-120, 2000.

Rossby, T., *The North Atlantic Current and surrounding waters: at the crossroads*, *Rev*. of Geophysics, 34, pp. 463-481, 1996.

Seager, R., Y. Kushnir, M. Visbeck, N. Naik, J. Miller, G. Krahmann, and H. Cullen, *Causes of Atlantic Ocean climate variability between 1958 and 1998*, J. Climate, 13, 2845-2862, 2000.

Schmitz, W.J., *On the interbasin-scale thermohaline circulation,* Rev. Geophys., 33, 151-173, 1995.

SSALTO/DUACS user hand book, Issue 1, CLS, Ramonville, 2001.

Stammer, D. and C. Wunsch, *Temporal changes in eddy energy of the oceans*, Deep-Sea Res. II, 46, 77-108, 1999.

Stammer, D., *Steric and wind-induced changes in TOPEX/Poseidon large scale sea surface topography observations*, J. Geophys. Res.,20987-21010, 1997.

Stammer, D. and C.W. Böning, *Generation and distribution of mesoscale eddies in the North Atlantic Ocean*. In: *The warmwatersphere of the North Atlantic Ocean* (ed. by W. Krauss), 159-193, Gebrüder Borntraeger, Berlin-Stutgard, 1996.

Steward, R.H., *Introduction to Physical Oceanography,* (available on-line http://oceanworld.tamu.edu/resources/ocng_textbook/contents.html) 2002.

Susanto, R.D., Q. Zheng, and X.-H. Yan, *Complex singular value decomposition analysis of equatorial waves in the Pacific observed by TOPEX/Poseidon altimeter*, J. Atmos. Ocean. Technol., 764-774, 1990.

Sverdup, H.U., *Wind-driven currents in a baroclinic ocean: with application to the equatorial currents of the eastern Pacific,* Proceedings of the National Academy of Sciences, 33 (11), 318-326, 1947.

Sverdrup, H.U., M.W. Johnson, and R.H. Fleming, *The oceans: their physics, chemistry, and general biology*, Englewood Cliffs, New Jersey,: Prentice-Hall, Inc., 1942.

Sy, A., Schauer, U. and Meinke, J., *The North Atlantic Current and its associated hydrographic structure above and eastwards of the Mid-Atlantic Ridge*, Deep-Sea Res., V39, No.5, 825-853, 1992.

Sy, A., *Investigation of large-scale circulation patterns in the central North Atlantic: the North Atlantic Current, the Azores Current, and the Mediterranean Water plume in the area of the Mid-Atlantic Ridge*, Deep-Sea Res., V35, No.3, 383-413, 1988.

Tapley, B.D., and M.-C. Kim, *Applications to Geodesy*, In: Satellite altimetry and earth sciences (ed. L.-L. Fu and A. Cazenave): a handbook of techniques and applications, Academic Press, International Geophysics Series, V69, 2001.

Taylor, A.H., and J.A. Stephens, *The North Atlantic Oscillation and the latitude of the Gulf Stream*, Tellus, 50A, 134-142, 1998.

Te Raa, L.A., *Internal variability of the thermohaline ocean circulation*, PhD thesis, ISBN 90-393-3345-9, pp.158, 2003.

Tokmakian, R.T. and P.G. Challenor, *Observations in the Canary Basin and the Azores frontal region using Geosat data*, J. Geophys. Res., 98, 4761-4773, 1993.

Valdimarsson, H., and S.-A. Malmberg, *Near-surface circulation in Icelandic waters derived from satellite-tracked drifters*, Rit Fiskideildar, 16, 23-29, 1999.

Van Aken, H.M., *Decadal changes of the hydrography between Ireland and Cape Farewell*, ICES Marine Science Symposia, 219: *Hydrobiological Variability in the ICES Area*, 1990 – 1999, pp. 80-85, 2003.

Van Aken, H.M., and G. Becker, *Hydrography and through-flow in the north-eastern North Atlantic Ocean: the NANSEN project,* Prog. Oceanog., 38, 297-346, 1996.

Verbrugge, N. and G. Reverdin, *Contribution of horizontal advection to the interannual variability of sea surface temperature in the North Atlantic*, J. Phys. Oceanogr., 33, 964-978, 2003.

Vivier, F., K.A. Kelly, L. Thompson, *Contributions of wind forcing, waves, and surface heating to sea surface height observations in the Pacific Ocean*, J. Geophys. Res., 104, 20767-20788, 1999.

Volkov, D.L. and H.M. van Aken (1), *Annual and interannual variability of sea level in the northern North Atlantic Ocean*, J. Geophys. Res., 108, 3204, doi: 10.1029/2002JC001459, 2003.

Volkov, D.L. and H.M. van Aken (2), *Low frequency change of sea level in the North Atlantic Ocean as observed with satellite altimetry*, In: Satellite altimetry for geodesy, geophysics and oceanography (eds. C.Hwang, C.Shum and L. Jiangcheng), International Association of Geodesy Symposia, Vol. 126, pp. 167-174, Springer-Verlag, 2003.

Volkov, D.L., *The interannual variability of the altimetry-derived eddy field and associated surface circulation in the North Atlantic Ocean in 1993-2001*, J. Phys. Oceanography, in press, 2004.

Wang, L. and C. Koblinsky, *Annual variability of the subtropical recirculations in the North Atlantic and North Pacific: a TOPEX/Poseidon study*, J. Phys. Oceanogr., 26, 2462-2479, 1996.

Walker, G.T. and E.W. Bliss, *World weather V. Mem. Roy. Meteor. Soc*., 4, 53-84, 1932.

White, M.A. and K.J. Heywood, *Seasonal and interannual changes in the North Atlantic subpolar gyre from Geosat and Topex/Poseidon altimetry*, J. Geophys. Res., 100, C12, 24931-24941, 1995.

White, W.B. and C.K. Tai, *Inferring interannual changes in global upper-ocean heat storage from TOPEX altimetry*, J. Geophys. Res., 100, 24,943-24,954, 1995.

Wood, R.A., *Unstable waves on oceanic fronts: large amplitude behavior and mean flow generation*, J. Phys. Oceanogr., 18, 775-787, 1988.

Wunsch, C., and Stammer, D., *Atmospheric loading and the oceanic "inverted barometer" effect*, Rev. Geophys., 35, 79-107, 1997.

Wyrtki, K., L. Magaard, and J. Hager, *Eddy energy in the oceans*, J. Geophys. Res., 81, 2641 - 2646, 1976.

Zhang, Y., J.M. Wallace, D.S. Battisti, *ENSO-like interdecadal variability: 1900-93*, J. Climate, 10, 1004-1020, 1997.

Samenvatting

(translated from English by Hendrik M. van Aken)

Variabiliteit in de oceaan vindt plaats met verschillende temporele (van seconden tot interjaarlijks en langer) en ruimtelijke schalen (millimeters tot oceaanschaal). De hoofddoelstelling van dit proefschrift was de studie, met behulp van satellietaltimetriewaarnemingen, van de aan het klimaat gebonden variabiliteit van het zeeniveau en de oceaancirculatie in the Noord-Atlantische Oceaan. De variabiliteit van het zeeniveau is een goede aanwijzing voor veranderingen die plaatsvinden in de eigenschappen van het water in de bovenste lagen van de oceaan (uitzetting en samentrekking van de waterkolom ten gevolge van veranderingen in temperatuur en saliniteit) en in de oceaancirculatie (verplaatsing van de positie van zeestromen en fronten).

De opkomst van de satellietaltimetrie heeft de studie van de variabiliteit van het zeeniveau en de oppervlaktecirculatie aanzienlijk vergemakkelijkt (Fu en Cazenave, 2001). Satellieten, uitgerust met een altimeter, leveren vaak en regelmatig waarnemingen, bijna mondiaal, van de hoogte van het zeeoppervlak. De geostrofische oppervlaktecirculatie kan worden bepaald uit de dynamische topografie van het zeeoppervlak; het verschil tussen de hoogte van het zeeoppervlak en de hoogte van een equipotentiaalvlak of geoïde. In dit proefschrift worden gegevens gebruikt van de recentste hoge-nauwkeurigheidaltimetriemissies, uitgevoerd met de gemeenschappelijk Frans/ Amerikaanse TOPEX/Poseidon en Jason-1 satellieten en de Europese ERS-1 en -2 satellieten van de ESA. Sinds de lancering van TOPEX/Poseidon op 10 augustus 1992 tot op heden zijn meer dan 10 jaar aan hoge-nauwkeurigheidsgegevens verzameld. De combinatie van gegevens van verschillende satellietmissies geeft een betere ruimtelijke bedekking (Ducet en LeTraon, 2000). Te tijdsresolutie van de gegevens wordt bepaald door de herhaalperiode van de satellietbaan. Voor de in dit proefschrift gebruikte gegevens is dit ongeveer een maal per 10 dagen (de herhaalperiode voor de TOPEX/Poseidon en Jason-1 satellieten). Daarom houdt dit proefschrift zich bezig met variabiliteit met mesoschaal-, seizoens- en interjaarlijkse tijdschalen. Variaties van het zeeniveau op deze tijdschalen worden voornamelijk veroorzaakt door fluxen van zout en warmte (drijfvermogen-fluxen) aan het zeeoppervlak, de variaties van het warmte- en zoutbudget vanwege de advectie van watermassa's met verschillende eigenschappen, wervelgeneratiemechanismen vanwege de instabiliteit van oceaanstromingen, Rossby-golven, enz.

Verschillende specifieke vragen werden behandeld in dit proefschrift. Er werd aangetoond hoe het zeeniveau op gematigde breedten in de Noord-Atlantische Oceaan veranderde gedurende de periode 1993-2003. De mesoschaal- seizoens- en interjaarlijkse modi van de variabiliteit werden ontsluierd, en de grootte en relatieve bijdrage van iedere modus aan de totale variantie werden vastgesteld. De interjaarlijkse verandering van het zeeniveau in the noordlijke Noord-Atlantische Oceaan werd gekoppeld aan in-situ-waarnemingen langs de trans-Atlantische AR7E sectie, die bijna jaarlijks tussen 1990 en 2003 werd onderzocht in het kader van de hydrografisch programma's van WOCE (World Ocean Circulation Experiment) en CLIVAR (CLImate VARiability). Dit maakte het

mogelijk de interjaarlijks verandering van het zeeniveau te interpreteren in termen van veranderingen van zeewatereigenschappen en verdeling van watermassa's. Een volgende stap was het vaststellen of the veranderingen, waargenomen in de gematigde Noord-Atlantische Oceaan verschilden van die in de gematigde noordelijke Stille Oceaan. De grootte, ruimtelijke patronen en trends in de waargenomen variatie van het zeeniveau en de daaraan verbonden oppervlaktecirculatie werden bestudeerd met gebruik van jaarlijkse schattingen van de kinetische energie van oceaanwervels (EKE) als benadering voor de loop van de belangrijkste zeestromingen. Een van de belangrijke zaken die door het proefschrift worden geïllustreerd is de waarschijnlijke afhankelijkheid van de interjaarlijkse verandering van zeeniveau en oceaancirculatie van de verandering van het atmosferische circulatiepatroon dat verband houdt met atmosfeer-zeewisselwerking. De voornaamste modi voor deze interactie in de noordelijke bekkens van de Atlantische en Stille Oceaan, de Noord-Atlantische Oscillatie (NAO) en de Pacifische Decadale Oscillatie (PDO), waren gekoppeld aan de waargenomen interjaarlijkse variaties van zeeniveau en oppervlakteciculatie.

In hoofstuk 3 werd aangetoond dat de seizoens- en interjaarlijkse signalen van de variabiliteit van het zeeniveau dominant zijn in de noordelijke Noord-Atlantische Oceaan (noord van 50ºNB). De seizoensvariabiliteit buiten de Noord-Atlantische Stroom bleek het sterkst bij te dragen aan de totale variantie, van 30 tot 50%. De interjaarlijkse verandering bleek het meest uitgesproken in het Irmingerbekken, met een relatieve bijdrage van meer dan 40%. De grootste amplitudes van de jaarlijkse gang van het zeeniveau (5-6 cm) werden in het IJslandbekken waargenomen, en toegeschreven aan de seizoensverandering in de positie van het Subarctische Front in dit gebied. Een tak van de Noord-Atlantische Stroom, geassocieerd met the Subarctische Front in het IJslandbekken, ondervindt ook seizoensverschuivingen en veranderingen in intensiteit. Aangezien de seizoensveranderingen van het zeeniveau niet volledig konden worden verklaard uit de seizoensvariaties van de warmteflux, dragen advectieve veranderingen van de positie van het Subarctische Front waarschijnlijk bij aan de seizoensverandering van het zeeniveau in het IJslandbekken. Advectie blijkt een belangrijke rol te spelen bij de interjaarlijks variatie van het zeeniveau, zoals werd gesuggereerd door Reverdin et al. (1999).

Op interjaarlijkse tijdschalen vertoonde het zeeniveau in de Noord-Atlantische Oceaan, gemeten met satellietaltimetrie, een grootschalige toename, van een minimumwaarde in 1994 tot een maximum in 1997-1998. Daarna nam het zeeniveau af, tot het weer begon te stijgen na 2000. De hydrografische gegevens, verkregen gedurende de WOCE en CLIVAR onderzoekstochten langs de trans-Atlantische AR7E sectie, bevestigden de verandering van het zeeniveau, gemeten met satellietaltimetrie. Op grote ruimtelijke schaal werd een goede overeenkomst gevonden tussen de altimetrische hoogte en de hydrografische dynamische hoogte, afgeleid van de temperatuur en het zoutgehalte. Dit impliceert een overwegend baroklien karakter van de waargenomen variatie van het zeeniveau, d.w.z. de veranderingen van het zeeniveau worden voornamelijk verklaard door veranderingen in de dichtheid van het zeewater.Dit verschilt met een barotrope verandering van het zeeniveau die wordt veroorzaakt door veranderingen in de totale hoeveelheid water en is waarschijnlijk belangrijker is in kustgebieden en randzeeën. Het bleek dat de laag tussen 200 en 800 m, waar het Subpolaire Modus Water (SPMW) wordt gevonden, de grootste bijdrage levert aan de interjaarlijkse variaties van het zeeniveau. SPMW wordt geproduceerd door menging en convectie van subtropische en polaire watermassa's (McCartney and Talley,

1982). Het zit bij benadering in de bovenste 1000 m van de zee en vertegenwoordigt de meest dynamische watermassa in de noordlijke Noord-Atlantische Oceaan. De voorname rol van dit water in de interjaarlijkse variatie van het zeeniveau werd ook verwacht, want het is de watermassa waar grote veranderingen in advectie en drijfvermogen kunnen plaatsvinden. De interjaarlijkse verandering van het zeeniveau in de Noord-Atlantische Oceaan bleek samen te hangen met veranderingen in de winterindex voor de NAO.

Er werd aangetoond dat op interjaarlijkse tijdschalen de gematigde Noord-Atlantische Oceaan als een dipoolsysteem reageert op de atmosferische forcering, uitgedrukt als de winterindex van de NAO (bijv. Esselborn en Eden, 2001). De verdeling van de atmosferische druk, en dientengevolge van de wind boven de oceaan, verschilt tussen positieve en negatieve NAO-fases. De verdeling van de atmosferische druk gedurende positieve/negatieve NAO-fase wordt gekarakteriseerd door een sterk/zwak Azoren-hogedrukgebied en een diep/zwak lagedrukgebied bij IJsland. (Hurrell et al., 2003). Gedurende een positieve NAO-fase, gekoppeld aan sterke westenwinden, is het zeeniveau hoog in de subtropische wervel en laag in de subpolaire wervel. Wanneer de NAO-fase verandert van positief naar negatief, en de westenwinden zwakker worden, zoals tweemaal gebeurde gedurende de onderzoeksperiode, neemt het zeeniveau toe in de subpolaire wervel terwijl het afneemt in de subtropische wervel. Aan de ene kant brengt de herstructurering van de atmosferische druk en circulatie gedurende een negatieve NAO-fase warme lucht naar de noordelijke en noordwestelijke gebieden van de subpolaire Noord-Atlantische Oceaan. Dit leidt to opwarming van de oceaan in deze gebieden. Aan de andere kant heeft een verandering van het atmosferische circulatiepatroon door de veranderde windschuifspanning uitwerking op het patroon van de grootschalige oceaancirculatie. Gedurende een negatieve NAO-fase worden de westenwinden zwakker, wat het oostwaartse transport van SPMW vermindert en leidt tot een westwaartse verschuiving van het subarctische front in het IJslandbekken (Bersch, 2001). Dit laat het transport van de Noord-Atlantische Stroom naar de noordelijke en noordwestelijke gebieden van de subpolaire Noord-Atlantische Oceaan toenemen. Op die manier draagt de advectie van warm en zouter water ook bij aan de toename van het zeeniveau in deze gebieden.

In hoofstuk 4 werden de grootte en ruimtelijke patronen van de variabiliteit van het zeeniveau in de noordelijke Atlantische Oceaan vergeleken met die in de noordelijke Stille Oceaan. Er werd aangetoond dat de ruimtelijke patronen van meso-schaal-, seizoens- en interjaarlijkse variabiliteit in beide oceanen lijken op lokale karakteristieken van de oppervlaktecirculatie. In de Noord-Atlantische Oceaan maakt de open verbinding met de Arctische Oceaan een noordoostelijke uitbreiding van de subpolaire wervel mogelijk. Dit veroorzaakt een divergentie van de belangrijkste oostwaartse stromingen wat relatief sterke mesoschaal variabiliteit veroorzaakt in een relatief groot gebied, samenhangen met de noordoostelijke stroming van de Noord-Atlantische Stroom en met de oostelijke Azorenstroom. In de noordelijke Stille Oceaan is een dergelijke noordoostelijke uitbreiding van de subpolaire wervel niet mogelijk vanwege de geografische grenzen en de nauwe en ondiepe Beringstraat. Daarom is het gebied met grote meso-schaalvariabiliteit in de Atlantische Oceaan relatief groter dan in the Noordelijke Stille Oceaan, en is de meso-schaalvariabiliteit in de Atlantische Oceaan dominanter. In het oostelijke gedeelte van de Stille Oceaan bleek de meso-schaalvariabiliteit erg klein, met uitzondering van de randstromingen langs de Noord-Amerikaanse kust. In de Noord-Atlantische Oceaan werd relatief sterke meso-schaalvariabiliteit bijna overal in het noordelijke gedeelte van de

subtropische wervel (noord van 30ºNB) aangetroffen. De meso-schaalvariabiliteit toont seizoensvariaties, waarschijnlijk veroorzaakt door de met de seizoenen veranderende windschuifspanning. In beide oceanen werd de sterkste seizoensmodulatie van de meso-schaalvariabiliteit waargenomen in de subpolaire gebieden. De grootste corresponderende variantie in het zeeniveau werd overwegend in de later herfst en de winter waargenomen. Deze periode valt samen met de periode van de grootste windschuifspanning, wat de afhankelijkheid van de meso-schaalactiviteit van de variërende wind ondersteunt. De seizoensveranderingen van het zeeniveau in de noordelijke Atlantische en Stille Oceaan blijken van de zelfde grootte en hebben hetzelfde ruimtelijke patroon. Er werd echter een verschil gevonden in de ruimtelijke verdeling van de fase van het seizoenssignaal. In de noordelijke Stille oceaan was de verdeling hiervan overwegend zonaal, met het maximum zeeniveau in de subtropische wervel in oktober en in de subpolaire wervel in september. In de noordelijke Atlantische Oceaan werd een zeeniveaumaximum in september alleen waargenomen in het Irmingerbekken en de Labradorzee. Zo'n faseverdeling in de Noord-Atlantische Oceaan wordt mogelijk veroorzaakt door het bestaan van een poolwaartse stroming en het bijbehorende doordringen van Atlantisch water in de arctische en polaire delen van de Atlantische Oceaan. De seizoensvariaties van het zeeniveau in de extensies van de Golfstroom en de Kuroshio toonden een meridionale verschuiving van de intensiviteit van de stroming: zuidwaarts in het voorjaar en noordwaarts in het najaar. De waargenomen grootte van de interjaarlijkse variabiliteit in de noordelijke Stille Oceaan bleek groter dan in de Atlantische Oceaan, terwijl de ruimtelijke patronen wel overeen kwamen.

Er werd een poging ondernomen de aan het klimaat gerelateerde verandering van het zeeniveau en de oppervlaktecirculatie in de noordelijke Atlantische en Stille Oceaan te analyseren. In de context van dit proefschrift wordt de aan het klimaat gerelateerde variabiliteit gezien als de interjaarlijkse en interdecadale veranderingen, samenhangend met wijzigingen in de niet-lineaire lucht-zee-wisselwerking. De belangrijkste modi voor deze interacties zijn de NAO in de Noord-Atlantische Oceaan en de PDO in de Stille Oceaan. De eerste empirisch modi in beide oceanen vertoonden een oscillerend dipoolkarakter. In de Noord-Atlantische oceaan vertoonde de eerste empirisch orthogonale modus voor 1993-2003 een bijna lineaire toename van het zeeniveau in de subpolaire en oostelijke gebieden.Deze toename ging vergezeld van een afnamen van het zeeniveau in de Golfstroomextensie en de Noord-Atlantische Stroom west van de Mid-Atlantische Rug. In de Noordelijke Stille Oceaan gaf de eerste empirische modus een stapsgewijze verandering in 1998 weer. In dat jaar begon het zeeniveau in de subpolaire gebieden af te nemen, in het bijzonder in de Beringzee, en toe te nemen in het noordelijke gedeelte van de subtropische wervel. De eerste empirische modus van de variabiliteit van het zeeniveau op interjaarlijkse tijdschalen bleek coherent te zijn met een laagfrequent lopend gemiddelde van de PDO-index. Hoewel de tijdreeks van iets meer dan 10 jaar, gebruikt in deze studie, te kort is om aan het klimaat gerelateerde veranderingen grondig te bestuderen, werden sommige conclusies ondersteund door eerder onderzoek (Cabanes et al., 2001; Häkkinen, 2003). De lineaire trend van het zeeniveau in de noordelijke Noord-Atlantische en Stille Oceaan, geschat met een lineaire regressie, bleek een patroon te hebben, bijna identiek aan de eerste empirische modi van de interjaarlijkse variabiliteit van het zeeniveau. Hieruit werd geconcludeerd dat deze modi een inter-decadale lange-termijntrend in het zeeniveau beschrijven. Deze trend verschilt van die, beschreven door Cabanes et al. (2001) voor een

vroegere periode. Voor de periode 1955 tot 1996 vonden zij een negatieve trend van het sterische zeeniveau in de subpolaire wervel en een positieve trend in de subtropische wervel van de Noord-Atlantische Oceaan, wat het tegengestelde is van de voor 1993 tot 2003 waargenomen verandering. In de noordelijke Stille Oceaan bestonden afnemende trends van het zeeniveau tussen 1955 en 1996 in de subtropische wervel, terwijl het zeeniveau toenam in de subpolaire en oostelijke gebieden. Klaarblijkelijk trad een omkering van het teken van de zeeniveautrends in beide oceanen op, mogelijk samenhangend met de inter-decadale klimaatvariabiliteit. De PDO zelf wordt gedefinieerd als de inter-decadale modus van atmosferische variabiliteit boven de noordelijke Stille Oceaan. De NAO vertoont vele frequenties, maar heeft ook een inter-decadale modus (zie hoofdstuk 1). De verandering van de trend in het zeeniveau van de noordelijke Stille Oceaan vond plaats in 1998. Om te begrijpen of dit een sprongverandering was van één PDO fase naar een andere, en geen kort-durende fluctuatie veroorzaakt door de el Niño en de daaropvolgende la Niña, hebben we meer daaropvolgende jaren nodig dan nu beschikbaar. Zoals werd aangetoond in hoofdstuk 3, was de interjaarlijkse verandering van het zeeniveau gecorreleerd met de NAO-index voor de wintermaanden. De toename van het zeeniveau in de subpolaire Noord-Atlantische Oceaan volgde op veranderingen van de NAO-fase van positief naar negatief in de winters van 1995/1996 en 2000/2001. De zeeniveautrends in de Noord-Atlantische Oceaan, waargenomen tussen 1993 en 2003, lijken op de negatieve NAO-index. Het is echter met zo'n korte reeks waarnemingen niet mogelijk vast te stellen of dit patroon blijft bestaan of dat het alleen ging om onafhankelijke korte-termijnfluctuaties. Op grond van de waarnemingen zou men ook kunnen suggereren dat op inter-decadale tijdschalen het zeeniveau in the Noord-Atlantische Oceaan uit fase varieert met het zeeniveau in de Stille Oceaan. Een gelijktijdige stijging van het zeeniveau in de subpolaire en oostelijke Noord-Atlantisch Oceaan en een daling in de Golfstroomextensie en de Noord-Atlantische Stroom gaan mogelijk vergezeld van een afname van het zeeniveau in de subpolaire en oostelijke Stille Oceaan en een een stijging in de Kuroshioextensie en in de Noord-Pacifische Stroom. De decadale trends van het zeeniveau in beide oceanen geeft ook een edecadale trend in de geostrofische oppervlaktecirculatie weer. Deze liet een afname zien van de subtropische en subpolaire wervels in de Noord-Atlantische Oceaan, en een intensivering van de wervels in de noordelijke Stille Oceaan. Flatau et al., (2003) en Häkkinen en Rhines (2003) toonden ook een afname van de Noord-Atlantische subpolaire circulatie aan.

In hoofdstuk 5 werd de variabiliteit van de kinetische energie van de meso-schaalwervels (EKE) geanalyseerd om de interjaarlijkse verandering van positie en intensiteit van de voornaamste stromingen in de gematigde Noord-Atlantische Oceaan te bestuderen. De voorgestelde interpretatie steunt op het feit dat zeestromingen de voornaamste bron vormen van EKE die wordt gegenereerd door instabiliteitsprocessen in frontale stromingen. Er werd aangetoond dat de grootste EKE geconcentreerd is langs de voornaamste frontale stromingen in de Noord-Atlantische Oceaan. Een vergelijking van de dichtheidsverdeling langs de AR7E sectie en de EKE aan het zeeoppervlak toonde aan dat de kernen van hoge EKE-waardes samenvielen met frontale zones met een hoge dichtheidsgradiënt. Hiermee werd getoond dat in afwezigheid van voldoende nauwkeurige schattingen van de geostrofische snelheden uit altimetriegegevens EKE een bruikbare parameter is om de variabiliteit van de oppervlaktecirculatie vast te leggen. Een gedetailleerde beschrijving van de interjaarlijkse variabiliteit van de EKE en de daarbij

behorende oppervlaktecirculatie in verscheidene gebieden van de gematigde Noord-Atlantische Oceaan werd gepresenteerd. In de Golfstroomextensie liet de interjaarlijkse variabiliteit van de EKE en van geostrofische snelheidsanomalieën meridionale verplaatsingen zien van de kern van de stroming. De zuidelijkste positie werd in 1998 vastgelegd, ongeveer 2 jaar na de verandering van de NAO-index van positief naar negatief in de winter van 1995/1996. De interjaarlijkse variabiliteit van de EKE in de Noord-Atlantische Stroom werd gedomineerd door de herverdeling van EKE tussen drie zones, gecentreerd rond 43ºNB, 47ºNB, en 50ºNB. De zuidelijkste zone wordt geassocieerd met de anti-cyclonale Mann-wervel. De twee andere vertegenwoordigen oostwaartse takken van de Noord-Atlantische Stroom. Het bleek dat, wanneer positieve EKE-anomalieën werden waargenomen in de Mann-wervel en langs de noordelijke wand van de Noord-Atlantische Stroom op 50ºNB, negatieve anomalieën werden waargenomen bij 47ºNB, en *vice versa*. Positieve/negatieve EKE-anomalieën in de Noord-Atlantitische Stroom kwamen in het algemeen overeen met oostwaartse/westwaartse geostrofische snelheidsanomalieën. Aangezien de Noord-Atlantische Stroom in het algemeen een brede oost tot noordoostelijke drift vertegenwoordigt, werden positieve/negatieve EKE-anomalieën in geassocieerd met versterking of verzwakking van de oostelijke stroming. On de Azorenstroom werd een EKE-maximum waargenomen in 1993-1995, gevolgd door een verzwakking van deze stroming, veroorzaakt door een verzwakking van de westenwinden in 1996. De interjaarlijkse verandering van EKE en geostrofische snelheidsanomalieën gaven de bovengenoemde westwaartse verschuiving van het Subarctische Front in het IJslandbekken weer, die gebeurde na 1995. Er werd aangetoond dat de noordoostelijke stroming in het Rockallkanaal intensiever was in 1993-1995 dan in latere jaren. In zowel het IJslandbekken als het Rockallkanaal was het seizoenssignaal van de EKE met een maximum in de winter veel sterker dan het interjaarlijkse signaal. Dit suggereert een verband tussen de EKE en de met het seizoen variërende windschuifspanning, die het sterkst is in de winter. In het Irmingerbekken werd een lange-termijntrend in de EKE waargenomen. Dit bekken bleek het enige in de Noord-Atlantische Oceaan waar de seizoensvariatie van de EKE kleiner was dan de interjaarlijkse verandering. In het Irmingerbekken was de EKE geconcentreerd in twee parallelle banden. De waargenomen toename van de EKE hatd betrekking op beide banden. Deze was echter niet verbonden met een intensivering van de oppervlaktecirculatie. Zoals al was aangetoond in andere studies (bijv. Flatau et al., 2003) en was bevestigd in hoofdstuk 5, nam de cyclonale circulatie van de subpolaire Noord-Atlantische wervel af. Er werd gesuggereerd dat de aan de NAO verandering gekoppelde westelijke verschuiving van het Subarctische Front dat het Irmingerbekken bereikte de generatie van meso-schaalwervels stimuleerde en de toename van de EKE in het Irmingerbekken veroorzaakte. Deze verschuiving kan de meest oostelijke EKE-band beïnvloed hebben, terwijl de westelijke band waarschijnlijk gehandhaafd bleef door een convectief gegenereerd oppervlaktefront in het centrum van het Irmingerbekken. In de Labradorzee bleek de variabiliteit van de EKE erg complex te zijn. Het seizoenssignaal was significant veel sterker dan het interjaarlijkse signaal. Een maximum in EKE wed waargenomen in de winters van 1996/1997, 1997/1998 en 1998/1999 met een hoge NAO-index , maar nier in het eerdere gedeelte van de waarnemingsreeks.

In hoofdstuk 6 werd de interjaarlijkse EKE-tijdreeks van de Noord-Atlantische Stroom tussen de Grand Banks en de Mid-Atlantische Rug onderzocht op zich voortplantende verschijnselen. Deze studie werd gemotiveerd door de bijzonderheden van de verdeling van

de EKE in dit gebied, beschreven in hoofdstuk 5. De meeste EKE werd in de Mann-wervel gevonden, en oost van Flemish Cap op 47ºNB. Door het gebruik van de Complexe Singuliere-waardedecompositie, een versie van de Complexe Empirisch Orthogonale Functiesanalyse, werden de zich voortplantende signalen in het EKE-veld zichtbaar gemaakt. Er werd aangetoond dat het EKE-signaal, samenhangend met de eerste empirische modus, zich stroomafwaarts voortplant in de Noord-Atlantische Stroom die rond de Grand Banks stroomt. Er werden voor het bestudeerde tijdsinterval 1993-2003 bijna twee EKE-golven met een periode van ongeveer 6 jaar waargenomen. Het bleek dat het EKE-signaal zich sneller voortplant op de westelijke en noordelijke rand van de Mann-wervel dan verder stoomop– of –afwaarts. Binnen de Mann-wervel werd geen voortplanting van een EKE-signaal waargenomen, daar had de EKE-variatie het karakter van een staande golf. De interjaarlijkse verandering van de EKE in de noord-Atlantische Stroom bleek coherent met de NAO. Positieve EKE-anomalieën in de Mann-wervel werden vastgesteld voor 1996-1997 en 2001-2002, direct nadat de NAO-index veranderde van positief naar negatief in de winters van 1995/1996 en 2000/2001. De 1996-1997 EKE-anomalie, waargenomen in de Mann-wervel, bereikte 47ºNB in 2000. De positieve EKE-anomalieën bleken voornamelijk samen te hangen met een geïntensiveerde oostelijke stroming. Met de beschikbare korte reeks waarnemingen is het nog niet mogelijk vast te stellen of de waargenomen EKE-voortplanting een periodiek verschijnsel is met een vaste periode. Het is waarschijnlijk dat de voortplanting gerelateerd is aan de meridionale verschuiving van takken van de Noord-Atlantische Stroom. De waargenomen coherentie met de NAO suggereert dat er een verband is met de atmosferische forcering. Aangezien de oppervlaktecirculatie in het algemeen door de wind wordt aangedreven, kan de meridionale verschuiving van stromingen, weergegeven door het zich voortplantende EKE-signaal, veroorzaakt worden door meridionale verschuivingen van de windschuifspanning.

Краткое изложение

Состояние вод Мирового Океана подвержено изменчивости, которая происходит на различных временных (от секунд до межгодовых и дольше) и пространственных (от нескольких миллиметров до размеров океанских бассейнов) масштабах. Главной целью этой диссертации было проведение исследования климатической изменчивости уровня океана и поверхностной циркуляции в Северной Атлантике по данным спутниковой альтиметрии. Изменчивость уровня океана является хорошим показателем изменений состояния морской воды в околоповерхностном слое (расширение или сжатие водной толщи вследствие изменений температуры и солености морской воды) и изменений в океанической циркуляции (смещения местоположений океанических фронтов и течений).

Начало использования спутниковой альтиметрии поверхности океана значительно упростило задачу исследования изменений уровня океана и океанической циркуляции (Fu and Cazenave, 2001). Околоземные спутники, оснащённые бортовыми альтиметрами, обеспечивают возможность проведения регулярных и практически глобальных измерений высоты поверхности океана относительно эллипсоида отсчёта, который представляет собой модель земного шара в виде сферы приплюснутой у полюсов. Разность между высотой поверхности океана и высотой поверхности геоида относительно эллипсоида отсчёта - есть динамическая топография поверхности океана. Уклоны поверхности океана, отраженные динамической топографией, позволяют определить геострофическую циркуляцию на поверхности. В этой диссертации использовались данные, полученные последними высокоточными альтиметрами, установленными на франко-американских спутниках TOPEX/Poseidon и Jason-1, а также на спутниках Европейского Космического Агенства ERS-1 и ERS-2. Начиная с запуска спутника TOPEX/Poseidon 10 августа 1992 года и до настоящего времени, было собрано более десяти лет высококачественных данных. Совмещение данных, полученных с разных спутников, помогает получить большее пространственное разрешение (Ducet et al., 2000). Временно́е разрешение альтиметрических данных определяется промежутком времени между двумя последовательными измерениями над одной и той же точкой поверхности океана. Для спутников TOPEX/Poseidon и Jason-1 оно составляет почти 10 суток. Подобное разрешение позволяет исследовать океанические процессы, характеризуемые пространственно-временной изменчивостью, начиная с мезомасштабной. Поэтому, данная диссертация включает исследования мезомасштабной, сезонной и межгодовой изменчивости. Изменения уровня поверхности океана на этих пространственно-временных масштабах в основном обусловлены вариациями обмена теплом и массой на поверхности раздела океан-атмосфера, изменениями теплосодержания и солености морской воды в результате адвекции инородных водных масс, процессами вихреобразования, благодаря динамической неустойчивости океанских течений, волнами Россби, и т.д.

Диссертация освещает несколько специфических вопросов. Она иллюстрирует, как изменялся уровень океана в различных внетропических районах Северной Атлантики в течение рассматриваемого времени с 1993 по 2003 годы. Были выявлены мезомасштабные, сезонные и межгодовые компоненты временных рядов и были оценены величина и относительный вклад каждой компоненты в общую изменчивость уровня поверхности океана. Межгодовые изменения уровня океана в северной части Северной Атлантики сравнивались с регулярными *in situ* гидрографическими наблюдениями вдоль трансатлантической секции AR7E, проводимыми практически ежегодно, начиная с 1990 года, в рамках програм WOCE (World Ocean Circulation Experiment) и CLIVAR (CLImate VARiability). Такое сравнение дало возможность объяснить межгодовые изменения уровня океана, выявленные спутниковой альтиметрией, в единицах изменений температуры и солености морской воды и распределения водных масс. Следующим шагом было сравнение колебаний уровня океана, произошедших во внетропической части Северной Атлантики, с изменениями во внетропической части Северного Тихого океана. Сравнивались величины, пространственный характер, а также тренды наблюдаемых изменений уровня океана и циркуляции на поверхности. Межгодовая изменчивость поверхносной циркуляции исследована с использованием ежегодных оценок кинетической вихревой энергии (КВЭ), которая использовалась как параметр для определения положения основных фронтальных течений. Одним из основных вопросов, рассмотренных в диссертации, является возможная зависимость межгодовых изменений уровня океана и циркуляции на поверхности от изменений в циркуляции атмосферы, которые связаны с взаимодейтсвием океана и атмосферы. Главные моды этих взаимодействий в Северной Атлантике и Северной Пацифике, известные под названиями Северной Атлантической Осцилляции (САО) и Тихоокеанской Декадной Осцилляции (ТДО), сопоставлялись с выявленными изменениями уровня океана и циркуляции на его поверхности.

В главе 3 показано, что сезонные и межгодовые вариации являются доминирующими в изменчивости уровня поверхности океана в северной части Северной Атлантики (к северу от 50° с.ш.). Оказалось, что сезонные колебания, вне зоны Северо-Атлантического течения, имеют наибольший вклад в общую изменчивость, варьируемый от 30% до 50%. Наибольшие межгодовые колебания уровня океана были обнаружены в бассейне Ирмингера, где их относительный вклад в общую изменчивость местами превышал 40%. Наибольшие амплитуды (5-6 см) сезонных изменений уровня океана наблюдались в Исландском бассейне и могли быть вызваны сезонными изменениями местоположения субарктического фронта в данном районе. Один из рукавов Северо-Атлантического течения, связанный с субарктическим фронтом, течёт через Исландский бассейн и вместе с фронтом подвержен сезонным изменениям местоположения и интенсивности. Учитывая, что сезонные колебания уровня океана в Исланском бассейне не удалось полностью объяснить сезонными изменениями потоков тепла между океаном и атмосферой, было сделано предположение, что адвекция, зависящая от местоположения субарктического фронта, возможно, также вносит определённый вклад в сезонные колебания уровня океана в Исландском бассейне. Согласно Reverdin et al. (1999),

адвекция также может играть важную роль в межгодовых изменениях уровня поверхности океана.

С помощью спутниковой альтиметрии был зафиксирован всеобщий рост уровня поверхности океана в северной части Северной Атлантики, начиная с минимального значения в 1994 году до максимальных значений в 1997-1998 годах. Затем уровень несколько понизился, но с 2000-го года начал снова расти. Гидрографические данные, полученные во время экспедиций вдоль трансатлантической секции AR7E, в рамках програм WOCE и CLIVAR, подтвердили вышеупомянутые изменения уровня океана, зарегестрированные альтиметрическими спутниками. На достаточно больших пространственных масштабах, высоты поверхности океана, измеренные альтиметрами, практически совпали с динамическими высотами, рассчитанными из данных температуры и солености. Это совпадение позволило сделать вывод о бароклинном характере колебаний уровня поверхности океана, т.е. высота поверхности океана менялась, в основном, благодаря изменениям термодинамических свойств морской воды. Подобные изменения отличаются от баротропных флюктуаций, которые обусловлены изменениями массы водной толщи. Баротропные флюктуации, вероятно, являются более важными в прибрежных районах и окраинных морях, подверженных штормовым нагонам. Оказалось, что водный слой между 200 и 800 м, занимаемый Субполярной водной массой, обеспечивает наибольший вклад в межгодовые колебания динамических высот вдоль секции AR7E. Субполярная водная масса образуется в результате смешения и последующей конвекции Субтропической и Полярной водных масс (McCartney and Talley, 1982). Она занимает верхний, приблизительно тысячеметровый слой воды и представляет собой самую динамичную водную массу в северной части Северной Атлантики. То, что этот слой играет основную роль в межгодовых изменениях уровня поверхности океана - не является удивительным, т.к. именно этот слой подвержен наибольшим колебаниям адвекции и потоков тепла, связанным с теплообменом между океаном и атмосферой.

Известно, что на межгодовых временных масштабах внетропическая часть Северного Атлантического океана реагирует на атмосферные воздействия, выраженные зимними значениями индекса САО. Океан реагирует в виде двухполярной осцилляционной системы (напр. Esselborn and Eden, 2001). Положительная и отрицательная фазы САО характеризуются разным распределением атмосферного давления и, следственно, полем ветра над океаном. Во время положительной/отрицательной САО фазы, распределение атмосферного давления характеризуется сильным/слабым центром высокого давления над Азорскими островами и сильным/слабым центром низкого давления над Исландией (Hurrell et al., 2003). Для положительной САО фазы, ассоциированной с интенсивными западными ветрами, характерны высокие значения уровня поверхности океана в зоне субтропического антициклонального круговорота и низкие значения уровня в зоне субполярной циклонической циркуляции. Когда происходит смена положительной фазы САО на отрицательную, как случилось дважды в течение исследуемого времени, уровень океана растет в субполярном круговороте и понижается в субтропическом. С другой стороны, смена распределения атмосферного давления и направлений атмосферных потоков в результате наступления отрицательной фазы САО вызывает приток теплых

воздужных масс в северные и северо-восточные субполярные районы Севрной Атлантики. Во время отрицательной САО фазы западные ветры ослабевают, что влечет за собой уменьшение транспорта вод Субполярной водной массы на восток и сопровождается перемещением субарктического фронта в Иландском бассейне в западном направлении (Bersch, 2001). Последнее приводит к увеличению адвекции вод Северо-Атлантического течения в северные и северо-западные субполярные районы Северной Атлантики. Таким образом, адвекция теплых и более соленых вод Северо-Атлантического течения может также способствовать росту уровня поверхности океана в субполярных районах.

В главе 4 приведен сравнительный анализ размеров и пространственного распределения мезомасштабной, сезонной и межгодовой изменчивости во внетропических районах Северной Атлантики и Северной Пацифики. В этой главе показано, что пространственные характеристики изменчивости на рассматриваемых временных масштабах определены особенностями местной циркуляции вод на поверхности. Отсутсвие труднопреодолимых естественных границ между Северным Атлантическим океаном и Северным Ледовитым океаном позволяет субполярному круговороту глубоко проникать на северо-восток. Это обусловливает дивергенцию основных течений восточного направления и создает широкую зону с относительно высокой мезомасштабной изменчивостью, в основном связанной с северо-восточным потоком Северо-Атлантического течения и восточным Азорским течением. В Северном Тихом океане, из-за наличия материков на севере и узкостью мелководного Берингова пролива, подобная дивергенция потока не является возможной. Поэтому, территория, характеризуемая большой мезомасштабной изменчивостью, в Северной Атлантике значительно шире чем в Северной Пацифике, и, следовательно, мезомасштабная изменчивость в Северной Атлантике играет более важную роль, чем в Северной Пацифике. В восточной части Северного Тихого океана мезомасштабная изменчивость очень мала, кроме зон окраинных течений вдоль берега Северной Америки. Относительно большая мезомасштабная изменчивость наблюдалась практически во всех районах северной части Североатлантического субтропического круговорота (к северу от 30° с.ш.). Мезомасштабная изменчивость подвержена сезонным колебаниям, возможно вызванным сезонными изменениями в поле ветра. В обоих океанах наибольшие сезонные колебания были обнаружены в субполярных районах. Наибольшая дисперсия значений высоты поверхности океана в основном характерна для осенне-зимнего периода, когда наблюдаются наибольшие колебания силы воздействия ветра на водную поверхность. Данный факт свидетельствует в пользу зависимоти сезонных изменений мезомасштабной активности от сезоных вариаций в поле ветра. Было показано, что сезонные колебания уровня поверхности океана в Северной Атлантике и в Северной Пацифике в основном имеют схожие размеры и пространственные характеристики. Тем не менее, различие было обнаружено в пространственном распределении фазы сезонных колебаний. В Северном Тихом океане сезонная фаза оказалась распределена зонально: в северной части субтропического круговорота максимальные значения уровня океана наблюдаются в октябре, в то время как в субполярном круговороте максимальные значения уровня океана имеют место в сентябре. В Северной Атлантике сентябрьский максимум уровня океана в субполяром круговороте был обнаружен

только в бассейне Ирмингера и в море Лабрадор. Подобное пространственное распределение фазы сезонных колебаний уровня океана в Северной Атлантике, предположительно обусловлено наличием потока, направленного к Арктическому бассейну, и как следствие, глубоким проникновением вод Северо-Атлантического течения в приарктические части Северной Атлантики. Сезонные колебания уровня океана в Гольфстриме и Курошио выявили сезонные меридианальные сдвиги интенсивности потоков: к югу весной, и к северу осенью. Величины межгодовой изменчивости, наблюдавшиеся в Северном Тихом океане, оказались больше, чем в Северной Атлантике, хотя её пространственные харатеристики оказались схожими.

Был проведен анализ климатических изменений уровня поверхности океана и циркуляции на поверхности в Северной Атлантике и Северной Пацифике. В контектсе этой диссертации климатические изменения отнесены к межгодовым и междекадным изменениям, которые связаны с нелинейными процессами взаимодействия океана и атмосферы. Первые эмпирические моды межгодовой изменчивости уровня в обоих океанах имеют пространственные харатеристики дипольных осцилляционных систем. В Северной Атлантике первая эмпирическая мода показала квази-линейный рост уровня в течение декады с 1993 по 2003 годы в субполярных и восточных районах океана. Этот рост сопровождался падением уровня океана в зонах Гольфстрима и Северо-Атлантического течения к западу от Срединно-Атлантического хребта. В Северной Пацифике первая эмпирическая мода проиллюстрировала ступенчатое изменение уровня океана, которое произошло в 1998 году. В этом году уровень океана начал уменьшаться в субполярных районах, особенно в Беринговом море, и увеличиваться в северной части субтропического круговорота. Первая эмпирическая мода межгодовой изменчивости уровня поверхности океана в Северной Пацифике оказалась коррелированной с низкочастотными изменениями индекса ТДО. Немногим более десяти лет наблюдений, рассмотренных в этой диссертации, являются очень коротким сроком для оценки климатических изменений. Несмотря на это, оказалось возможным сделать некоторые выводы, учитывая предыдущие исследования (Cabanes et al., 2001; Häkkinen and Rhines, 2004). Обнаружено, что линейные тренды уровня поверхности океана в Северной Атлантике и Северной Пацифике с 1993 по 2003 годы, оцененные посредством линейной регрессии, имеют пространственные характеристики идентичные первым эмпирическим модам межгодовой изменчивости уровня. Таким образом, был сделан вывод, что первые эмпирические моды описывают долговременные, возможно междекадные, изменения уровня океана. Тренды, представленные в данной диссертации, отличаются от трендов оцененных Cabanes et al. (2001) для более раннего временного интервала. За период с 1955 по 1996 Cabanes et al. (2001) обнаружили отрицательные тренды стерического (обусловленного только потоками тепла между океаном и атмосферой) уровня поверхности океана в субполярном круговороте и положительные тренды в субтропическом круговороте Северной Атлантики, что является диаметрально противоположным наблюдениям за 1993 - 2003 годы. В Северном Тихом океане с 1993 по 2003 годы имели место отрицательные тренды уровня океана в субтропическом круговороте и положительные тренды уровня океана в субполярных и восточных областях. Таким образом, в обоих океанах произошло изменение знака трендов уровня поверхности, вероятно связанное с междекадной изменчивостью. ТДО сама по себе определяется

как междекадная мода изменчивости в Северной Пацифике. САО имеет множество частот, но также включает в себя междекадные колебания (см. главу 1). Инверсия трендов уровня океана в Северной Пацифике предположительно произошла в 1998 году. Чтобы выяснить была ли эта инверсия связана с долговременным изменением фазы ТДО или это была только краткосрочная флюктуация, вызванная сильным Эль-Ниньо в 1997 году и последующим Ля-Нинья, требуются, как минимум, несколько добавочных лет наблюдений. Как было показано в главе 3, в субполярных областях Северного Атлантического океана межгодовая изменчивость уровня с 1993 по 2003 годы коррелирована с зимними значениями САО индекса. Рост уровня океана в субполярной Северной Атлантике последовал после изменения САО фазы с положительной на отрицательную в зимы 1995/1996 и 2000/2001 годов. Линейные тренды уровня океана в Северной Атлантике, наблюдавшиеся с 1993 по 2003 годы, соответсвуют условиям отрицательной фазы САО. Несмотря на это, имея такую короткую выборку, невозможно с уверенностью сказать будут ли эти условия удерживаться долгое время, или изменения фазы САО были только кратковременными колебаниями. Из данных наблюдений можно сделать предположение, что на междекадных временных масштабах уровень океана в Северной Атлантике может изменяться в противофазе к уровню океана в Северной Пацифике. Одновременный рост уровня океана в субполярных и восточных областях Северной Атлантики и падение уровня в зонах Гольфстрима и Северо-Атлантического течения вероятно сопровождаются падением уровня океана в субполярных и восточных областях Северной Пацифики и повышением уровня в зонах Курошио и Северо-Тихоокеанского течений. Декадные тренды уровня поверхности в обоих океанах также отражают декадные тренды геострофиической циркуляции на поверхности. Последние выявили замедление субполярного и субтропического круговоротов в Северной Атлантике и интенсификацию субполярного и субтропического круговоротов в Северной Пацифике. Свидетельства замедления циркуляции в субполярных районах Северной Атлантики уже были представлены в Flatau et al. (2003) и Häkkinen and Rhines (2004).

В главе 5 для изучения межгодовых изменений местоположения и интенсивности основных течений во внетропической части Северной Атлантики использовались данные межгодовой изменчивости кинетической вихревой энергии (КВЭ). Предложенная интерпретация основана на том факте, что течения являются основным источником вихревой энергии, генерируемой через процессы неустойчивости фронтальных потоков. Было показано, что в Северной Атлантике наибольшие значения КВЭ сконцентрированы вдоль основных фронтальных течений. Сравнительный анализ вертикального распределения плотности вдоль регулярной гидрографической секции AR7E и поверхностной КВЭ продемонстировал, что центры зон с высокой КВЭ совпадают с фронтальными зонами, характеризуемыми наибольшими горизонтальными градиентами плотности. Таким образом, в диссертации показано, что в отсутствие достаточно точных оценок скоростей геострофических течений, полученных из данных спутниковой альтиметрии, КВЭ может служить полезным параметром для мониторинга изменчивости поверхностной циркуляции. В главе представлено детальное описание межгодовой изменчивости КВЭ и ассоциированной поверхностной циркуляции в

нескольких регионах внетропической части Северной Атлантики. На основе межгодовой изменчивости КВЭ продемонстрировано, что ядро Гольфстрима в рассматриваемой области претерпевает меридианальные сдвиги. В 1998 году зафиксировано самое южное положение потока, произошедшее приблизительно 2 года после того, как САО индекс перешёл из положительной в отрицательную фазу зимой 1995/1996 годов. Межгодовая изменчивость КВЭ в Северо-Атлантическом течении характеризовалась перераспределением КВЭ между тремя зонами с центрами около 43° с.ш., 47° с.ш. и 50° с.ш.. Южная зона связана с антициклоническим вихрем Манна. Две других зоны, вероятно, представляют собой ответвления Северо-Атлантического течения направленные на восток. Оказалось, что во время положительных аномалий КВЭ, наблюдавшихся в вихре Манна и вдоль северной границы Северо-Атлантического течения около 50° с.ш., отрицательные аномалии КВЭ имели место около 47° с.ш., и наоборот. Положительные/отрицательные аномалии КВЭ в Северо-Атлантическом течении в основном соответствовали восточным/западным аномалиям скоростей геострофических течений. Так как Северо-Атлантическое течение представляет собой широкий, преимущественно восточно-северо-восточный поток, то положительные/отрицательные аномалии КВЭ, главным образом, обозначают его усиление/ослабление. Максимальные значения КВЭ в Азорском течении наблюдались в 1993-1995 годах. После этого последовал спад КВЭ, который был интерпретирован как результат ослабления течения, вызванный ослаблением западных ветров в 1996 году. Межгодовые изменения КВЭ и аномалий геострофических скоростей в Иландском бассейне отразили вышеупомянутый сдвиг субарктического фронта на запад , произошедший после 1995 года. Было также продемонстрировано, что северо-восточный поток в котловине Роколл в 1993-1995 годы был интенсивнее, чем в последующие годы. Как в Исландском бассейне, так и в котловине Роколл, сезонные, с максимальными значениями преимущественно в зимний период, флюктуации КВЭ превалировали над межгодовой изменчивостью. Этот факт подтверждает взаимосвязь между КВЭ и сезонными изменениями в поле ветра, максимум которых приходится также на зиму. Долговременный тренд увеличения КВЭ был зафиксирован в бассейне Ирмингера. Этот бассейн оказался единственной областью в субполярной Северной Атлантике, где наблюдавшиеся сезонные изменения КВЭ оказались меньше межгодовых колебаний. В бассейне Ирмингера КВЭ оказалась сконцентрированной вдоль двух полос параллельных хребту Рейкянес. Наблюдавшийся рост КВЭ охватил обе полосы и, очевидно, не был связан с усилением поверхностных течений. Как было показано в предыдущих исследованиях (напр. Flatau et al., 2003) и подтверждено в главе 5, интенсивность циклонической циркуляции Северо-Атлантического субполярного круговорота уменьшилась. Было предложено, что вызванный САО сдвиг субарктического фронта к западу в направлении бассейна Ирмингера и внутрь его мог благодаря фронтальным процессам вихреобразования обусловить рост КВЭ в этом бассейне. Подобный сдвиг субарктического фронта мог задеть восточную полосу с высокой КВЭ, в то время как наличие высокой КВЭ вдоль западной полосы может поддерживаться околоповерхностным конвективным фронтом в центре бассейна Ирмингера. Характер изменчивости КВЭ в море Лабрадор до конца не исследован. Сезонные колебания КВЭ в этом регионе значительно превысили межгодовые.

Наибольшая КВЭ наблюдалась во время высоких значений САО в зимы 1996/1997, 1997/1998, и 1998/1999 годы, но не в более раннее время выборки.

В главе 6 были исследованы данные годовых значений КВЭ в зоне Северо-Атлантического течения между Большой Ньюфаундлендской банкой и Срединно-Атлантическим хребтом, чтобы определить содержат ли эти данные пространственно-распространяющиеся сигналы. Это исследование было мотивировано особенностями распределения КВЭ в данном районе, описанными в главе 5. Наиболшие значения КВЭ были обнаружены в вихре Манна и к востоку банки Флемиш-Кап около 47° с.ш. Было показано, что первая эмпирическая мода описывает распространение сигнала КВЭ вниз по течению вокруг Большой Ньюфаундлендской банки. В течение исследуемого времени с 1993 по 2003 годы зарегестрированы почти две волны КВЭ с периодом около 6 лет. Оказалось, что на западной окраине вихря Манна скорость распространения сигнала КВЭ больше, чем вверх или вниз по течению от вихря Манна. В самом вихре Манна пространственного распространения КВЭ обнаружено не было, а межгодовая изменчивость КВЭ характеризовалась стационарными колебаниями. Межгодовые колебания КВЭ в Северо-Атлантическом течении оказались когерентными с САО. Положительные аномалии КВЭ в вихре Манна были зарегестрированы в 1996-1997 и 2001-2002 годах. Это произошло после того, как положительные значения индекса САО сменились отрицательными в зимы 1995/1996 и 2000/2001 годов. Положительная аномалия КВЭ, которая наблюдалась в вихре Манна в 1996-1997 годах, достигла широты 47° с.ш. в 2000 году. Положительные аномалии КВЭ в Северо-Атлантическом течении оказались, главным образом, связаны с интенсификацией восточного потока. Тем не менее, располагая короткими временными рядами наблюдений, невозможно определить является ли наблюдавшееся пространственное распространение КВЭ периодическим явлением и имеет ли оно характерный период. Вполне вероятно, что распространение КВЭ связано с меридианальными сдвигами рукавов Северо-Атлантического течения. Зафиксированная когерентность с САО предполагает наличие связи с атмосферным воздействием. Так как поверхностная циркуляция, в основном, движима ветром, то меридианальные сдвиги потоков течений, отождествлённые с пространственным распространением КВЭ, могут быть вызваны меридианальными сдвигами в поле напряжения ветра.

Acknowledgements

This Ph.D. thesis is the result of about 4 years of research conducted at the Department of Physical Oceanography of the Royal Netherlands Institute for Sea Research (NIOZ). As “onderzoeker in opleiding” or a researcher in training I enjoyed highly encouraging atmosphere at the department and at the whole institute. I would like to express my gratitude to all those involved in the research and in the everyday life beyond work.

First of all, I sincerely wish to thank my co-supervisor Hendrik van Aken and supervisor Will de Ruijter for inviting me to the Netherlands and offering the opportunity to do the Ph.D. research. Hendrik was always an active and responsive helper, advisor and teacher. I am grateful to him for assistance in solving different research tasks, reviewing manuscripts, and also translating the summary of this thesis into Dutch.

Merci beaucoup, Alima, pour ton amour, amitié et pour avoir été auprès de moi durant ces années. I am very grateful to all friends on Texel, with whom I shared many great and unforgettable moments, particularly to Phil, Khalid, Anne-Claire, Yann, Alina, Pedro, Teresa, Joana and Ben, Astrid, Jérôme, Furu, Micha, and Jasper. Special thanks to Phil for often correcting my English. Many thanks to Julia Vdovenko, Kirill and Julia Duz, Svetlana, Sergey Kirillov, Sergey Grigoriev and Irina, Alexey and Svetlana Negulyaev for your long and so valuable friendship. I also want to thank all people I met at conferences and at the summer school in Les Diablerets, especially Rory Bingham, with whom we not only climbed the Swiss Alps, but also explored the expanses of the Saint-Lawrence river.

I wish to thank all my colleagues at the department for warm reception and team spirit. It was a pleasure to work beside all of you. Astrid and Femke, thank you for being nice officemates. I very enjoyed playing football for the NIOZ team and I thank all my team-mates for the great time we had.

Наконец, я хочу поблагодарить моих родителей и брата за любовь, огромную заботу и бесценную поддержку, без чего написание этой диссертации было бы просто немыслимо.

Curriculum Vitae

Denis Volkov was born on 30 April 1975 in Taganrog, south Russia. Having finished secondary school in Tallinn (Estonia), he entered the Saint-Petersburg State University (Russia) in 1992. After two years of general education at the Faculty of Geography and Geoecology, he started to specialize in physical oceanography. He passed his Bachelor in 1997, and after the successful defence of his Master's thesis in 1999, he graduated *cum laude* with the degree of the Master of Hydrometeorology. The Master's thesis was dedicated to the study of the factors responsible for the variability of the sea fast ice edge in the Russian Arctic seas. This research was done during several months of work at the Arctic and Antarctic Research Institute in Saint-Petersburg. In June 2000, Denis Volkov started his Ph.D. research at the Royal Netherlands Institute for Sea Research on the project "Climatic variability of the sea surface height and circulation in the North Atlantic Ocean observed with satellite altimetry". Along with the preparation for the defence, he is now hoping that by the time the reader reads this CV he will have found a postdoctoral research position somewhere on our Blue planet to continue exploring her mysteries.